Genetics and Pathogenesis of Inherited Neuropathies

Yo-Tsen Liu

A thesis submitted to the University College London for

the degree of Doctor of Philosophy

2015

Department of Molecular Neuroscience,

Institute of Neurology,

University College London

Declaration

I, Yo-Tsen Liu, confirm that the vast majority of laboratory genetic work presented in this thesis is my own. For the results generated from others' work including the clinical assessments, electrophysiology and pathology, I confirm that these have been indicated clearly in this thesis.

Yo-Tsen Liu

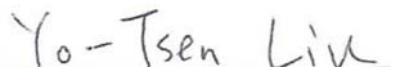

Abstract

Inherited neuropathies are a clinically and genetically heterogeneous group of diseases affecting the peripheral nervous system (PNS). More than 70 causative genes have been recognised, however, there are still patients whose disease-causing genes have not been identified, particularly those presenting with complex phenotypes which also involve the central nervous system (CNS) and other organs. The main objective of my PhD was to establish the genetic diagnosis in these patients through an integrated approach combining conventional Sanger sequencing and the next generation sequencing (NGS) technologies which include whole exome sequencing (WES) and targeted resequencing.

Based on this integrated approach, mutations in several genes for inherited neuropathies and related disorders have been identified. My thesis focuses on: (1) screening studies in large cohorts of patients conducted by Sanger sequencing to define the frequency of the mutations in the *NEFL* gene in Charcot-Marie-Tooth disease (CMT), in the *SPTLC*2 gene in hereditary sensory neuropathy type I and in the *PDYN* gene in autosomal dominant cerebellar ataxia (ADCA) in British population; (2) WES studies to identify mutations in patients with inherited neuropathies or autosomal recessive cerebellar ataxia (ARCA), including a novel *ADCK3* mutation in ARCA and two novel genes causing CMT, *MARS* and *C12orf65;* (3) the development of two targeted resequencing panels for CMT and hereditary spastic paraplegia (HSP) with axonal neuropathy to identify disease-causing mutations in two cohorts; (4) the broadening of the phenotypic spectrum of *KIF5A* in patients with HSP and CMT type 2.

In this thesis functional studies for some of the identified mutations were also performed such as the impairment of the mitochondrial respiratory enzymes in the lymphoblasts of patients with the *C12orf65* mutation and in fibroblasts of patients with the *ADCK3* mutation.

The challenges faced by the use of NGS in genetic diagnosis and how to address these challenges in the future are discussed.

Acknowledgement

Firstly, I would like to thank the Department of Molecular Neuroscience and MRC Centre for Neuromuscular Diseases, UCL Institute of Neurology and my principal supervisor Professor Mary M Reilly for giving me the opportunity and support to undertake this project. I would also express my appreciation to the Ministry of Education of Taiwan government who issued me the Studying Abroad Scholarship in support of my PhD study. I am extremely grateful to my secondary supervisors, Professor Henry Houlden for the guidance in study concepts, laboratory experiment and the much needed strictness that really helped bring this project together. I owe a special appreciation to my third supervisor, Dr. Matilde Laurá for constant encouragement and an infinite amount of patience in the guidance of my academic writing.

Thanks are given to all the laboratory colleagues the Department of Molecular Neuroscience and the genetic unit at the National Hospital for Neurology and Neurosurgery for their guidance and assistance. I would especially like to thank Dr. James M Polke for sharing with me much knowledge of sequencing procedures and data analysis. I would also express my appreciation to Dr. Vincent Plagnol, Dr. Katherine Fawcett, Dr. Alan Pittman and Ms Deborah Hughes for their very useful advice over next generation sequencing. I am thankful to Dr.Iain P Hargreaves, Dr. Kate EC Duberley and Ms Elisavet Preza for all their assistance on the studies of mitochondrial enzyme activities, CoQ10 measurement and cellular cultures.

Special thanks will go to Dr. Joshua Hersheson and Dr. Alejandro Horga for their help in collecting clinical information of the patients. I would like to thank my friends and colleague Dr. Amelie Pandraud, Ms Ellen Cottenie, Ms Alice Gardiner for their support and encouragement through the course of my PhD studying.

I am grateful to all the patients and their families, without whom none of this research would have been possible.

My sincerest thankfulness would be delivered to my mother, sister, mother-in-law and brother-in-law who are always my strongest back up and cheered my up from the frustration. Lastly, this thesis is dedicated with the deepest love and the hugest thanks to my husband Dr. Yu-Ping Su and my lovely daughter Vivian. Their understanding and support all these years make my dream come true.

Table of content

Abbreviations

AAA metalloprotease	ATPases associated with various cellular activities metalloprotease complex
AARS	The alanyl-trna-synthetase gene
AD	Autosomal dominant
ADCA	Autosomal dominant cerebellar ataxia
ADCA-DN	Autosomal dominant cerebellar ataxia, deafness and narcolepsy
ADCK3	The aarf domain containing kinase 3 gene
AFG3L2	The AFG3 atpase family gene 3-like 2 gene
AIFM1	The apoptosis-inducing factor, mitochondrion-associated, 1 gene
ALS	Amyotrophic lateral sclerosis
AOA1	Ataxia with oculomotor apraxia type 1
AOA2	Ataxia with oculomotor apraxia type 2
AR	Autosomal recessive
ARCA	Autosomal recessive cerebellar ataxia
ARSACS	Autosomal recessive Charlevoix-Saguenay-Spastic Ataxia
AT	Ataxia telangiectasia
ATL1	The atlastin-1 gene
ATP	Adenosine triphosphate
ATP7A	The atpase, Cu++ transporting, alpha polypeptide gene
BICD2	The bicaudal D homolog 2 gene
BN-PAGE	Blue native polyacrylamide gel electrophoresis
BSCL2	The Berardinelli-Seip congenital lipodystrophy 2 gene
C12orf65	The chromosome 12 open reading frame 65 gene
CCDS	Consensus CDS (coding DNA sequence)
CCFDN	Congenital cataracts, facial dysmorphism, and neuropathy
CCT5	The epsilon subunit of the cytosolic chaperonin-containing t-complex peptide-1 gene
cDNA	Complementary DNA
CHN	Congenital hypomyelinating neuropathy
cHSP	Complex hereditary spastic paraplegia
CIPA	Congenital insensitivity to pain with anhidrosis
CMT	Charcot–Marie–Tooth disease
CMT1	CMT type 1
CMT2	CMT type 2
CNS	The central nervous system
CoQ10	Coenzyme Q10
CTDP1	The CTD (carboxy-terminal domain, RNA polymerase II, polypeptide A) phosphatase, subunit 1 gene
DCTN1	The dynactin 1 gene

ddNTP	2', 3' dideoxynucleotides
DFNA6	Autosomal dominant deafness 6
dHMN	Distal hereditary motor neuropathy
DHTKD1	The dehydrogenase E1 and transketolase domain containing 1 gene
DI-CMT	Dominant intermediate CMT
DIDMOAD	Diabetes Insipidus, Diabetes Mellitus, Optic Atrophy, and Deafness
DNA	Deoxyribonucleic acid
DNAJB2	The dnaj (Hsp40) homolog, subfamily B, member 2 gene
DNM2	The dynamin 2 gene
DNMT1	The DNA-methyltransferase 1 gene
DRPLA	Dentatorubro-pallidoluysian atrophy
DSN	Dejerine Sottas neuropathy
DYNC1H1	The cytoplasmic dynein heavy chain 1 gene
DYT1	Early-onset primary dystonia
EGR2	The early growth response 2 gene
EMG	Electromyography
ER	Endoplasmic reticulum
ESV	National Heart, Lung, and Blood Institute Exome Sequencing Variant database
FAM134B	The family with sequence similarity 134 member B gene
FBLN5	The FBLN5 fibulin 5 gene
FCCP	Trifluorocarbonylcyanide phenylhydrazone
FGD4	The FYVE, rhogef and PH domain containing 4 gene
FIG4	The FIG4 homolog, SAC1 lipid phosphatase domain containing gene
FXTAS	Fragile-X tremor ataxia syndrome
GARS	The glycyl-trna synthetase gene
GDAP1	The ganglioside induced differentiation associated protein 1 gene
gDNA	Genomic DNA
GJB1	The gap junction protein, beta 1 gene
GJB3	The GJB3 gap junction protein, beta 3, 31kda, gene
GNB4	The guanine nucleotide binding protein (G protein), beta polypeptide 4 gene
GO	Gene ontology
HARS	The histidyl-trna synthetase gene
HINT1	The histidine triad nucleotide binding protein 1gene
HK1	The hexokinase 1 gene
HMSN	Hereditary motor and sensory neuropathy
HNPP	Hereditary neuropathy with liability to pressure palsies
HSAN	Hereditary sensory and autonomic neuropathy
HSN	Hereditary sensory neuropathy
HSN2	The hereditary sensory neuropathy, type II gene

HSP	Hereditary spastic paraplegia
HSPB1(HSP27)	The heat shock 27-kda protein 1 gene
HSPB3	The heat shock 27kda protein 3 gene
HSPB8(HSP22)	The heat shock 22-kda protein 1 gene
I-CMT	Intermediate CMT
IGHMBP2	The immunoglobulin mu binding protein 2 gene
IGV	The Integrative Genomics Viewer
IKBKAP	The inhibitor of kappa light polypeptide gene enhancer in B-cells, kinase complex-associated protein gene
INF2	The inverted formin, FH2 and WH2 domain containing gene
IPNMD	Inherited peripheral neuropathies mutation database
KARS	The lysyl t-RNA synthetase gene
KCND3	The potassium voltage-gated channel, Shal-related subfamily, member 3 gene
KHC	Kinesin heavy chain
KIF1A	The kinesin family member 1A gene
KIF1B	The kinesin family member 1B gene
KIF5A	The kinesin family member 5A gene
LITAF	The lipopolysaccharide-induced tumor necrosis factor gene
LMN	Lower motor neuron
LMNA	The lamin A/C gene
LRSAM1	The leucine rich repeat and sterile alpha motif containing 1 gene
MAF	Minor allele frequency
MAP	Motor action potential
MARS	The methionyl-trna synthetase gene
MED25	The mediator complex subunit 25 gene
MFN2	The mitofusin 2 gene
MNCV	Motor nerve conduction velocity
MPZ	The myelin protein zero gene
MRC	Mitochondrial respiratory chain
MRI	Magnetic resonance imaging
mRNA	Messenger ribonucleic acid
MT-ATP6	The mitochondrially encoded ATP synthase 6 gene
MTMR13	The myotubularin-related protein 13 gene
MTMR2	The myotubularin-related protein 2 gene
MYH14	The myosin, heavy chain 14, non-muscle gene
NADH	Nicotinamide adenine dinucleotide
NAV2	The neuron navigator 2 gene
NCS	Nerve conduction study
NCV	Nerve conduction velocity
NDRG1	The N-myc downstream regulated 1 gene

NEFL	The neurofilament, light polypeptide gene
NFL	Neurofilament light chain
NGFB	The nerve growth factor (beta polypeptide) gene
NGS	Next-generation sequencing
NHNN	The National Hospital for Neurology and Neurosurgery
NIH	National Institutes of Health
NIPA1	The non imprinted in Prader-Willi/Angelman syndrome 1 gene
NMD	Genome Variant Database for Neuromuscular Diseases
NTRK1	The neurotrophic tyrosine kinase, receptor, type 1
OMIM	Online Mendelian Inheritance in Man
OXPHOS	The oxidative phosphorylation system
PCR	Polymerase chain reaction
PDK3	The pyruvate dehydrogenase kinase, isozyme 3 gene
PDXK	The pyridoxal (pyridoxine, vitamin B6) kinase gene
PDYN	The prodynorphin gene
pHSP	Pure hereditary spastic paraplegia
PLEKHG5	The pleckstrin homology domain containing, family G member 5 gene
PMP22	The peripheral myelin protein 22 gene
PNMHH	Peripheral neuropathy, myopathy, hoarseness, and hearing loss
PNPLA6	The patatin-like phospholipase domain containing 6 gene
PNS	Peripheral nervous system
POLG	The polymerase gamma gene
Polyphen2	Polymorphism Phenotyping v2
PRNP	The prion protein gene
PRPS1	The phosphoribosylpyrophosphate synthetase 1 gene
PRX	The periaxin gene
qRT-PCR	Quantitative Real Time PCR (qrt-PCR)
RAB7	The RAS-related GTP-binding family member 7 gene
REEP1	Receptor accessory protein 1
RI-CMT	Recessive intermediate CMT
RNA	Ribonucleic acid
RNF216	The ring finger protein 216 gene
RT	Room temperature
SA	Sphinganine
SACS	The spastic ataxia of Charlevoix-Saguenay gene
SAP	Sensory nerve action potential
SBF1	The SET binding factor 1 gene
SCA	Spinocerebellar ataxia
SCAN1	Spinocerebellar ataxia with axonal neuropathy
SCN9A	The sodium channel, voltage-gated, type IX, alpha subunit gene

SD	Standard deviation
SETX	The senataxin gene
SH3TC2	The SH3 domain and tetratricopeptides repeats 2 gene
SIFT	Sorting intolerant from tolerant
SLC5A7	The solute carrier family 5 (sodium/choline cotransporter), member 7 gene
SMA	Spinal muscular atrophy
SMA-LED	Spinal muscular atrophy with lower limb predominance
SMAN	Sensory motor axonal neuropathy
SMARD1	Spinal muscular atrophy with respiratory distress type 1
SNP	Single nucleotide polymorphism
SO	Sphingosine
SOX10	The SRY (sex determining region Y)-box 10 gene
SPAST	The spastin gene
SPG7	The spastic paraplegia 7 gene
SPT	Serine palmitoyltransferase
SPTLC1	The serine palmitoyltransferase long chain base subunit 1 gene
SPTLC2	The serine palmitoyltransferase long chain base subunit 2 gene
SSCP	Single strand conformation polymorphism
STRING	Search Tool for the Retrieval of Interacting Genes/Proteins
SURF1	The surfeit 1 gene
TDP1	The tyrosyl-DNA phosphodiesterase 1 gene
TFG	The TRK-fused gene
TiGER	Tissue-specific Gene Expression and Regulation
TRIM2	The tripartite motif containing 2 gene
TRPV4	The transient receptor potential cation channel, subfamily V, member 4 gene
TSCA	Truseq Custom Amplicon
UGI	Ucl genetics institute
UK	United kingdom
UMN	Upper motor neuron
US	United states
UTR	Untranslated region
VCF	Variant call format
WES	Whole exome sequencing
WFS	Wolfram syndrome
WFS1	The Wolfram syndrome 1 gene
WGS	Whole genome sequencing
WNK1	The WNK lysine deficient protein kinase 1 gene
WUNDC	Washington university neuromuscular disease center database
YARS	The tyrosyl-trna synthetase gene
ZFYVE26	The zinc finger, FYVE domain containing 26 gene

List of figures

List of tables

Publications arisen from this thesis

1. Extended phenotypic spectrum of KIF5A mutations: from spastic paraplegia to axonal neuropathy. **Liu YT***, Laurá M, Hersheson J, Horga A, Jaunmuktane Z, Brandner S, PittmanA, Hughes D, Polke JM, Sweeney MG, Proukakis C, Janssen JC, Auer-Grumbach M, Zuchner S, Shields KS, Reilly MM, Houlden H. Neurology. 2014 Jul 9. [Epub ahead of print].

2. Autosomal-recessive cerebellar ataxia caused by a novel ADCK3 mutation that elongates the protein: clinical, genetic and biochemical characterisation. **Liu YT***, Hersheson J, Plagnol V, Fawcett K, Duberley KE, Preza E, Hargreaves IP, Chalasani A, Laurá M, Wood NW, Reilly MM, Houlden H.J Neurol Neurosurg Psychiatry. 2014 May;85(5):493-8.

3. Novel C12orf65 mutations in patients with axonal neuropathy and optic atrophy. Tucci A, **Liu YT**, Preza E, Pitceathly RD, Chalasani A, Plagnol V, Land JM, Trabzuni D, Ryten M; on behalf of UKBEC, Jaunmuktane Z, Reilly MM, Brandner S, Hargreaves I, Hardy J, Singleton AB, Abramov AY, Houlden H. J Neurol Neurosurg Psychiatry. 2014 May;85(5):486-92

4. Exome sequencing identifies a significant variant in methionyl-tRNA synthetase (MARS) in a family with late-onset CMT2. Gonzalez M, McLaughlin H, Houlden H, Guo M, **Liu YT***, Hadjivassilious M, Speziani F, Yang XL, Antonellis A, Reilly MM, Züchner S; Inherited Neuropathy Consortium. J Neurol Neurosurg Psychiatry. 2013 Nov;84(11):1247-9.

5. Hereditary sensory and autonomic neuropathy type 1 (HSANI) caused by a novel mutation in SPTLC2. Murphy SM, Ernst D, Wei Y, Laurà M, **Liu YT***, Polke J, Blake J, Winer J, Houlden H, Hornemann T, Reilly MM. Neurology. 2013 Jun 4;80(23):2106-11.

6. The frequency of spinocerebellar ataxia type 23 in a UK population. Fawcett K, Mehrabian M, **Liu YT***, Hamed S, Elahi E, Revesz T, Koutsis G, Herscheson J, Schottlaender L, Wardle M, Morrison PJ, Morris HR, Giunti P, Wood N, Houlden H. J Neurol. 2013 Mar;260(3):856-9. Epub 2012 Oct 30. Erratum in: J Neurol. 2013 Mar;260(3):860.

7. Charcot-Marie-Tooth disease: frequency of genetic subtypes and guidelines for genetic testing. Murphy SM, Laura M, Fawcett K, Pandraud A, **Liu YT***, Davidson GL, Rossor AM, Polke JM, Castleman V, Manji H, Lunn MP, Bull K, Ramdharry G, Davis M, Blake JC, Houlden H, Reilly MM. J Neurol Neurosurg Psychiatry. 2012 Jul;83(7):706-10.

Contribution from collaborative researchers

I would like to express the deepest acknowledgements to the following people and institutions who collaborative with my genetic studies in this thesis. These collaborators were all from Department of Molecular Neuroscience, UCL Institute of Neurology unless who are specially described. Their contribution is listed below.

C12orf65 sequencing, RNA purification and cDNA synthesis and RT-qPCR were conducted in collaboration with Dr. Arianna Tucci.

SPTLC2 sequencing was conducted in collaboration with Dr. Sinéad M Murphy. *PDYN* sequencing was conducted in collaboration with Dr. Katherine Fawcett and Mohadeseh Mehrabian. *KCND3* sequencing was conducted in collaboration with Dr. Katherine Fawcett and Joshua Hersheson. *AFG3L2* sequencing was conducted in collaboration with Dr. Katherine Fawcett.

Lymphoblast and fibroblast cell cultures were performed by Ms. Elisabeth Preza.

Fibroblast lines from matched healthy controls were kindly provided by Dr. Jan-Willem Taanman, UCL Institute of Neurology and the MRC CNMD Biobank London.

Blue native in-gel assay was performed by Andrey Y. Abramov.

Mitochondrial O_2 consumption determination.and respiratory enzyme activity assay were performed by Dr. Iain P. Hargreaves from Neurometabolic unit, NHNN.

Determination of the CoQ10 level of fibroblasts was conducted by Dr. Kate E. C. Duberley.

Photographs of the sural nerve biopsies were provided by Dr. Zane Jaunmuktane from Division of Neuropathology and Department of Neurodegenerative Disease, UCL Institute of Neurology.

Structural model of human MetRS, Cloning and mutagenesis of MES1, and Yeast viability assays were performed by the laboratory of Dr. Stephan Züchner in Dr. John T. McDonald Foundation Department of Human Genetics and John P. Hussman Institute for Human Genomics, University of Miami Miller School of Medicine, Miami, US.

Cloning and mutagenesis of *SPTLC2*, metabolic labeling assay, SPT in vitro activity assay, lipid-base extraction, acid-base extraction and analysis of sphingoid bases were performed by the laboratory of Dr. Thorsten Hornemann from Institute for Clinical Chemistry, University

Hospital Zurich and Institute of Physiology and Zurich Center for Integrative Human Physiology, University of Zurich, Zurich, Switzerland.

For WES performed at Department of Molecular Neuroscience, UCL Institute of Neurology, sample preparation, whole exome capturing and enrichment at were performed by Ms Deborah Hughes. The bioinformatics annotation was performed by Dr. Alan Pittman.

Bioinformatic annotation of WES in the patient with *ADCK3* mutation was performed by Dr. Vincent Plagnol from UCL Genetics Institute. WES analysed for the patient with ADCK3 mutation was performed in collaboration with Dr. Katherine Fawcett.

WES of the patients with KIF5A R280C mutation (K6) was performed in collaboration with Dr. Michaela Auer-Grumbach from Department of Orthopaedics, Medical University Vienna, Vienna, Austria and Dr. Stephan Züchner in Dr. John T. McDonald Foundation Department of Human Genetics and John P. Hussman Institute for Human Genomics, University of Miami Miller School of Medicine, Miami, US.

Chapter 1

Introduction

Inherited neuropathies are a clinically and genetically heterogeneous group of diseases affecting the PNS. More than 70 causative genes have been recognised, however, there are still patients whose disease-causing genes have not been identified, particularly those presenting with complex and atypical phenotypes involving the CNS and even other organs. The objective of this thesis was to investigate the genetics and pathogenesis of inherited neuropathies via the approach of NGS in combination with conventional methods. The research projects undertaken were divided into the following parts: (1) screening of disease-causing mutations in newly-identified genes or in rare genes responsible for inherited neuropathies, (2) screening of disease-causing mutations in genes responsible for other inherited neurological disorders associated with peripheral neuropathies, (3) WES in patients in which genetic diagnosis has not been reached by conventional methods, (4) applications of targeted resequencing in cohorts of patients with inherited neuropathies and related disorders. Functional studies for some of the mutations identified were also performed.

This chapter provides an overview of the neurological diseases studied in this thesis which include inherited neuropathies, hereditary cerebellar ataxia and hereditary spastic paraplegia (HSP). A brief introduction on NGS and its applications on genetic diagnosis is also outlined.

1.1 Overview of inherited neuropathies

The commonest type of inherited neuropathies are Charcot-Marie-Tooth disease (CMT), hereditary sensory neuropathies (HSN) and the distal hereditary motor neuropathies (dHMN).(Reilly et al. 2009; Saporta et al. 2013; Siskind et al. 2013). These three disorders represent a continuum from pure motor neuropathies (dHMN), involvement of both motor and sensory nerves (CMT) to sensory-predominant neuropathies (HSN). In the past two decades a great advancement has been achieved in the genetic diagnosis of inherited neuropathies with the identification of mutations in more than 70 causative genes.(Rossor et al. 2013) Interestingly, increasing overlaps in clinical phenotypes and genetic aetiologies between these disorders have been recognised.

1.1.1 Charcot-Marie-Tooth disease (CMT)

CMT was named after the three clinicians: Jean-Marie Charcot, Pierre Marie and Howard Henry Tooth who first described the familial neurological syndrome “peroneal muscular atrophy” in 1886. CMT has now been recognised as the commonest inherited neuromuscular disorder affecting approximately 1 in 2,500 individuals.(Azzedine et al. 2012; Skre 1974) Also termed as hereditary motor sensory neuropathy (HMSN), CMT is a heterogeneous group of sensorimotor peripheral neuropathies characterised by distal muscle weakness and atrophy, distal sensory loss, decreased or absent tendon reflexes. The weakness results in foot drop and steppage gait. Foot deformities occur frequently. The onset is usually in the first two decades. Patients may have autosomal dominant (AD), autosomal recessive (AR) or X-linked inheritance; however, de novo dominant cases are not rare and thus some patients do not have a family history. In the north European and United States (US) populations, AD and X-linked are the commonest inheritance pattern accounting for near 90% of all cases of CMT. ARCMT cases are less common, although in countries with a higher rate of consanguineous marriages it can account for up to 40% of all CMT cases.(Dubourg et al. 2006a)

CMT was first classified in demyelinating CMT1 [median motor nerve conduction velocity (MNCV) <38 m/s] and CMT2 (median MNCV >38 m/s) on the base of neurophysiological parameters.(Harding et al.1980) This classification remains the cornerstone of modern diagnosis. In all populations, CMT1 is consistently reported as the commonest form, accounting 50~75% of all affected patients, followed by CMT2 (30~50 %). A small group of patients (2~15%) have median MNCV ranging between 25~45 m/s and have been classified as the intermediate CMT (I-CMT).(Braathen et al. 2011; Nicolaou et al. 2010) Congenital hypomyelinating neuropathies (CHN) or Dejerine Sottas neuropathy (DSN) is used to indicate severe forms of CMT with onset during infancy. CMT4 is currently used to characterise ARCMT1.(Reilly et al. 2009)

The identification of PMP22 as the first causative gene for CMT in 1991 was the breakthrough point in the understanding of CMT.(Lupski et al. 1991) Since then there have been rapid advances in the molecular genetics of the disease with the identification of more than 70 causative genes.(Reilly et al. 2011; Rossor et al. 2013) The classification of CMT is in continuous evolution due to the rapid development of molecular genetics. Current classification is based on clinical, electrophysiological, genetic and pathological criteria. Clinical features and causative genes are summarised in table 1-1 (p22).

Autosomal dominant CMT1 (ADCMT1) is the largest subgroup of CMT. The majority of ADCMT1 are caused by mutations or rearrangement in the following five genes: *PMP22*, *MPZ*, *LITAF*, *EGR2* and *NEFL*.(Azzedine et al. 2012; Murphy et al. 2012) CMT1A caused by the chromosome 17 duplication containing *PMP22* gene is the commonest form and accounts for 70% of all CMT1 cases in European/North American populations.(Saporta et al. 2011) A deletion in the same segment of DNA is associated with Hereditary Neuropathy with Liability to Pressure Palsies (HNPP), an autosomal dominant condition characterised by recurrent nerve palsies at points vulnerable to pressure. Point mutations in the same *PMP22* gene are associated with variable phenotypes including classical CMT1A, more severe CMT1 and HNPP.(Relly et al. 2009, Russo et al. 2011) CMT1B caused by *MPZ* mutations accounts for approximately 10% of ADCMT1 cases. CMT1B patients are more likely to have an early-onset neuropathy and a more severe disease course (Shy et al. 2004), however late-onset CMT2, I-CMT and recessive CMT have all been described with *MPZ* mutations.(Azzedine et al. 2012) ADCMT1 caused by mutations of the other genes (*LITAF, EGR2* and *NEFL)* are rare (<1% each),(Street et al. 2003; Sevilla et al. 2004; Warner et al. 1998)

CMT2, the axonal form of CMT, is clinically heterogeneous and it can present as the classical CMT phenotype or as predominant sensory neuropathy or as predominant motor neuropathy.(Bienfait et al. 2011; Reilly et al. 2011) For ADCMT2, mutations in at least 22 genes have been reported and genetic testing is mainly guided by patient's phenotype. CMT2A secondary to *MFN2* mutations is the commonest form, representing approximately 20% of all patients with ADCMT2.(Murphy et al. 2012; Relly et al. 2009; Zuchner et al. 2004) In CMT2 with predominant sensory impairment the following genes should be considered as the priority: *RAB7* (the causative gene for CMT2B), *SPTLC1* and *SPTLC2*.(Auer-Grumbach et al. 2003; Rotthier et al. 2010; Verhoeven et al. 2003) *SPTLC1* and *SPTLC2* are the causative gene of HSN but patients usually have significant motor involvement and hence the overlap with CMT2.(Bejaoui et al. 2001)

CMT2 with predominant motor involvement is usually associated with mutations in four genes: *GARS, HSP27/HSPB1, HSP22/HSPB8* and *TRPV4*.(Reilly et al. 2009) Predominant upper limb involvement is commonly described in patients carrying *GARS* mutations (Antonellis et al. 2003) Mutations in *HSPB1* and *HSPB8* are otherwise more commonly identified in patients with predominant lower limb involvement.(Murphy et al. 2012) Mutations in *TRPV4* are associated with variable phenotypes. Dominant mutations were originally described causing skeletal dysplasia, brachyolmia type 3. Subsequently mutations were identified in patients with CMT2C, scapuloperoneal muscular atrophy and congenital distal spinal muscle atrophy (SMA).(Rossor et al. 2012)

Table 1-1. Classification of Charcot-Marie-Tooth disease (CMT)

Subtype	Gene/Locus	Phenotype
CMT1 (ADCMT1)		
CMT1A	17p dup *PMP22* (pm)	CMT1/DSN/CHN
CMT1B	*MPZ*	CMT1/DSD/CHN/rarely CMT2
CMT1C	*LITAF*	CMT1
CMT1D	*EGR2*	CMT1/DSN/CHN/rarely recessive
CMT1F	*NEFL*	CMT2/rarely CMT1/rarely I-CMT/rarely recessive
Other	*FBLN5*	CMT1/d-HMN with macular degeneration & hyperelastic skin
	SOX10	CMT1/CHN with hypopigmentation & enteric aganglionosis
	GJB3	Demyelinating polyneuropathy & hearing loss
CMT2 (ADCMT2)		
CMT2A2	*MFN2*	CMT2/progressive/optic atrophy/pyramidal signs/rarely recessive
CMT2A1	*KIF1B*	CMT2/usually severe/optic atrophy
CMT2B	*RAB7*	CMT2B or HSN 1, predominant sensory involvement and sensory complications
CMT2C	*TRPV4*	CMT2/dHMN(Congenital SMA)/Scapuloperoneal SMA with respiratory involvement/ arthrogryposis, laryngomalacia and vocal cord paresis
CMT2D	*GARS*	CMT2/dHMN-V with predominant hand wasting
CMT2E	*NEFL*	CMT2/rarely CMT1/rarely I-CMT/rarely recessive
CMT2F	*HSPB1*	CMT2, motor predominant/dHMN-II/rarely recessive
CMT2I	*MPZ*	Late-onset CMT2
CMT2J	*MPZ*	CMT2 with hearing loss and pupillary abnormalities
CMT2K	*GDAP1*	CMT1, severe and early-onset /ARCMT2C/RI-CMT with vocal cord and diaphragm paralysis
CMT2L	*HSPB8*	CMT2, motor predominant/dHMN-II
CMT2M	*DNM2*	Intermediate CMT (DI-CMTB)/CMT2 with cataracts, ophthalmoplegia, ptosis
CMT2N	*YARS*	CMT2/d-HMN
CMT2O	*DYNC1H1*	CMT2 with learning difficulties/SMA-LED
CMT2P	*LRSAM1*	CMT2
CMT2Q	*DHTKD1*	CMT2
Other	*TFG*	CMT2 with proximal involvement
	MARS	Late-onset CMT2
	HARS	CMT2
	KIF5A	CMT2 with pyramidal signs/SPG10
	MT-ATP6	CMT2 with pyramidal signs

Table 1-1. (cont)

Subtype	Gene/Locus	Phenotype & additional feature
CMT4 (ARCMT1)		
CMT4A	*GDAP1*	CMT1, severe and early-onset /ARCMT2C/RI-CMT with vocal cord and diaphragm paralysis
CMT4B1	*MTMR2*	severe CMT1with facial weakness, bulbar palsy and focally folded myelin
CMT4B2	*MTMR13*	severe CMT1with glaucoma and focally folded myelin
CMT4B3	*SBF1*	CMT1 and focally folded myelin
CMT4C	*SH3TC2*	severe CMT1with scoliosis
CMT4D	*NDRG1*	severe CMT1 with deafness and tongue atrophy, gypsy
CMT4E	*EGR2*	CMT1/DSN/CHN
CMT4F	*PRX*	CMT1, predominant sensory, and focally folded myelin
CMT4G		
(HMSN-Russe)	*HK1*	severe and early-onset CMT1, Russe type
CMT4H	*FGD4*	CMT1
CMT4J	*FIG4*	CMT1, predominant motor, progressive
CCFDN	*CTDP1*	CMT1/gypsy/cataracts/dysmorphic features
Other	*SURF1*	severe and early-onset demyelinating neuropathy with lactic acidosis and cerebellar ataxia
	EGR2	
	NEFL	
ARCMT2		
ARCMT2A	*LMNA*	CMT2 with proximal involvement, rapid progression/muscular dystrophy/cardiomyopathy/lipodystrophy
ARCMT2B	*MED25*	CMT2
ARCMT2C	*GDAP1*	CMT1, severe and early-onset /ARCMT2C/CMT-RIA with vocal cord and diaphragm paralysis
Other	*NEFL*	
	MFN2	
	TRIM2	very early onset CMT2
	HINT1	CMT and neuromyotonia
CMT X		
CMTX1	*GJB1 (Cx32)*	CMT1/CMT2/I-CMT, male MCVs < female MCVs
CMTX4	*AIFM1*	Cowchock sydnrome
CMTX5	*PRPS1*	severe CMT2 with deafness and optic atrophy
CMTX6	*PDK3*	CMT2
Dominant intermediate CMT (DI-CMT)		
CMT-DIB	*DNM2*	I-CMT/CMT2; with cataracts, ophthalmoplegia; ptosis
CMT-DIC	*YARS*	I-CMT/CMT2
CMT-DID	*MPZ*	I-CMT/CMT2
CMT-DIE	*INF2*	I-CMT with glomerulonephritis
CMT-DIF	*GNB4*	I-CMT
Other	*NEFL*	CMT2/rarely CMT1/rarely I-CMT/rarely recessive
Recessive intermediate CMT (RI-CMT)		
CMT-RIA	*GDAP1*	CMT1, severe and early-onset /ARCMT2C/CMT-RIA with vocal cord and diaphragm paralysis
CMT-RIB	*KARS*	I-CMT with learning difficulty, vestibular schwannoma
CMT-RIC	*PLEKHG5*	I-CMT/SMA

CCFDN: congenital cataracts, facial dysmorphism, and neuropathy; **CHN**: congenital hypomyelinating neuropathy; **DSN**: Dejerine Sottas neuropathy; **dup**: duplication; **pm:** point mutation; **SMA**: spinal muscular atrophy; **SMA-LED**: spinal muscular atrophy with lower limb predominance; **SPG10**: spastic paraplegia type 10.

Autosomal recessive CMT (ARCMT) includes both demyelinating (CMT4) and axonal forms (ARCMT2) and more than 20 causative genes have been identified so far.(Rossor et al. 2013; Tazir et al. 2013) These are rarer forms and account for approximately 30-50% of CMT in Mediterranean or Middle East countries. These patients generally have an early onset and a more severe course of disease than patients with typical ADCMT1. Patients can have delayed motor milestones and weakness often progresses to involve proximal muscle and may result in early loss of ambulation. *GDAP1* is the first gene identified for ARCMT and its mutations can cause either demyelinating or axonal neuropathy. Vocal cord paralysis is a frequent associated feature. Recent reports suggest that CMT4C due to mutations of *SH3TC2* is emerging as the commonest form in many populations and severe and early scoliosis is a characteristic clinical feature.(Houlden et al. 2009b; Murphy et al. 2012) Another subtype in which the mutation has been identified in the British/Irish population is CMT4H secondary to *FGD4* mutations. The patients had very slowly progressive demyelinating neuropathy.(Houlden et al. 2009a) Recently, CMT4J secondary to *FIG4* mutations were described in patients with rapidly progressive asymmetrical demyelinating neuropathy, resembling an acquired inflammatory neuropathy.(Cottenie et al. 2013) Autosomal recessive CMT2 (ARCMT2) is a very rare condition. It can be associated with *LMNA* mutations (ARCMT2A) and patients usually presents with a severe neuropathy involving proximal muscles. *LMNA* mutations are also associated with Emery-Dreifuss muscular dystrophy and Dunnigan-type familial partial lipodystrophy.(Agarwal et al. 2003; De Sandre-Giovannoli et al. 2002) ARCMT2B is a milder subtype caused by *MED25* mutations.(Leal et al. 2009) Very rarely, recessive mutations in *GDAP1*, *NEFL* and *HSPB*1 have been also reported.(Houlden et al. 2008; Reilly et al. 2011; Yum et al. 2009)

CMTX1 caused by *GJB1* mutations is the commonest form of X-linked CMT and also the second most frequent subtype of CMT. CMTX1 is an X-linked dominant disorder in which males are usually more severely affected than females. NCVs are usually slow in the demyelinating range in males while in females are usually in the axonal range, but for both it is common to have NCVs in the intermediate range as mentioned above. Patchy or asymmetric distribution is frequently observed.(Reilly et al. 2011) *GJB1* mutations (52.8%) are responsible for the majority of intermediate CMT (MNCV ranging between 35 and 45 m/s).(Miller et al. 2011; Nicholson et al. 1993). Therefore patients with intermediate conduction velocities, a classical phenotype in the absence of male-to-male transmission, should be first tested for *GJB1* mutations (CMT1X). If this testing is negative, testing should proceed to *MPZ* mutations (CMT-DID/CMT1B). Alternatively, if there is male-to-male transmission, testing for *MPZ* mutations should occur first.(Miller et al. 2011; Nicholson et al. 2006)

The group with intermediate MNCV but negative for *GJB1* mutations is then subdivided into

dominant intermediate (DI-CMT) and recessive intermediate CMT (RI-CMT).(Kim et al. 2013; Nicholson et al. 2006) Some rare genes causing DI-CMT include *DNM2* (CMT-DIB) and *YARS* (CMT-DIC) mutations. Recently, a few new genes have been identified for DI-CMT, like *INF2* (CMT-DIE) and *GNB4* (CMT-DIF).(Soong et al. 2013; Toyota et al. 2013) RI-CMT is very rare and the responsible genes may cause other atypical manifestations, for example, vestibular Schwannoma and developmental delay caused by *KARS* (CMT-RIA) and elevated serum creatine kinase levels with *PLEKHG5* (CMT-RIC) mutations.(Kim et al. 2013; McLaughlin et al. 2010)

1.1.2 Hereditary sensory neuropathies (HSN)

Hereditary sensory neuropathies (HSN) are a group of diseases caused by degeneration of peripheral sensory neurons. The hallmark feature is prominent distal sensory loss with insensitivity to pain in some patients. The sensory loss frequently leads to chronic ulcerations and osteomyelitis resulting in amputations of toes and fingers. HSN was also termed hereditary sensory and autonomic neuropathies (HSAN) due to the autonomic involvement occurring in these neuropathies.(Dyck et al. 1993) Autonomic dysfunction observed in some patients includes anhidrosis, fever, blood pressure fluctuations and gastro-intestinal disturbances. Neurophysiology usually shows changes consistent with a sensory axonal neuropathy.(Auer-Grumbach et al. 2003; Dyck et al. 1993; Rotthier et al. 2009; Rotthier et al. 2012) At least 14 genes have been identified as causative genes of HSN (table 1-2, p26). Nevertheless, a genetic diagnosis can currently be reached in approximately 19% of patients, suggesting that further genes associated with HSN are waiting to be identified.(Davidson et al. 2012) In a study which included 140 HSN British patients, mutations in six genes were identified*: SPTLC1, RAB7, WNK1/HSN2, FAM134B, NTRK1* and *NGFB*. The *SPTLC1* Cys133Trp (C133W) mutation was the most frequently identified mutation.(Davidson et al. 2012)

The current classification of HSN includes at least eight clinical subtypes and can be divided in two groups by the inheritance pattern. Patients with AD-HSN typically show a juvenile or adult onset sensory neuropathy with minimal autonomic disturbances and frequent motor involvement, whereas typical manifestations of AR-HSN are congenital or early onset, pronounced autonomic symptoms and minimal motor involvement.

Five genes have been identified as the causative genes for AD-HSN: *SPTLC1*, *SPTLC2*, *ATL1*, *DNMT1* and *PRNP*. Patients with mutations in *SPTLC1* or *SPTLC2* are almost phenotypically indistinguishable. They sometimes have significant motor involvement and hence the clinical overlap with CMT2.(Auer-Grumbach 2008; Rotthier et al. 2010) *ATL1* is originally known as the causative gene for SPG3A, a dominant form of HSP, but its mutation have been identified in

Table 1-2. Classification of hereditary sensory neuropathies (HSN)

Subtype	Inheritance	Gene	Phenotype
HSN-IA	AD	*SPTLC1*	pan-sensory loss/lancinating pain /variable distal motor involvement/amputations/adolescence onset
HSN-IC	AD	*SPTLC2*	pan-sensory loss/lancinating pain /variable distal motor involvement/amputations/adolescence or adulthood onset
CMT2B	AD	*RAB7*	predominant sensory involvement and sensory complications
HSN-ID	AD	*ATL1*	severe distal sensory loss and amyotrophy in lower limbs/ skin and nail changes/acromutilation/adult onset
HSN-IE	AD	*DNMT1*	pan-sensory loss /sensorineuronal hearing loss/dementia/early adult onset
HSN with chronic diarrhea	AD	*PRNP*	Dementia/ autonomic dysfunction/ sensory loss/diarrhoea
HSN-IIA	AR	*HSN2 (WNK1)*	severe mutilations in hands and feet/acropathy/congenital or early childhood onset
HSN-IIB	AR	*FAM134B*	impaired nociception /childhood onset
HSN-IIC	AR	*KIF1A*	impaired propioception and vibration sense/minor distal weakness/ childhood to adolescence onset/SPG30
HSN-III	AR	*IKBKAP*	Riley-Day syndrome/prominent autonomic involvement with vasomotor instability and hyperhidrosis/absence of lingual fungiform papillae/congenital
HSN-IV	AR	*NTRK1*	Congenital insensitivity to pain with anhydrosis (CIPA) / episodic fever/ mental retardation/unmyelinated fibers mainly affected
HSN-V	AR	*NGFB*	Congenital insensitivity to pain/severe loss of deep pain perception/ minimal autonomic/no mental retardation unmyelinated fibers affected
HSN with spastic paraplegia	AR	*CCT5*	loss of all sensory modalities/acromutilation/spastic paraplegia
Channelopathy associated insensitive to pain	AR	*SCN9A*	Congenital insensitivity to pain/Erythromelagia

patients with AD-HSN.(Guelly et al. 2011) *DNMT1* mutations cause hereditary sensory neuropathy with dementia and hearing loss (HSN/HSAN-IE), a neurodegenerative disorder characterised by dementia, sensorineural hearing loss and sensory neuropathy. Affected patients usually present with sensory impairment and hearing loss at the age of 20-35 and subsequently develop dementia in the third or fourth decade.(Klein 2012; Klein et al. 2011)

Several causative genes have been identified in AR-HSN. Mutations in *WNK1*/*HSN2, FAM134B* and *KIF1A* (HSN II) are typically associated with early-onset sensory neuropathy. HSN-III caused by *IKBKAP* mutations, also called familial dysautonomia or Riley–Day syndrome, manifests at birth with prominent and progressive autonomic disturbances and small-fiber sensory dysfunction which reduce life expectancy in affected patients. The disease occurs

almost solely in the eastern European Jewish population.(Slaugenhaupt et al. 2001) HSN-IV caused by *NTRK1* mutation*s*, also known as congenital insensitivity to pain with anhidrosis (CIPA), typically presents with a combination of absence of normal responses to painful stimuli, markedly decreased or absent sweating associated with recurrent episodes of fever and variable mental retardation with self-mutilating behaviour.(Langer et al. 1981; Nolano et al. 2000) HSN-V is caused by mutations in *NGFB.* Patients with HSN-V show hypohidrosis rather than anhidrosis and do not have mental retardation.(Dyck et al. 1983) However, the distinction between HSN-IV and HSN-V is not always clear, as one patient with *NGFB* mutation presenting with a HSN-IV phenotype (Carvalho et al. 2011) and another patient with HSN-V was identified with a homozygous *NTRK1* mutation.(Houlden et al. 2001)

1.1.3 Distal hereditary motor neuropathies (dHMN)

Distal hereditary motor neuropathy (dHMN), also known as distal spinal muscular atrophy (SMA) or the spinal form of CMT, it is a clinically and genetically heterogeneous condition characterised by the selective involvement of motor neurons.(Dierick et al. 2008) The cardinal feature is an almost exclusive motor involvement with distal wasting and weakness of upper and lower limbs though minor sensory abnormalities may be observed. dHMNs are quite often associated with additional features, including vocal cord paralysis and pyramidal signs.(Irobi et al. 2006) To date, at least 17 causative genes have been identified for the dHMNs. However, in only 20% of patients can a definite genetic diagnosis can be achieved.(Dierick et al. 2008; Irobi et al. 2006; Rossor et al. 2012) The classification of dHMN is based on the system proposed by Harding (Harding 1993b) but has been expanded to include the currently known genes (table 1-3, p28).

Patients with dHMN can be divided into two main groups according to the inheritance pattern. Among AD-dHMN, affected patients typically present with length-dependent neuropathy with weakness starting in the lower limbs.(Houlden et al. 2008) They can be caused by mutations in several genes, however, *HSPB1* and *HSPB8* are the two genes in which most of the mutations have been identified so far.(Irobi et al. 2006) Interestingly, a recessive *HSPB1* mutation has been identified in a family with neuropathy.(Houlden et al. 2008) There is often an overlap between AD-dHMN with mild sensory abnormalities and CMT2 with predominant motor involvement. At least five genes have been identified causing both CMT2 and dHMNs: *TRPV4, GARS, HSPB1, HSPB8* and *DYNC1H1*.(Dubourg et al. 2006b; Reilly et al. 2011; Rossor et al. 2012; Sivakumar et al. 2005) Both phenotypes have been observed within a family with the same *HSBP1* mutation.(Solla et al. 2010)

AD-HMNs caused by mutations in other genes are rare.(Rossor et al. 2012) Patients presenting with predominant hand involvement usually carry mutations in *BSCL2* or *GARS* genes.(Reilly et

al. 2011) Patients with *BSCL2* mutations have a variable phenotype ranging from typical dHMN to spastic paraplegia with hand amyotrophy (Silver Syndrome). Recently mutations in two genes related to dynein, *DYNC1H1* and *BICD2*, were documented to be the cause of spinal muscular atrophy with lower limb predominance (SMA-LED), a form of AD-SMA overlapping with dHMN. SMA-LED is clinically characterised by early onset, predominant lower limb involvement and very slow disease progression.(Harms et al. 2012; Peeters et al. 2013; Tsurusaki et al. 2012; Weedon et al. 2011) The identification of these two new genes highlights the importance of dynein-mediated motility in motor neuron function in humans.

Table 1-3. Classification of distal hereditary motor neuropathies (dHMN)

Subtype	Inheritance	Gene	Phenotype
dHMN2A	AD	*HSPB8*	Adult onset typical dHMN/CMT2L
dHMN2B	AD	*HSPB1*	Adult onset typical dHMN/CMT2F
dHMN2C	AD	*HSPB3*	Adult onset typical dHMN
dHMN5A	AD	*GARS*	Upper limb onset/CMT2D
		BSCL2	Upper limb onset, frequent spasticity in lower limbs/ Silver syndrome (SPG17)
dHMN5B	AD	*REEP1*	Predominant hand wasting /SPG31
dHMN6	AR	*IGHMBP2*	SMARD1/infantile onset, respiratory distress
dSMA5	AR	*DNAJB2*	early adult onset, predominantly in lower limbs
SPSMA	AD	*TRPV4*	Adult onset/vocal cord paralysis
dHMN7A	AD	*SLC5A7*	Vocal cord palsy
dHMN7B	AD	*DCTN1*	Adult onset/vocal cord paralysis/facial weakness
dHMN and pyramidal features	AD	*SETX*	HMN/ALS4/early onset/pyramidal signs
dHMN/SMA	AD	*TRPV4*	vocal cord paralysis, distal weakness, congenital SMA/CMT2/arthrogryposis
SMAX3	X-linked	*ATP7A*	distal-onset wasting and weakness
dHMN	AD	*AARS*	Typical HMN
SMA-LED	AD	*BICD2*	Congenital, contractures, lower-limb predominant, pyramidal signs
		DYNC1H1	Congenital, contractures, lower-limb predominant, pyramidal signs, learning difficulties
PNMHH	AD	*MYH14*	distal myopathy, hoarseness, hearing loss

ALS: amyotrophic lateral sclerosis, **PNMHH**: peripheral neuropathy, myopathy, hoarseness, and hearing loss, **SMARD1**: spinal muscle atrophy with respiratory distress type 1.

AR-dHMN is very rare. dHMN-6 caused by mutations in *IGHMBP2*, also termed spinal muscular atrophy with respiratory distress type 1 (SMARD1), is characterised by severe distal weakness and diaphragmatic palsy occurring in early infancy . This is one of the most severe forms of dHMN and it is associated with poor prognosis. Patients usually die from respiratory complications before the age of 20.(Pitt et al. 2003) Only one X-linked form of dHMN has been so far described. This condition is caused by mutations in the *ATP7A* gene which was firstly described as the gene responsible for Menke's disease, a severe developmental disorder due to abnormal copper metabolism with onset during infancy. The two mutations associated with dHMN have not been reported in Menke's disease and the affected individuals had normal serum copper concentrations.(Kennerson et al. 2010)

1.2 Peripheral neuropathies associated with other related disorders

There is increasing evidence of overlap between inherited neuropathies and other neurological syndromes. In many conditions, inherited neuropathy is part of a multisystem disorder affecting also the CNS or other non-neurological systems. Cerebellar ataxias and spasticity are two additional features frequently observed in patients with inherited neuropathies. Conversely, peripheral neuropathy can be part of the clinical picture of hereditary cerebellar ataxias or hereditary spastic paraplegia (HSP).

1.2.1 Peripheral neuropathies and hereditary spastic paraplegia

HSP is a group of clinically and genetically heterogeneous disorders characterised by spasticity in the limbs, gait abnormalities, urinary disturbances with over 60 loci or genes recognised.(Behan et al. 1974; Bruyn 1992; Schule et al. 2012) HSPs are classified into pure HSPs (pHSP) which have isolated pyramidal system involvement and complex HSPs (cHSP) in which the pyramidal signs are associated with variable combinations of additional neurological or extra-neurological involvement.(Harding 1983) Clinically, peripheral neuropathy has been recognised as the most frequent associated feature in cHSP, including mutations in one of the commonest genes: *ATL1*(SPG3A) and *SPAST* (SPG4*)*.(Al-Maawali et al. 2011; Kumar et al. 2012) Nerve conduction studies (NCS) are now routinely included in the evaluation of patients with spastic paraplegia. SPG6 was previously considered a form of pHSP until the identification of a heterozygous missense *NIPA1* mutation in a family with peripheral neuropathy and spastic paraplegia.(Du et al. 2011) *REEP1*(SPG31) mutations can be associated with amyotrophy, peripheral nerve involvement and bulbar palsy.(Hewamadduma et al. 2009) Up to two thirds of SPG10 patients with *KIF5A* mutations have peripheral neuropathy.(Crimella et al. 2012; Goizet et al. 2009) As mentioned earlier, mutations in genes for HSP can occasionally cause isolated neuropathy, such as *ATL1*(SPG3A) in AD-HSN and *BSCL2* (SPG17) in dHMN.(Guelly et al. 2011; Windpassinger et al. 2004)

Conversely, mutations in genes causing primarily inherited neuropathies have been identified in patients with HSP. For example, mutations of *KIF1A*, the gene for HSN-IIC, have been found in patients with SPG30.(Erlich et al. 2011; Klebe et al. 2012) Another example is *CCT5* in which the mutations result in autosomal recessive mutilating sensory neuropathy with spastic paraplegia.(Bouhouche et al. 2006) CNS involvement is well recognized in CMT2A patients due to *MFN2* mutations.(Chung et al. 2006). *SOX10* mutations cause a rare form of demyelinating CMT associated with spastic quadriplegia and sensorineural deafness.(Inoue et al. 1999) The group of inherited neuropathies with significant upper motor neuron (UMN) component is continuously expanding. The coexistence of peripheral neuropathies and

pyramidal signs highlights common pathophysiological pathways in these disorders.

1.2.2 Peripheral neuropathies and hereditary cerebellar ataxia

Hereditary cerebellar ataxias are a clinically and genetically heterogeneous group of disorders characterised by slowly progressive cerebellar ataxia associated with dysarthria and abnormal eye movements.(Anheim 2011; Harding 1993a) The clinical phenotype is often complicated by involvement of other neurological or non-neurological systems. Peripheral neuropathy is frequently present. Therefore neurophysiological assessment is often included in the evaluation of patients with hereditary cerebellar ataxia.(Anheim et al. 2011)

In autosomal dominant cerebellar ataxias (ADCA) / spinocerebellar ataxia (SCA), the commonest type of neuropathy is sensory motor axonal neuropathy (SMAN) which has been frequently observed in patients of SCA1, 2, 3, 4, 6, 8, 12, 18, 22, 25, 27 and DRPLA (Dentatorubro-pallidoluysian atrophy) and is particularly prevalent in patients with SCA2 (up to 68%).(Manto et al.2009; Durr 2010)

SMAN is also associated with many forms of autosomal recessive cerebellar ataxias (ARCA) which include cerebrotendinous xanthomatosis, ataxia telangiectasia (AT) and AT-like disorder, oculomotor apraxia type 1 (AOA1), oculomotor apraxia type 2 (AOA2) and ataxia with coenzyme Q10 deficiency.(Anheim 2011; Embirucu et al. 2009; Manto et al.2009) Another well-known example is spinocerebellar ataxia with axonal neuropathy (SCAN1) secondary to *TDP1* mutations. Patients are characterised by areflexia, steppage gait and pes cavus.(Takashima et al. 2002).

In addition to SMAN, other types of neuropathies have been described in ARCA. For example patients with autosomal recessive Charlevoix-Saguenay-spastic ataxia (ARSACS) secondary to *SACS* mutations have usually sensory motor demyelinating neuropathy.(Vermeer et al. 2008) *DNMT1* mutations can lead to either HSN-IE or autosomal dominant cerebellar ataxia, deafness and narcolepsy (ADCA-DN).(Winkelmann et al. 2012) In both phenotypes, affected patients may have co-existing sensory axonal neuropathy and cerebellar ataxia. Sensory axonal neuropathy is also a prominent feature in Friedreich ataxia, abetalipoproteinemia, ataxia with vitamin E deficiency, and ataxia with *POLG* mutation. Otherwise, sensory demyelinating neuropathy frequently presents in Refsum disease.(Embirucu et al. 2009; Milone et al. 2008; Van Goethem et al. 2004; Weiss et al. 2010)

Peripheral neuropathy is also observed in X-linked ataxia. Variable degrees of peripheral and autonomic nerve involvement can be found in patients with fragile-X tremor ataxia syndrome

(FXTAS).(Leehey et al. 2012; Verkerk et al. 1991)

Cerebellar ataxia with neuropathy and bilateral vestibular areflexia syndrome (CANVAS) is a distinct syndrome with cerebellar ataxia, non-length-dependent sensory neuropathy and absent visually enhanced vestibulo-ocular reflex. The majority of patients had evidence of cerebellar atrophy involving anterior and dorsal vermis on brain magnetic resonance image (MRI) and absent sensory nerve action potential (SAP). Nevertheless, the disease-causing gene has not been identified yet.(Szmulewicz et al. 2011)

1. 3 Applications of next generation sequencing in genetic diagnosis

An accurate diagnosis of inherited neuropathy requires detailed information of the phenotype (type of neuropathy, mode of inheritance, associated clinical features) and the updated knowledge of genetic subtypes including their frequencies in different populations. Current diagnostic strategy is based on a sequential genetic screening strategy guided by the phenotype.(Murphy et al. 2012a; Saporta et al. 2011) as illustrated in figure 1-1.

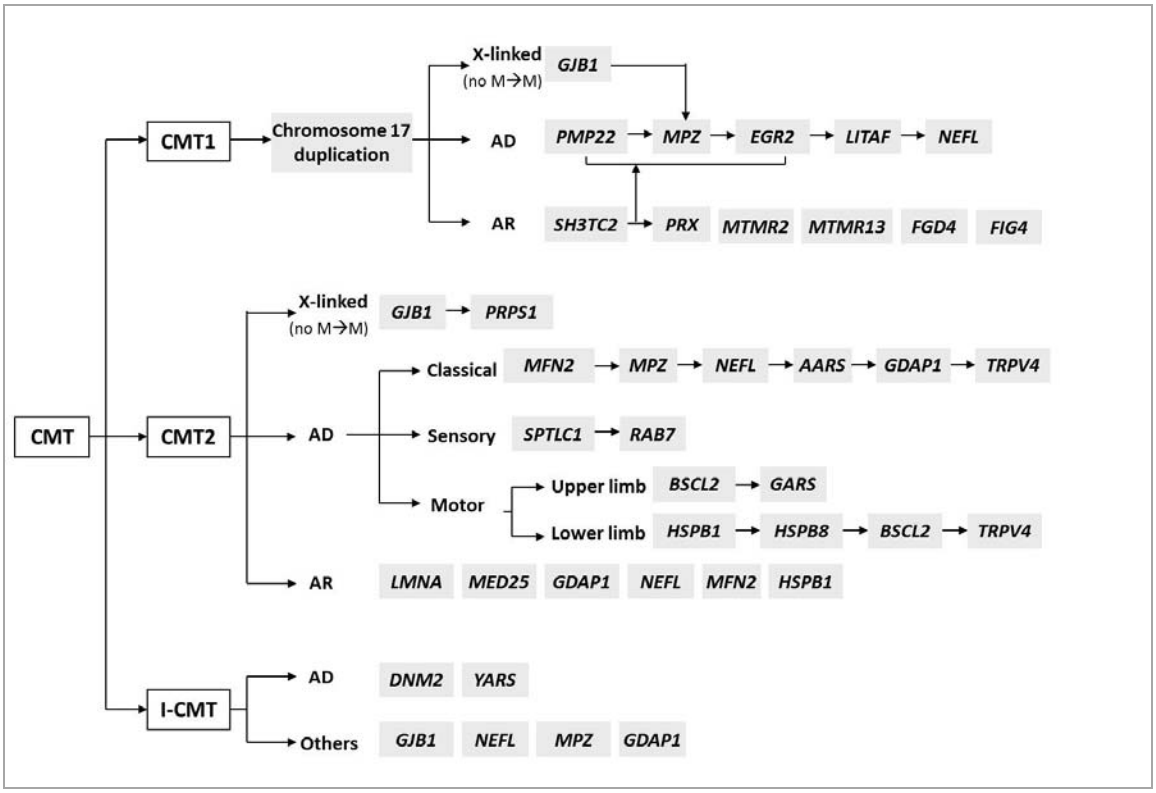

Figure 1-1. Current diagnostic strategy for CMT

Molecular diagnosis of CMT starts with classification of the phenotypes according to the patient's neurophysiological features: CMT1, CMT2 or I-CMT. For CMT1 and CMT2, the arrows indicate a sequential genetic screening strategy. M→M: male to male inheritance

Although a genetic diagnosis is currently achieved in approximately 60~70% of CMT patients via conventional approach, pursuing a definite diagnosis in the rest patients remains a great challenge.(Braathen et al. 2011; Miller et al. 2011; Reilly et al. 2011) The major reason is the constantly growing number of genes that have to be screened due to increasing overlap in phenotypes and genotypes. Sanger sequencing, the current main method of genetic diagnosis, can only get the maximal read length at around 800 bps and screens usually one exon in a single round. Thus the identification of the disease-causing mutations is often a time-consuming and expensive process.

For patients in which a genetic diagnosis has not been achieved the traditional approach employs linkage analysis as the core method to define the candidate region, followed by positional cloning to narrow the candidate region until the gene and its mutations are found. Nevertheless, there are several factors which may prevent a successful outcome: small families with a limited number of affected individuals, sporadic cases, reduced penetrance, locus heterogeneity, and alleles that impair reproductive fitness.

Since the commercial launch of the first platform in 2005, next-generation sequencing (NGS) has revolutionised the process of identifying novel genes and markedly accelerated multiple areas of genomics research. NGS, also known as high-throughput sequencing, allows massively parallel sequencing of deoxyribonucleic acid (DNA) molecules so that hundreds of megabases to gigabases of nucleotide-sequence can be generated in a single instrument run.(Hirschhorn 2009) The most widely used NGS technologies for genetic diagnosis is exome sequencing (exome capture) with the concept of using a complex pool of biotinylated RNA probes to hybridize and then to capture the exons for sequencing (figure 1-2).(Choi et al. 2009; Gnirke et al. 2009) Exome sequencing can be applied in two ways: (1) whole exome sequencing (WES) to capture all the known coding exons and exon/intron boundaries of the genome (2) targeted resequencing capture only genomic specific regions of interest instead of whole exome, for example, exons of specific genes.(Voelkerding et al. 2009)

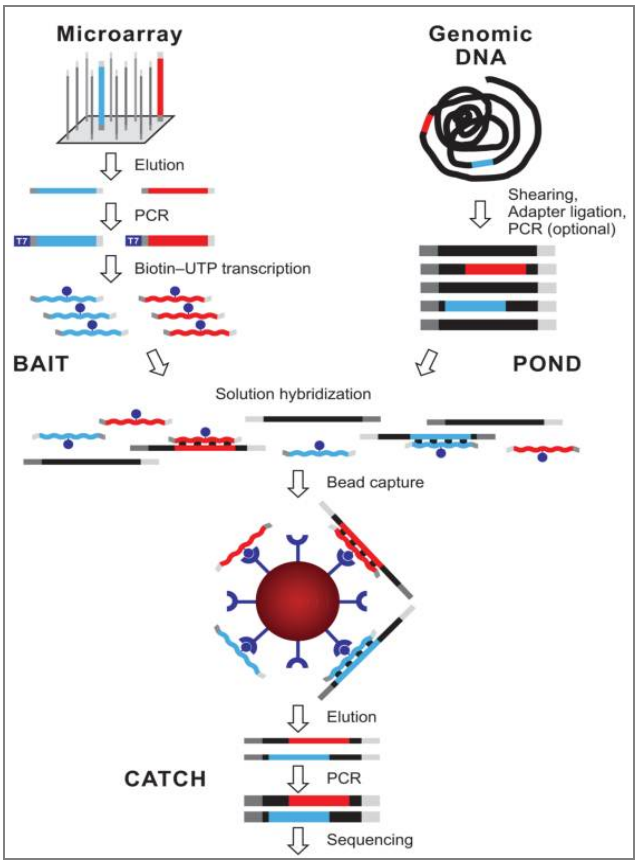

Figure 1-2. Overview of exome sequencing using the hybrid selection method.

The steps involved in the preparation of a complex pool of capture probes ("bait"; top left), genome fragment input library ("pond"; top right) and hybrid-selected enriched output library ("catch"; bottom) are illustrated. Two sequencing targets and their respective baits are shown in red and blue. Thin and thick lines represent single and double strands, respectively. Universal adapter sequences are grey. The excess of single-stranded non-self-complementary RNA (wavy lines) drives the hybridization. (modified from Gnirke et al. 2009)

1.3.1 Whole exome sequencing (WES)

The “exome” represents all the exons in the human genome and accounts for about 180,000 exons and for around 1% of the human genome which translates to about 30 Mb in length. It is estimated that about 85% of disease-causing mutations lie within the protein-coding regions of the human genome. Because most mutations causing monogenic disorders are exomic, whole exome sequencing has been introduced as an efficient strategy to identify novel genes associated with rare mendelian disorders.(Choi et al. 2009; Ng et al. 2009; Singleton et al.)

Inherited neuropathy is an attractive model in which WES could be employed as a diagnostic tool because of the genetically heterogeneity of the disease. WES was first successfully used in the identification of a novel *GJB1* mutation in a CMT family.(Montenegro et al. 2011) Several studies subsequently documented WES as a powerful tool in the identification of novel CMT genes (figure 1-3).(Pandra et al. 2012; Rossor et al. 2013)

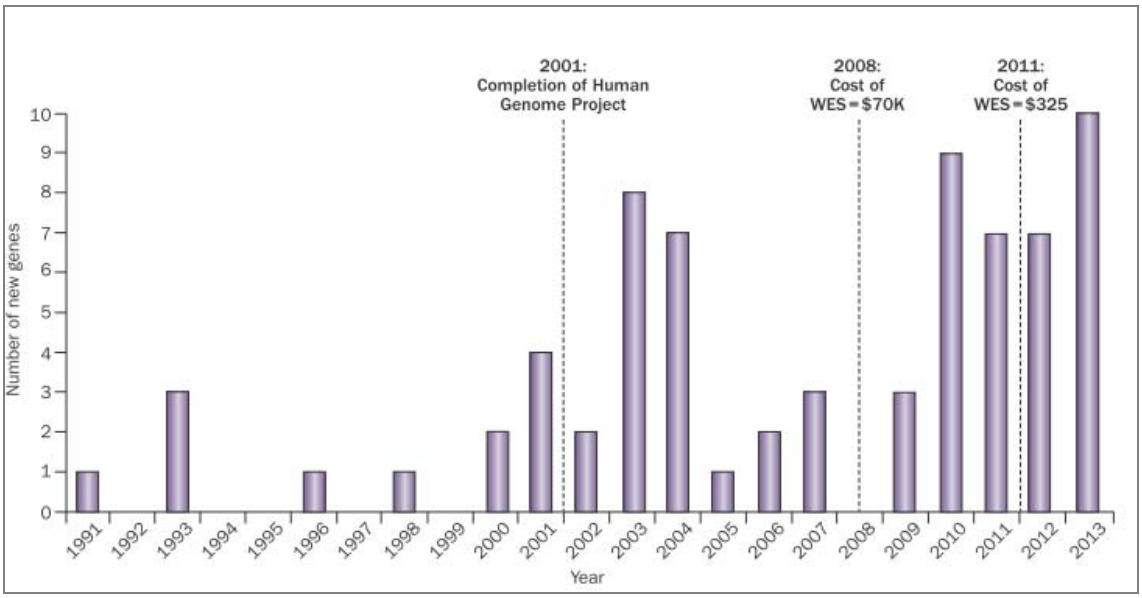

Figure 1-3. A timeline of discovery of genes involved in Charcot–Marie–Tooth disease and related disorders.

WES: whole-exome sequencing. (cited from Rossor et al. 2013)

WES is also helpful in unraveling new pathogenic variants and genotype-phenotype associations. Genes can be found to cause a phenotype which was previously unexpected. For example, *ATL1* was known to cause SPG3A but it was subsequently detected by WES causing HSN.(Guelly et al. 2011) WES has also identified new types of mutations in many known genes thus broadening the phenotypic spectrum of the diseases due to these genes. Heterozygous mutations in the ATPase family gene 3-like 2 gene (*AFG3L2)* can cause SCA28, a type of ADCA frequently associated with pyramidal signs and ophthalmoplegia.(Koppen et al. 2007) By WES, a homozygous *AFG3L2* mutation was identified in a recessive family with a spastic-ataxia-neuropathy syndrome, a phenotype very close to recessive SPG7 caused by *SPG7*

mutations (figure1-4).(Pierson et al. 2011). Interestingly, *AFG3L2* and *SPG7* are paralogous genes and both of them carry the AAA (ATPases associated with various cellular activities) metalloprotease domain and proteolytic domain in their coding proteins. The genetic finding suggests that a common pathway is involved in the pathogenesis of peripheral neuropathy, spasticity and cerebellar ataxia.

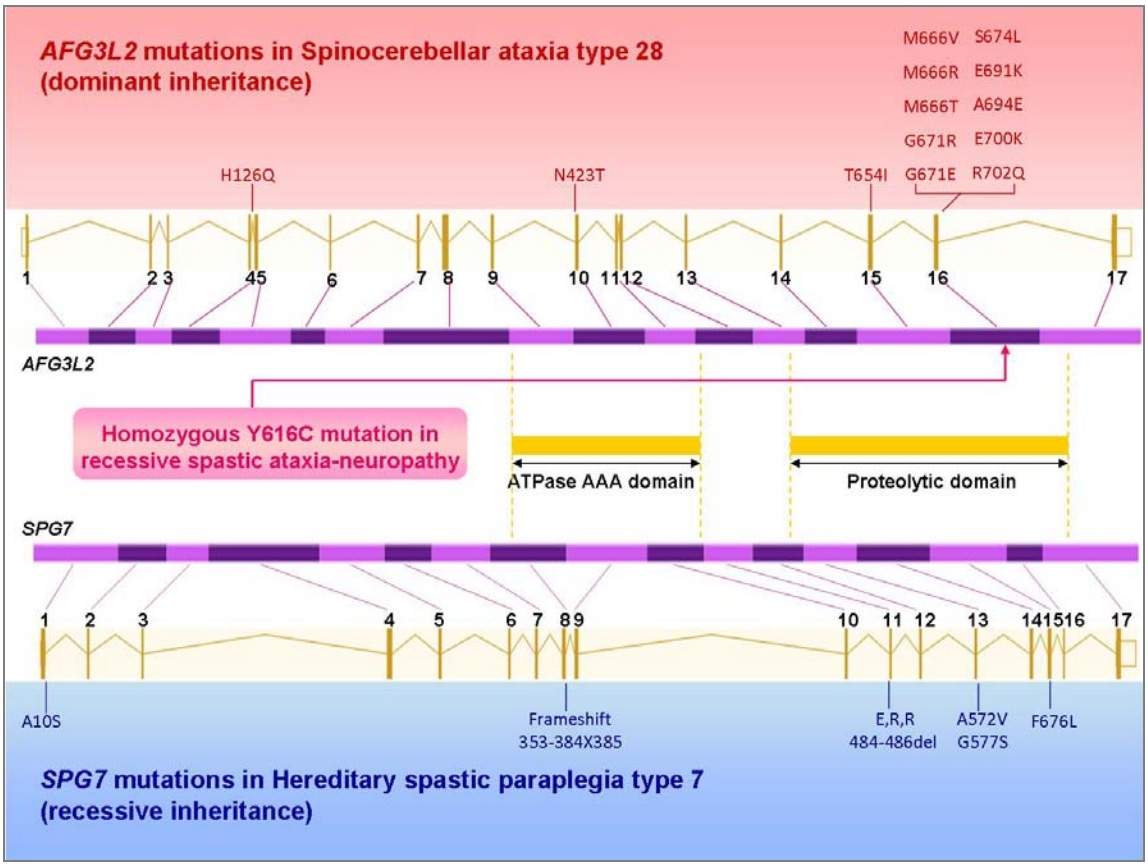

Figure 1-4. A homozygous *AFG3L2* mutation causes recessive spastic ataxia-neuropathy, a phenotype overlapping between SCA28 and SPG7.

Top. The genomic organization of *AFG3L2* and the domain structure of the coding protein. All published mutations are marked in red. **Bottom.** The genomic organization of *SPG7* and the domain structure of the coding protein. Other published mutations are marked in blue. Homozygous Y616C mutation in the proteolytic domain was identified in a recessive family with spastic paraplegia, peripheral neuropathy, and cerebellar ataxia.(the picture has been published in Pandraud et al. 2012)

1.3.2 Targeted resequencing

Targeted resequencing is a NGS technique which is able to sequence only those exons of the human genome of interest for a particular disease. The aim is therefore to reduce the amount of false positive signals and to enhance the efficiency of the analysis as compared to WES. Furthermore, the overall time and cost of a sequencing experiment can be reduced. Targeted resequencing allows high throughput and massive parallel sequencing of multiple genes with

various NGS sequencing platforms and different target enrichment strategies, including microarray-based capture, in-solution capture and PCR-based amplification.(Albert et al. 2007; Gnirke et al. 2009; Hodges et al. 2009; Hodges et al. 2007; Okou et al. 2007) By customization of the targeted coordinates, targeted resequencing is more flexible to fit for the specific aim and sample size of the research project and capable of supporting a wider range of genomic applications more quickly and efficiently than WES. Resequencing panels have been applied in different research projects, such as sequencing of a single gene with numerous exons for multiple samples, to establish molecular diagnosis of particular disorders, or to screen multiple genes which are known to cause overlapping phenotypes.(Denning et al. 2007; Dufke et al. 2012; Kothiyal et al. 2010; Nemeth et al. 2013; Schlipf et al. 2011; Waldmuller et al. 2008)

1.4. Objectives

1.4.1 Investigating genetic aetiologies in patients with inherited neuropathies and associated disorders

The aim of my research was to establish the genetic diagnosis in several cohorts of patients affected by CMT, HSN, or peripheral neuropathy in complex syndromes. The phenotypic-genotypic correlations of identified mutated genes were investigated. To achieve the above objectives, an integrated approach combining conventional Sanger sequencing and NGS technology was taken. My research projects were divided into the following parts:

(1) Screening of disease-causing mutations in newly-identified genes or rare genes for inherited neuropathies in large cohorts of patients. The investigated genes included:
   (a) *NEFL* gene and the five prime untranslated region (5'UTR) of *PMP22* in CMT patients
   (b) Two novel genes, *MARS* and *C12orf65,* in CMT patients
   (c) *SPTLC*2 gene in HSN patients

(2) Screening of disease-causing mutations in genes responsible for other disorders which may be also associated with peripheral neuropathies in cohorts of patients. The studied genes included:
   (a) *KIF5A* (SPG10) in patients with cHSP with axonal neuropathy and CMT2 with spasticity
   (b)*PDYN* (SCA23), *AFG3L2* (SCA28) and *KCND3* (SCA19/SCA22) in patients with cerebellar ataxia

(3) WES of selected families or sporadic patients in which a genetic diagnosis has not been reached by conventional methods. The phenotypes of the investigated patients included:
   (a) HSN with cerebellar ataxia.
   (b) X-linked HSN
   (c) ARCMT2
   (d) ARCA or ARCA-plus syndromes

(4) Targeted resequencing in patients with inherited neuropathies and related disorders. The development of an effective screening panel included design of the probe library, recruitment of patients, execution of the library preparation and validation of the panel using positive and negative controls. Two panels using different technology were developed to explore the potentiality for targeted resequencing as a tool in genetic diagnosis,:
   (a) ARCMT1 panel using the Truseq system (Illumina)
   (b) HSP with axonal neuropathy panel using the HaloPlex system (Agilent)

1.4.2 Investigating the pathogenesis of inherited neuropathies and associated disorders

Functional studies were also performed for two identified mutations/variations:

(1) Gene expression and the pathogenic effects of a novel *C12orf65* mutation were studied in lymphoblasts of CMT patients

(2) The pathogenic effect of a novel *ADCK3* mutation was studied in fibroblasts of patients with ARCA.

The scope of this thesis was summarised in figure 1-5.

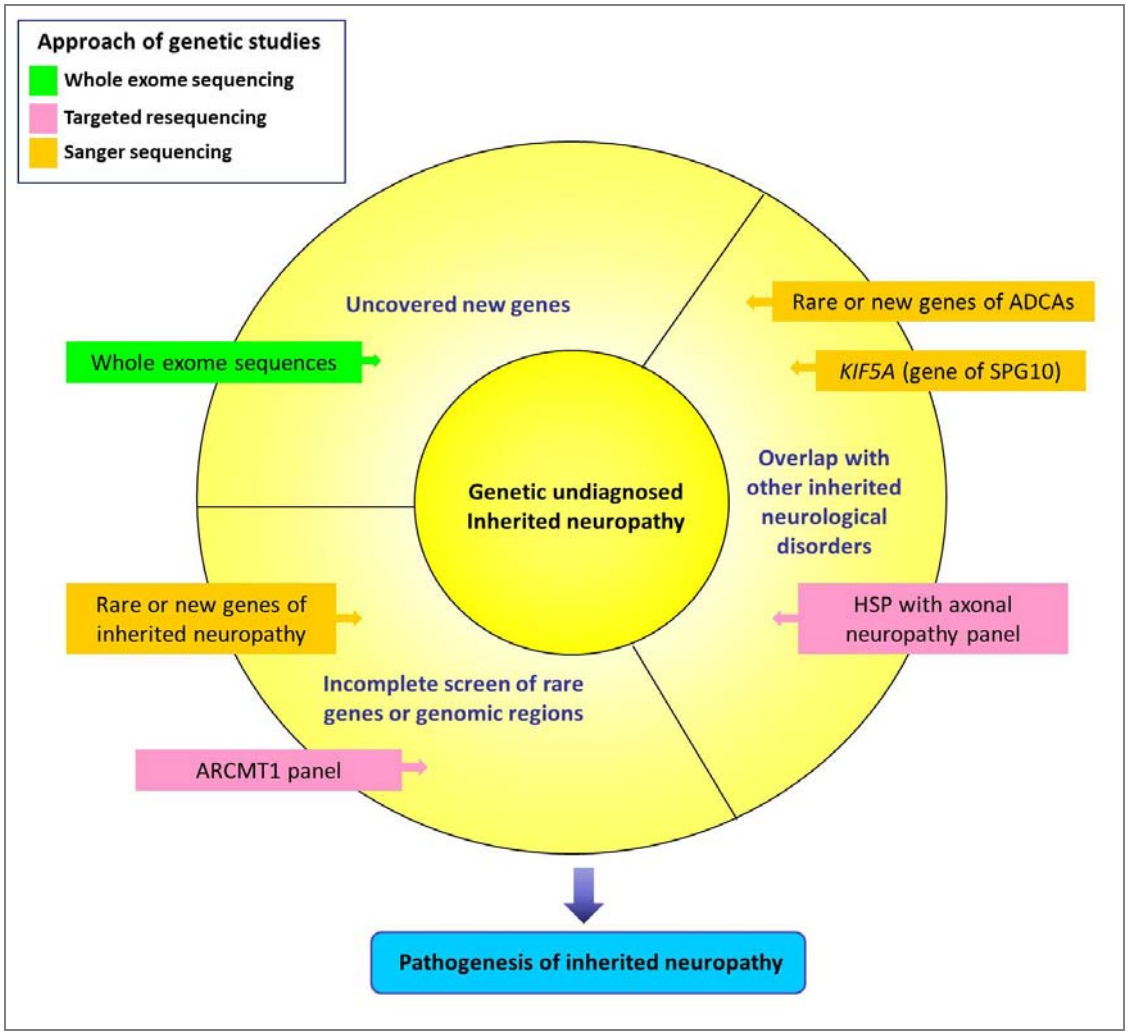

Figure 1-5. Scope of this thesis

Reference

Agarwal AK, Simha V, Oral EA, Moran SA, Gorden P, O'Rahilly S, Zaidi Z, Gurakan F, Arslanian SA, Klar A, Ricker A, White NH, Bindl L, Herbst K, Kennel K, Patel SB, Al-Gazali L, Garg A (2003) Phenotypic and genetic heterogeneity in congenital generalized lipodystrophy. J Clin Endocrinol Metab 88: 4840-7

Al-Maawali A, Rolfs A, Klingenhaeger M, Yoon G (2011) Hereditary spastic paraplegia associated with axonal neuropathy: a novel mutation of SPG3A in a large family. J Clin Neuromuscul Dis 12: 143-6

Albert TJ, Molla MN, Muzny DM, Nazareth L, Wheeler D, Song X, Richmond TA, Middle CM, Rodesch MJ, Packard CJ, Weinstock GM, Gibbs RA (2007) Direct selection of human genomic loci by microarray hybridization. Nat Methods 4: 903-5

Anheim M (2011) Autosomal recessive cerebellar ataxias. Rev Neurol (Paris) 167: 372-84

Anheim M, Tranchant C (2011) [Peripheral neuropathies associated with hereditary cerebellar ataxias]. Rev Neurol (Paris) 167: 72-6

Antonellis A, Ellsworth RE, Sambuughin N, Puls I, Abel A, Lee-Lin SQ, Jordanova A, Kremensky I, Christodoulou K, Middleton LT, Sivakumar K, Ionasescu V, Funalot B, Vance JM, Goldfarb LG, Fischbeck KH, Green ED (2003) Glycyl tRNA synthetase mutations in Charcot-Marie-Tooth disease type 2D and distal spinal muscular atrophy type V. Am J Hum Genet 72: 1293-9

Auer-Grumbach M (2008) Hereditary sensory neuropathy type I. Orphanet J Rare Dis 3: 7

Auer-Grumbach M, De Jonghe P, Verhoeven K, Timmerman V, Wagner K, Hartung HP, Nicholson GA (2003) Autosomal dominant inherited neuropathies with prominent sensory loss and mutilations: a review. Arch Neurol 60: 329-34

Azzedine H, Senderek J, Rivolta C, Chrast R (2012) Molecular genetics of charcot-marie-tooth disease: from genes to genomes. Mol Syndromol 3: 204-14

Behan WM, Maia M (1974) Strumpell's familial spastic paraplegia: genetics and neuropathology. J Neurol Neurosurg Psychiatry 37: 8-20

Bejaoui K, Wu C, Scheffler MD, Haan G, Ashby P, Wu L, de Jong P, Brown RH, Jr. (2001) SPTLC1 is mutated in hereditary sensory neuropathy, type 1. Nat Genet 27: 261-2

Bienfait HM, Baas F, Koelman JH, de Haan RJ, van Engelen BG, Gabreels-Festen AA, Ongerboer de Visser BW, Meggouh F, Weterman MA, De Jonghe P, Timmerman V, de Visser M (2007) Phenotype of Charcot-Marie-Tooth disease Type 2. Neurology 68: 1658-67

Bouhouche A, Benomar A, Bouslam N, Chkili T, Yahyaoui M (2006) Mutation in the epsilon subunit of the cytosolic chaperonin-containing t-complex peptide-1 (Cct5) gene causes autosomal recessive mutilating sensory neuropathy with spastic paraplegia. J Med Genet 43: 441-3

Braathen GJ, Sand JC, Lobato A, Hoyer H, Russell MB (2011) Genetic epidemiology of Charcot-Marie-Tooth in the general population. Eur J Neurol 18: 39-48

Bruyn RP (1992) The neuropathology of hereditary spastic paraparesis. Clin Neurol Neurosurg 94 Suppl: S16-8

Carvalho OP, Thornton GK, Hertecant J, Houlden H, Nicholas AK, Cox JJ, Rielly M, Al-Gazali L, Woods CG (2011) A novel NGF mutation clarifies the molecular mechanism and extends the phenotypic spectrum of the HSAN5 neuropathy. J Med Genet 48: 131-5

Choi M, Scholl UI, Ji W, Liu T, Tikhonova IR, Zumbo P, Nayir A, Bakkaloglu A, Ozen S, Sanjad S,

Nelson-Williams C, Farhi A, Mane S, Lifton RP (2009) Genetic diagnosis by whole exome capture and massively parallel DNA sequencing. Proc Natl Acad Sci U S A 106: 19096-101

Chung KW, Kim SB, Park KD, Choi KG, Lee JH, Eun HW, Suh JS, Hwang JH, Kim WK, Seo BC, Kim SH, Son IH, Kim SM, Sunwoo IN, Choi BO (2006) Early onset severe and late-onset mild Charcot-Marie-Tooth disease with mitofusin 2 (MFN2) mutations. Brain 129: 2103-18

Cottenie E, Menezes MP, Rossor AM, Morrow JM, Yousry TA, Dick DJ, Anderson JR, Jaunmuktane Z, Brandner S, Blake JC, Houlden H, Reilly MM (2013) Rapidly progressive asymmetrical weakness in Charcot-Marie-Tooth disease type 4J resembles chronic inflammatory demyelinating polyneuropathy. Neuromuscul Disord 23: 399-403

Crimella C, Baschirotto C, Arnoldi A, Tonelli A, Tenderini E, Airoldi G, Martinuzzi A, Trabacca A, Losito L, Scarlato M, Benedetti S, Scarpini E, Spinicci G, Bresolin N, Bassi M (2012) Mutations in the motor and stalk domains of KIF5A in spastic paraplegia type 10 and in axonal Charcot-Marie-Tooth type 2. Clin Genet 82(2):157-64

Davidson GL, Murphy SM, Polke JM, Laura M, Salih MA, Muntoni F, Blake J, Brandner S, Davies N, Horvath R, Price S, Donaghy M, Roberts M, Foulds N, Ramdharry G, Soler D, Lunn MP, Manji H, Davis MB, Houlden H, Reilly MM (2012) Frequency of mutations in the genes associated with hereditary sensory and autonomic neuropathy in a UK cohort. J Neurol 259(8):1673-85

De Sandre-Giovannoli A, Chaouch M, Kozlov S, Vallat JM, Tazir M, Kassouri N, Szepetowski P, Hammadouche T, Vandenberghe A, Stewart CL, Grid D, Levy N (2002) Homozygous defects in LMNA, encoding lamin A/C nuclear-envelope proteins, cause autosomal recessive axonal neuropathy in human (Charcot-Marie-Tooth disorder type 2) and mouse. Am J Hum Genet 70: 726-36

Denning L, Anderson JA, Davis R, Gregg JP, Kuzdenyi J, Maselli RA (2007) High throughput genetic analysis of congenital myasthenic syndromes using resequencing microarrays. PLoS One 2: e918

Dierick I, Baets J, Irobi J, Jacobs A, De Vriendt E, Deconinck T, Merlini L, Van den Bergh P, Rasic VM, Robberecht W, Fischer D, Morales RJ, Mitrovic Z, Seeman P, Mazanec R, Kochanski A, Jordanova A, Auer-Grumbach M, Helderman-van den Enden AT, Wokke JH, Nelis E, De Jonghe P, Timmerman V (2008) Relative contribution of mutations in genes for autosomal dominant distal hereditary motor neuropathies: a genotype-phenotype correlation study. Brain 131: 1217-27

Du J, Hu YC, Tang BS, Chen C, Luo YY, Zhan ZX, Zhao GH, Jiang H, Xia K, Shen L (2011) Expansion of the phenotypic spectrum of SPG6 caused by mutation in NIPA1. Clin Neurol Neurosurg 113: 480-2

Dubourg O, Azzedine H, Verny C, Durosier G, Birouk N, Gouider R, Salih M, Bouhouche A, Thiam A, Grid D, Mayer M, Ruberg M, Tazir M, Brice A, LeGuern E (2006a) Autosomal-recessive forms of demyelinating Charcot-Marie-Tooth disease. Neuromolecular Med 8: 75-86

Dubourg O, Azzedine H, Yaou RB, Pouget J, Barois A, Meininger V, Bouteiller D, Ruberg M, Brice A, LeGuern E (2006b) The G526R glycyl-tRNA synthetase gene mutation in distal hereditary motor neuropathy type V. Neurology 66: 1721-6

Dufke C, Schlipf N, Schule R, Bonin M, Auer-Grumbach M, Stevanin G, Depienne C, Kassubek J, Klebe S, Klimpe S, Klopstock T, Otto S, Poths S, Seibel A, Stolze H, Gal A, Schols L, Bauer P (2012) A high-throughput resequencing microarray for autosomal dominant spastic paraplegia genes.

Neurogenetics 13: 215-27

Durr, A. (2010). Autosomal dominant cerebellar ataxias: polyglutamine expansions and beyond. Lancet Neurol 9(9): 885-94

Dyck PJ, Chance, P., Lebo, R. & Carney, J. A. (1993) Hereditary motor and sensory neuropathies. In: Dyck PJ, Thomas, P.K., Griffin, J.W., ALow, P. & Poduslo J.F. (ed) Peripheral Neuropathy W.B. Saunders Company, Philadelphia, pp 1094-1136

Dyck PJ, Mellinger JF, Reagan TJ, Horowitz SJ, McDonald JW, Litchy WJ, Daube JR, Fealey RD, Go VL, Kao PC, Brimijoin WS, Lambert EH (1983) Not 'indifference to pain' but varieties of hereditary sensory and autonomic neuropathy. Brain 106 (Pt 2): 373-90

Embirucu EK, Martyn ML, Schlesinger D, Kok F (2009) Autosomal recessive ataxias: 20 types, and counting. Arq Neuropsiquiatr 67: 1143-56

Erlich Y, Edvardson S, Hodges E, Zenvirt S, Thekkat P, Shaag A, Dor T, Hannon GJ, Elpeleg O (2011) Exome sequencing and disease-network analysis of a single family implicate a mutation in KIF1A in hereditary spastic paraparesis. Genome Res 21: 658-64

Gnirke A, Melnikov A, Maguire J, Rogov P, LeProust EM, Brockman W, Fennell T, Giannoukos G, Fisher S, Russ C, Gabriel S, Jaffe DB, Lander ES, Nusbaum C (2009) Solution hybrid selection with ultra-long oligonucleotides for massively parallel targeted sequencing. Nat Biotechnol 27: 182-9

Goizet C, Boukhris A, Mundwiller E, Tallaksen C, Forlani S, Toutain A, Carriere N, Paquis V, Depienne C, Durr A, Stevanin G, Brice A (2009) Complicated forms of autosomal dominant hereditary spastic paraplegia are frequent in SPG10. Hum Mutat 30: E376-85

Guelly C, Zhu PP, Leonardis L, Papic L, Zidar J, Schabhuttl M, Strohmaier H, Weis J, Strom TM, Baets J, Willems J, De Jonghe P, Reilly MM, Frohlich E, Hatz M, Trajanoski S, Pieber TR, Janecke AR, Blackstone C, Auer-Grumbach M (2011) Targeted high-throughput sequencing identifies mutations in atlastin-1 as a cause of hereditary sensory neuropathy type I. Am J Hum Genet 88: 99-105

Harding AE (1983) Classification of the hereditary ataxias and paraplegias. Lancet 1: 1151-5

Harding AE (1993a) Clinical features and classification of inherited ataxias. Adv Neurol 61: 1-14

Harding AE (1993b) Inherited neuronal atrophy and degeneration predominantly of lower motor neurons. In: Dyck PJ, Thomas, P.K., Griffin, J.W., ALow, P. & Poduslo J.F. (ed) Peripheral Neuropathy W.B. Saunders Company, Philadelphia, pp 1051-1064

Harding AE, Thomas PK (1980) The clinical features of hereditary motor and sensory neuropathy types I and II. Brain 103: 259-80

Harms MB, Ori-McKenney KM, Scoto M, Tuck EP, Bell S, Ma D, Masi S, Allred P, Al-Lozi M, Reilly MM, Miller LJ, Jani-Acsadi A, Pestronk A, Shy ME, Muntoni F, Vallee RB, Baloh RH (2012) Mutations in the tail domain of DYNC1H1 cause dominant spinal muscular atrophy. Neurology 78: 1714-20

Hewamadduma C, McDermott C, Kirby J, Grierson A, Panayi M, Dalton A, Rajabally Y, Shaw P (2009) New pedigrees and novel mutation expand the phenotype of REEP1-associated hereditary spastic paraplegia (HSP). Neurogenetics 10: 105-10

Hirschhorn JN (2009) Genomewide association studies--illuminating biologic pathways. N Engl J Med 360: 1699-701

Hodges E, Rooks M, Xuan Z, Bhattacharjee A, Benjamin Gordon D, Brizuela L, Richard McCombie W,

Hannon GJ (2009) Hybrid selection of discrete genomic intervals on custom-designed microarrays for massively parallel sequencing. Nat Protoc 4: 960-74

Hodges E, Xuan Z, Balija V, Kramer M, Molla MN, Smith SW, Middle CM, Rodesch MJ, Albert TJ, Hannon GJ, McCombie WR (2007) Genome-wide in situ exon capture for selective resequencing. Nat Genet 39: 1522-7

Houlden H, Hammans S, Katifi H, Reilly MM (2009a) A novel Frabin (FGD4) nonsense mutation p.R275X associated with phenotypic variability in CMT4H. Neurology 72: 617-20

Houlden H, King RH, Hashemi-Nejad A, Wood NW, Mathias CJ, Reilly M, Thomas PK (2001) A novel TRK A (NTRK1) mutation associated with hereditary sensory and autonomic neuropathy type V. Ann Neurol 49:521-5

Houlden H, Laura M, Ginsberg L, Jungbluth H, Robb SA, Blake J, Robinson S, King RH, Reilly MM (2009b) The phenotype of Charcot-Marie-Tooth disease type 4C due to SH3TC2 mutations and possible predisposition to an inflammatory neuropathy. Neuromuscul Disord 19: 264-9

Houlden H, Laura M, Wavrant-De Vrieze F, Blake J, Wood N, Reilly MM (2008) Mutations in the HSP27 (HSPB1) gene cause dominant, recessive, and sporadic distal HMN/CMT type 2. Neurology 71: 1660-8

Inoue K, Tanabe Y, Lupski JR (1999) Myelin deficiencies in both the central and the peripheral nervous systems associated with a SOX10 mutation. Ann Neurol 46: 313-8

Irobi J, Dierick I, Jordanova A, Claeys KG, De Jonghe P, Timmerman V (2006) Unraveling the genetics of distal hereditary motor neuronopathies. Neuromolecular Med 8: 131-46

Kennerson ML, Nicholson GA, Kaler SG, Kowalski B, Mercer JF, Tang J, Llanos RM, Chu S, Takata RI, Speck-Martins CE, Baets J, Almeida-Souza L, Fischer D, Timmerman V, Taylor PE, Scherer SS, Ferguson TA, Bird TD, De Jonghe P, Feely SM, Shy ME, Garbern JY (2010) Missense mutations in the copper transporter gene ATP7A cause X-linked distal hereditary motor neuropathy. Am J Hum Genet 86: 343-52

Kim HJ, Hong YB, Park JM, Choi YR, Kim YJ, Yoon BR, Koo H, Yoo JH, Kim SB, Park M, Chung KW, Choi BO (2013) Mutations in the PLEKHG5 gene is relevant with autosomal recessive intermediate Charcot-Marie-Tooth disease. Orphanet J Rare Dis 8: 104

Klebe S, Lossos A, Azzedine H, Mundwiller E, Sheffer R, Gaussen M, Marelli C, Nawara M, Carpentier W, Meyer V, Rastetter A, Martin E, Bouteiller D, Orlando L, Gyapay G, El-Hachimi KH, Zimmerman B, Gamliel M, Misk A, Lerer I, Brice A, Durr A, Stevanin G (2012) KIF1A missense mutations in SPG30, an autosomal recessive spastic paraplegia: distinct phenotypes according to the nature of the mutations. Eur J Hum Genet 20(6):645-9

Klein CJ (2012) DNMT1-Related Dementia, Deafness, and Sensory Neuropathy. In: Pagon RA, Bird TD, Dolan CR, Stephens K, Adam MP, editors. GeneReviews™ [Internet]. Seattle (WA): University of Washington, Seattle; 1993-2012 Feb 16 [updated 2012 May 17].

Klein CJ, Botuyan MV, Wu Y, Ward CJ, Nicholson GA, Hammans S, Hojo K, Yamanishi H, Karpf AR, Wallace DC, Simon M, Lander C, Boardman LA, Cunningham JM, Smith GE, Litchy WJ, Boes B, Atkinson EJ, Middha S, PJ BD, Parisi JE, Mer G, Smith DI, Dyck PJ (2011) Mutations in DNMT1 cause hereditary sensory neuropathy with dementia and hearing loss. Nat Genet 43: 595-600

Koppen M, Metodiev MD, Casari G, Rugarli EI, Langer T (2007) Variable and tissue-specific subunit

composition of mitochondrial m-AAA protease complexes linked to hereditary spastic paraplegia. Mol Cell Biol 27: 758-67

Kothiyal P, Cox S, Ebert J, Husami A, Kenna MA, Greinwald JH, Aronow BJ, Rehm HL (2010) High-throughput detection of mutations responsible for childhood hearing loss using resequencing microarrays. BMC Biotechnol 10: 10

Kumar KR, Sue CM, Burke D, Ng K (2012) Peripheral neuropathy in hereditary spastic paraplegia due to spastin (SPG4) mutation - A neurophysiological study using excitability techniques. Clin Neurophysiol 123(7):1454-9

Langer J, Goebel HH, Veit S (1981) Eccrine sweat glands are not innervated in hereditary sensory neuropathy type IV. An electron-microscopic study. Acta Neuropathol 54: 199-202

Leal A, Huehne K, Bauer F, Sticht H, Berger P, Suter U, Morera B, Del Valle G, Lupski JR, Ekici A, Pasutto F, Endele S, Barrantes R, Berghoff C, Berghoff M, Neundorfer B, Heuss D, Dorn T, Young P, Santolin L, Uhlmann T, Meisterernst M, Sereda MW, Stassart RM, Zu Horste GM, Nave KA, Reis A, Rautenstrauss B (2009) Identification of the variant Ala335Val of MED25 as responsible for CMT2B2: molecular data, functional studies of the SH3 recognition motif and correlation between wild-type MED25 and PMP22 RNA levels in CMT1A animal models. Neurogenetics 10: 275-87

Leehey MA, Hagerman PJ (2012) Fragile X-associated tremor/ataxia syndrome. Handb Clin Neurol 103: 373-86

Lupski JR, de Oca-Luna RM, Slaugenhaupt S, Pentao L, Guzzetta V, Trask BJ, Saucedo-Cardenas O, Barker DF, Killian JM, Garcia CA, Chakravarti A, Patel PI (1991) DNA duplication associated with Charcot-Marie-Tooth disease type 1A. Cell 66: 219-32

Manto M, Marmolino D (2009) Cerebellar ataxias. Curr Opin Neurol 22: 419-29

McLaughlin HM, Sakaguchi R, Liu C, Igarashi T, Pehlivan D, Chu K, Iyer R, Cruz P, Cherukuri PF, Hansen NF, Mullikin JC, Biesecker LG, Wilson TE, Ionasescu V, Nicholson G, Searby C, Talbot K, Vance JM, Zuchner S, Szigeti K, Lupski JR, Hou YM, Green ED, Antonellis A (2010) Compound heterozygosity for loss-of-function lysyl-tRNA synthetase mutations in a patient with peripheral neuropathy. Am J Hum Genet 87: 560-6

Miller LJ, Saporta AS, Sottile SL, Siskind CE, Feely SM, Shy ME (2011) Strategy for genetic testing in Charcot-Marie-disease. Acta Myol 30: 109-16

Milone M, Brunetti-Pierri N, Tang LY, Kumar N, Mezei MM, Josephs K, Powell S, Simpson E, Wong LJ (2008) Sensory ataxic neuropathy with ophthalmoparesis caused by POLG mutations. Neuromuscul Disord 18: 626-32

Montenegro G, Powell E, Huang J, Speziani F, Edwards YJ, Beecham G, Hulme W, Siskind C, Vance J, Shy M, Zuchner S (2011) Exome sequencing allows for rapid gene identification in a Charcot-Marie-Tooth family. Ann Neurol 69(3):464-70

Murphy SM, Laura M, Fawcett K, Pandraud A, Liu YT, Davidson GL, Rossor AM, Polke JM, Castleman V, Manji H, Lunn MP, Bull K, Ramdharry G, Davis M, Blake JC, Houlden H, Reilly MM (2012) Charcot-Marie-Tooth disease: frequency of genetic subtypes and guidelines for genetic testing. J Neurol Neurosurg Psychiatry 83: 706-10

Nemeth AH, Kwasniewska AC, Lise S, Parolin Schnekenberg R, Becker EB, Bera KD, Shanks ME, Gregory L, Buck D, Zameel Cader M, Talbot K, de Silva R, Fletcher N, Hastings R, Jayawant S,

Morrison PJ, Worth P, Taylor M, Tolmie J, O'Regan M, Valentine R, Packham E, Evans J, Seller A, Ragoussis J (2013) Next generation sequencing for molecular diagnosis of neurological disorders using ataxias as a model. Brain 136: 3106-18

Ng SB, Turner EH, Robertson PD, Flygare SD, Bigham AW, Lee C, Shaffer T, Wong M, Bhattacharjee A, Eichler EE, Bamshad M, Nickerson DA, Shendure J (2009) Targeted capture and massively parallel sequencing of 12 human exomes. Nature 461: 272-6

Nicholson G, Myers S (2006) Intermediate forms of Charcot-Marie-Tooth neuropathy: a review. Neuromolecular Med 8: 123-30

Nicholson G, Nash J (1993) Intermediate nerve conduction velocities define X-linked Charcot-Marie-Tooth neuropathy families. Neurology 43: 2558-64

Nicolaou P, Zamba-Papanicolaou E, Koutsou P, Kleopa KA, Georghiou A, Hadjigeorgiou G, Papadimitriou A, Kyriakides T, Christodoulou K (2010) Charcot-Marie-Tooth disease in Cyprus: epidemiological, clinical and genetic characteristics. Neuroepidemiology 35: 171-7

Nolano M, Crisci C, Santoro L, Barbieri F, Casale R, Kennedy WR, Wendelschafer-Crabb G, Provitera V, Di Lorenzo N, Caruso G (2000) Absent innervation of skin and sweat glands in congenital insensitivity to pain with anhidrosis. Clin Neurophysiol 111: 1596-601

Okou DT, Steinberg KM, Middle C, Cutler DJ, Albert TJ, Zwick ME (2007) Microarray-based genomic selection for high-throughput resequencing. Nat Methods 4: 907-9

Pandraud A, Liu Y-T, Houlden H (2012) Advances in the genetics of peripheral nerve disorders. Advances in clinical neuroscience and rehabilitation 12: 8-13

Peeters K, Litvinenko I, Asselbergh B, Almeida-Souza L, Chamova T, Geuens T, Ydens E, Zimon M, Irobi J, De Vriendt E, De Winter V, Ooms T, Timmerman V, Tournev I, Jordanova A (2013) Molecular Defects in the Motor Adaptor BICD2 Cause Proximal Spinal Muscular Atrophy with Autosomal-Dominant Inheritance. Am J Hum Genet 92(6):955-64

Pierson TM, Adams D, Bonn F, Martinelli P, Cherukuri PF, Teer JK, Hansen NF, Cruz P, Mullikin For The Nisc Comparative Sequencing Program JC, Blakesley RW, Golas G, Kwan J, Sandler A, Fuentes Fajardo K, Markello T, Tifft C, Blackstone C, Rugarli EI, Langer T, Gahl WA, Toro C (2011) Whole-exome sequencing identifies homozygous AFG3L2 mutations in a spastic ataxia-neuropathy syndrome linked to mitochondrial m-AAA proteases. PLoS Genet 7: e1002325

Pitt M, Houlden H, Jacobs J, Mok Q, Harding B, Reilly M, Surtees R (2003) Severe infantile neuropathy with diaphragmatic weakness and its relationship to SMARD1. Brain 126: 2682-92

Reilly MM, Murphy SM, Laura M (2011) Charcot-Marie-Tooth disease. J Peripher Nerv Syst 16: 1-14

Reilly MM, Shy ME (2009) Diagnosis and new treatments in genetic neuropathies. J Neurol Neurosurg Psychiatry 80: 1304-14

Rossor AM, Kalmar B, Greensmith L, Reilly MM (2012) The distal hereditary motor neuropathies. J Neurol Neurosurg Psychiatry 83: 6-14

Rossor AM, Polke JM, Houlden H, Reilly MM (2013) Clinical implications of genetic advances in Charcot-Marie-Tooth disease. Nat Rev Neurol 9(10):562-71

Rotthier A, Auer-Grumbach M, Janssens K, Baets J, Penno A, Almeida-Souza L, Van Hoof K, Jacobs A, De Vriendt E, Schlotter-Weigel B, Loscher W, Vondracek P, Seeman P, De Jonghe P, Van Dijck P, Jordanova A, Hornemann T, Timmerman V (2010) Mutations in the SPTLC2 subunit of serine

palmitoyltransferase cause hereditary sensory and autonomic neuropathy type I. Am J Hum Genet 87: 513-22

Rotthier A, Baets J, De Vriendt E, Jacobs A, Auer-Grumbach M, Levy N, Bonello-Palot N, Kilic SS, Weis J, Nascimento A, Swinkels M, Kruyt MC, Jordanova A, De Jonghe P, Timmerman V (2009) Genes for hereditary sensory and autonomic neuropathies: a genotype-phenotype correlation. Brain 132: 2699-711

Rotthier A, Baets J, Timmerman V, Janssens K (2012) Mechanisms of disease in hereditary sensory and autonomic neuropathies. Nat Rev Neurol 8: 73-85

Russo, M., Laura M, et al. (2011) Variable phenotypes are associated with PMP22 missense mutations. Neuromuscul Disord 21(2): 106-14

Saporta AS, Sottile SL, Miller LJ, Feely SM, Siskind CE, Shy ME (2011) Charcot-Marie-Tooth disease subtypes and genetic testing strategies. Ann Neurol 69: 22-33

Saporta MA, Shy ME (2013) Inherited peripheral neuropathies. Neurol Clin 31: 597-619

Schlipf NA, Schule R, Klimpe S, Karle KN, Synofzik M, Schicks J, Riess O, Schols L, Bauer P (2011) Amplicon-based high-throughput pooled sequencing identifies mutations in CYP7B1 and SPG7 in sporadic spastic paraplegia patients. Clin Genet 80: 148-60

Schule R, Schols L (2012) Genetics of hereditary spastic paraplegias. Semin Neurol 31: 484-93

Sevilla T, Vilchez JJ (2004) [Different phenotypes of Charcot-Marie-Tooth disease caused by mutations in the same gene. Are classical criteria for classification still valid?]. Neurologia 19: 264-71

Shy ME, Jani A, Krajewski K, Grandis M, Lewis RA, Li J, Shy RR, Balsamo J, Lilien J, Garbern JY, Kamholz J (2004) Phenotypic clustering in MPZ mutations. Brain 127: 371-84

Singleton AB, Hardy J, Traynor BJ, Houlden H Towards a complete resolution of the genetic architecture of disease. Trends Genet 26: 438-42

Siskind CE, Panchal S, Smith CO, Feely SM, Dalton JC, Schindler AB, Krajewski KM (2013) A Review of Genetic Counseling for Charcot Marie Tooth Disease (CMT). J Genet Couns

Sivakumar K, Kyriakides T, Puls I, Nicholson GA, Funalot B, Antonellis A, Sambuughin N, Christodoulou K, Beggs JL, Zamba-Papanicolaou E, Ionasescu V, Dalakas MC, Green ED, Fischbeck KH, Goldfarb LG (2005) Phenotypic spectrum of disorders associated with glycyl-tRNA synthetase mutations. Brain 128: 2304-14

Skre H (1974) Genetic and clinical aspects of Charcot-Marie-Tooth's disease. Clin Genet 6: 98-118

Slaugenhaupt SA, Blumenfeld A, Gill SP, Leyne M, Mull J, Cuajungco MP, Liebert CB, Chadwick B, Idelson M, Reznik L, Robbins C, Makalowska I, Brownstein M, Krappmann D, Scheidereit C, Maayan C, Axelrod FB, Gusella JF (2001) Tissue-specific expression of a splicing mutation in the IKBKAP gene causes familial dysautonomia. Am J Hum Genet 68: 598-605

Solla P, Vannelli A, Bolino A, Marrosu G, Coviello S, Murru MR, Tranquilli S, Corongiu D, Benedetti S, Marrosu MG (2010) Heat shock protein 27 R127W mutation: evidence of a continuum between axonal Charcot-Marie-Tooth and distal hereditary motor neuropathy. J Neurol Neurosurg Psychiatry 81: 958-62

Soong BW, Huang YH, Tsai PC, Huang CC, Pan HC, Lu YC, Chien HJ, Liu TT, Chang MH, Lin KP, Tu PH, Kao LS, Lee YC (2013) Exome sequencing identifies GNB4 mutations as a cause of dominant intermediate Charcot-Marie-Tooth disease. Am J Hum Genet 92: 422-30

Street VA, Bennett CL, Goldy JD, Shirk AJ, Kleopa KA, Tempel BL, Lipe HP, Scherer SS, Bird TD, Chance PF (2003) Mutation of a putative protein degradation gene LITAF/SIMPLE in Charcot-Marie-Tooth disease 1C. Neurology 60: 22-6

Szmulewicz DJ, Waterston JA, MacDougall HG, Mossman S, Chancellor AM, McLean CA, Merchant S, Patrikios P, Halmagyi GM, Storey E (2011) Cerebellar ataxia, neuropathy, vestibular areflexia syndrome (CANVAS): a review of the clinical features and video-oculographic diagnosis. Ann N Y Acad Sci 1233: 139-47

Takashima H, Boerkoel CF, John J, Saifi GM, Salih MA, Armstrong D, Mao Y, Quiocho FA, Roa BB, Nakagawa M, Stockton DW, Lupski JR (2002) Mutation of TDP1, encoding a topoisomerase I-dependent DNA damage repair enzyme, in spinocerebellar ataxia with axonal neuropathy. Nat Genet 32: 267-72

Tazir M, Bellatache M, Nouioua S, Vallat JM (2013) Autosomal recessive Charcot-Marie-Tooth disease: from genes to phenotypes. J Peripher Nerv Syst 18: 113-29

Toyota K, Ogino D, Hayashi M, Taki M, Saito K, Abe A, Hashimoto T, Umetsu K, Tsukaguchi H, Hayasaka K (2013) INF2 mutations in Charcot-Marie-Tooth disease complicated with focal segmental glomerulosclerosis. J Peripher Nerv Syst 18: 97-8

Tsurusaki Y, Saitoh S, Tomizawa K, Sudo A, Asahina N, Shiraishi H, Ito J, Tanaka H, Doi H, Saitsu H, Miyake N, Matsumoto N (2012) A DYNC1H1 mutation causes a dominant spinal muscular atrophy with lower extremity predominance. Neurogenetics 13: 327-32

Van Goethem G, Luoma P, Rantamaki M, Al Memar A, Kaakkola S, Hackman P, Krahe R, Lofgren A, Martin JJ, De Jonghe P, Suomalainen A, Udd B, Van Broeckhoven C (2004) POLG mutations in neurodegenerative disorders with ataxia but no muscle involvement. Neurology 63: 1251-7

Verhoeven K, De Jonghe P, Coen K, Verpoorten N, Auer-Grumbach M, Kwon JM, FitzPatrick D, Schmedding E, De Vriendt E, Jacobs A, Van Gerwen V, Wagner K, Hartung HP, Timmerman V (2003) Mutations in the small GTP-ase late endosomal protein RAB7 cause Charcot-Marie-Tooth type 2B neuropathy. Am J Hum Genet 72: 722-7

Verkerk AJ, Pieretti M, Sutcliffe JS, Fu YH, Kuhl DP, Pizzuti A, Reiner O, Richards S, Victoria MF, Zhang FP, et al. (1991) Identification of a gene (FMR-1) containing a CGG repeat coincident with a breakpoint cluster region exhibiting length variation in fragile X syndrome. Cell 65: 905-14

Vermeer S, Meijer RP, Pijl BJ, Timmermans J, Cruysberg JR, Bos MM, Schelhaas HJ, van de Warrenburg BP, Knoers NV, Scheffer H, Kremer B (2008) ARSACS in the Dutch population: a frequent cause of early-onset cerebellar ataxia. Neurogenetics 9: 207-14

Voelkerding KV, Dames SA, Durtschi JD (2009) Next-generation sequencing: from basic research to diagnostics. Clin Chem 55: 641-58

Waldmuller S, Muller M, Rackebrandt K, Binner P, Poths S, Bonin M, Scheffold T (2008) Array-based resequencing assay for mutations causing hypertrophic cardiomyopathy. Clin Chem 54: 682-7

Warner LE, Mancias P, Butler IJ, McDonald CM, Keppen L, Koob KG, Lupski JR (1998) Mutations in the early growth response 2 (EGR2) gene are associated with hereditary myelinopathies. Nat Genet 18: 382-4

Weedon MN, Hastings R, Caswell R, Xie W, Paszkiewicz K, Antoniadi T, Williams M, King C, Greenhalgh L, Newbury-Ecob R, Ellard S (2011) Exome sequencing identifies a DYNC1H1

mutation in a large pedigree with dominant axonal Charcot-Marie-Tooth disease. Am J Hum Genet 89: 308-12

Weiss MD, Saneto RP (2010) Sensory ataxic neuropathy with dysarthria and ophthalmoparesis (SANDO) in late life due to compound heterozygous POLG mutations. Muscle Nerve 41: 882-5

Windpassinger C, Auer-Grumbach M, Irobi J, Patel H, Petek E, Horl G, Malli R, Reed JA, Dierick I, Verpoorten N, Warner TT, Proukakis C, Van den Bergh P, Verellen C, Van Maldergem L, Merlini L, De Jonghe P, Timmerman V, Crosby AH, Wagner K (2004) Heterozygous missense mutations in BSCL2 are associated with distal hereditary motor neuropathy and Silver syndrome. Nat Genet 36: 271-6

Winkelmann J, Lin L, Schormair B, Kornum BR, Faraco J, Plazzi G, Melberg A, Cornelio F, Urban AE, Pizza F, Poli F, Grubert F, Wieland T, Graf E, Hallmayer J, Strom TM, Mignot E (2012) Mutations in DNMT1 cause autosomal dominant cerebellar ataxia, deafness and narcolepsy. Hum Mol Genet 21: 2205-10

Yum SW, Zhang J, Mo K, Li J, Scherer SS (2009) A novel recessive Nefl mutation causes a severe, early-onset axonal neuropathy. Ann Neurol 66: 759-70

Zuchner S, Mersiyanova IV, Muglia M, Bissar-Tadmouri N, Rochelle J, Dadali EL, Zappia M, Nelis E, Patitucci A, Senderek J, Parman Y, Evgrafov O, Jonghe PD, Takahashi Y, Tsuji S, Pericak-Vance MA, Quattrone A, Battaloglu E, Polyakov AV, Schroder JM, Vance JM (2004) Mutations in the mitochondrial GTPase mitofusin 2 cause Charcot-Marie-Tooth neuropathy type 2A. Nat Genet 36: 449-51

Chapter 2

Methods

2.1 Patients

All studies in the thesis were approved by the joint ethics committee of UCL Institute of Neurology and The National Hospital for Neurology and Neurosurgery (NHNN). Clinical evaluation, blood or other biological samples were obtained after written or oral informed consents from the affected patients and family members according to the regulations of NHNN or other institutes and then sent to our laboratories. When mutations were identified patients were assessed and had detailed clinical and neurophysiological examinations if necessary. NCS was performed using standard technique.

2.2 Mutation nomenclature

The mutation and polymorphisms identified were labelled based on the published complementary deoxyribonucleic acid (cDNA) sequence (http://www.ncbi.nlm.nih.giv). The nomenclature system followed the recommendation of the Human Genome Variation Society.(den Dunnen et al.2003) Gene cDNA sequence was prefixed c. for cDNA nucleotide and numbering +1 refers to the first nucleotide of the ATG translation initiation codon. The amino acid numbering was taken from the published cDNA sequence.

2.3 Sanger sequencing

2.3.1 DNA extraction from blood

Genomic DNA (gDNA) was extracted from 4~5 ml of whole blood using Promega Wizard DNA extraction kit or using the Qiagen Gentra Puregene Blood Kit, following manufacturer's instructions. DNA extracted from blood was stored at -80˚C freezer.

2.3.2 DNA quantification

The amount of gDNA was measured by the NanoDrop Spectrophotometer equipped with the interactive software ND-1000 V2.3.2 (NanoDrop Technologies). The NanoDrop spectrophotometer was loaded with 1~2 µl of solution and the gDNA concentration was expressed in ng/µl. DNA absorbed at 260 nm and contributed to the total absorbance. For quality control, the ratios of absorbance at 260/280 nm and 260/230 nm were used to assess the purity of DNA. Ratios of 260/280 around 1.8 and 260/230 around 2.0~2.2 denoted pure DNA. If in both cases the ratio was appreciably lower than expected, it might indicate the presence of

contaminants which absorbed at 280 and/or 230 nm.

2.3.3 Polymerase chain reaction (PCR)

DNA was prepared at a concentration of 10~30 ng/µl for the polymerase chain reaction (PCR). PCR was performed using Roche Faststart PCR Master (400 RXN/10 ml), primers at a dilution of 10 pmol/µl and DNA at a concentration of 10~30 ng/µl. Reagents were added in a total volume of 25 µl as following: Roche Master 12.5 µl, forwarded and reverse primers 0.75µl for each, autoclave water 10 µl and DNA 1 µl in a single run of reaction. With difficult PCR's, usually due to GC rich regions, DMSO was added at 10% of PCR total volume.

2.3.4 Agarose gel electrophoresis

Agarose gel electrophoresis was used to verify the quality and size of PCR amplification product. The 1.0~1.5% gel was prepared using Ultrapure Agarose (Invitrogen) and TBE 1X buffer (VWR). Samples and the DNA ladder (1 Kb) (Novagen) were loaded on the gels and a run at 50~70 mV was performed for 30~45 minutes. DNA fragments were visualized and photographed using UV transluminator.

2.3.5 PCR product purification

PCR product was filtered using the 96 wells PCR filter plates (Millipore). 80 µl of autoclave water was then added for each sample to filter the PCR product on the manifold. Then the filter plate was seated onto the vacuum platform (Eppendorf) with the vacuum on and the lid off for 5 minutes. Subsequently PCR product was re-suspended in 50 µl of autoclave water and shaken on the thermoshaker (Eppendorf) at room temperature (RT, 15~25°C) at 300 rpm for 5~30 minutes. The ~50 µl resuspended, purified PCR product was transferred to a labelled blue skirted plate (Eppendorf). It was used for sequencing reaction. The rest of the purified PCR product was stored at -20˚C freezer.

2.3.6 Sequencing reaction

Reagents were added in a total volume of 10 µl as following : 0.5 µl of BigDye Terminator (V3.1 or V3.3), 2 µl of 5X Sequencing Buffer (Applied Biosystems), 0.5µl of forward or reverse primers at the concentration 3.2 pmol/µl, 3.5 µl of purified PCR product and 6.5 µl of autoclave water. Sequencing reaction was performed using the settings as following:

a. 24 cycles of:
   96°C for 10 seconds
   55°C for 5 seconds
   60°C for 4 minutes
b. 4°C forever

2.3.7 Dye removal of sequencing product

The purpose of this step is to remove excess fluorescently labelled 2',3' dideoxynucleotides (ddNTPs), primers and salts from the sequencing reactions. Two methods were used depending availability of reagents and consumables.

(1) Millipore plate clean up

Sequencing product was filtered using the 96 wells PCR filter plates (Millipore). 80 µl of autoclave water was then added for each sample to filter the PCR product on the manifold. Then the filter plate was seated onto the vacuum platform with the vacuum on and the lid off for 5 minutes. Subsequently sequencing product was re-suspended in 20 µl of autoclave water and shaken on the thermoshaker (Eppendorf) at RT at 300 rpm for 5~30 minutes. The ~20 µl purified sequencing product was transferred to a 96-well reaction plate and run in the 3730 Genetic Analyser (Applied Biosystems).

(2) Dye terminator removal plate clean up

A dye terminator removal plate (ABgene) containing a gel separation matrix of spheres with pores in them was used. The matrix retained the smaller ddNTPs and allowed the DNA fragments to pass through into the filtrate. Dye removal was performed in the following steps:

1. The dye removal plate was removed from its silver foil. The bottom cover was removed from the plate and placed over one of the plates with the rounded wells.
2. The top cover was removed and the plate was spun in the centrifuge at 2150 rpm for 3 minutes.
3. The dye removal plate was sit over a fresh, labelled PCR plate.
4. 10 µl of autoclave water was added to each sequencing reaction (well).
5. All 20 µl of diluted sequencing reaction agents were pipetted gently into the centre of the filters in the dye removal plate wells.
6. The dye removal plate and PCR plate were spun at 2150 rpm for 3 minutes
7. After spinning, the PCR plate should contain ~20 µl of filtrate in each well. The PCR plate was placed into a black, plastic holder and then submitted to the 3730 Genetic Analyser for sequence analysis.

2.3.8 Sequence analysis

The 3730 Genetic Analyser was used for gene sequencing. The resulting sequences were aligned and analysed with Sequencher software (Gene Codes Corporation). Sequence variants were confirmed by repeat sequencing.

2.4 PCR based messenger ribonucleic acid (mRNA) expression studies

2.4.1 RNA isolation

Ribonucleic acid (RNA) was extracted from lymphoblasts of patient and healthy controls in *C12orf65* gene expression study (Section 3.1). The RNA had to be pure and intact and free of contaminants such as DNA and other potential inhibitors, for example, RNAses. Therefore, a sterile technique was employed at all times when handling reagents and equipment used for RNA isolation.

Purification of total RNA was performed with the RNeasy Mini Kit (Qiagen) which combines phenol/guanidine-based lysis of samples and silica-membrane–based purification of total RNA. RNA isolation was performed as the following procedures:

1. 700 µl QIAzol Lysis Reagent was added and mixed evenly to loosen the cell pellet thoroughly by vortex.
2. The tube containing the homogenate was placed at RT for 5 minutes.
3. 140 µl chloroform was added to the tube which contained the homogenate and capped it securely. The tube was shook vigorously for 15 seconds.
4. The tube containing the homogenate was placed at RT for 2~3 minutes.
5. The tube containing the homogenate was then centrifuged for 15 minutes at 12,000 x g at 4°C. After centrifugation, the sample separated into 3 phases: an upper, colorless, aqueous phase containing RNA; a white interphase; and a lower, red, organic phase. The volume of the aqueous phase was approximately 350 µl.
6. The upper aqueous phase was transferred to a new collection tube. 1.5 volumes (usually 525 µl) of 100% ethanol were added and mix thoroughly by pipetting up and down several times. Continue without delay with step 7.
7. 7Up to 00 µl of the sample, including any precipitate that may have formed, was pipetted into an RNeasy Mini spin column in a 2 ml collection tube. The lid was closed gently. The tube was centrifuged at ≥8000 x g (≥10,000 rpm) for 15 seconds at RT. The flow-through was discarded. The collection tube would be reused in step 8.
8. Step 7 was repeated using the remainder of the sample. The flow-through was discarded. The collection tube would be reused in step 9.
9. 700 µl Buffer RWT was added to the RNeasy Mini spin column. The lid was closed gently and the tube was centrifuged for 15 s at ≥8000 x g (≥10,000 rpm) to wash the column. The flow-through was discarded.
10. 500 µl Buffer RPE was pipetted onto the RNeasy Mini spin column. The lid was closed gently and the tube was centrifuged for 15 s at ≥8000 x g (≥10,000 rpm) to wash the column. The flow-through was discarded. The collection tube would be reused in step 11.

11. Another 500 µl Buffer RPE was added to the RNeasy Mini spin column. The lid was closed gently and the column was centrifuged for 2 minutes at ≥8000 x g (≥10,000 rpm) to dry the RNeasy Mini spin column membrane. The long centrifugation dried the spin column membrane, ensuring that no ethanol was carried over during RNA elution.
12. The RNeasy Mini spin column was transferred to a new 1.5 ml collection tube. 30~50 µl RNase-free water was pipetted directly onto the RNeasy Mini spin column membrane. The lid was closed gently and the column was centrifuged for 1 min at ≥8000 x g (≥10,000 rpm) to elute the RNA.
13. The RNA concentration was measured and assessed the quality with spectrophotometer by evaluating the 260/280 nm and 260/230 nm ratio.

The procedures were summarised in figure 2-1.

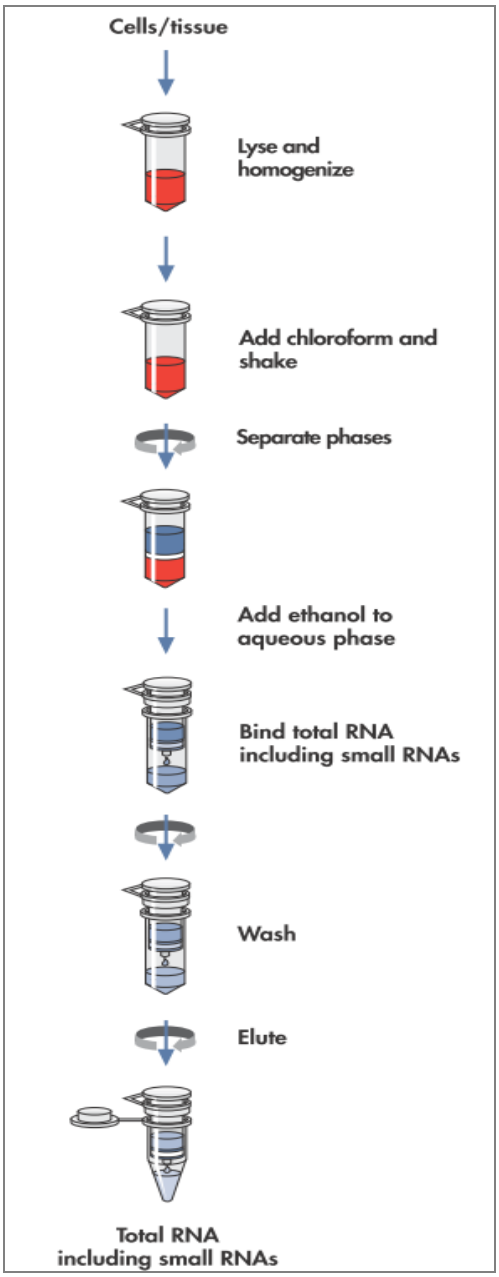

Figure 2-1. The miRNeasy Mini procedures

2.4.2 cDNA synthesis

RNA was reverse transcribed form cDNA using the First-Strand cDNA synthesis Superscript II RT kit (Invitrogen). The reaction constituted 2µg of total RNA, 1 µl of random primers, 1 µl of dNTP mix (10mM) and 8 µl of RNAase-free water. The mixture was heated to 65°C for 5 minutes, followed by a quick chill on ice. The contents were then centrifuged and the remaining cDNA synthesis mixture was added which included 4 µl of 5X First-Strand Buffer, 2 µl of 0.1 M dithiothreitol (DTT), followed by 1 µl of RNAse OUT (40 units/µl). RNaseOUT is optional and required when the starting RNA is less than 50ng. The contents were then mixed gently and incubated 25°C for 2 minutes. 1 µl (200 units) of SuperScript II RT was added by pipetting gently up and down. The mixture was incubated at 42°C for 50 minutes, followed by 70°C for 15 minutes to inactivate the reaction. The synthetic cDNA can be stored at -20°C.

2.4.3 Quantitative Real Time PCR (qRT-PCR)

A multiplex quantitative real-time PCR assay for the levels *of C12orf65* and *RPL13A* were performed using SYBR Green PCR Master Mix kit (Applied Biosystems) with a Corbett Rotor-Gene real-time quantitative thermal cycler (Corbett Research/Qiagen). The 25µl reaction required 5µl of cDNA (50ng/µl), 12.5µl SYBR-green, 2.25µl primers (900nM) and 3µl ddH_2O. Thermal cycling consisted of 10 minutes at 94°C for initial denaturation and DNA polymerase activation, followed by 40 cycles of denaturation at 94°C for 15 seconds and annealing/extension at 60°C for 1 minute. Each assay contained template negative controls and a quantitative standard curve dilution run in duplicate. All reactions were performed in triplicate in a final volume of 10 µl. Dissociation curves were run to detect nonspecific amplification, and single amplified product was confirmed in each reaction. Standard curves showed that all duplexed assays had equal efficiencies (99.9%), satisfying criteria for the comparative Ct method of quantification. The quantities of each test gene and internal controls were then determined from the standard curve using the Rotor-Gene 6000 series software 1.7 (Corbett Research/Quiagen). Relative quantity of each *C12orf65* level normalized by the *RPL13A* level was then calculated. The results were expressed as percentage of control.

2.5 Targered resequencing

2.5.1 Design of the probe library in targeted resequencing

(1) TruSeq Custom Amplicon project

The library of probes for the ARCMT1 panel was designed though TruSeq Custom Amplicon (TSCA) system (Illumina).(Section 6.1) Custom oligonucleotide probes were first designed in web-based DesignStudio (https://icom.illumina.com/). Each panel was designed for a *project*, referring to a group of diseases, e.g. ARCMT1. A project contained several target regions of interest. A *target region* comprised a pair of coordinates that define a continuous sequence in the genome, usually CCDS (Consensus coding DNA sequence) of the target gene. Each target region then was divided into several targets. *Targets* were the actual coordinates used for designing probes to make each amplicon ~250 bps in length. The TSCA kit allowed the procession of up to 384 amplicons per sample and integrated indexes to support up to 96 samples per run. The reference genome was based on UCSC iGenomes (hg19) (Homo sapiens) (http://genome.ucsc.edu). Figure 2-2 illustrated the online DesignStudio.

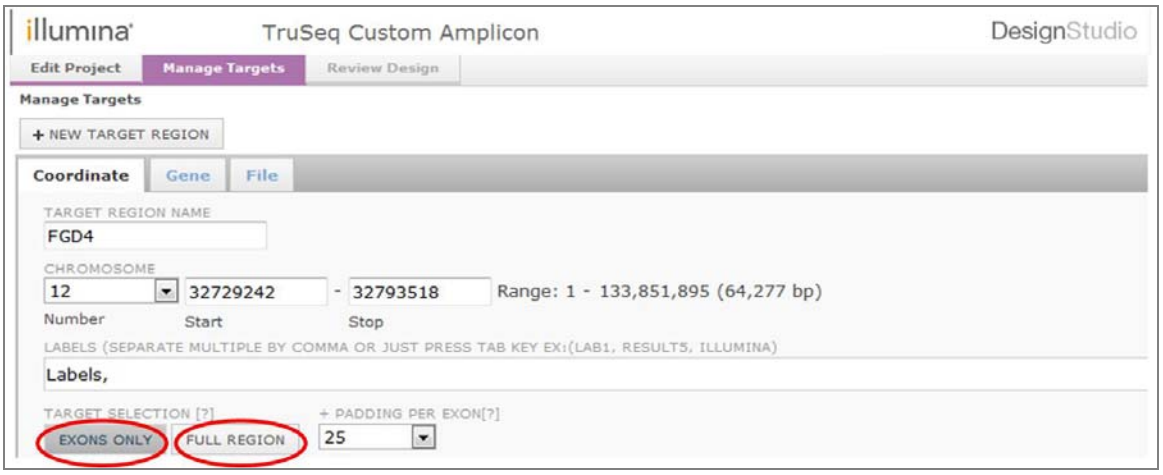

Figure 2-2. Design of custom oligonucleotide probes in web-based DesignStudio.

Target probes could be designed across the entire target region (full region), or these targets could be discontinuous if the probes were designed for just the exons (exon only). Padding per exon was to add from 0 to 25 bases upstream and downstream of each exon.

(2) Halo Design Wizard

The target sequencing panel of the HSP-neuropathy panel was designed with the web-based Agilent Halo Design Wizard (http://www.halogenomics.com/haloplex/custom-reagent-kits) (Section 6.2). The design procedure was started to input a list of target genes or a set of genomic coordinates. Then regions of interest for each gene were defined as required, for example, CCDS only or the whole genomic gene. After reviewing the target regions on Halo design servers, the project was assigned the name and then submitted to the server.

(3) Report of the design

By selection of the way to design probes and adjustment of the settings, the amplicons were optimized with the attempt to get a full coverage of the target regions. After the design was completed, a report containing the location and coverage of the custom amplicons was generated. In table 2-1 amplicons of *FGD4* are provided as an example.

Table 2-1. Report of the design of *FGD4* custom amplicons

Target	Chr	Start	Stop	Length (bp)	Amplicon	Avoid SNP	Coverage	Score
FGD4 ex3	12	32729242	32729383	142	1	Yes	100	95
FGD4 ex4	12	32734894	32735401	508	4	Yes	100	85
FGD4 ex5	12	32751431	32751520	90	1	Yes	100	95
FGD4 ex6	12	32754212	32754357	146	1	Yes	100	95
Amplicon	Chr	Start	Stop	Target	Length (bp)	Strand	Avoid SNP	Score
Amplicon (3081506)	12	32729100	32729327	Exon_2193735	228	R	Yes	95
Amplicon (3081507)	12	32729276	32729513	Exon_2193735	238	F	Yes	87
Amplicon (3081512)	12	32734742	32734974	Exon_2196253	233	R	Yes	74
Amplicon (3081513)	12	32734920	32735150	Exon_2196253	231	F	Yes	95

Chr= chromosome, Avoid SNP = indicating whether SNPs are being avoided for the target region and/or amplicon, Coverage = the total number of non-overlapping base covered by the attempted amplicons divided by the total number of bases in design, Score= an Illumina estimate of the percentage of attempted probes that will successfully enrich the targeted sequences. This prediction is based on GC content and probe uniformity. Actual assay performance and resultant sequencing depth may vary across targeted regions due to a variety of factors including library quality and probe hybridization efficiency. Only part of the targets and amplicons are listed in the table.

The following figure 2-3 (p57) illustrated how designed amplicons covered the targeted regions. All the short-fragmented custom amplicons for *FGD4* (black tracks) are inspected on the genome browser to check if they together could cover CCDS (green tracks) without any gaps.

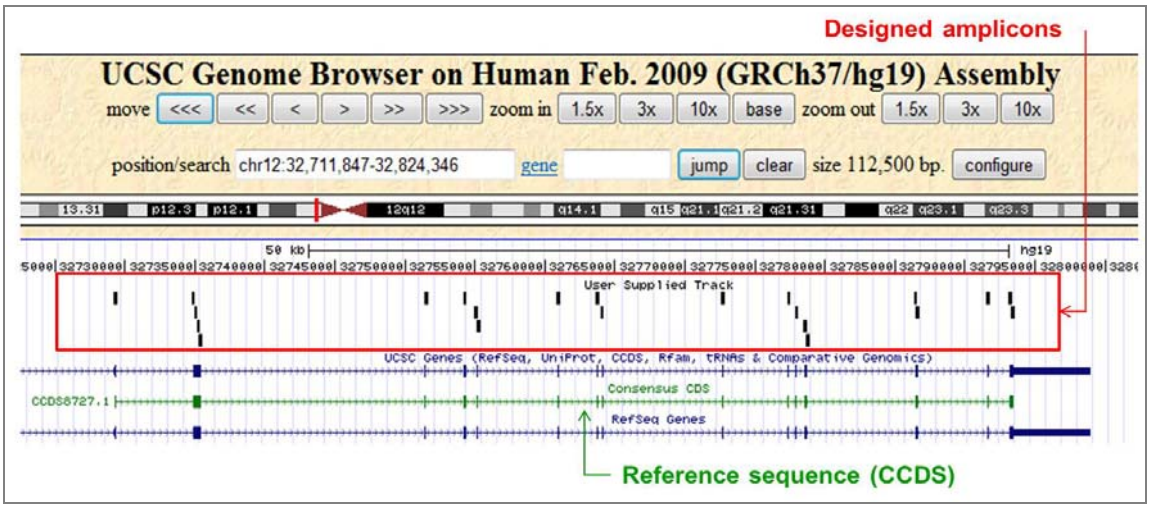

Figure 2-3. Designed custom amplicons can cover CCDS of *FGD4* without gaps

2.5.2 Sample assessment and preparation

Next generation sequencers require stringent control of sample preparation. To obtain an accurate quantification of the DNA library, the sample gDNA used in targeted resequencing and WES were assessed by the Qubit Fluorometry system with dsDNA BR Assay (Invitrogen) and the Qubit ® 2.0 Fluorometer (Invitrogen) using 2 µl of each gDNA sample with 198 µl of the Qubit working solution for sample quantification. Once high quality DNA had been extracted, the library was prepared using the TruSeq DNA Sample Prep Kit (Illumina) following manufacturer's instructions, which provided an indexed adapter sequence for each DNA sample, enabling multi-sample pooling in a single enrichment reaction.

2.5.3 Library enrichment- TruSeq Enrichment System

Library enrichment of WSE and the targeted resequencing ARCMT1 panel with reactions of a total of 96 samples were completed by using the TruSeq Custom Enrichment System, but different oligonucleotide reagents were used for WSE and targeted resequencing during the hybridization procedures. The workflow is summarised in figure 2-4 (p58).

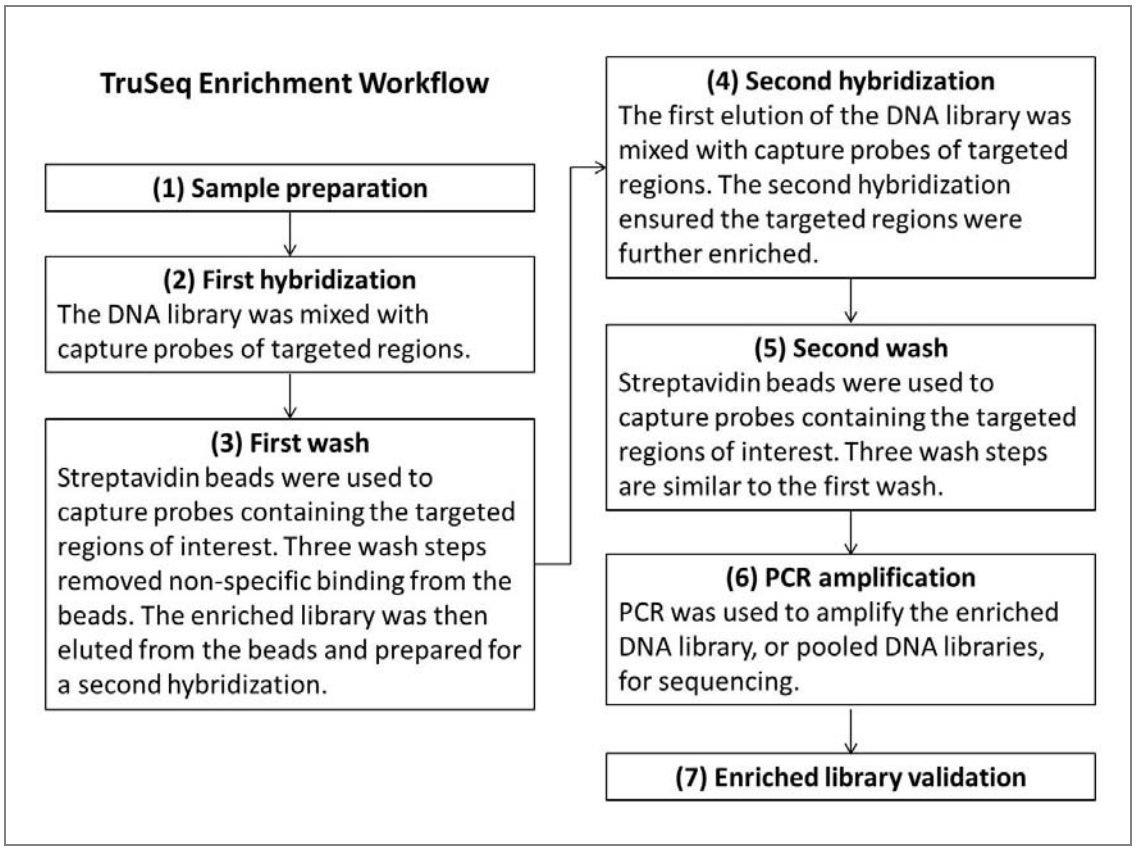

Figure 2-4. TruSeq enrichment system workflow

(1) Sample preparation

Prior to library enrichment, the human DNA library was prepared using the TruSeq DNA Sample Preparation kit as mentioned in Section 2.5.2

(2) First Hybridization

In this process, the DNA library was mixed with capture probes of targeted regions.

1. The Capture Target Buffer 1 tube (CTB1) was put on the vortex for 5 seconds to make sure no crystal structures were present.
2. The reaction mix was prepared in a total volume 100 µl per sample in each well of the new 96-well PCR plate labelled CTP1 in the following order: diluted DNA library 40 µl, CTB1 50 µl, Custom Selected Oligos10 µl. The entire volume was pipetted gently up and down 10~20 times to mix thoroughly.
3. The CTP1 plate was sealed with an adhesive seal tightly to prevent potential evaporation.
4. The CTP1 plate was centrifuged to 280 xg for 1 minute.
5. The sealed CTP1 plate was placed on the pre-programmed thermal cycler with the lid closed and incubated using the settings:

a. Pre-heated lid set to 100°C

b. 95°C for 10 minutes

c. 18 cycles of 1 minute incubations, starting at 93°C, then decreasing 2°C per cycle

d. 58°C for 16~20 hours

(3) First Wash

In this process, streptavidin beads were used to capture probes containing the targeted regions of interest. Three wash steps were performed to remove non-specific binding from the beads. The enriched library was then eluted from the beads and prepared for a second hybridization.

1. The CTP1 plate was removed from the thermal cycler.
2. The CTP1 plate was centrifuged to 280 xg for 1 minute.
3. The CTP1 plate was placed on a 96-well rack and the adhesive seal was removed from the plate.
4. The entire contents of each well was transferred from the CTP1 plate to the corresponding well of the new 96-well plate labelled WTP1.
5. The Streptavidin Magnetic Beads tube was put on the vortex until the beads are well dispersed, then 250 µl of well-mixed Streptavidin Magnetic Beads was added to the wells of the WTP1 plate. The entire volume was pipetted gently up and down 10 times to mix thoroughly.
6. The WTP1 plate was sealed with an adhesive seal.
7. The WTP1 plate was placed at RT for 30 minutes.
8. The WTP1 plate was centrifuged to 280 xg for 1 minute.
9. The adhesive seal was removed from the WTP1 plate.
10. The WTP1 plate was placed on the magnetic stand for 2 minutes at RT until the liquid appearing clearly.
11. All of the supernatant was removed and discarded from each well.
12. The WTP1 plate was removed from the magnetic stand.
13. The Wash Solution 1 tube was put on the vertex for 5 seconds to make sure that no crystal structures were present.
14. 200 µl Wash Solution 1 was added to each well of the WTP1 plate. The entire volume was pipetted gently up and down 10~20 times to make sure the beads were fully resuspended.
15. The WTP1 plate was placed on the magnetic stand for 2 minutes at RT until the liquid appearing clearly.
16. All of the supernatant was removed and discarded from each well.
17. The WTP1 plate was removed from the magnetic stand.
18. The Wash Solution 2 tube was put on the vertex or 5 seconds to make sure that the Wash

Solution 2 was mixed thoroughly.

19. 200 µl Wash Solution 2 was added to each well of the WTP1 plate. The entire volume was pipetted gently up and down 10~20 times to mix thoroughly and avoid excessive bubbling or foaming. The beads had to be fully resuspended.
20. The WTP1 plate was placed on the magnetic stand for 2 minutes at RT until the liquid appearing clearly.
21. All of the supernatant was removed and discarded from each well.
22. The WTP1 plate was removed from the magnetic stand.
23. 200 µl Wash Solution 2 was added to each well of the WTP1 plate. The entire volume was pipetted up and down 10~20 times to mix thoroughly and avoid excessive bubbling or foaming. The beads had to be fully resuspended.
24. The entire contents of each well was transferred of the WTP1 plate to the corresponding well of the new 96-well PCR plate labelled IWP1.
25. The IWP1 plate was sealed with an adhesive seal.
26. The IWP1 plate was incubated on the thermal cycler at 42°C for 30 minutes with a heated lid set to 100°C.
27. The magnetic stand was placed next to the thermal cycler for immediate access.
28. The IWP1 plate was removed from the thermal cycler and immediately placed on the magnetic stand for 2 minutes until the liquid appearing clearly.
29. The adhesive seal was removed from the IWP1 plate.
30. All of the supernatant was immediately removed and discarded from each well.
31. The IWP1 plate was removed from the magnetic stand.
32. 200 µl Wash Solution 2 was added to each sample well of the IWP1 plate. The entire volume was pipetted gently up and down 10~20 times to mix thoroughly and avoid excessive bubbling or foaming. The beads had to be fully resuspended.
33. Steps 25~30 were repeated once.
34. The IWP1 plate was removed from the magnetic stand.
35. 200 µl Wash Solution 3 was added to each well of the IWP1 plate. The entire volume was pipetted gently up and down 10~20 times to mix thoroughly.
36. The IWP1 plate was placed on the magnetic stand for 2 minutes at RT until the liquid appearing clearly.
37. All of the supernatant was removed and discarded from each well.
38. Steps 34~37 were repeated once.
39. To remove any residual Wash Solution 3, the IWP1 plate was sealed with an adhesive seal.
40. The IWP1 plate was centrifuged briefly to collect any residual Wash Solution 3.
41. The IWP1 plate was placed on the magnetic stand for 2 minutes at RT until the liquid appearing clearly.

42. The adhesive seal was removed carefully from the IWP1 plate.
43. Any residual supernatant was removed and discarded from each well.
44. The elution pre-mix was prepared in a total volume per sample 30 µl in in a separate PCR tube in the following order: Elute Target Buffer 1 (ETB1) 28.5 µl, 2N NaOH 1.5 µl.
45. The IWP1 plate was removed from the magnetic stand.
46. 30 µl of the elution pre-mix was added to each well of the IWP1 plate. The entire volume of each well was pipetted gently up and down 10~20 times to mix thoroughly.
47. The IWP1 plate was sealed with an adhesive seal tightly.
48. The IWP1 plate was placed at RT for 5 minutes.
49. The IWP1 plate was centrifuged to 280 xg for 1 minute.
50. The IWP1 plate was placed on the magnetic stand for 2 minutes until the liquid appearing clearly.
51. The adhesive seal was carefully removed from the IWP1 plate.
52. 29 µl of supernatant was transferred from each well of the IWP1 plate to the corresponding well of the new 96-well PCR plate labelled TTP1.
53. 5 µl Elute Target Buffer 2 (ETB2) was added to each well of the TTP1 plate containing samples to neutralize the elution. The entire volume was gently pipetted up and down 10~20 times to mix thoroughly.
54. The TTP1 plate was sealed with an adhesive seal tightly.
55. 2 µl of the first elution was diluted in 98 µl PCR grade water (1:50 dilution) in a new PCR tube labelled “First Elution for qPCR”. Each tube was capped and stored at -15° to -25°C.

(4) Second Hybridization

In this process, the first elution of the DNA library was mixed with the capture probes of target regions. The second hybridization made sure that the targeted regions were further enriched.

Reagents were prepared as following:

1. The Custom Selected Oligos tube was removed from -15°to -25°C storage and thawed on ice.
2. The Capture Target Buffer 1 tube was thawed at RT.
3. The TTP1 plate was thawed at RT. The thawed TTP1 plate was centrifuged to 280 xg for 1 minute. The adhesive seal was removed from the thawed TTP1 plate.

1. The Capture Target Buffer 1 tube was put on the vortex for 5 seconds to make sure that no crystal structures were present.
2. The reagents were prepared to a total volume per sample100 µl in the order listed to each well of the new 300 µl 96-well PCR plate labelled CTP2: Capture Target Buffer 1 50 µl, Custom Selected Oligos 10 µl, PCR Grade Water 10 µl and First Elution from TTP1 Plate 30 µl. The

entire volume was gently pipetted up and down 10~20 times to mix thoroughly. The tip had to be changed after each sample.

3. The CTP2 plate was sealed with an adhesive seal tightly.
4. The CTP2 plate was centrifuged to 280 xg for 1 minute.
5. The sealed CTP2 plate was placed on the pre-programmed thermal cycler with the lid closed and incubated using the pre-programmed settings:
   a. Pre-heated lid set to 100°C
   b. 95°C for 10 minutes
   c. 18 cycles of 1 minute incubations, starting at 93°C, then decreasing 2°C per cycle
   d. 58°C for 16–20 hours

(5) Second Wash

In this process, streptavidin beads were used to capture probes containing the targeted regions of interest. Three wash steps were performed to remove non-specific binding from the beads. The enriched library was then eluted from the beads and prepared for sequencing.

1. The CTP2 plate was removed from the thermal cycler.
2. The room temperature CTP2 plate was centrifuged to 280 xg for 1 minute.
3. The CTP2 plate was placed on a 96-well rack and the adhesive seal was removed from the plate.
4. The entire contents from each well of the CTP2 plate was transferred to the corresponding well of the new 96-well plate labelled WTP2.
5. The Streptavidin Magnetic Beads tube was put on the vortex until the beads were well dispersed, then 250 µl of well-mixed Streptavidin Magnetic Beads was added to the wells of the WTP2 plate. The entire volume was gently pipetted up and down 10 times to mix thoroughly.
6. The WTP2 plate was sealed with an adhesive seal.
7. The WTP2 plate was placed at RT for 30 minutes.
8. The WTP2 plate was centrifuged to 280 xg for 1 minute.
9. The adhesive seal was removed from the WTP2 plate.
10. The WTP2 plate was placed on the magnetic stand for 2 minutes at RT until the liquid appears clear.
11. All of the supernatant was removed and discarded from each well.
12. The WTP2 plate was removed from the magnetic stand.
13. The Wash Solution 1 tube was put on the vortex for 5 seconds to make sure that no crystal structures were present.
14. 200 µl Wash Solution 1 was added to each well of the WTP2 plate. The entire volume was gently pipetted up and down 10~20 times to make sure the beads were fully resuspended.

15. The WTP2 plate was placed on the magnetic stand for 2 minutes at RT until the liquid appearing clear.
16. All of the supernatant was removed and discarded from each well.
17. The WTP2 plate was removed from the magnetic stand.
18. The Wash Solution 2 tube was put on the vortex for 5 seconds to make sure that the Wash Solution 2 was mixed thoroughly.
19. 200 µl Wash Solution 2 was added to each well of the WTP2 plate. The entire volume was gently pipetted up and down 10~20 times to mix thoroughly and avoid excessive bubbling or foaming. The beads had to be fully resuspended.
20. The WTP2 plate was placed on the magnetic stand for 2 minutes at RT until the liquid appearing clear.
21. All of the supernatant was removed and discarded from each well.
22. The WTP2 plate was removed from the magnetic stand.
23. 200 µl Wash Solution 2 was added to each well of the WTP2 plate. The entire volume was gently pipetted up and down 10~20 times to mix thoroughly and avoid excessive bubbling or foaming. The beads had to be fully resuspended.
24. The entire contents of each well of the WTP2 plate was transferred to the corresponding well of the new 96-well PCR plate labelled IWP2.
25. The IWP2 plate was sealed with an adhesive seal tightly.
26. The IWP2 plate was incubated on the thermal cycler at 42°C for 30 minutes with a heated lid set to 100°C.
27. The magnetic stand was placed next to the thermal cycler for immediate access.
28. The IWP2 plate was removed from the thermal cycler and immediately placed on the magnetic stand for 2 minutes until the liquid appearing clear.
29. The adhesive seal was removed from the IWP2 plate.
30. All of the supernatant was removed and discarded from each well immediately.
31. The IWP2 plate was removed from the magnetic stand.
32. 200 µl Wash Solution 2 was added to each sample well of the IWP2 plate. The entire volume was gently pipetted up and down 10~20 times to mix thoroughly and avoid excessive bubbling or foaming. The beads had to be fully resuspended.
33. Steps 25~30 were repeated once.
34. The IWP2 plate was removed from the magnetic stand.
35. 200 µl Wash Solution 3 was added to each well of the IWP2 plate. The entire volume was gently pipetted up and down 10~20 times to mix thoroughly.
36. The IWP2 plate was placed on the magnetic stand for 2 minutes at RT until the liquid appearing clear.
37. All of the supernatant was removed and discarded from each well.

38. Steps 34~37 were repeated once.
39. To remove any residual Wash Solution 3, the IWP2 plate was sealed with an adhesive seal.
40. The IWP2 plate was briefly centrifuged to collect any residual Wash Solution 3.
41. The IWP2 plate was placed on the magnetic stand for 2 minutes at RT until the liquid appearing clear.
42. The adhesive seal was carefully removed from the IWP2.
43. Any residual supernatant was removed and discarded from each well.
44. The elution pre-mix was prepared in a total volume per sample 30 µl in in a separate PCR tube in the following order: ETB1 28.5 µl and 2N NaOH 1.5 µl.
45. The IWP2 plate was removed from magnetic stand
46. 30 µl of the elution pre-mix was added to each well of the IWP2 plate. The entire volume was gently pipetted up and down 10~20 times to mix thoroughly.
47. The IWP2 plate was sealed with an adhesive seal tightly.
48. The IWP2 plate was placed at RT for 5 minutes.
49. The IWP2 plate was centrifuged to 280 xg for 1 minute.
50. The IWP2 plate was placed on the magnetic stand for 2 minutes until the liquid appearing clearly.
51. The adhesive seal was carefully removed from the IWP2 plate.
52. 29 µl of supernatant from each well of the IWP2 plate was transferred to the corresponding well of the new 96-well PCR plate labelled TTP.
53. 5 µl ETB2 was added to each well of the TTP2 plate containing samples to neutralize the elution. The entire volume was gently pipetted up and down 10~20 times to mix thoroughly.

(6) PCR Amplification

In this process, PCR was performed to amplify the enriched DNA library for sequencing with the same PCR primer cocktail used in TruSeq DNA Sample Preparation.

Reagents were prepared as following:

1. One tube of PCR Master Mix and PCR Primer Cocktail were removed from -15° to -25°C storage to thaw, then the tubes were placed on ice.
2. The thawed PCR Primer Cocktail and PCR Master Mix tubes were briefly centrifuged for 5 seconds.
3. The AMPure XP beads were removed from storage and placed at RT for at least 30 minutes.

1. The following reagents were added in a total volume per sample 50 µl to each well of the new 96-well PCR plate labelled TAP1: Second Elution from TTP2 plate 20 µl, PCR Master Mix 25 µl and PCR Primer Cocktail 5 µl. Gently pipette the entire volume up and down 10 times

to mix thoroughly.

2. The TAP1 plate was sealed with an adhesive seal.
3. The TAP1 plate was centrifuged to 280 xg for 1 minute.
4. The sealed TAP1 plate was placed on the pre-programmed thermal cycler with the lid closed and incubated using the pre-programmed settings:
   a. Pre-heated lid set to 100°C
   b. 98°C for 30 seconds
   c. 10 cycles of :
      98°C for 10 seconds
      60°C for 30 seconds
      72°C for 30 seconds
   d. 72°C for 5 minutes
   e. Hold at 10°C
5. The adhesive seal was removed from the TAP1 plate.
6. The AMPure XP Beads were put on the vortex until the beads are well dispersed, then 90 µl of the mixed AMPure XP Beads was added to each well of the TAP1 plate containing 50 µl of the PCR amplified library. The entire volume was gently pipetted up and down 10~20 times to mix thoroughly.
7. The TAP1 plate was incubated at RT for 15 minutes.
8. The TAP1 plate was placed on the magnetic stand at RT for 5 minutes or until the liquid appearing clearly.
9. Using a 200 µl single or multichannel pipette, 140 µl of the supernatant was removed and discarded from each well of the TAP1 plate.
10. With the TAP1 plate remaining on the magnetic stand, 200 µl of freshly prepared 80% EtOH was added to each well without disturbing the beads.
11. The TAP1 plate was incubated for at least 30 seconds at RT, then the supernatant was removed and discarded from each well.
12. Steps 10~11 were repeated once for a total of two 80% EtOH washes.
13. The TAP1 plate was kept on the magnetic stand and placed at RT for 15 minutes to dry, then the plate was removed from the magnetic stand.
14. The dried pellet in each well was resuspended with 30 µl Resuspension Buffer. The entire volume was gently pipetted up and down 10 times to mix thoroughly.
15. The TAP1 plate was incubated at RT for 2 minutes.
16. The TAP1 plate was placed on the magnetic stand at RT until the liquid appearing clearly.
17. 30 µl of the clear supernatant from each well of the TAP1 plate was transferred to the corresponding well of the new 96-well PCR plate labelled CAP.

(7) Enriched library validation

Performing procedures for quality control analysis on sample library and quantification of the DNA library templates were crucial for a successful run. Data were assessed by the use of TruSeq Enrichment scripts after alignment with Illumina Consensus Assessment of Sequence and Variation (CASAVA) software programmes. CASAVA converted raw image data into intensity scores, base calls, quality scored alignments, and additional formats for downstream analysis, transforming data into biologically relevant information.

2.5.4 Library enrichment- HaloPlex Custom Enrichment System

The HSP-neuropathy panel was performed by the application of the HaloPlex Target Enrichment System. Reactions of a total of 72 samples were completed through seven runs of 12 samples each. The overall workflow of the HaloPlex Target Enrichment System is summarised in figure 2-5.

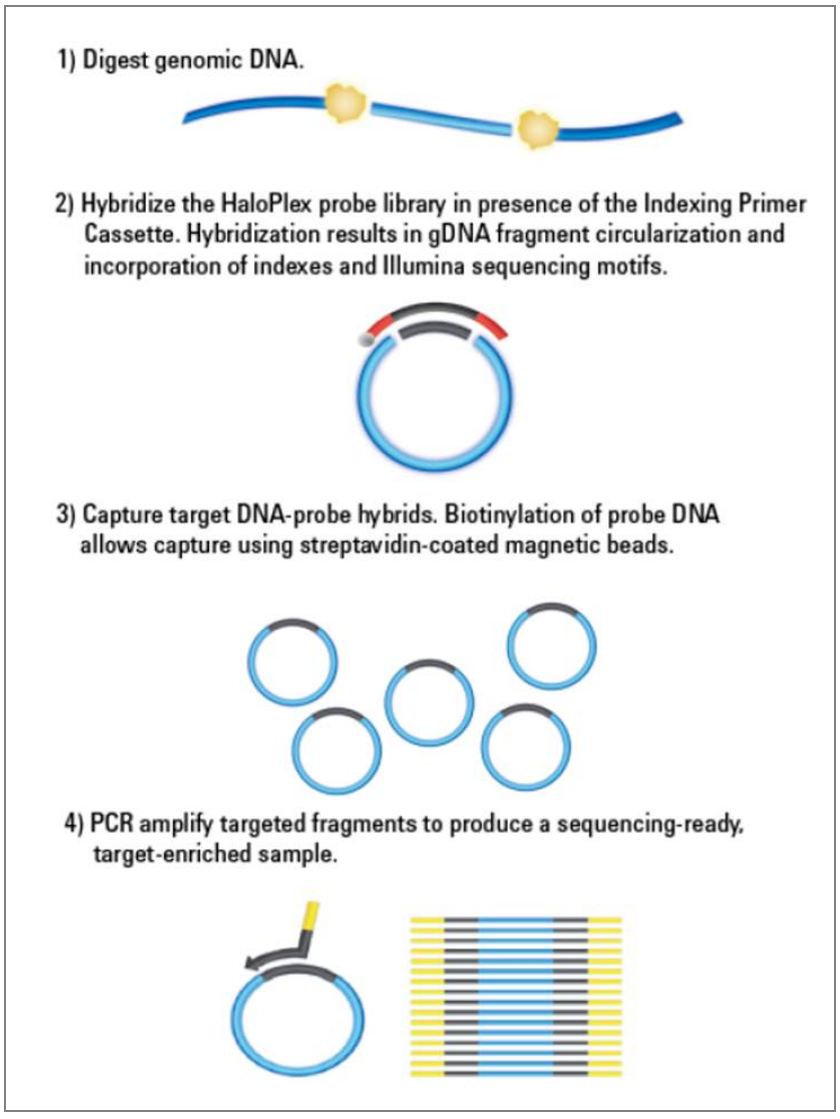

Figure 2-5. HaloPlex custom enrichment workflow

(1) Digest genomic DNA with restriction enzymes

1. The Qubit dsDNA BR Assay was used to determine the concentration of gDNA samples.
2. For 12-reaction runs, 11 gDNA samples and one Enrichment Control DNA sample (ECD) were prepared and stored on ice.
   a. In separate 0.2-mL PCR tubes, 225 ng of each gDNA sample was diluted in 45 µl nuclease-free water to reach a final DNA concentration of 5 ng/µl.
   b. In a separate 0.2-mL PCR tube, 45 µl of the supplied ECD was dispensed.
3. Eight separate restriction enzyme master mixes were prepared by combining two enzymes (from Enzyme Strips 1 and 2, each 0.5 µl for one reaction), restriction buffer (34 µl for one reaction), and BSA (0.85 µl for one reaction) in each well of an 8-well strip tube as shown in figure2-6 (A).
4. Using a multichannel pipette, 5 µl of each RE master mix was carefully distributed row-wise into each well of the restriction digest reaction plate (RD plate) as shown in figure 2-6 (B).
5. DNA samples (5 µl per well) were aliquot along the horizontal side of the RD plate as shown in figure 2-6 (C).

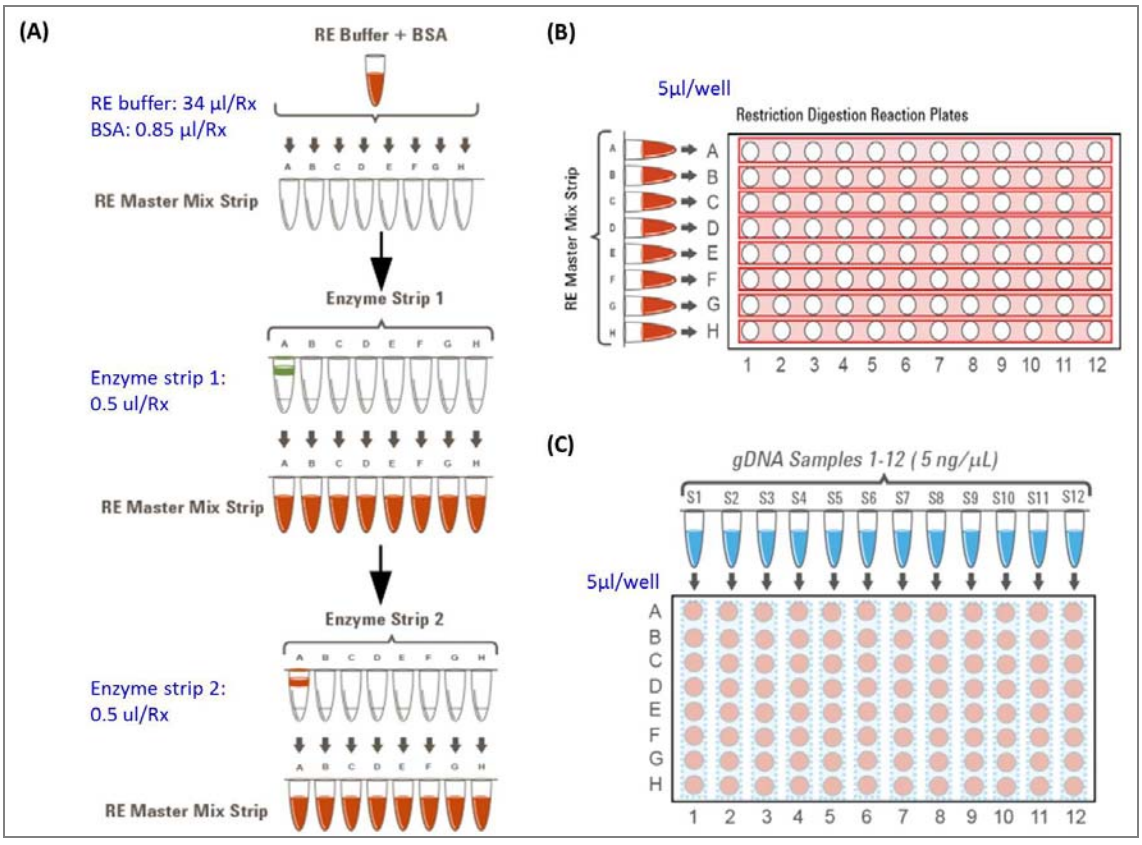

Figure 2-6. Preparation and distribution of the Restriction Enzyme Master Mix Strip for a 12-sample run

RE= restriction enzyme, Rx=reaction.

6. The plate was carefully vortexed to mix the digestion reactions.
7. The RD plate was briefly spun in a plate centrifuge.
8. The RD plate was placed in a thermal cycler with a heated lid and run the programme as 37°C for 30 min then hold at 8°C.
9. The restriction digestion reaction was validated by electrophoretic analysis of the ECD reactions. The RD plate was kept on ice during validation.

a. 4 µl of each ECD digestion reaction was transferred from wells of the digestion reaction plate to fresh 0.2-ml PCR tubes.

b. The removed 4 µl samples were incubated at 80°C for 5 minutes to inactivate the restriction enzymes.

c. An undigested DNA gel control was prepared by combining 2 µl of the ECD stock solution and 2 µl of nuclease-free water in a separate tube.

d. A HS DNA Kit was used to analyze the prepared samples using microfluidic electrophoresis on the 2100 Bioanalyzer. Each of the eight digested ECD samples should have a smear of gDNA restriction fragments between 100 and 2500 bp, overlaid with three predominant bands at approximately 125, 225 and 450 bp. These three bands corresponded to the 800-bp PCR product-derived restriction fragments, and precise sizes were differ after digestion in each of the eight RE master mixes (figure 2-7).

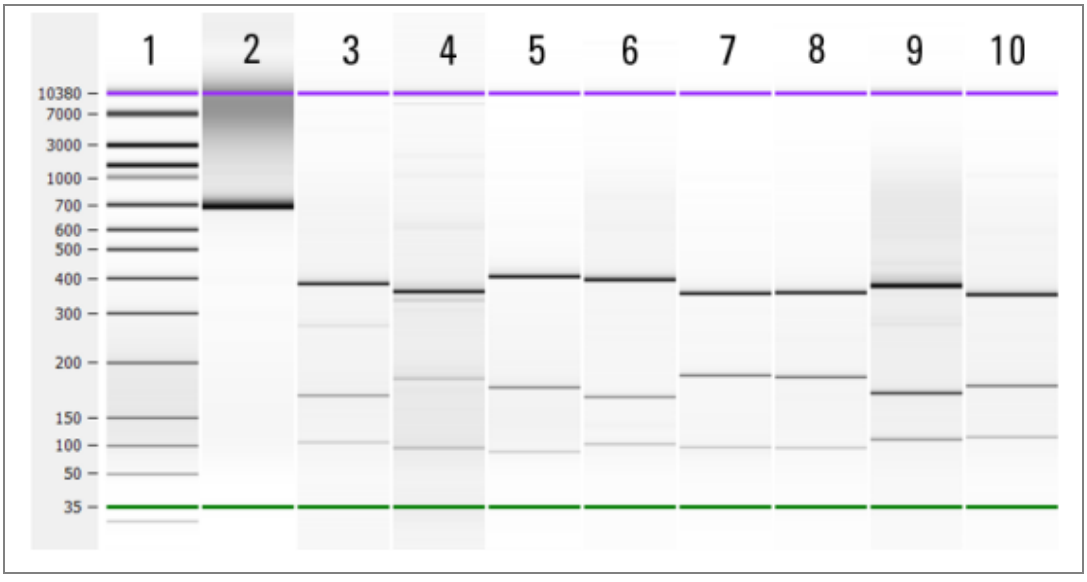

Figure 2-7. Validation of restriction digestion by 2100 Bioanalyzer analysis.

Lane 1: 50-bp DNA ladder, Lane 2: Undigested Enrichment Control DNA, Lanes 3~10: ECD digestion reactions A~H. (cited from HaloPlex Target Enrichment System Protocol Version C, June 2012)

(2) Hybridize digested DNA to HaloPlex probes for target

In this step, HaloPlex probes were hybridized selectively to fragments originating from target

regions of the genome and to direct circularization of the targeted DNA fragments. During the hybridization process, Illumina sequencing motifs including index sequences were incorporated into the targeted fragments.

1. A Hybridization Master Mix was prepared by combining Hybridization Solution (50 µl per reaction) and HaloPlex Probe (20 µl per reaction).
2. 70 µl of the Hybridization Master Mix was distributed to each of 12 tubes.
3. 10 µl of the appropriate Indexing Primer Cassette was added to each tube containing Hybridization Master Mix.
4. Digested DNA samples were transferred from the RD Plate directly into hybridization reaction tubes. All eight digestion reactions that correspond to one DNA sample were transferred into the appropriate hybridization reaction tube. The digestion samples would not pooled before adding to the hybridization reaction mixture as restriction enzymes were still active and might catalyze inappropriate cleavage events. After pooling, each hybridization reaction contained 70 µl Hybridization Master Mix, 10 µl Indexing Primer Cassette and approximately 80 µl pooled digested DNA samples.
5. The mixtures were put on the vortex and spun briefly. The hybridization reaction tubes were placed in a thermal cycler to run the programme:
   a. Pre-heated lid set to 100°C
   b. 95°C for 10 minutes
   c. 46°C for 3 hours
   d. Hold at 8°C

(3) Capture the target DNA

In this step, the circularized target DNA-HaloPlex probe hybrids, containing biotin, were captured on streptavidin beads.

1. The following reagents were placed at RT: the Capture Solution, Wash Solution, Ligation Solution , SSC Buffer, the HaloPlex Magnetic Beads and fresh 50 mM NaOH (25 µl per sample).
2. The provided HaloPlex Magnetic Beads were vigorously resuspended on a vortex mixer.
3. 40 µl (1 Volume) of HaloPlex Magnetic Beads per hybridization sample were prepared for the capture reaction:
   a. The appropriate volume of bead suspension was transferred to a 1.5-ml tube.
   b. The tube was put into a 1.5 ml tube-compatible magnetic rack for 5 minutes.
   c. After verifying that the solution has cleared, the supernatant was carefully removed and discarded using a pipette.
   d. An equivalent volume of Capture Solution was added to the beads and resuspended by pipetting up and down.

4. 40 µl of the prepared bead suspension was added to each 160-µl hybridization reaction.
5. After adding the magnetic beads, the capture reactions were mixed thoroughly by pipetting up and down 15 times using a 100-µl pipette set to 80 µl.
6. The capture reactions were incubated at RT for 15 minutes.
7. The tubes were briefly spun in a desktop centrifuge and then transferred to the Agencourt SPRIPlate Super Magnet magnetic plate.
8. After the solution being clear (about 30 seconds), the supernatant was then removed and discarded using a pipette set to 200 µl.
10. Wash the bead-bound samples:
   a. The capture reaction tubes were removed from the magnetic plate and 100 µl of Wash Solution was added to each tube.
   b The beads were resuspended thoroughly by pipetting up and down 10 times using a 100-µl multichannel pipette set to 80 µl.
   c. The tubes were incubated in a thermal cycler at 46°C for 10 minutes, using a heated lid.
   d. The tubes were briefly spun in a desktop centrifuge and then transferred to the magnetic plate.
   e. After the solution being clear (about 30 seconds), the supernatant was then removed and discarded using a pipette set to 120 µl.

(4) Ligate the captured, circularized fragments

In this step, DNA ligase was added to the capture reaction to close nicks in the circularized HaloPlex probe-target DNA hybrids.

1. A DNA ligation master mix was prepared by combining the reagents in the following table. The components were mixed thoroughly by gently vortexing and spinning the tube briefly.
2. 50 µl of the DNA ligation master mix was added to the beads in each DNA capture reaction tube.
3. The beads were resuspended thoroughly by pipetting up and down 15 times using a 100-µl multichannel pipette set to 40 µl.
4. The tubes were incubated in a thermal cycler at 55°C for 10 minutes, using a heated lid.

(5) Prepare the PCR Master Mix

In this step, a PCR master mix was prepared for the captured target DNA amplification step

1. The PCR master mix was prepared by combining the reagents in table 2-2 (p71):
2. The master mix components was mixed by gently vortexing, then 30-µl aliquots were distributed to fresh 0.2-ml reaction tubes.
3. The tubes were stored on ice until they were used in PCR amplification of the captured target libraries.

Table 2-2. Preparation of PCR master mix

Reagent	Volume for 1 reaction	Volume for 12 reactions (includes excess)	Volume for 16 reactions (includes excess)
5X Herculase II Reaction Buffer	10 µL	130 µL	170 µL
dNTPs (100 mM, 25 mM for each dNTP)	0.4 µL	5.2 µL	6.8 µL
Primer 1 (25 µM)	1 µL	13 µL	17 µL
Primer 2 (25 µM)	1 µL	13 µL	17 µL
2 M Acetic acid	0.5 µL	6.5 µL	8.5 µL
Herculase II Fusion DNA Polymerase	1 µL	13 µL	17 µL
Nuclease-free water	16.1 µL	209.3 µL	273.7 µL
Total	**30 µL**	**390 µL**	**510 µL**

(6) Elute captured DNA with NaOH

When the 10-minute ligation reaction period was complete, the following steps were proceeded to elute the captured DNA libraries.

1. The ligation reaction tubes were briefly spun in a desktop centrifuge and then transferred to the magnetic plate.
2. After the solution being clear (about 30 seconds), the supernatant was then removed and discarded using a pipette set to 50 µl.
3. The tubes were removed from the magnetic plate and 100 µl of the SSC Buffer was added to each tube.
4. The beads were resuspended thoroughly by pipetting up and down 10 times using a 100-µl multichannel pipette set to 80 µl.
5. The tubes were briefly spun and then put back to the magnetic plate.
6. After the solution being clear (about 30 seconds), the SSC Buffer was then carefully removed and discarded using a pipette set to 120 µl.
7. 25 µl of 50 mM NaOH was added to each tube.
8. The beads were resuspended thoroughly by pipetting up and down 10 times using a 100-µl multichannel pipette set to 15 µl.
9. Samples were incubated for 1 minute at RT to allow elution of the captured DNA.
10. The tubes were briefly spun and then transferred to the magnetic plate. PCR amplification had to be proceeded immediately the following section.

(7) PCR amplify the captured target libraries

1. The amplification reactions were prepared by transferring 20 µl of cleared supernatant from

each tube on the magnetic plate to a PCR Master Mix tube held on ice.

2. The liquid was mixed by gentle vortexing and then spun briefly.
3. The amplification reaction tubes were run in a thermal cycler with the programme:
   a. Pre-heated lid set to 100°C
   b. 98°C for 2 minutes
   c. 21 cycles of:
      98°C for 30 seconds
      60°C for 30 seconds
      72°C for 1 minute
   d. 72°C for 10 minutes
   e. Hold at 8°C

(8) Purify the amplified target libraries

In this step, the amplified target DNA was purified using AMPure XP beads.

1. The AMPure XP beads were placed at RT for at least 30 minutes.
2. 400 µl of 70% ethanol per sample were prepared.
3. 40 µl of each PCR reaction sample was transferred to a fresh 0.2-ml tube. The remaining volume of each sample was stored at –20°C for troubleshooting.
4. The AMPure XP bead suspension was resuspended well, until the suspension appeared homogeneous and consistent in color.
5. 60 µl (1.5 Volumes) of homogenous AMPure XP beads were added to each 40-µl amplified library sample and then vortexed thoroughly.
6. Samples were incubated for 5 minutes at RT.
7. The liquid was spun briefly to collect, then the tubes were placed in the magnetic plate until the solution being clear (approximately 2 minutes).
8. The tubes were kept in the magnetic plate. The cleared solution was carefully removed and discarded from each tube using a 100-µl pipette set to 100 µl. The beads could not be touched while removing the solution.
9. The tubes were kept in the magnetic plate while 200 µl of 70% ethanol was added into the tubes. Fresh 70% ethanol was used for optimal results.
10. After disturbed beads being settled (approximately 30 seconds), the ethanol was removed using a 200-µl pipette set to 200 µl.
11. Step 9 and step 10 were repeated once for a total of two washes.
12. Residual ethanol was removed with a 20-µl volume pipette.
13. The tubes were air-dried with open lids at RT until the residual ethanol completely evaporated.
14. The tubes were removed from the magnetic plate and 40 µl of 10 mM Tris-acetate or Tris-

HCl buffer (pH 8.0) was added to each sample. Room-temperature Tris-acetate or Tris-HCl buffer was used for elution at this step.

15. The liquid was mixed thoroughly by pipetting up and down 15 times using a 100-µl pipette set to 30 µl.
16. The samples were incubated for 2 minutes at RT to allow elution of DNA.
17. The tube in the magnetic plate was left for 2 minutes or until the solution was clear.
18. The cleared supernatant (approximately 40 µl) was removed to a fresh tube.

(9) Validate enrichment and quantify enriched target DNA

Each amplicon contained one target insert surrounded by sequence motifs required for multiplexed sequencing using the Illumina platform. Amplicons include 50 to 500 bp of target DNA insert and 125 bp of sequencing motifs, as shown in figure 2-8. The amplicons should range from 175 to 625 bp in length, with the majority of products sized 225 to 525 bp.

Figure 2-8. Content of HaloPlex-enriched target amplicons

Each amplicon contains one target insert (blue) surrounded by the Illumina paired-end sequencing elements (black), the sample index (red) and the library bridge PCR primers (yellow). (cited from HaloPlex Target Enrichment System Protocol Version C, June 2012)

Prior to sample pooling and sequencing sample preparation, the 2100 Bioanalyzer was used to validate enrichment and quantify the enriched target DNA in each library sample. The electropherogram for each sample was analyzed. The concentration of enriched target DNA in the sample was determined by integration under the peak between 175 and 625 bp. Any spurious DNA products outside of this size range in any sample were excluded from the target DNA quantitation results. See figure 2-9 for an example.

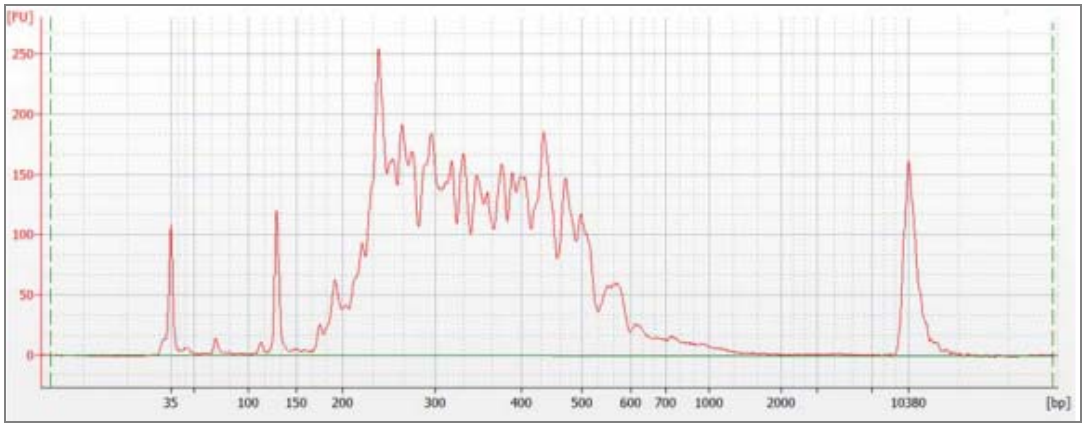

Figure 2-9. Validation of HaloPlex enrichment by 2100 Bioanalyzer analysis

(cited from HaloPlex Target Enrichment System Protocol Version C, June 2012)

(10) Sample pooling and sequencing platform

Samples with different indexes were pooled with equimolar amounts of each sample to optimize the use of sequencing capacity. The final HaloPlex enrichment pool was ready for 150 + 150 bp paired-end sequencing using standard Illumina primers and chemistry on the Illumina MiSeq. Sequence alignment and variant calling were performed against the reference human genome (UCSC hg19). Before aligning reads to the reference genome, the reads from Illumina adaptor sequences were trimmed with NextGene software (Softgenetics).

2.6 Whole exome sequencing

2.6.1 Sample assessment and preparation

The sample gDNA used in WES were assessed by the Qubit Fluorometry system with dsDNA BR Assay (Invitrogen) and the Qubit ® 2.0 Fluorometer (Invitrogen) with the same method described in Section 2.5.2. Once high quality DNA had been extracted, the Covaris E210 acoustic disruptor (LGC Genomics) was used to shear gDNA to be at 150 bp target size. The sheared gDNA was then purified and assessed using a High Sensitivity DNA Kit (p/n 5067-4626) and the 2100 Bioanalyzer system with 2100 Expert Software (version B.02.07) (Agilent).

After DNA fragmentation, the library was prepared using the TruSeq DNA Sample Preparation Kit (Illumina) following manufacturer's instructions, which provided an index for each DNA sample, enabling multi-sample pooling in a single enrichment reaction. For samples passing quality control, the 3' ends of the fragmented DNA was repaired using an End Repair Mix and then purified. The 3' to 5' exonuclease activity of this mix removed the 3' overhangs and the polymerase activity filled in the 5' overhangs. After purification, a single 'A' nucleotide was added to the 3' ends of the blunt fragments to prevent them from ligating to one another during the adapter ligation reaction. A corresponding single 'T' nucleotide on the 3' end of the adapter provided a complementary overhang for ligating the adapter to the fragment. This was to ensure a low rate of chimera (concatenated template) formation. The DNA was purified again. At this point the paired end adapters were ligated to the DNA sample. An additional purification step and assessment on the 2100 Bioanalyzer system were performed again. The adapter-ligated library was then amplified using 6 rounds of PCR, purified and assessed on a 2100 Bioanalyzer looking for peak enrichment at 200 bp. At this point enrichment of the DNA library for exome fragments could proceed.

2.6.2 Library enrichment

Library enrichment of WSE was completed by using the TruSeq Custom Enrichment System. The workflow was the same as which in targeted sequencing (Section 2.5.3) except for different oligonucleotide reagents were used for WSE.

2.6.3 Bioinformatics pipeline of data procession

A substantial amount of data is produced from next generation sequencing. After the genome analyser generated the raw sequencing images (image analysis), several steps were involved in the read conversion to variant calling.

(1) UCL Genetics Institute (UGI) pipeline

For the exomes which were annotated by Dr. Vincent Plagnol at UGI, the bioinformatics pipeline was described as following: FASTQ files were aligned to the hg19 reference sequence using Novoalign version 2.07.19, including hard and soft clipping, quality calibration and adapter trimming. Duplicate reads were excluded using the PICARD tool MarkDuplicates (http://picard.sourceforge.net/). Calling was performed using SAMtools v0.18 (http://samtools.sourceforge.net/) and single sample calling. The resulting calls were annotated with the software ANNOVAR. Candidate variants were typically filtered based on function: frameshift, premature stop, non-synonymous or potential splice altering variants (defined as being with 5 bp of the actual splice site) and frequency (< 0.5%in the 1,000 Genomes and NHLBI for homozygous and compound heterozygous variants, and absent from both of these databases for heterozygous variants). Variant Call Format (VCF) tools were used to annotate gene information for the remaining novel variants. The Integrative Genomics Viewer (IGV) was used to inspect variants.

Homozygosity mapping was performed based on the exome sequence data. An in-house R script that implemented a hidden Markov model with two hidden states was used. In the "homozygosity stretch" state, the proportion of heterozygous SNPs was set to 1%. In the "normal" state, the frequency of heterozygous SNPs was set to its exome-wide average. The most likely hidden chain of homozygosity states was reconstructed using a maximum likelihood Viterbi algorithm.

(2) UCL Institute of Neurology (ION) pipeline

For the exomes which were processed at ION, there were several steps involved in the read conversion to variant calling as following: 1) Initial base-calling with quality score generation was performed using the Illumina pipeline, 2) conversion of reads into Sanger format and 3) read trimming based on per lane quality score. Sequence was aligned against the human genome and converted into SAM files using BWA (http://bio-bwa.sourceforge.net/) and SAMTools. Building, indexing and sorting SAM files, recalibrating per base quality scores, removal of PCR duplicates, lane merging were performed when necessary by the use of BWA, SAMTools, Genomic Analysis Toolkit (GATK) (https://www.broadinstitute.org/gsa/wiki/index.php/TheGenomeAnalysisToolkit) and PICARD tool. Subsequently on target and per base coverage read statistics were generated based on NCBI consensus coding sequence project CCDS defined exom (http://www.ncbi.nlm.nih.gov/projects/CCDS/CcdsBrowse.cgi). Calling raw variants was performed using GATK and SAMTools, calling single nucleotide variants and short indels. IGV was used to inspect variants to check the sequencing depth and coverage. Variants were filtered based on quality control criteria and a genotype file was produced. Annotation and prediction of consequence (amino-acid change, predicted damage of variant) was conducted using the

package SIFT (Sorting Intolerant From Tolerant; http://sift.jcvi.org/) and PolyPhen2 (Polymorphism Phenotyping v2) prediction of functional effects of human nsSNPs; http://genetics.bwh.harvard.edu/pph2/).

2.6.4 Selecting and prioritizing variants

To distinguish genetic variations from true disease-causing mutations, a number of filtering strategies to prioritize variants were used as following:

(1) After total variants were generated, benign variants were filtered out by the following criteria: synonymous variants and any variant present at a global minor allele frequency (MAF) ≥ 1% in a range of publically available databases of sequence variation: dbSNP (www.ncbi.nlm.nih.gov/projects/SNP), 1000 Genomes Project (www.1000genomes.org), the National Heart, Lung, and Blood Institute Exome Sequencing Variant (ESV) database and the Genome Variant Database for Neuromuscular Diseases (NMD) (http://hihg.med.miami.edu/gvd-nmd/).

(2) Heterozygous or homozygous variants were selected according to the inheritance mode. If the inheritance is uncertain, all types of variants were included.

(3) Variants which were present in the genes located in known linkage and shared haplotype intervals from the literature were selected.

(4) Variants which were present in all patients of the same family (segregating with disease) or were present in multiple families and were absent in matched controls were selected.

(5) Variants in genes already known for related phenotypes were first considered. The gene list was based on PubMed (http://www.ncbi.nlm.nih.gov/pubmed), Washington University Neuromuscular Disease Center (WUNDC) Database (http://neuromuscular.wustl.edu/) and Inherited Peripheral Neuropathies Mutation (IPNMD) Database (http://www.molgen.ua.ac.be/cmtmutations/Mutations).

(6) If there was no candidate variants in the known genes, variants were prioritized by gene function and expression, mutation type, evidence from animal and cellular models. Variants which were highly expressed or had evidence of unique alternative splicing in the central or peripheral nerve system were selected. Variants which were present in genes causing associated phenotypes from known network pathways and known interactors were also picked. The following public genomic variant and in-house databases were used as reference:

Online Mendelian Inheritance in Man (OMIM) (www.omim.org/), (Search Tool for the Retrieval of Interacting Genes/Proteins (STRING) (http://string-db.org/), ESV, NMD, Tissue-specific Gene Expression and Regulation (TiGER) (http://bioinfo.wilmer.jhu.edu/tiger/) and HEX (hex.ion.ucl.ac.uk).

(7) The variants were expected to cluster in candidate genes and pathways and to overlap between cases with similar phenotypes. For cases with similar phenotype but without probable variants in the known genes, sequences were pooled together to look for any common mutated gene shared by more than one family.

(8) When variants in a candidate gene were identified, Sanger sequencing using the method described above was performed to confirm them. Variants would need to be confirmed with Sanger sequencing.

References:

Choi M, Scholl UI, Ji W, Liu T, Tikhonova IR, Zumbo P, Nayir A, Bakkaloglu A, Ozen S, Sanjad S, Nelson-Williams C, Farhi A, Mane S, Lifton RP (2009) Genetic diagnosis by whole exome capture and massively parallel DNA sequencing. Proc Natl Acad Sci U S A 106: 19096-101

den Dunnen JT, Antonarakis SE (2003) Mutation nomenclature. Curr Protoc Hum Genet Chapter 7: Unit 7.13. Review.

Chapter 3

Results: Genetic and functional studies in novel forms of inherited neuropathies and other inherited disorders

This chapter describes genetic and functional studies of four novel forms of inherited neuropathies and other inherited neurological disorders: 1) axonal neuropathy and optic atrophy due to a homozygous *C12orf65* mutation; 2) late-onset CMT2 due to the newly-identified *MARS* mutation; 3) hereditary sensory neuropathy type 1 due to a novel *SPTLC2* mutation; 4) juvenile complex autosomal cerebellar ataxia due to a novel *ADCK3* mutation. Genetic screening in various cohorts of patients was performed to investigate the mutation frequencies of these genes. Functional studies were also performed with the aim of providing further understanding of the pathogenesis of each mutation.

3.1 A novel *C12orf65* mutation in patients with axonal neuropathy and optic atrophy

3.1.1 Introduction

The association between CMT and optic atrophy, also known as CMT6 (OMIM_601152), has been reported in families with different modes of inheritance, comprising over 50 cases.(Chalmers et al. 1996; Chalmers et al. 1997; Ippel et al. 1995) Clinical features of CMT6 are distal weakness, wasting and sensory loss in the lower limbs associated with optic atrophy. *MFN2* mutations have been already described causing dominant forms of CMT6 (Zuchner et al. 2006) and *PRPS1* mutations have been linked to X-linked form of CMT6 (Kim et al. 2007), but homozygous mutations causing recessive form of the disease have never been identified. In this study a novel homozygous mutation c.346delG; p.Val116X [V116X]) in the chromosome 12 open reading frame 65 gene (*C12orf65*) was identified in a large consanguineous Gujerati family by the combination of WES and homozygosity mapping.(Tucci et al. 2014) Affected family members presented with axonal neuropathy, optic atrophy, mental retardation and pyramidal signs. The family was previously reported by MacDermot et al.1987 but the disease-causing gene was not identified at the time of publication.

C12orf65 encodes a 166-amino-acid mitochondrial matrix protein which is involved in the translation and assembly of the mitochondrial oxidative phosphorylation system (OXPHOS).(Antonicka et al. 2010) Before this study, three pathogenic *C12orf65* mutations have been documented causing defects in the translation and assembly of the mitochondrial OXPHOS, which was defined as combined oxidative phosphorylation deficiency 7 (COXPD7) (MIM_613559). Patients carrying these mutations presented with a wide range of phenotypes: from a severe early onset encephalomyopathy with respiratory failure to a slowly progressive spastic paraplegia with mild neuropathy and reduced vision (SPG55).(Antonicka et al. 2010; Shimazaki et al. 2012) The novel V116X mutation is associated with recessive axonal neuropathy associated with optic atrophy, a phenotype not previously reported in patients with *C12orf65* mutations. Segregation analysis and *C12orf65* screening in additional cohorts with a similar phenotype were performed to support the pathogenic role of this novel mutation. Levels of gene expression were measured to investigate whether the nonsense mutation resulted in mRNA decay. Mitochondrial function assays were performed to study functional impacts of this mutation.

3.1.2 Patients and methods

(1) *C12orf65* sequencing

DNAs from both parents of the index patient were sequenced for the coding exons of *C12orf65* (NM_001143905). Two series of patients were also screened for *C12orf65* mutation. The first

series included DNA extracted from blood of 93 patients who had axonal neuropathy with one of the following features: optic atrophy, retinitis pigmentosa, psychomotor retardation, cerebellar ataxia, or pyramidal sign (the neuropathy series). All these patients had been previously resulted negative for mutations in the *PMP22, GJB1, MFN2, MPZ, GDAP1, BSCL2, TRPV4, NEFL, HSPB1, HSPB8* and *GARS* genes. The second series was a collection of DNA extracted from muscles of 90 patients who presented a decreased activity of mitochondrial respiratory chain (MRC) complex V or combined oxidative phosphorylation enzymes deficiency in the blue native polyacrylamide gel electrophoresis (BN-PAGE) (the mitochondrial dysfunction series, kindly provided by the Neurometabolic Unit at the NHNN). Clinical presentations of patients in the second cohort included Leigh-like phenotype, neuropathy, cerebellar ataxia and/or optic atrophy.

(2) RNA purification and cDNA synthesis

Purification of total RNA from lymphoblasts of the index patient, her parents and two healthy controls was performed with the Qiagen miRNeasy Mini Kit (Hilden, Germany) according to the manufacturer's instructions. RNA concentration was then measured with spectrophotometer and quality was assessed evaluating 260/280 nm and 260/230 nm ratio. cDNA was synthesized from RNA by the use of Qiagen Omniscript RT Kit (Hilden, Germany). (The details of experiment method were described in Section 2.4)

(3) Reverse transcription and quantitative real-time PCR (RT-qPCR).

Multiplex quantitative real-time PCR assays for the cDNA / mRNA levels of *C12orf65* and the house-keeping gene *RPL13A* were performed using SYBR Green PCR Master Mix kit (Applied Biosystems) with a Corbett Rotor-Gene real-time quantitative thermal cycler (Corbett Research/Qiagen). Thermal cycling consisted of 10 minutes at 94℃ for initial denaturation and DNA polymerase activation, followed by 40 cycles of denaturation at 94℃ for 15 seconds and annealing/extension at 60℃ for 1 minute. All reactions were performed in triplicate in a final volume of 10 μl. Relative quantity of *C12orf65* level normalized by *RPL13A* level was then calculated. (The details of experiment method were described in Section 2.4)

(4) Lymphoblast cell cultures

Lymphoblast cells were obtained from Case 1 and two unaffected relative carriers. Lymphoblastoid cell lines were established by Epstein–Barr virus transformation of lymphocytes isolated from peripheral blood. Cell lines were stored at the European Collection of Cell Cultures. Informed consent was obtained for all samples. Patient and control lymphoblasts were thawed and maintained in culture in modified RPMI-1640 medium containing 300 mg/L L-Glutamine and HEPES (Invitrogen) supplemented with 10% heat-

inactivated Fetal Bovine Serum (FBS) (Invitrogen) at 37℃ and 5% CO_2 . Fresh medium was added every 3 days and cultures were expanded accordingly.

(5) Blue native in-gel complex V assay

The mitochondrial fraction was obtained from the lymphoblastoid cell pellets (7.5×10 5 cells) using two low-speed centrifugation steps (600 g×10 min) at 4℃, separated by a homogenization step. Then, the mitochondrial membranes were solubilised with a 750 mM amino hexanoic acid/50 mM Bis Tris buffer + 4% n-dodecyl β-D maltoside detergent. Samples were left on ice for 30 min and a further high spin (14000 g×10 min) was used to pellet insoluble material. An equal quantity of mitochondrial protein was loaded from each sample. Blue Native (BN) gel was run using a 3~12% Bis–Tris gel (Invitrogen) to ensure discrete separation of complex V. Complex V activity was measured in a reverse direction. Complex V assay was performed by incubating the gel overnight in stain containing 34 mM Tris, 270 mM glycine, 14 mM magnesium chloride, 6 mM lead (II) nitrate and 8 mM ATP.

(6) O_2 consumption

To measure mitochondrial respiration rate in intact cells, approximately 1×10^7 cells were suspended in respiration medium (HBSS with 10 mM D-glucose) in a Clark-type oxygen electrode thermostatically maintained at 37℃. The oxygen electrode was calibrated with air-saturated water, assuming 406 nmol O_2 atoms/mL at 37℃. Oxygen consumption was measured over 10 min with addition of oligomycin (final concentration 2 μg/mL) and trifluorocarbonylcyanide phenylhydrazone (FCCP) (0.5 μM). All data were obtained using an Oxygraph Plus System (Hansatech Instruments, UK) with chart recording software. For measurements of mitochondrial membrane potential (Δψm), cells were loaded with 25 nM tetramethylrhodaminemethylester (TMRM) for 30 min at room temperature in HBSS (156 mM NaCl, 3 mM KCl, 2 mM $MgSO_4$, 1.25 mM KH_2PO_4, 2 mM $CaCl_2$, 10 mM glucose and 10 mM HEPES, pH adjusted to 7.35), and the dye was present during the experiment. TMRM was used in the redistribution mode and therefore a reduction in TMRM fluorescence represents Δψm depolarisation. Z-stack images were obtained for accurate analysis. The values for wild-type (WT) were set to 100% and the other genotypes were expressed relative to WT. Confocal images were obtained using a Zeiss 710 LSM with a 40X oil immersion objective. TMRM was excited using the 560 nm laser and fluorescence was measured at 580 nm.

3.1.3 Results

(1) Clinical features

The pedigree of the family is shown in figure 3-1 (p84). Two brothers (Case 1 and 2) and their maternal cousin (Case 3) had axonal neuropathy, optic atrophy, mental retardation and

pyramidal signs with onset in the first 3 years of life.(MacDermot et al. 1987) The symptoms progressed very slowly and all patients were still able to walk in their 20s. Two other maternal cousins had isolated retinitis pigmentosa.

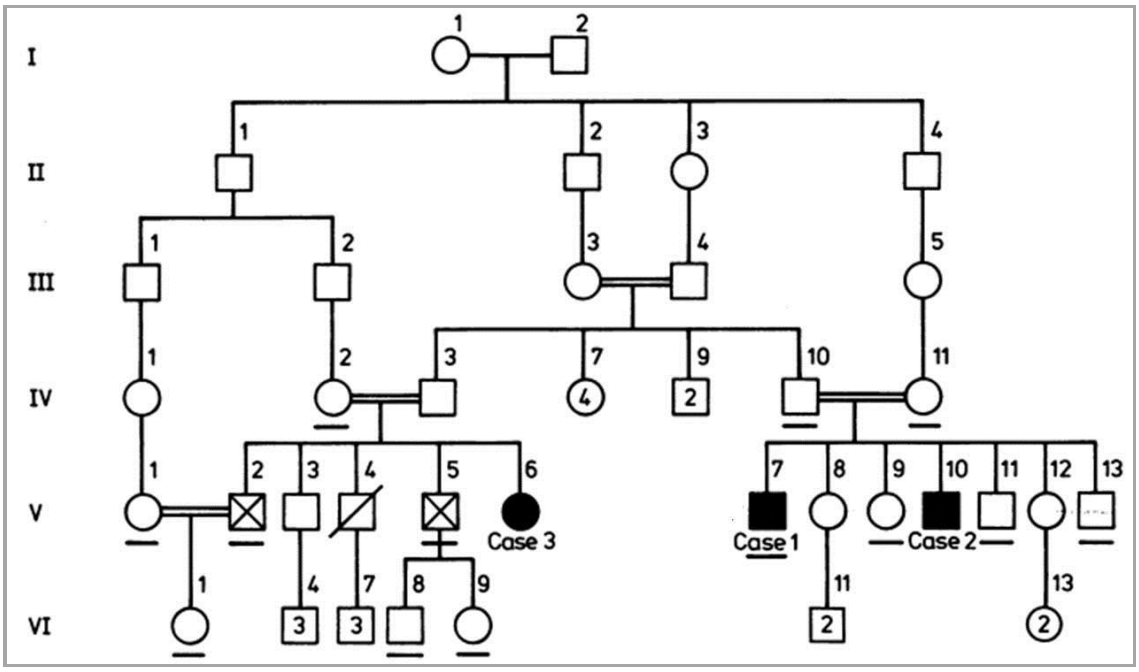

Figure 3-1. Pedigree of the family with *C12orf65* V116X mutation

Affected individuals of axonal neuropathy and optic atrophy are filled in black, ☒ = affected by retinitis pigmentosa, number in ☐ or ○ = number of unaffected siblings. __= examined family member. (modified from MacDermot et al, 1987)

WES was performed in Case 2 and Case 3 in order to establish the genetic diagnosis and detected a novel homozygous mutation c.346delG; p.Val116X [V116X]) in the *C12orf65* gene. Details of their clinical features are listed in table 3-1.

Table 3-1. Clinical features of patients with *C12orf65* V116X mutation

Patient	AAO/ ALE	Presenting symptom	Neuropathy	Eyes	Reflexes	Additional symptoms
Case2 (M)	3/30	delayed walking	wasting and weakness started in LL, and involving later UL	Bilateral optic atrophy with macular colloid bodies	Generalized brisk reflexes except absent ankle reflexes	Mental retardation, primary position and gaze induced nystagmus
Case 3 (F)	1/22	delayed walking	wasting and weakness started in LL, and involving later UL	Bilateral optic atrophy with macular colloid bodies	Normal UL, brisk knee and abductor reflexes, reduced ankle jerks	Mental retardation

AAO= age at onset; ALE= age of last exam; F= female; LL = lower limbs; M=male; UL = upper limbs.

Neurophysiology of the affected members showed reduced sensory action potentials (SAPs) in the lower limbs with preserved nerve conduction velocities (NCV), compatible with an axonal neuropathy (table 3-2).

Table 3-2. Nerve conduction studies of the patient with *C12orf65* V116X mutation

	Case 1	Case 2	Case 3	V-1	IV-II
CMAP (uV):					
Ulnar	NA	40	NA	NA	NA
SAP amplitude (uV):					
Median	10	NA	15	40	NA
Ulnar	6	NA	12	20	16
Sural	2	NA	5	NA	NA
MCV (m/s):					
Ulnar	41	46	51	54	60

CMAP = compound muscle action potentials; NA=not available; MCV= motor conduction velocity, recorded over abductor digiti minimi (Case 1, V-1 and IV-II) and flexor carpi ulnaris (Cases 2 and 3); SAP=sensory action potentials, median and ulnar SAPs were recorded from second and fifth fingers to wrist. (modified from Tucci et al.2014)

Sural nerve biopsy from Case 1 showed a marked reduction of large myelinated fibres and numerous small myelinated fibres, the majority of which were associated with regeneration clusters, consistent with axonal degeneration (figure 3-2, p86). The neuropathological findings were similar to previously described patients with documented *MFN2* mutation, another subtype of axonal CMT.

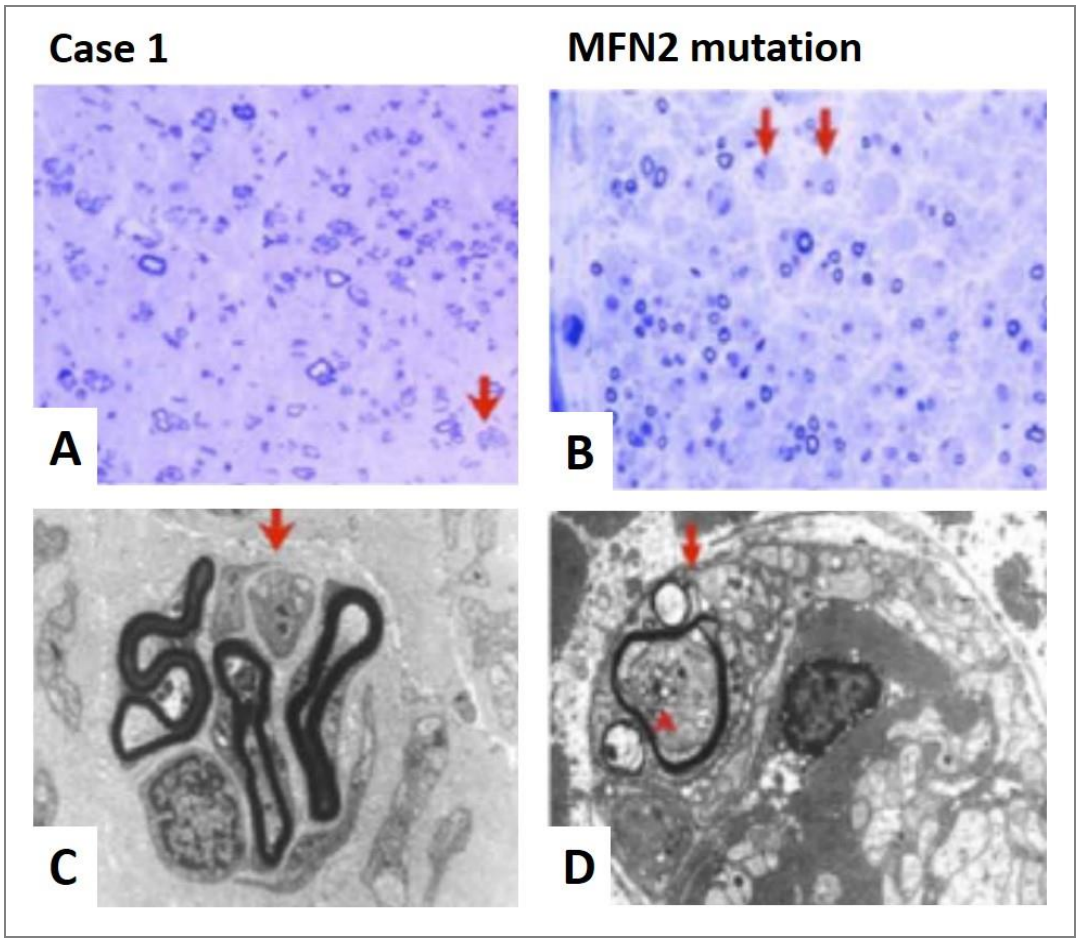

Figure 3-2. Sural nerve biopsy of the patient with C12orf65 V116X mutation

Semi-thin resin sections stained with toluidine blue show marked reduced numbers of large myelinated fibres in the sural nerve from Case 1 with the *C12orf65* V116X mutation **(A).** Numerous regeneration clusters of unmyelinated axons (red arrows) were also revealed and further highlighted by ultrastructure assessment **(C).** These above histological features were similar to those in a CMT2 patient with proved *MFN2* mutation **(B and D).**

(2) Mutation validation

Sanger sequencing validated that Case 2 and Case 3 shared a common homozygous 1bp deletion causing premature translational termination at the Val 116 codon of *C12orf65* (c.345delG; V116X). Both parents of Case 3 were heterozygous carriers of this mutation confirming segregation of the mutation within family (figure 3-3, p87).

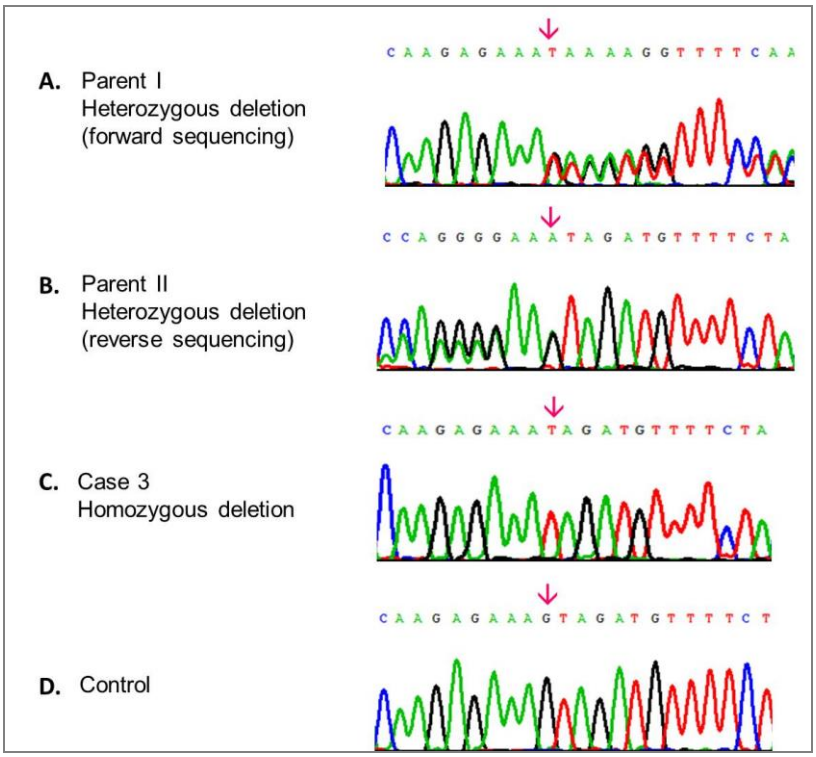

Figure 3-3. Segregation of *C12orf65* V116X mutation within the family

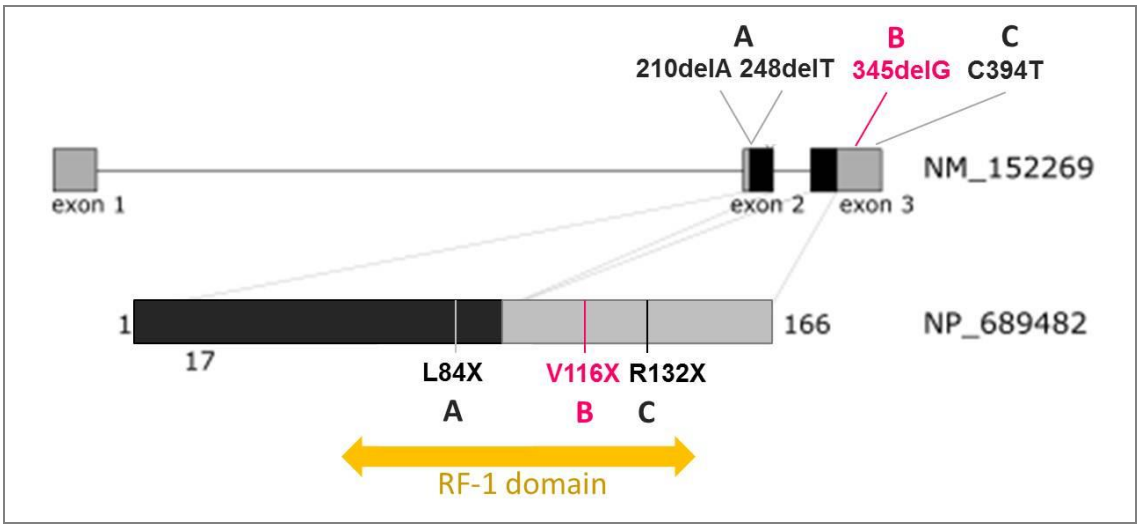

Figure 3-4. Genomic structure of *C12orf65* and the locations of its mutations

A. Both 210delA and 238delT cause stop gain at the same amino acid Leu84. They were identified from patients with a severe early encephalopathy.(Antonicka et al. 2010)

B. 345delG; V116X in exon 3 is associated with AR-CMT6 (this study, Tucci et al. 2014).

C. The missense mutation C394T leads to translational termination at the R132 codon and was associated with SPG55.(Shimazaki et al. 2012)

As shown in figure 3-4 (p87), V116X, similarly to three other previously reported *C12orf65* mutations, is a nonsense mutation. It is localized in the RF-1 domain, a highly conserved motif with peptidyl-tRNA hydrolase activity.(Song et al. 2000).

(3) Screening in additional cohorts

A total of 183 patients were screened for *C120rf65* mutations but no additional mutations were found except for one heterozygous synonymous mutation and two known SNPs which were identified in three patients (table 3-3).

Table 3-3. *C12orf65* variations identified in patients of the neuropathy series

cDNA	Codon	Variation type		SNP ID
c.G952A	Q103	Heterozygous	synonymous coding	.
c.C917T	I91	Heterozygous	synonymous coding	rs2280424
c.G688A	R15Q	Heterozygous	non-synonymous coding	rs78651634

(4) Gene expression study

The mRNA level of *C12orf65* in lymphoblasts from Case 3 was measured by multiplex qRT-PCR assays. There was no significant difference between the *C12orf65* mRNA levels of the patient, his parents and the control (figure 3-5). This documented that the nonsense mutation V116X did not induce mRNA nonsense-mediated decay.

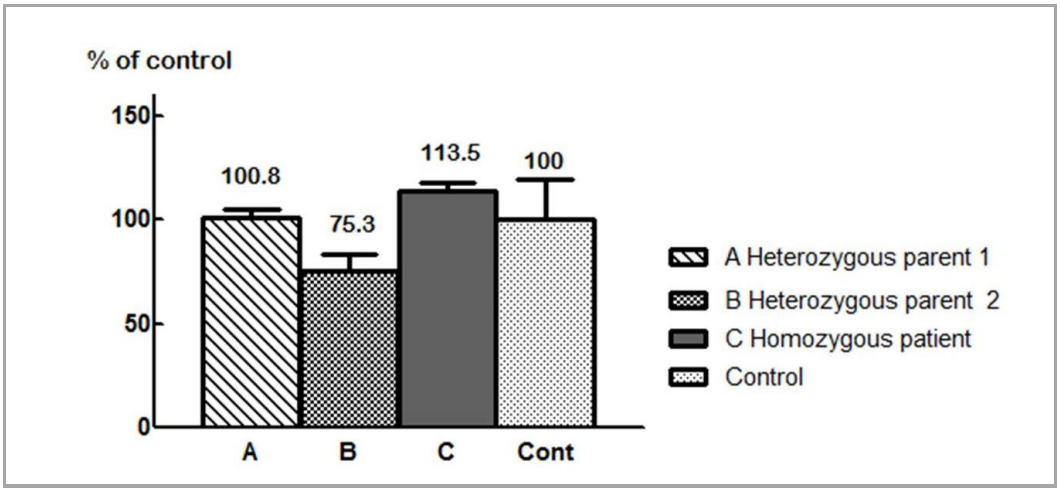

Figure 3-5. *C12orf65* mRNA levels in lymphoblasts

The bar graphs represented the relative *C12orf65* mRNA levels which were normalized to *RPL13A* levels and were shown as the percentage of the average in the control. There was no significant difference in *C12orf65* mRNA levels between all samples. Data are shown as means of 3 experiments, with error bars representing SDs. SDs were calculated using 1-way analysis of variance with Bonferroni multiple correction. Cont= control.

(4) MRC complex assembly

BN-PAGE was used to study the assembly pattern of MRC protein complexes and their in-gel activity of lymphoblasts. A significant decrease in the activity as well as an assembly defect in complex V were observed in cells from Case 3 when compared to cells from the control and the parents (figure 3-6, A, p90).

(5) Oxygen consumption

The rates of oxygen consumption in lymphoblasts were measured to investigate the effect of this mutation on mitochondrial respiration (figure 3-6, B). The rate basal oxygen consumption in cells from Case 3 was significantly reduced up to 49% compared with control cells ($p<0.001$). When Oligomycin (an inhibitor of MRC complex V) was added to inhibit the respiration coupled to oxidative phosphorylation, respiration was inhibited but to a significantly lesser extent in patient's cells compared with control cells ($p<0.001$). These findings provided evidence of profound mitochondrial uncoupling and confirmed decreased complex V activity in Case 3 cells. FCCP could uncouple the electron transport system from the oxidative phosphorylation system and accelerate respiration to maximal levels in control lymphocytes but to a significantly lesser degree in Case 3 cells, suggesting that the activity of respiratory chain enzymes in the patient's cells were limited.

(6) Mitochondrial membrane potential ($\Delta\psi m$)

$\Delta\psi m$ is a major indicator of mitochondrial function. $\Delta\psi m$ in Case 3 and control lymphoblasts were assessed by the fluorescent indicator TMRM. Mutant cells were associated with a significant reduction in the TMRM signal (and hence in $\Delta\psi m$) to $77.5\pm3.9\%$ compared with controls ($p<0.001$) (figure 3-6, C).

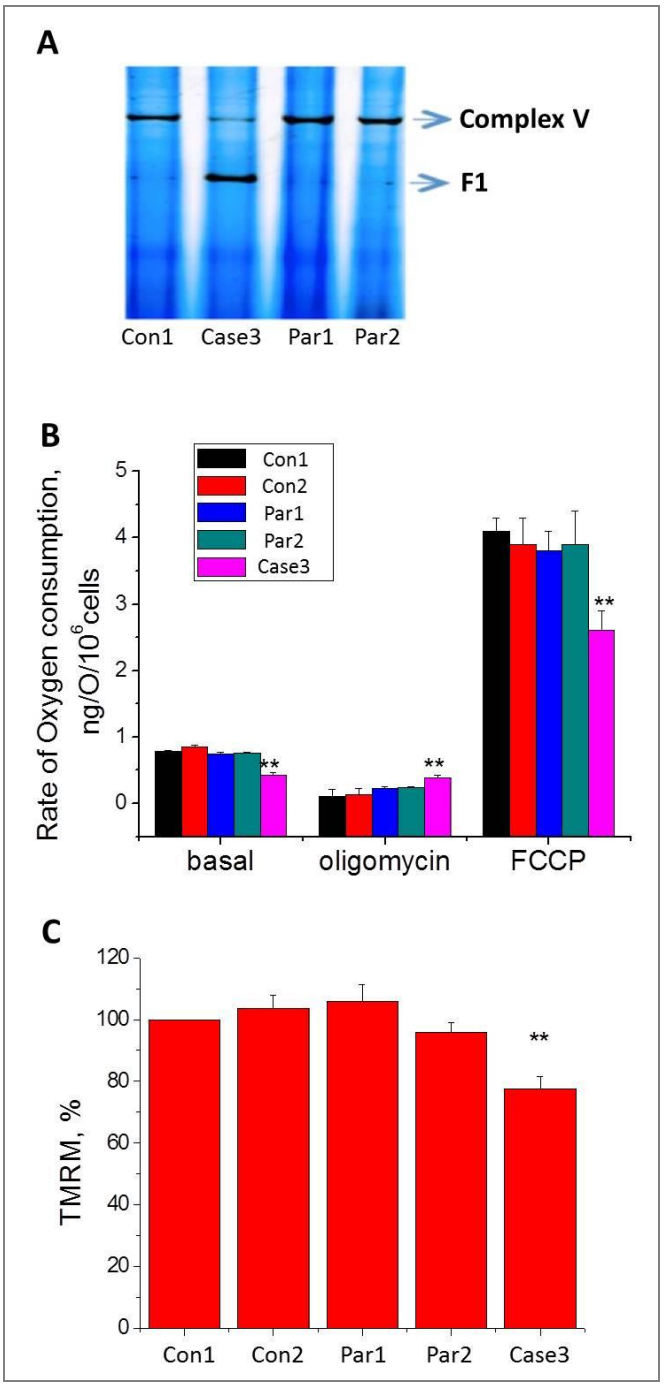

Figure 3-6. Mitochondrial function assays in lymphoblasts with *C12orf65* V116 mutation

A. Blue native polyacrylamide gel electrophoresis (in gel activity)
Reduced complex V activity in Case 3 is demonstrated by reduced band density. Complex V = complex V holoenzyme; F1 = catalytic site of complex V only.

B. Oxygen consumption rate (OCR)
Data are represented as mean ± SEM. The basal OCR in Case 3: 0.42±0.02 nmol/O2/min/106cells; n=4 experiments; the average OCR of Con1 and Con2: 0.85±0.03 nmol O2/min/106 cells; n=5 experiments ($p<0.001$). OCR in Case 3 was less inhibited by oligomycin (inhibitor of complex V; 2µg/m) and less accelerated by the FCCP (uncoupler of MRC; 1µM) as compared to controls ($p<0.001$).

C. Mitochondrial membrane potential (Δψm)
Δψm in lymphoblasts from control, parents and Case3 were determined by TMRM fluorescence. The TMRM signal representing Δψm in mutant cells was 77.5±3.9% of controls ($p<0.001$). n=3 experiments. Con= control; Par= parent; * = $p<0.05$; ** = $p<0.001$.

All the above experiments were performed double blindly. (The figure is modified from Tucci et al. 2014)

3.1.4 Discussion

This study describes for the first time a novel homozygous mutation in *C12orf65* gene in patients with recessive CMT6. Functional studies confirm that the nonsense mutation V116X could cause mitochondrial dysfunction. The multi-systemic involvement of PNS, CNS and non-neurological organs in the affected patients reflect the critical impacts of mitochondrial dysfunction which is caused by mutant *C12orf65*.

V116X in our family, similarly to other three pathogenic *C12orf65* mutations, leads to a premature translational termination in the RF-1 domain. Interestingly, these mutations were associated with various phenotypes. Both two homozygous mutations, c.248delT and c.210delA, caused premature termination at Leu84 and were associated with infantile subacute necrotizing encephalomyelopathy, also called Leigh syndrome, presenting with generalized psychomotor retardation, peripheral neuropathy and ventilator-dependent respiratory failure.(Antonicka et al. 2010) Another nonsense mutation (c.394C>T, p.R132X) was identified in patients with SPG55, a newly-defined recessive cHSP presenting with predominant spastic paraplegia in association with optic atrophy and axonal neuropathy.(Shimazaki et al. 2012) There seemed to be an inverse correlation between the severity of phenotype and the length of intact protein: the longer the preserved segment, the milder the phenotype (figure 3-4, p87).

C12orf65 mutations have been associated with different patterns of assembly defects in the subunit of mitochondrial OXPHOS. Whereas V116X mutation in this study caused defects in the MRC complex V only, other mutations resulted in multiple MRC complexes defects: complex I~IV in fibroblasts with L84X mutation and complexes I and IV in R132X mutant cells.(Antonicka et al. 2010; Shimazaki et al. 2012) We have documented that V116X did not cause disease through mRNA nonsense mediated decay, indicating that different segment of the protein may have distinct functions and variable impact on the stability of MRC complexes.

Several genes in which the mutations result in defects of the mitochondrial OXPHOS subunits or in mitochondrial dysfunction have been identified in peripheral neuropathy, suggesting a common pathway of nerve degeneration.(Diaz 2010) For example, *MFN2*, the major cause of AD-CMT2, is a mitochondrial membrane protein involved in mitochondrial fusion, the regulation of mitochondrial membrane potential and the OXPHOS.(Pich et al. 2005) Mutations in *GDAP1*, which encodes a mitochondrial membrane protein, can cause both dominant and recessive CMT2. Recently, mutations in the mitochondrial DNA encoded ATP synthase 6 gene (*MT-ATP6*, MIM_516060), encoding the ATP6 subunit of the mitochondrial OXPHOS complex V, were recognized to cause axonal type of CMT.(Pitceathly et al. 2012) The identification of *C12orf65* and *MT-ATP6* mutations suggested that complex V defects may have a key role in axonal degeneration of peripheral nerves though the detail is still not clear. In addition by confirming *C12orf65* as a new gene in AR-CMT6 and revealing its effects on the MRC complex, our results provided new insights on the pathogenesis of axonal neuropathy.

3.2 A significant variant in *MARS* may cause late-onset CMT2

3.2.1. Introduction

Despite the high number of genes identified in various forms of CMT2, many families are still genetically undiagnosed. During the past few years, WES has helped identifying several new genes causing CMT2.(Weedon et al. 2011; Weterman et al. 2012) For example using WES we identified a novel missense mutation [c.852C<T; p.Arg618Cys (R618C)] in the methionyl-tRNA synthetase gene (*MARS*) in a family with late onset CMT2 and incomplete penetrance. Following the identification of *MARS* as a possible new gene for CMT2, the screening of *MARS* in additional CMT2 patients was performed. Also, functional studies were conducted to investigate the pathogenicity of the identified mutation.

3.2.2 Patients and methods

(1) Mutation screening in the additional cohorts

Direct sequencing for all coding exons (exon 1-21) of *MARS (*NM_004990) was performed in 48 patients with a clinical diagnosis of AD-CMT2. Because of the incomplete penetrance of the identified mutation, exon 15 (where the mutation was localized) was also screened in further 140 patients with sporadic CMT2. In view of the frequent presence of pyramidal signs in patients carrying previously identified mutations in another aminoacyl-tRNA synthetase gene (*GARS)*, exon 15 was also sequenced in 140 patients with axonal neuropathy and pyramidal signs. Mutations of *GJB1*, *MFN2*, *MPZ*, *GDAP1*, *BSCL2*, *TRPV4*, *NEFL*, *HSPB1* and *HSPB8* genes had been excluded in these patients.

(2) Structural model of human MetRS

Structural model of human MARS encoding protein (MetRS) was generated by homology modeling based on the crystal structure of MetRS from archaea Pyrococcus abyssi (pdb 1RGG) using the Phyre2 server (www.sbg.bio.ic.ac.uk/phyre2/). Out of the total 900 residues of human MetRS, 576 residues that contain the catalytic domain (Residue 251-658) and the anticodon binding domain (Residue 659-806) were modeled. The N-terminal GST domain and the C-terminal WHEP domain are eukaryotic specific extensions and were omitted from the structural modeling.The model was verified manually by comparison with available crystal structures of MetRS from different species (pdb 1PG2, 2FMT and 1PFU).

(3) Cloning and mutagenesis

DNA constructs were generated using Gateway cloning technology (Invitrogen, Carlsbad, CA). The Saccharomyces cerevisiae MES1 locus (including the open reading frame and 783 base pairs of proximal promoter sequence and 321 base pairs of distal termination sequence) were

PCR amplified using Saccharomyces cerevisiae genomic DNA. The cloning primer was designed to include flanking Gateway attB1 (forward) and attB2 (reverse) sequences. Subsequently, purified MES1 PCR products were recombined into the pDONR221 vector and sequenced to yield appropriate entry clones. Mutagenesis of MES1 was performed using the QuikChange II XL Site-Directed Mutagenesis Kit (Agilent Technologies, Santa Clara, CA) and appropriate mutation-bearing oligonucleotides. Subsequently, plasmid DNA purified from each entry clone was subcloned into a gateway-compatible pRS315 or pRS316 destination vector according to the manufacturer's instructions. Each resulting expression construct was analyzed by restriction enzyme digestion with BsrGI (New England Biosystems, Ipswich, MA) to confirm the presence of an appropriately-sized insert.

(4) Yeast viability assays

To assess the functional consequences of *MARS* R618C variant in vivo, the variant was introduced in the yeast ortholog MES1. The ability to rescue deletion of endogenous MES1 was determined in wild-type MES1, an insert-free pRS315 construct, R618C MES1 and R727Q MES1 (a common variation, dbSNP rs113808165). Two independently generated mutant-bearing constructs were analysed. Cultures of each yeast strain were inoculated and grown on solid growth medium containing 5-FOA (Fluoroorotic Acid Monohydrate, Teknova, Hollister, CA). A commercially-available diploid heterozygous mes1Δ yeast strain (MATa/α, his3Δ1/his3Δ1, leu2Δ0/leu2Δ0, LYS2/lys2Δ0, met15Δ0/MET15, ura3Δ0/ura3Δ0; Open Biosystems, Huntsville, AL) was transformed with a URA3-bearing pRS316 vector containing wild-type MES1. Lithium acetate transformations were performed at 30℃ using 200 ng of plasmid DNA. Subsequently, sporulation and tetrad dissections were performed to yield a haploid mes1Δ strain that also contains the wild-type MES1 pRS316 maintenance vector. Two resulting haploid mes1Δ strains bearing a wild-type MES1 pRS316 maintenance vector were then transformed with LEU2-containing pRS315 constructs containing wild-type or mutant MES1 (described above). For each transformation, three colonies were selected for analysis on 0.1%5-FOA. Because 5-FOA is toxic to yeast cells bearing a functional URA3 allele, only cells that lost the URA3 maintenance plasmid and for which the LEU2 test plasmid could complement the chromosomal mes1Δ allele were expected to grow.

3.2.3 Results

(1) Clinical feature

The index case (figure 3-7, III.1, p94) had progressive sensory loss and weakness in the distal upper and lower limbs since the age of 50. He had also pain in his feet. Examination revealed bilateral foot drop, distal wasting in the upper and lower limbs, mild distal weakness in the upper limbs to Medical Research Council (MRC) scale grade 4. In the lower limbs he had equal

distal and proximal weakness with both hip flexion and ankle dorsiflexion and plantar flexion being grade 4. All sensory modalities were affected with impairment of pinprick and vibration sensation up to knees bilaterally. His maternal uncles had an axonal neuropathy with onset at age 67. His mother was clinically unaffected and had normal examination and neurophysiology at age 85. For the index patient, causes of acquired peripheral neuropathy were excluded and screening for mutations in the *MFN2, MPZ, PMP22, CX32, GDAP1, HSPB8, HSPB1, TRPV4* and *NEFL* genes were all negative.

(2) Genetic analysis

WES identified a variant R618 in *MARS* gene. The variant was a highly conserved amino acid residue in multiple species alignment (figure 3-7, B). The variant showed high conservation scores in other prediction softwares (GERP = 5.04, PhastCons =1) The strict conservation of the amino acid residue supported the pathogenic role of this variant. No further nucleotide variations in *MARS* were identified in 48 patients with AD-CMT2 or in the other two cohorts of patients (280 patients in total).

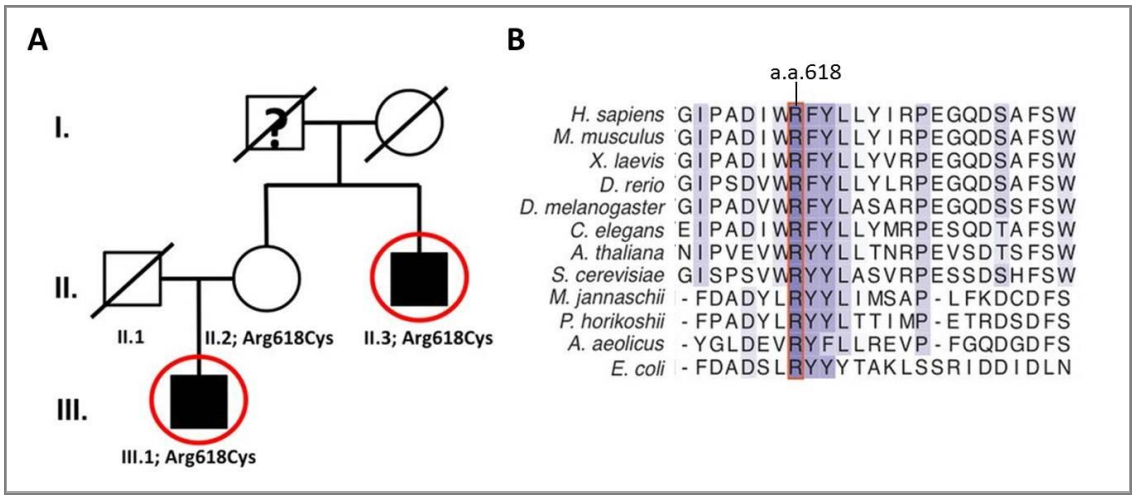

Figure 3-7. Pedigree of the family with *MARS* R618C mutation and conservation of the R618 codon

A. Pedigree of the dominant CMT2 family displaying segregation but incomplete segregation of R618C mutation. Two affected male individuals (III.1 and II.3) were analysed by WES (in red circles). The mother of the index patient, II.2, was an obligate carrier although she was clinically unaffected.

B. Sequence alignment of MetRS with multiple species showing that Arg618 is a strictly conserved residue.(modified from (Gonzalez et al. 2013)

(3) Structural change of mutant MetRS protein

In silico modeling of the core domains of human MetRS showed that R618 is located at the interface of the catalytic domain (Figure 3-8, A). Interactions with both domains suggest that R618 plays an important role in stabilising the domain interface. The R618C variation is predicted to create a disulfide bond and cause a neomorphic structural opening in the protein. The hypothetic structural opening may affect the tRNA aminoacylation function of *MARS*, which is essential for the translation process.

(4) Loss of function in mutant yeasts

Both R618C MES1 and the insert-free construct failed to rescue the MES1 allele, whereas wild type and R727Q MES1 were able to fully complement MES1 (Figure 3-8, B). The results confirmed that MES1 is an essential gene and suggested a loss-of-function effect caused by R618C variant.

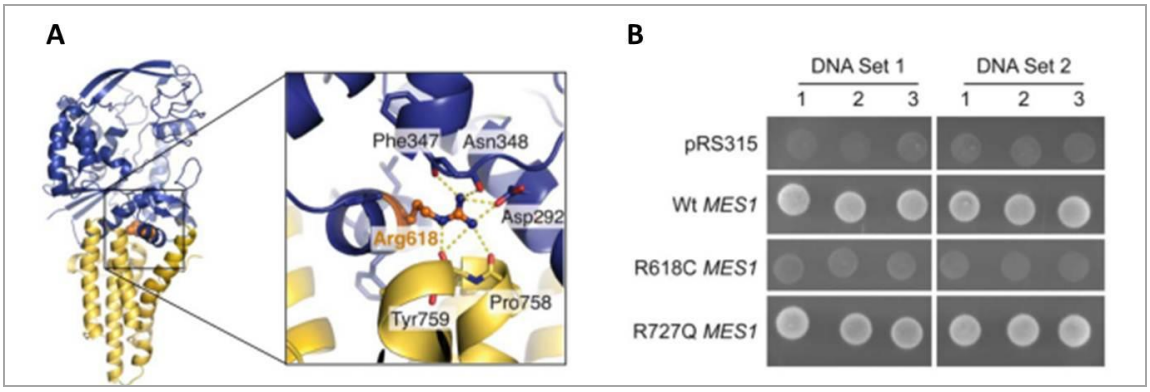

Figure 3-8. Structural and functional impacts of *MARS* R618C mutation

A. Structural model of human MetRS showed that Arg618 (R618) is localized at the interface of the catalytic domain (blue) and the anticodon-binding domain (yellow), with the guanidinium side chain forming a strong salt-bridge with the side chain of Asp292 from the catalytic domain, and extensive hydrogen-bonding interactions with the backbone carbonyl oxygens of Phe347 and Asn348 from the catalytic domain and of Pro758 and Tyr759 from the anticodon-binding domain.

B. Cultures of yeast strains previously transfected with a vector containing no insert (pRS315), wild-type MES1 (wt MES1) or the indicated variant form of MES1. Three representative cultures of each yeast strain were shown. Two independently generated mutant-bearing constructs were analysed (DNA Set 1 and DNA Set 2). (modified from Gonzalez et al. 2013)

3.2.4 Discussion

This study identified *MARS* R618C variation in a family with late-onset CMT2 and incomplete penetrance. Although this was the only family with CMT2 identified to carry *MARS* mutation, there are multiple lines of evidence supporting *MARS* as a novel rare CMT2 gene: (1)

segregation of this mutation with the phenotype in the family, (2) unusually strong conservation of the R618 codon across species, (3) a demonstrated loss-of-function effect of R618C variant, and (4) the negative screening results in a large cohort of CMT2 patients which ruled out the possibility that R618C is a rare ethnic polymorphism. The disease phenotype associated with *MARS* mutation is expanding. Following the identification of the CMT2 family in this study, compound heterozygous *MARS* mutations (F370L and I523T) in highly conserved regions were reported in a recessive family with infantile multi-organ complex including myopathy and seizure.(van Meel E et al. 2013) This report provides additional evidence that mutations in MARS can lead to a variety of clinical manifestations including the peripheral nervous system.

MARS encodes a member of aminoacyl-tRNA synthetases (ARSs), a family of enzymes that covalently attach transfer RNA (tRNA) and amino acids. Before *MARS*, mutations in five genes in the ARS family have been described to cause axonal forms of CMT or documented to be neurotoxic: glycyl-tRNA synthetase *(GARS),* tyrosyl-tRNA synthetase *(YARS),* alanyl-tRNA synthetase *(AARS),* lysyl-tRNA synthetase *(KARS)* and histidyl-tRNA synthetase (*HARS*).(Antonellis et al. 2003; Jordanova et al. 2003; Jordanova et al. 2006; Latour et al. 2010; Stum et al. 2010; Vester et al. 2013) The loss-of-function effect of *MARS* R618C in our family is similar to many other CMT-associated mutations in these ARS genes.(Antonellis et al. 2006; Jordanova et al. 2006; McLaughlin et al. 2010; Vester et al. 2013) Recently, DARS mutations have been identified in recessive neurologic phenotypes presenting with brain stem and spinal cord involvement and leg spasticity.(Taft et al. 2013) Interestingly, while these ARSs are ubiquitously expressed, these diseases are characterized by neurodegeneration and neuropathy. The increasing numbers of neuropathy-related variants in aminoacyl-tRNA synthetases genes implies that they may have nerve-specific roles in addition to the well-known ubiquitously expressed function.

In summary the genetic and functional studies for a late-onset CMT2 family suggest that *MARS* is a novel, yet very rare cause of the disease.

3.3 HSN type 1 caused by a novel *SPTLC2* mutation

3.3.1 Introduction

HSN type I (HSN-I) is clinically and genetically heterogeneous and includes all autosomal dominant forms of HSN. Two of the HSN-I genes encode the subunits of the serine palmitoyltransferase (SPT), a heteromeric enzyme composed of three subunits (SPTLC1~3) localized in the outer membrane of the endoplasmic reticulum.(Hanada 2003; Hornemann et al. 2006) *SPTLC1* encodes the first subunit of SPT and its mutations are the commonest cause of HSN-I in the British population accounting for 12% of cases.(Bejaoui et al. 2001; Davidson et al. 2012; Dawkins et al. 2001) Mutations in the second subunit (*SPTLC2)* were subsequently found in patients with a very similar phenotype.(Rotthier et al. 2010)

SPT catalyzes the first and rate limiting step in the de novo sphingolipid synthesis pathway: the condensation of L-serine and palmitoyl-CoA. Mutations in *SPTLC1* and *SPTLC2* can cause a shift in the substrate specificity of SPT leading to the alternative use of L-alanine and L-glycine over its canonical substrate L-serine.(Penno et al. 2010; Zitomer et al. 2009) This leads to the formation of probable neurotoxic 1-deoxysphingolipids (1-deoxySLs), which impedes the formation of complex sphingolipids but also their canonical degradation. Elevated 1-deoxySL levels have been found in the plasma and lymphoblasts of patients with HSN-I.(Penno et al. 2010; Rotthier et al. 2010)

In this study, *SPTLC2* was sequenced in a cohort of HSN patients and a novel *SPTLC2* mutation was identified in a family with ulceromutilating sensory-predominant neuropathy accompanied by early and severe motor involvement. The plasma level of 1-deoxySLs in patients and the biochemical properties of the mutant protein were also investigated.

3.3.2 Materials and methods

(1) Genetic sequencing

Nucleotide variants in all 12 exons and flanking introns of *SPTLC2* were screened in a cohort of 107 genetically undetermined HSN-I patients. Diagnosis was based on clinical phenotype and neurophysiology. These patients presented with distal progressive sensory loss, with or without ulceromutilating complications or autonomic dysfunction. Patients who had motor involvement were still included when the sensory features were predominant. All patients were negative for mutations in *SPTLC1* and the majority of patients were also negative for mutations in *RAB7, NGFB, FAM134B* and *NTRK1*.

(2) Cloning

The A182P was introduced into the *SPTLC2* cDNA by site-directed mutagenesis. All constructs were verified by sequencing. HEK293 cells (ATCC, Manassas, VA) were stably transfected with the empty vector (control), *SPTLC2* wild type (wt), or the A182P mutant. Expression of the constructs was confirmed by RT-PCR and immune blotting.

(3) Metabolic labeling assay

Transfected HEK293 cells were cultured in Dulbecco's modified Eagle medium for 3 days before medium was changed to Dulbecco's modified Eagle medium without L -serine (Genaxxon BioScience, Ulm, Germany). After 2 hours of preincubation, isotope-labeled (2,3,3-d 3 , 15 N) L -serine (1 mM) and (2,3,3,3)-d 4–labeled L -alanine (5 mM) (Cambridge Isotope Laboratories, Inc., Andover, MA) were added to the cells. In some cases, cells were treated with Fumonisin B1 (FB1) (35 mM). Cells were harvested after 24 hours, counted (Z2 Coulter Counter; Beckman Coulter, Brea, CA), and pelleted (800g, 5 minutes at 4℃). Pellets were stored at 220℃.

(4) SPT in vitro activity assay and lipid-base extraction

SPT in vitro activity was measured as described previously.(Rütti et al.2009) In modification to the original protocol, 64 mM L -serine or 320 mM L –alanine (Sigma, St. Louis, MO) was used.

(5) Acid-base extraction and analysis of sphingoid bases

The plasma sphingoid base levels of patients and healthy controls were analyzed after acid-base extraction as described before.(Penno et al. 2010) MetOH 500 mL including 200 pmol internal standard (d7-sphinganine and d7-sphingosine; Avanti Polar Lipids, Alabaster, AL) were added to 100 mL of plasma or frozen cell pellets which were resuspended in 100 mL phosphate-buffered saline. Lipid extraction was performed for 1 hour at 37℃ with constant agitation at 1,000 rpm (Thermomixer Comfort; Eppendorf, Hamburg, Germany). Precipitated protein was removed by centrifugation (5 minutes at 16,000g). After transferring the supernatant into a new tube, lipids were extracted and analyzed by liquid chromatography–mass spectrometry.

3.3.3 Results

(1) Genetic analysis

In the selected cohort, a novel mutation c.544G>C, p.Ala182Pro (A182P) was found in one British patient belonging to a four-generation family. The family had autosomal dominant inheritance. Segregation analysis revealed the mutation in the affected daughter (pedigree shown in figure 3-9, p99). The mutation was not detected in 358 British control chromosomes and PolyPhen2 and SIFT both predicted damaging and intolerable effects of the mutation.

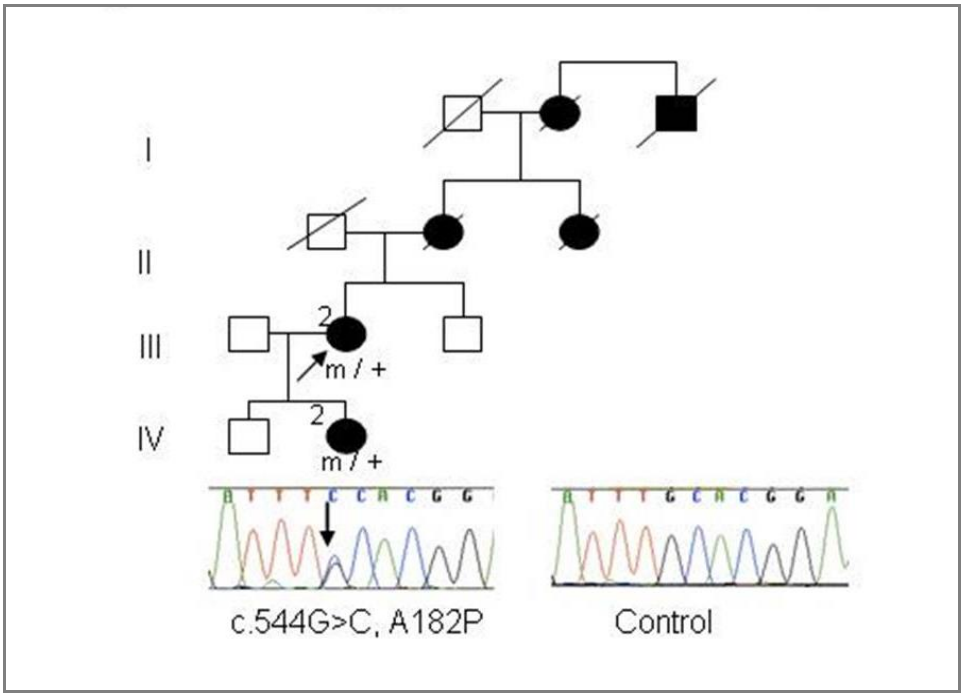

Figure 3-9. Pedigree of the family with *SPTLC2* A182P mutation

The chromatograms of affected patient and control are shown in the bottom. m/+: heterozygous mutation; arrow: proband. (cited from (Murphy et al. 2013)

(2) Clinical feature

In both affected individuals, the presenting symptoms were reduced sensation in the feet during the first decade. Sensory complications including ulcers and accidental burns developed later. Patient III-2 had painful tingling in the hands whereas IV-2 had no history of pain. Furthermore, they had marked motor involvement soon after the onset of sensory impairment. On examination, both had a glove-and-stocking sensory loss with pinprick appreciation more severely affected than vibration perception. They also had severe distal wasting and weakness in all four limbs. They did not report hearing loss or autonomic dysfunction. The clinical features are summarised in table 3-4 (p100).

Table 3-4. Clinical features of patients with *SPTLC2* A182P mutation

Patient	AAO/ ALE	Symptom at onset	Positive sensory symptoms	Sensory	Motor	Reflexes	CMTNS2
III-2 (F)	10/63	Numb feet	Painful tingling in hands	Vib to knees, pin above wrists and above knees	Severe distal UL and LL	Brisk UL, absent at ankles	25/36
IV-2 (F)	5/29	Numb feet	No	Vib to ankle, pin above elbow and above knee	Mild proximal and severe distal UL/severe distal LL	Brisk UL, reduced at ankles	27/36

F= female; AAO= age at onset; ALE= age of last exam; Vib = vibration; Pin= pinprick; UL = upper limbs; LL = lower limbs; CMTNS2 = Charcot- Marie-Tooth Neuropathy Score version 2. (Murphy et al. 2011)

Neurophysiology of the affected individuals is presented in table 3-5. Overall, NCS demonstrated a sensorimotor axonal neuropathy. SAPs were absent in the lower limbs and reduced or absent in the upper limbs. Motor responses were absent or reduced in the lower limbs and normal or reduced in the upper limbs. In patient III-2, mild slowing of MNCV with reasonable MAPs in the upper limbs were observed (<38 m/s).

Table 3-5. Neurophysiology of patients with *SPTLC2* A182P mutation

Patient	Median				Ulnar				Common peroneal			Sural
	DML ms	CV m/s	CMAP mV	SAP uV	DML ms	CV m/s	CMAP mV	SAP uV	DML ms	CV m/s	CMAP mV	SAP uV
III-2	3.5	32	4.5	NR	3.9	33	3.1	NR	NR	NR	NR	NR
IV-2	3.1	25	0.2	NR	3.1	29	0.3	NR	5.4	30	0.2	NR

DML = distal motor latency; CV = conduction velocity; CMAP = compound motor action potential; SAP = sensory action potential; ms = milliseconds; m/s = metres per second; mV = millivolts; uV = microvolts (modified from Murphy et al. 2013)

(3) Plasma sphingoid and deoxysphingoid base levels

Although total sphinganine (SA) or sphingosine (SO) levels showed no difference between *SPTLC2*-A182P patients and healthy controls (figure 3-10, A, p101), the 1-deoxySL levels were significantly elevated in the plasma of the two A182P carriers (figure 3-10, B). Also, the 1-deoxySL plasma levels were higher in patient IV-2 who was more severely affected (figure 3-10, B).

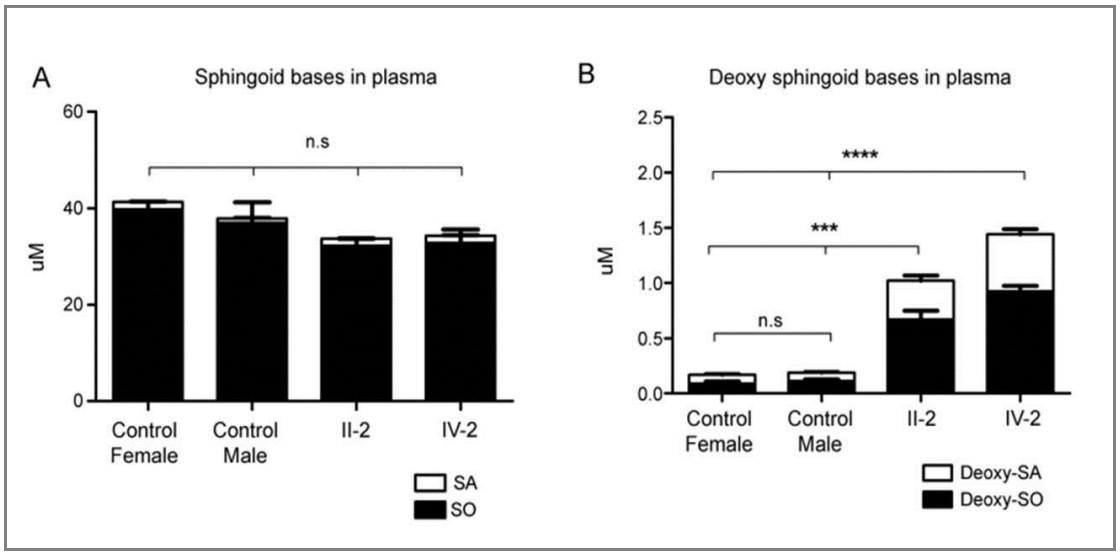

Figure 3-10. Plasma sphingoid and deoxysphingoid base levels of patients with *SPTLC2*-A182P mutation

A. There was no difference between the plasma levels of sphinganine (SA) or sphingosine (SO) of *SPTLC2*-A182P patients and healthy controls.

B. Significantly elevated 1-deoxysphingolipid levels were found in the two patients carrying *SPTLC2*-A182P mutation. Higher 1-deoxySL plasma levels were found in the more severely affected patient IV-2.

Data are represented as mean, with error bars representing SDs. SDs were calculated using 1-way analysis of variance with Bonferroni multiple correction. n.s.= not significant; SA= sphinganine; SO = sphingosine. ***p , 0.001; ****p , 0.0001. (cited from Murphy et al. 2013)

(4) Effect of the *SPTLC2*-A182P mutation on SPT activity

Two metabolic labeling assays checking the accumulation of SA, a measure for cellular SPT activity, confirmed that the *SPTLC2*-A182P expressing HEK293 cells showed significantly reduced activity with L -serine and increased activity with L -alanine. The first in vitro assay showed that the *SPTLC2* mutant had a 65% reduced activity with L-serine and a 3.5-fold increased activity with L-alanine in comparison with *SPTLC2*wt cells (figure 3-11, p102, A and B, p97). The second assay in which isotope-labelled (d_3, ^{15}N)L-serine (1 mM) and (d_4)L-alanine (5 mM) would lead to the formation of isotope-labeled (M+3)SA and (M+3)de-oxySA separately also revealed the same phenomenon (figure 3-11, C, p100).(Ikushiro et al. 2008)

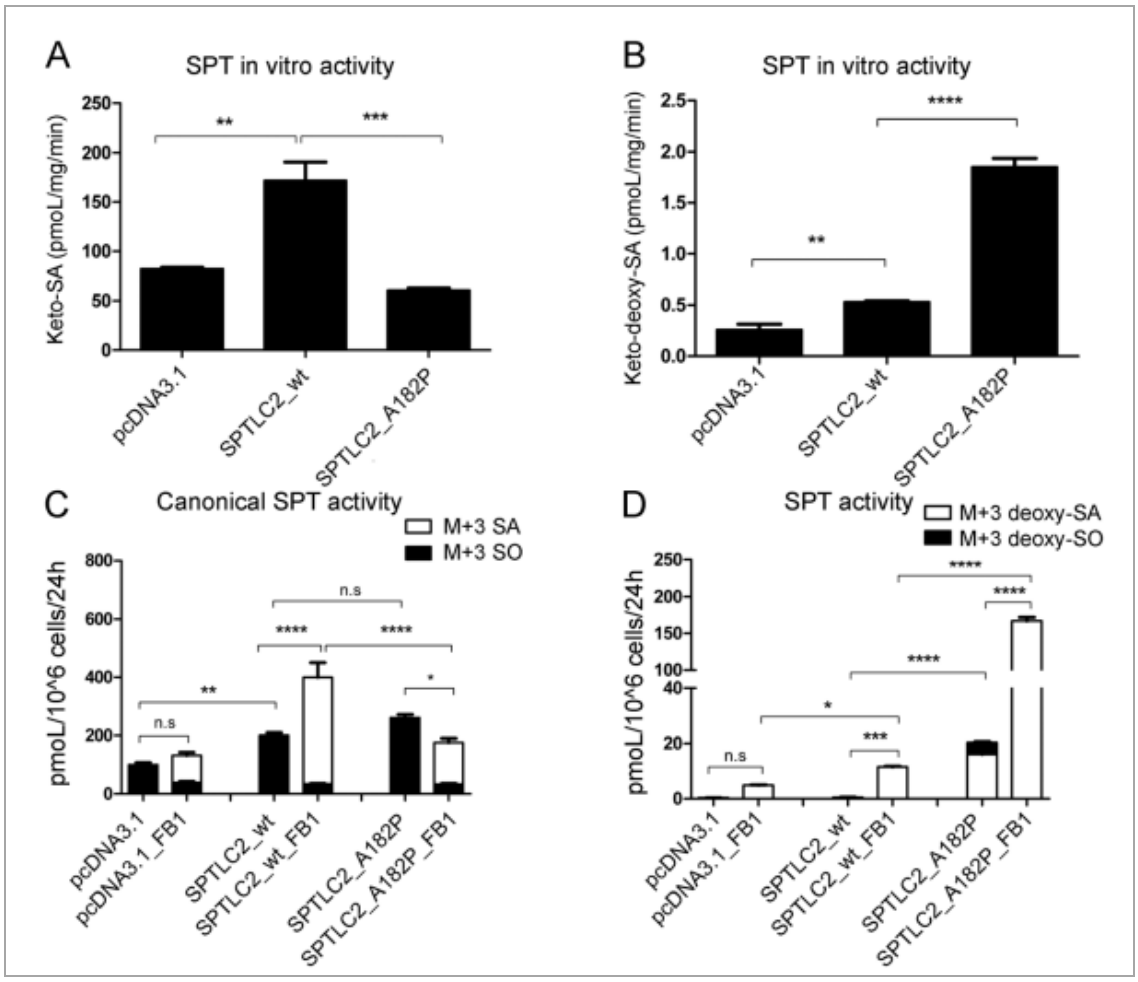

Figure 3-11. SPT activity of the *SPTLC2* A183P mutant cell

A. *In vitro* SPT activity with L-serine measured in 1 mg total protein lysate extracted from HEK293 cells. The A182P mutation leads to a significant decrease in keto-SA compared with the *SPTLC2*wt-expressing control ($p<0.001$).

B. *In vitro* SPT activity with L-alanine measured in 1 mg total protein lysate extracted from HEK293 cells. The A182P mutation leads to a significant increase in keto-deoxySA compared with the *SPTLC2*wt-expressing control ($p<0.0001$).

C. SPT activity measured in HEK293 cells. SPT activity in the *SPTLC2*wt is increased in the presence of FB1, whereas this increase is lost for the A182P mutant ($p<0.0001$). Without FB 1, SPT activity is not different between mutant and *SPTLC2*wt.

D. Generation of deoxySLs in HEK293 cells. The A182P mutation leads to a significant increase in deoxySL formation compared with *SPTLC2*wt cells ($p<0.0001$). In the presence of FB1, deoxySLs are also generated by SPTLC2wt cells ($p<0.001$), but the formation was significantly higher in the A182P cells ($p<0.0001$).

FB1 = Fumonisin B1; deoxy-SA = deoxysphinganine; deoxy-SO = deoxysphingosine; deoxySL = deoxysphingolipid; SA = sphinganine; SO = sphingosine; SPT = serine palmitoyltransferase; wt = wild-type. Data are shown as means, with error bars representing SDs. SDs were calculated using 1-way analysis of variance with Bonferroni multiple correction. n.s.= not significant; SA= sphinganine; SO = sphingosine. **p, 0.01; ***p, 0.001; ****p, 0.0001. (cited from Murphy et al. 2013)

The isotope-labelled assay was performed in the presence or absence of FB1, an inhibitor for ceramide synthase leading to the accumulation of SA, which is a measure for cellular SPT activity. In the absence of FB1, the sphingoid bases were mostly metabolized into (M+3) SO after acid hydrolysis (figure 3-11, C) whereas deoxySLs were predominantly present as (M+3) deoxySA (figure 3-11, D). In the presence of FB1, the *SPTLC2*wt cells showed a 2- to 3-fold higher accumulation of (M+3)SA and (M+3)deoxySA compared with controls (figure 3-11, C and D). In the A182P cells, the formation of (M+3)SA was reduced 2- to 3-fold (figure 3-11, C) whereas (M+3)deoxySA formation was 15-fold higher than in *SPTLC2*wt cells (figure 3-11, D).

3.3.4 Discussion

This study reports a novel A182P mutation in the *SPTLC2* gene identified from a dominant family and provides functional data demonstrating its pathogenic role. The age of onset in the affected patients was in the first decade, younger than is typically seen in HSN-I patients. To date, only three *SPTLC2* mutations have been described (V359M, G382V and I504F) and one of these has been also associated with onset in the first decade.(Rotthier et al. 2010) Patients developed significant motor involvement in the early stages of the disease, suggesting a wide phenotypic spectrum of *SPTLC2* mutations. Slowing of motor conduction velocities suggestive of demyelinating changes was noted in one of the patients, a finding which has been previously observed in patients with *SPTLC1* mutations.(Houlden et al. 2006)

In both A182P carrier, elevated serum 1-deoxySL levels were described confirming the pathogenicity of the mutation, and a higher level was found in the more severely affected daughter. The in vitro cell study and two metabolic labeling assays confirmed that the A182P mutant reduced significantly the SPT activity with L-serine and increased the activity with L-alanine. The combined genetic, clinical and functional data confirmed the association of this novel *SPTLC2* mutation with HSN-I. The findings confirmed the observation that other mutations in *SPTLC1* and *SPTLC2* genes are associated with reduced canonical activity and increased 1-deoxySL formation.(Bejaoui, Wu et al. 2001; Dawkins, Hulme et al. 2001; Houlden, King et al. 2006; Rotthier, Auer-Grumbach et al. 2010)

This study also supported the pathogenic role of 1-deoxySLs in HSN-I, indicating that it may be a metabolic disorder and 1-deoxySLs can be considered relevant biomarkers in HSN-I.

3.4 Autosomal recessive cerebellar ataxia caused by a novel *ADCK3* mutation

3.4.1 Introduction

Autosomal-recessive cerebellar ataxias (ARCAs) are a group of inherited neurodegenerative disorders characterised primarily by cerebellar ataxia, but are frequently associated with other neurological manifestations including spasticity, peripheral neuropathy, seizures and optic atrophy. ARCAs are genetically heterogeneous with more than 20 causative genes currently recognized.(Degardin et al. 2012; Jayadev et al.2013; Sailer et al.2012) Coenzyme Q10 (CoQ10) deficiency (MIM_607426) is one of the potentially treatable causes of ARCA as the symptoms in many patients improve with CoQ10 supplementation.(Emmanuele et al. 2013; Potgieter et al. 2013) CoQ10 is a lipid-soluble component located in the inner mitochondrial membrane. It plays a pivotal role in the OXPHOS by shuttling electrons derived from MRC complexes I [Nicotinamide adenine dinucleotide (NADH) ubiquinone oxidoreductase] and II (succinate ubiquinone oxidoreductase) to complex III (ubiquinol cytochrome c oxidoreductase) and also participates in other cellular processes as a potent antioxidant and by influencing pyrimidine metabolism.(DiMauro et al. 2007; Quinzii et al. 2010)

The AarF domain containing kinase 3 gene (*ADCK3*, MIM_606980) is one of the genes involved in the biosynthetic pathway of CoQ10 thus their mutations can cause CoQ10 deficiency where most mutations are loss of function. *ADCK3* is the homologue of the yeast Coq8 gene and encodes a mitochondrial protein which functions in an electron-transferring membrane protein complex in the MRC.(Lagier-Tourenne et al. 2008) Patients with *ADCK3* mutations usually have disease onset in infancy or early childhood and can present with pure cerebellar ataxia or a complex phenotype with additional features such as seizures, cognitive impairment, depression, peripheral neuropathy, strabismus or exercise intolerance.(Gerards et al. 2010; Horvath et al. 2012; Lagier-Tourenne et al. 2008; Mollet et al. 2008)

In this study, WES identified a homozygous frameshift mutation in *ADCK3* in a patient affected by cerebellar ataxia, myoclonus and dysarthria. This is a read-though mutation resulting in the loss of the stop codon and extension of the protein by 81 amino acids. CoQ10 level and the MRC enzyme activities in the index patient's fibroblasts were also investigated and CoQ10 supplementation was given to her based on the genetic and functional results.

3.4.2 Materials and methods

(1) Patients

The index patient and the affected siblings were examined and blood samples were obtained

after informed consent. A skin biopsy was also obtained from the index patient.

(2) Genetic analysis

WES was carried out on the index patient at the National Institutes of Health (NIH) (Bethesda, US). Nimblegen SeqCap EZ Exome kit (in solution capture) was used for the exome capture. Shotgun sequencing libraries were generated from 3 µg genomic DNA. Sequencing was performed on a Genome Analyzer IIx, according to the manufacturer's instruction. Sanger sequencing of exon 15 and the adjacent intronic junctions of the *ADCK3* gene (NM_020247) was performed in the index patient and the affected sibling to validate the identified variant (DNAs of the parents were unavailable).

(3) Cell culture

Primary fibroblasts were obtained from a skin biopsy from the index patient. The fibroblasts were cultured in Dulbecco's modified Eagle's medium (DMEM) GlutaMAX supplemented with 10% (v/v) heat-inactivated foetal bovine serum (FBS) and 1% (v/v) penicillin-streptomycin and they were maintained at 37oC, humidified and 5% CO2 in air.

(4) Quantification of CoQ10 levels

CoQ10 levels were quantified using a tandem mass spectrometer with a 2975 HPLC (Waters, Manchester, UK) as previously described.(Duberley et al. 2013) A hexane: ethanol (5:2, v/v) extraction was initially performed and the upper hexane layer was retained for analysis. Samples were re-suspended in 50:50 HPLC grade ethanol and methanol. Separation was achieved using a 3M Hypersil Gold C4 (150mm x 3mm, 3µm) with a Gold C4 guard column (3mm, 10mm length, 3µm) operated at 40℃ at a flow rate of 0.4ml/min. The mobile phases consisted of methanol, 4mM ammonium acetate 0.1% formic acid and methanol:isopropanol: formic acid (45:55:0.5, v/v/v) containing 5mM methylamine as an ion pair reagent. Isocratic delivery of the mobile phase ensured elution of the CoQ10 methylammonium adduct at approximately 8 minutes. D6-CoQ10 was used as an internal standard.

(5) MRC enzyme activities

Activities of MRC complex I, complex II-III , complex IV (cytochrome c oxidase) and citrate synthase (CS) were determined in the fibroblast cells according to methods previously described.(Hargreaves et al, 2006) Results were expressed as a ratio to CS activity and were normalized against protein. Protein quantification was determined using the Lowry method using bovine serum albumin as a standard.(Lowry et al.1951)

3.4.3 Results

(1) Clinical features

The proband was a 35-year-old lady who started experiencing myoclonus and jerky tremor in the head and limbs at the age of 10. In her second decade she developed slurred speech and unsteady gait. Symptoms did not respond to levodopa. By the age of 30, she became wheelchair dependent because of the ataxic myoclonic gait. She also had difficulty in writing and holding objects due to ataxia and involuntary movements. Her speech fatigued easily, was often tremulous and dysarthric and she also complained of muscle fatigue on exertion. One of the four siblings, had a similar presentation with myoclonus, tremor and unsteady gait with onset at age 14. Their parents were first cousins and were originally from Pakistan (pedigree shown in figure 3-12, B, p107).

Examination of the index case at the age of 35 showed cerebellar dysarthria with a tremulous quality to her speech. Eye movements were full with jerky pursuit, marked coarse tremor of the hands and head, which was both jerky and dystonic in nature. There was upper limb myoclonus and both upper and lower limb movements were uncoordinated when performing the finger nose task and the heel-knee-shin test. Her gait was ataxic and interrupted by frequent myoclonic jerks and she was unable to tandem walk. Her cognition and visual acuity were normal. She had symmetrical normal reflexes, flexor plantars, normal sensory examination and full muscle power. Her affected brother also had myoclonic movements, ataxic gait and dysarthria when examined at age 32.

Brain magnetic resonance imaging (MRI) of the index case at the age of 35 showed mild cerebellar atrophy which was consistent with previous reports of patients with *ADCK3* mutations. NCS and needle electromyography were normal. In both affected siblings, acquired causes of ataxia were excluded as well as Friedreich's ataxia, AOA1, AOA2, ataxia telangiectasia, early-onset primary dystonia (DYT1), Vitamin E-deficiency, Wilson's disease and SCA type 1-3.

(2) Genetic analysis

The process of variant prioritization is summarised in figure 3-12, A. A total of 17,240 exonic variants were identified in the index patient. According to the Consensus Coding Sequences hg19 definition of the exome, 92% of exome capture baits had at least 10× depth and 85% at least 30× depth. After excluding synonymous variants and those with MAF >1%, 78 coding variants remained. None of these variants were detected in genes known to be associated with ARCAs and related neurological disorders. A homozygous 1bp insertion in the *ADCK3* (NM_020247; c.1844_1845insG; p.Ser616Leufs*114) was identified (figure 3-12, C). The

variant was validated by Sanger sequencing. Genetic analysis of the affected brother documented the segregation of this variant within the family (figure 3-12, D).

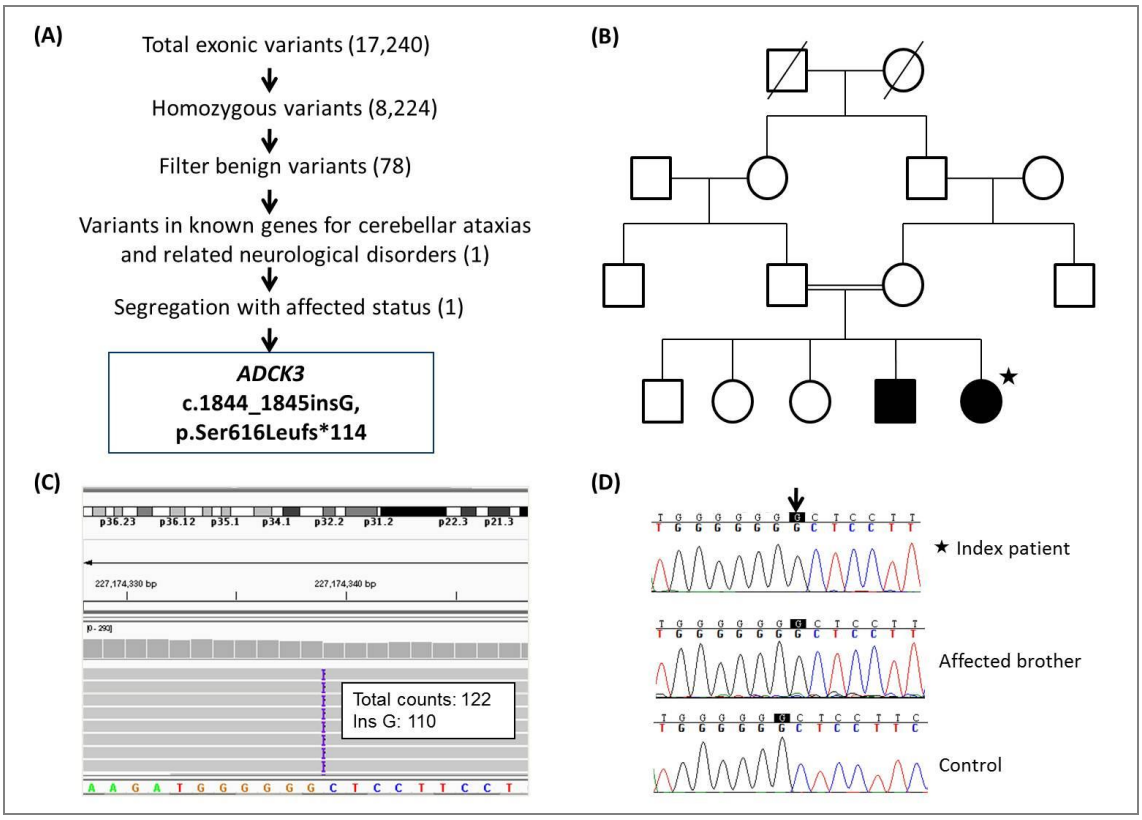

Figure 3-12. Genetic study and pedigree of the family with *ADCK3* S616Lfs mutation

(A) Filtering and prioritization of variants from WES in the index patient. The criteria of filters were described in Method (Secton 2.6.1)

(B) Pedigree of the family. The index patient is labelled with a black star. Based on the consanguinity, only homozygous variants were selected.

(C) A good sequence depth up to 122X and the homozygosity of the novel *ADCK3* mutation as the insertion G was detected in 110 of the total 122 counts were shown when inspected with the Integrative Genomics Viewer (IGV).

(D) Sanger sequencing validated the mutation and proved its segregation within the family. (Picture cited from Liu et al. 2014)

The genomic structure of the human *ADCK3* gene and mutations in this gene are illustrated in figure 3-13, A (p109). These mutations were classified by the patients' age of onset. The family described in this chapter is the second kindred of *ADCK3* mutation with a juvenile onset of disease (between 10 to 20 years) as only a single study has previously reported a family with compound heterozygous missense mutations in *ADCK3*: R271C and A304T.(Horvath et al. 2012) The novel frameshift mutation is localised to the C-terminal of *ADCK3* resulting in an alteration of several highly-conserved codons in the last coding exon. Furthermore, the frameshift is predicted to eliminate the original stop codon and allow translation to continue on

into the three prime untranslated region (3'UTR), extending the peptide by 81 amino acids (figure 3-13, B).

(3) CoQ10 level and MRC enzyme activity

The serum CoQ10 level of the patient was found to be within the normal range, however, the CoQ10 level in the patient's fibroblasts was low: 35% of the average CoQ10 level of controls. The assay of MRC enzymes in fibroblasts obtained from a skin biopsy from the index patient also revealed that the activities of complex I and complex II-III were significantly reduced as compared with controls. A decrease in complex II-III activity is compatible with CoQ10 deficiency, as the activity of this linked enzyme system is dependent upon endogenous CoQ10.(Rahman et al. 2001) Details of these analyses are shown in table 3-6.

Table 3-6. CoQ10 levels and the mitochondrial respiratory chain enzyme activities in the patient with *ADCK3* S616Lfs mutation

	Patient	**Control**	**P/C ratio**	**P value**
CoQ 10 levels (pmol/mg]				
in serum	43.00	37~133[#]	/	
in fibroblasts	**31.29**	89.3[§] (*n*=50)	**35.0%**	***p*<0.05**
MRC enzyme activity				
CI/CS	**0.15±0.167**	0.82±0.18 (*n*=3)	**18.3%**	***p*<0.05**
CII+CIII/CS	**0.046±0.03**	0.122±0.02 (*n*=3)	**37.7%**	***p*<0.05**
CIV/S	0.017±0.0052	0.015±0.004 (*n*=3)	113.3%	ns

P/C ratio, the ratio of patient's measurement to control value; **CI**, complex I (NADH ubiquinone oxidoreductase); **CII**, complex II (succinate ubiquinone oxidoreductase); **CIII**, complex III (ubiquinol cytochrome c oxidoreductase); **CIV**, complex IV (cytochrome c oxidase: EC 1.9.3.1); **CS**, citrate synthase; **MRC enzyme activity**, the mitochondrial respiratory chain enzyme activities assessed in patient's fibroblasts. Abnormal values are shown in bold. When experiments were done more than once, values are given as means± standard error of the mean. [#] From the diagnostic laboratory at National Hospital of Neurology and Neurosurgery, Queen Square, London, UK**.** [§]Reference range 57.0~121.6 pmol/mg, average 89.3 pmol/mg; Age: 20.75±1.4 years (range, 0.03~55 years); ratio of males to females, 2:3.(Duberley et al. 2013)

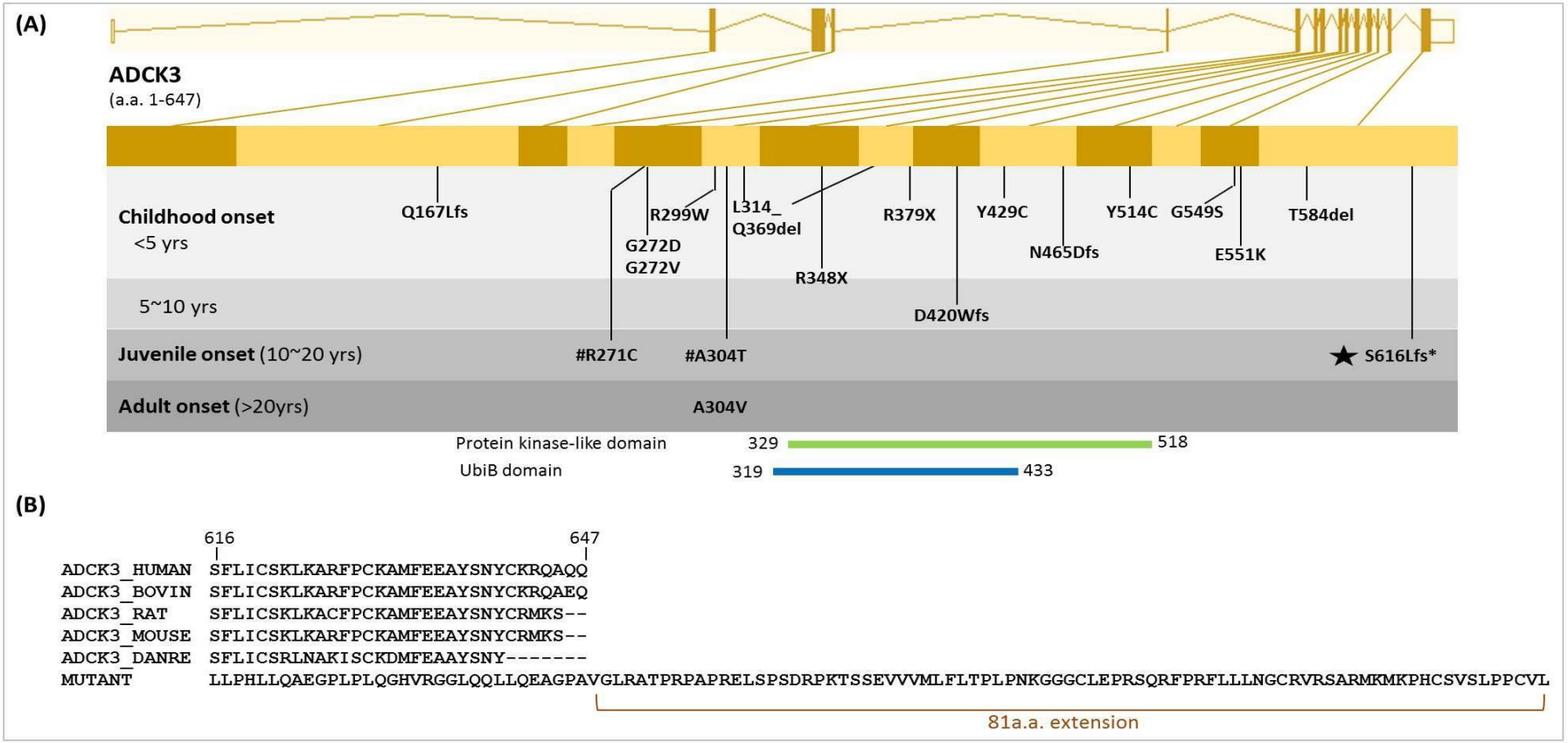

Figure 3-13. Genomic location of *ADCK3* S616Lfs mutation and the mutant peptide sequence

(A) Genomic structure of the human ADCK3 gene is shown. All *ADCK3* mutations reported in literature to date are shown in the gene and grouped by the average of patient's age of onset in each family. The novel mutation identified in this study is marked with a black star. #R271C and A304T are two compound heterozygous mutations detected within a previously reported family. D420Wfs, Q167Lfs,Y514C, T584del, L314_Q369del and G549S were reported in Lagier-Tourenne 2008. E551K, R213W, G272V, G272D and N465Dfs were reported in Mollet 2008. R348X, R348X and L379X were reported in Gerald 2010. R271C, A304T, A304V, R299W and Y429C were reported in Horvath 2012.

(B) Multiple species alignment shows this frameshift mutation changes several highly conserved amino acid codons in the terminal segment of *ADCK3* and eliminates the original stop codon thus extends the peptide by 81 amino acids. (the picture has been published in Liu et al. 2014)

(4) Treatment and outcome

Following the identification of primary CoQ10 deficiency in the index patient, CoQ10 replacement was initiated with a starting dose of 200mg bd. After 3 months of therapy, myoclonus dramatically improved whereby she was able to discontinue clonazepam which she had been taking for the previous 2 years to manage her frequent myoclonic jerking. The quality of her speech also improved and was less tremulous although she continued to have residual dysarthria. Self-reported symptoms of fatigue also improved.

These improvements were sustained when she was reviewed 6 months after initiation of CoQ10 replacement. There was subjective and objective improvement in her ataxia with a reduction in SARA (scale for the assessment and rating of ataxia) scores dropped from 17 to 13 (table 3-7).(Schmitz-Hubsch et al. 2006) Her affected sibling has also shown improvement in speech and fatigue after taking CoQ10 100mg twice daily for three months.

Table 3-7. SARA scores of the patient with *ADCK3* S616Lfs mutation before and after 6 months of CoQ10 supplement

SARA score	Before treatment	After 6 months of treatment
(1) Gait	4	3
(2) Stance	4	3
(3) Sitting	1	1
(4) Speech disturbance	1	1
(5) Finger chase*	2	1
(6) Nose-finger test*	2	1
(7) Fast alternating hand movements*	1.5	1.5
(8) Heel-shin slide*	1.5	1.5
Total	**17**	**13**

SARA (scale for the assessment and rating of ataxia) has eight items that yield a total score of 0 (no ataxia) to 40 (most severe ataxia): (1) Gait (score 0 to 8), (2) Stance (score 0 to 6), (3) Sitting: (score 0 to 4), (4) Speech disturbance (score 0 to 6), (5) finger chase (score 0 to 4), (6) nose-finger test (score 0 to 4), (7) fast alternating hand movements (score 0 to 4), (8) Heel-shin slide (score 0 to 4). *Limb kinetic functions (items 5 to 8) are rated independently for both sides, and the arithmetic mean of both sides is included in the SARA total score.

3.4.4 Discussion

In this study genetic and biochemical data were demonstrated in a family with a complex ataxia-myoclonus phenotype CoQ10 deficiency and abnormal MRC enzyme activities due to a novel frameshift mutation in the *ADCK3* gene and. One of the unusual features of this family was the onset in the second decade, which is later than most of previously reported cases with *ADCK3* mutations. Also, this family was affected with marked myoclonic-dystonic movements but relatively mild cerebellar ataxia, suggesting a wide phenotypic spectrum of *ADCK3* mutations.

To date, autosomal recessive mutations in *ADCK3* have only been identified in 22 patients from 13 families, and these mutations have been associated with clinically heterogeneous diseases.(Horvath et al. 2012) Patients usually present with a complex neurological phenotype, with cerebellar ataxia as the predominant manifestation.(Gerards et al. 2010; Horvath et al. 2012; Lagier-Tourenne et al. 2008; Mollet et al. 2008) In this family, cerebellar symptoms were relatively mild compared to the disabling myoclonus and involuntary movements which affected both siblings. This report shows that *ADCK3* mutations should be considered a potential cause of unexplained complex neurological syndromes even when cerebellar ataxia is not the predominant feature.

Unlike previous reports in which the majority of patients had the onset in their childhood or infancy (figure 3-13) (Gerards et al. 2010; Horvath et al. 2012; Lagier-Tourenne et al. 2008; Mollet et al. 2008), this is the second kindred with a juvenile onset providing further evidence that *ADCK3* mutations can cause complex cerebellar ataxia with a variable age of onset.

In our patient, the diagnosis of CoQ10 deficiency was confirmed biochemically by CoQ10 levels measured in fibroblasts. Significantly reduced activities of MRC enzymes were also observed in fibroblasts. CoQ10 measurement in muscle is the gold standard for diagnosis of CoQ10 deficiency as plasma concentrations of CoQ10 are not reliable and may be influenced by dietary factors.(Duberley et al. 2013) However, the measurement in muscle may be normal particularly when the deficiency is mild.(Emmanuele et al. 2013) Assessing CoQ10 levels in fibroblasts has been documented to be a reliable method to diagnose CoQ10 deficiency.(Duberley et al. 2013; Duncan et al. 2009; Hargreaves et al. 1999; Rahman et al. 2001) Therefore measuring CoQ10 levels in fibroblasts can be an alternative to muscle measurement.

CoQ10 replacement therapy resulted in subjective and objective improvement in patient symptoms and function. The most marked improvements were the reduction of myoclonus and

speech improvement although there were also improvements in ataxic symptoms as measured by the SARA scale. CoQ10 deficiency is one of the few treatable causes of ataxia and symptom improvement following replacement has been observed in a number of patients, although treatment protocols are yet to be standardized.(Emmanuele et al. 2013; Horvath 2012) There are few long-term studies however and it is not clear for how long these benefits might be sustained or if they alter the overall disease course.

ADCK3 mutations are very rare and the number of patients reported is still low. This is partly due to the nonspecific genotype-phenotype correlations of CoQ10-associated genes and the difficulty in screening all potentials genes in suspicious cases. CoQ10 deficiency is associated with clinically heterogeneous diseases, including cerebellar ataxia, encephalomyopathy, severe infantile multisystemic disease, nephropathy, myopathy and multiple-system atrophy, and the number of genes involved in the biosynthetic pathway for CoQ10 is increasing.(Emmanuele et al. 2013) In this study WES has been demonstrated to be a powerful tool to detect mutations in rare known genes, particularly in unexplained complex syndromes with high genetic heterogeneity. It is likely that the application of WES and other NGS technology will allow the identification of more patients with CoQ10 deficiency. The novel mutation identified in this study also provides new insights into the pathogenesis of *ADCK3* mutations. This is the first *ADCK3* mutation which results in the loss of the stop codon and translation into the UTR. CoQ10 deficiency and reduced respiratory enzymes activities in the patient's fibroblast confirmed the pathogenicity of this mutation. It is not yet clear through what mechanism the function of the protein is impaired by the extended C-terminal sequence. The elongated mutant protein may bear less structure stability and thus be incompetent to carry out its function in mitochondria and CoQ10 biosynthesis. However, given the relatively mild disease course, it is likely that some residual function remains.

In summary, this study extends the phenotypic spectrum of *ADCK3* mutations associated with ARCA. Mutations are not only restricted to childhood-onset ataxias, and other neurological features such as myoclonus may be prominent. This study also increases the understanding of genetic and functional effects of *ADCK3* mutations. The loss of a stop codon mutation identified in this gene suggests that the terminal segment of *ADCK3* may play an unknown but essential role in its normal function. The good response to treatment highlights the importance of identifying a potentially treatable cause, CoQ10 deficiency, in unexplained recessive cerebellar ataxia or ataxia-associated complex syndromes.

References

Antonellis A, Ellsworth RE, Sambuughin N, Puls I, Abel A, Lee-Lin SQ, Jordanova A, Kremensky I, Christodoulou K, Middleton LT, Sivakumar K, Ionasescu V, Funalot B, Vance JM, Goldfarb LG, Fischbeck KH, Green ED (2003) Glycyl tRNA synthetase mutations in Charcot-Marie-Tooth disease type 2D and distal spinal muscular atrophy type V. Am J Hum Genet 72: 1293-9

Antonellis A, Lee-Lin SQ, Wasterlain A, Leo P, Quezado M, Goldfarb LG, Myung K, Burgess S, Fischbeck KH, Green ED (2006) Functional analyses of glycyl-tRNA synthetase mutations suggest a key role for tRNA-charging enzymes in peripheral axons. J Neurosci 26: 10397-406

Antonicka H, Ostergaard E, Sasarman F, Weraarpachai W, Wibrand F, Pedersen AM, Rodenburg RJ, van der Knaap MS, Smeitink JA, Chrzanowska-Lightowlers ZM, Shoubridge EA (2010) Mutations in C12orf65 in patients with encephalomyopathy and a mitochondrial translation defect. Am J Hum Genet 87: 115-22

Bejaoui K, Wu C, Scheffler MD, Haan G, Ashby P, Wu L, de Jong P, Brown RH, Jr. (2001) SPTLC1 is mutated in hereditary sensory neuropathy, type 1. Nat Genet 27: 261-2

Chalmers RM, Bird AC, Harding AE (1996) Autosomal dominant optic atrophy with asymptomatic peripheral neuropathy. J Neurol Neurosurg Psychiatry 60: 195-6

Chalmers RM, Riordan-Eva P, Wood NW (1997) Autosomal recessive inheritance of hereditary motor and sensory neuropathy with optic atrophy. J Neurol Neurosurg Psychiatry 62: 385-7

Davidson GL, Murphy SM, Polke JM, Laura M, Salih MA, Muntoni F, Blake J, Brandner S, Davies N, Horvath R, Price S, Donaghy M, Roberts M, Foulds N, Ramdharry G, Soler D, Lunn MP, Manji H, Davis MB, Houlden H, Reilly MM (2012) Frequency of mutations in the genes associated with hereditary sensory and autonomic neuropathy in a UK cohort. J Neurol

Dawkins JL, Hulme DJ, Brahmbhatt SB, Auer-Grumbach M, Nicholson GA (2001) Mutations in SPTLC1, encoding serine palmitoyltransferase, long chain base subunit-1, cause hereditary sensory neuropathy type I. Nat Genet 27: 309-12

Degardin A, Dobbelaere D, Vuillaume I, Defoort-Dhellemmes S, Hurtevent JF, Sablonniere B, Destee A, Defebvre L, Devos D (2012) Spinocerebellar ataxia: a rational approach to aetiological diagnosis. Cerebellum 11: 289-99

Diaz F (2010) Cytochrome c oxidase deficiency: patients and animal models. Biochim Biophys Acta 1802: 100-10

DiMauro S, Quinzii CM, Hirano M (2007) Mutations in coenzyme Q10 biosynthetic genes. J Clin Invest 117: 587-9

Duberley KE, Hargreaves IP, Chaiwatanasirikul KA, Heales SJ, Land JM, Rahman S, Mills K, Eaton S (2013) Coenzyme Q10 quantification in muscle, fibroblasts and cerebrospinal fluid by liquid chromatography/tandem mass spectrometry using a novel deuterated internal standard. Rapid Commun Mass Spectrom 27: 924-30

Duncan AJ, Bitner-Glindzicz M, Meunier B, Costello H, Hargreaves IP, Lopez LC, Hirano M, Quinzii CM, Sadowski MI, Hardy J, Singleton A, Clayton PT, Rahman S (2009) A nonsense mutation in COQ9 causes autosomal-recessive neonatal-onset primary coenzyme Q10 deficiency: a potentially

treatable form of mitochondrial disease. Am J Hum Genet 84: 558-66

Emmanuele V, Lopez LC, Berardo A, Naini A, Tadesse S, Wen B, D'Agostino E, Solomon M, DiMauro S, Quinzii C, Hirano M (2013) Heterogeneity of coenzyme Q10 deficiency: patient study and literature review. Arch Neurol 69: 978-83

Gerards M, van den Bosch B, Calis C, Schoonderwoerd K, van Engelen K, Tijssen M, de Coo R, van der Kooi A, Smeets H (2010) Nonsense mutations in CABC1/ADCK3 cause progressive cerebellar ataxia and atrophy. Mitochondrion 10: 510-5

Gonzalez M, McLaughlin H, Houlden H, Guo M, Liu YT, Hadjivassilious M, Speziani F, Yang XL, Antonellis A, Reilly MM, Zuchner S (2013) Exome sequencing identifies a significant variant in methionyl-tRNA synthetase (MARS) in a family with late-onset CMT2. J Neurol Neurosurg Psychiatry 84(11):1247-9

Hanada K (2003) Serine palmitoyltransferase, a key enzyme of sphingolipid metabolism. Biochim Biophys Acta 1632: 16-30

Hargreaves IP, Heales SJ, Land JM (1999) Mitochondrial respiratory chain defects are not accompanied by an increase in the activities of lactate dehydrogenase or manganese superoxide dismutase in paediatric skeletal muscle biopsies. J Inherit Metab Dis 22: 925-31

Hornemann T, Richard S, Rutti MF, Wei Y, von Eckardstein A (2006) Cloning and initial characterization of a new subunit for mammalian serine-palmitoyltransferase. J Biol Chem 281: 37275-81

Horvath R (2012) Update on clinical aspects and treatment of selected vitamin-responsive disorders II (riboflavin and CoQ 10). J Inherit Metab Dis 35: 679-87

Horvath R, Czermin B, Gulati S, Demuth S, Houge G, Pyle A, Dineiger C, Blakely EL, Hassani A, Foley C, Brodhun M, Storm K, Kirschner J, Gorman GS, Lochmuller H, Holinski-Feder E, Taylor RW, Chinnery PF (2012) Adult-onset cerebellar ataxia due to mutations in CABC1/ADCK3. J Neurol Neurosurg Psychiatry 83: 174-8

Houlden H, King R, Blake J, Groves M, Love S, Woodward C, Hammans S, Nicoll J, Lennox G, O'Donovan DG, Gabriel C, Thomas PK, Reilly MM (2006) Clinical, pathological and genetic characterization of hereditary sensory and autonomic neuropathy type 1 (HSAN I). Brain 129: 411-25

Ikushiro H, Fujii S, Shiraiwa Y, Hayashi H (2008) Acceleration of the substrate Calpha deprotonation by an analogue of the second substrate palmitoyl-CoA in Serine Palmitoyltransferase. J Biol Chem 283: 7542-53

Ippel EF, Wittebol-Post D, Jennekens FG, Bijlsma JB (1995) Genetic heterogeneity of hereditary motor and sensory neuropathy type VI. J Child Neurol 10: 459-63

Jayadev S, Bird TD (2013) Hereditary ataxias: overview. Genet Med 15(9):673-83

Jordanova A, Irobi J, Thomas FP, Van Dijck P, Meerschaert K, Dewil M, Dierick I, Jacobs A, De Vriendt E, Guergueltcheva V, Rao CV, Tournev I, Gondim FA, D'Hooghe M, Van Gerwen V, Callaerts P, Van Den Bosch L, Timmermans JP, Robberecht W, Gettemans J, Thevelein JM, De Jonghe P, Kremensky I, Timmerman V (2006) Disrupted function and axonal distribution of mutant tyrosyl-tRNA synthetase in dominant intermediate Charcot-Marie-Tooth neuropathy. Nat Genet 38: 197-202

Kim HJ, Sohn KM, Shy ME, Krajewski KM, Hwang M, Park JH, Jang SY, Won HH, Choi BO, Hong SH,

Kim BJ, Suh YL, Ki CS, Lee SY, Kim SH, Kim JW (2007) Mutations in PRPS1, which encodes the phosphoribosyl pyrophosphate synthetase enzyme critical for nucleotide biosynthesis, cause hereditary peripheral neuropathy with hearing loss and optic neuropathy (cmtx5). Am J Hum Genet 81: 552-8

Lagier-Tourenne C, Tazir M, Lopez LC, Quinzii CM, Assoum M, Drouot N, Busso C, Makri S, Ali-Pacha L, Benhassine T, Anheim M, Lynch DR, Thibault C, Plewniak F, Bianchetti L, Tranchant C, Poch O, DiMauro S, Mandel JL, Barros MH, Hirano M, Koenig M (2008) ADCK3, an ancestral kinase, is mutated in a form of recessive ataxia associated with coenzyme Q10 deficiency. Am J Hum Genet 82: 661-72

Latour P, Thauvin-Robinet C, Baudelet-Mery C, Soichot P, Cusin V, Faivre L, Locatelli MC, Mayencon M, Sarcey A, Broussolle E, Camu W, David A, Rousson R (2010) A major determinant for binding and aminoacylation of tRNA(Ala) in cytoplasmic Alanyl-tRNA synthetase is mutated in dominant axonal Charcot-Marie-Tooth disease. Am J Hum Genet 86: 77-82

Liu YT, Hersheson J, Plagnol V, Fawcett K, Duberley KE, Preza E, Hargreaves IP, Chalasani A, Laura M, Wood NW, Reilly MM, Houlden H (2014) Autosomal-recessive cerebellar ataxia caused by a novel ADCK3 mutation that elongates the protein: clinical, genetic and biochemical characterisation. J Neurol Neurosurg Psychiatry 85(5):493-8.

Lowry OH, Rosebrough NJ, Farr AL, Randall RJ (1951) Protein measurement with the Folin phenol reagent. J Biol Chem 193:265-75

MacDermot KD, Walker RW (1987) Autosomal recessive hereditary motor and sensory neuropathy with mental retardation, optic atrophy and pyramidal signs. J Neurol Neurosurg Psychiatry 50: 1342-7

McLaughlin HM, Sakaguchi R, Liu C, Igarashi T, Pehlivan D, Chu K, Iyer R, Cruz P, Cherukuri PF, Hansen NF, Mullikin JC, Biesecker LG, Wilson TE, Ionasescu V, Nicholson G, Searby C, Talbot K, Vance JM, Zuchner S, Szigeti K, Lupski JR, Hou YM, Green ED, Antonellis A (2010) Compound heterozygosity for loss-of-function lysyl-tRNA synthetase mutations in a patient with peripheral neuropathy. Am J Hum Genet 87: 560-6

Mollet J, Delahodde A, Serre V, Chretien D, Schlemmer D, Lombes A, Boddaert N, Desguerre I, de Lonlay P, de Baulny HO, Munnich A, Rotig A (2008) CABC1 gene mutations cause ubiquinone deficiency with cerebellar ataxia and seizures. Am J Hum Genet 82: 623-30

Murphy SM, Ernst D, Wei Y, Laura M, Liu YT, Polke J, Blake J, Winer J, Houlden H, Hornemann T, Reilly MM (2013) Hereditary sensory and autonomic neuropathy type 1 (HSANI) caused by a novel mutation in SPTLC2. Neurology Epub May 8.

Murphy SM, Herrmann DN, McDermott MP, Scherer SS, Shy ME, Reilly MM, Pareyson D (2011) Reliability of the CMT neuropathy score (second version) in Charcot-Marie-Tooth disease. J Peripher Nerv Syst 16: 191-8

Penno A, Reilly MM, Houlden H, Laura M, Rentsch K, Niederkofler V, Stoeckli ET, Nicholson G, Eichler F, Brown RH, Jr., von Eckardstein A, Hornemann T (2010) Hereditary sensory neuropathy type 1 is caused by the accumulation of two neurotoxic sphingolipids. J Biol Chem 285: 11178-87

Pich S, Bach D, Briones P, Liesa M, Camps M, Testar X, Palacin M, Zorzano A (2005) The Charcot-Marie-Tooth type 2A gene product, Mfn2, up-regulates fuel oxidation through expression of

OXPHOS system. Hum Mol Genet 14: 1405-15

Pitceathly RD, Murphy SM, Cottenie E, Chalasani A, Sweeney MG, Woodward C, Mudanohwo EE, Hargreaves I, Heales S, Land J, Holton JL, Houlden H, Blake J, Champion M, Flinter F, Robb SA, Page R, Rose M, Palace J, Crowe C, Longman C, Lunn MP, Rahman S, Reilly MM, Hanna MG (2012) Genetic dysfunction of MT-ATP6 causes axonal Charcot-Marie-Tooth disease. Neurology 79: 1145-54

Potgieter M, Pretorius E, Pepper MS (2013) Primary and secondary coenzyme Q10 deficiency: the role of therapeutic supplementation. Nutr Rev 71: 180-8

Quinzii CM, Hirano M (2010) Coenzyme Q and mitochondrial disease. Dev Disabil Res Rev 16: 183-8

Rahman S, Hargreaves I, Clayton P, Heales S (2001) Neonatal presentation of coenzyme Q10 deficiency. J Pediatr 139: 456-8

Rütti MF, Richard S, Penno A, von Eckardstein A, Hornemann T (2009) An improved method to determine serine palmitoyltransferase activity. J Lipid Res 50:1237-44

Rotthier A, Auer-Grumbach M, Janssens K, Baets J, Penno A, Almeida-Souza L, Van Hoof K, Jacobs A, De Vriendt E, Schlotter-Weigel B, Loscher W, Vondracek P, Seeman P, De Jonghe P, Van Dijck P, Jordanova A, Hornemann T, Timmerman V (2010) Mutations in the SPTLC2 subunit of serine palmitoyltransferase cause hereditary sensory and autonomic neuropathy type I. Am J Hum Genet 87: 513-22

Sailer A, Houlden H (2012) Recent advances in the genetics of cerebellar ataxias. Curr Neurol Neurosci Rep 12: 227-36

Schmitz-Hubsch T, du Montcel ST, Baliko L, Berciano J, Boesch S, Depondt C, Giunti P, Globas C, Infante J, Kang JS, Kremer B, Mariotti C, Melegh B, Pandolfo M, Rakowicz M, Ribai P, Rola R, Schols L, Szymanski S, van de Warrenburg BP, Durr A, Klockgether T, Fancellu R (2006) Scale for the assessment and rating of ataxia: development of a new clinical scale. Neurology 66: 1717-20

Shimazaki H, Takiyama Y, Ishiura H, Sakai C, Matsushima Y, Hatakeyama H, Honda J, Sakoe K, Naoi T, Namekawa M, Fukuda Y, Takahashi Y, Goto J, Tsuji S, Goto Y, Nakano I (2012) A homozygous mutation of C12orf65 causes spastic paraplegia with optic atrophy and neuropathy (SPG55). J Med Genet 49: 777-84

Song H, Mugnier P, Das AK, Webb HM, Evans DR, Tuite MF, Hemmings BA, Barford D (2000) The crystal structure of human eukaryotic release factor eRF1--mechanism of stop codon recognition and peptidyl-tRNA hydrolysis. Cell 100: 311-21

Stum M, McLaughlin HM, Kleinbrink EL, Miers KE, Ackerman SL, Seburn KL, Antonellis A, Burgess RW (2010) An assessment of mechanisms underlying peripheral axonal degeneration caused by aminoacyl-tRNA synthetase mutations. Mol Cell Neurosci 46: 432-43

Taft RJ, Vanderver A, Leventer RJ, Damiani SA, Simons C, Grimmond SM, Miller D, Schmidt J, Lockhart PJ, Pope K (2013) Mutations in DARS cause hypomyelination with brain stem and spinal cord involvement and leg spasticity. Am J Hum Genet 14(5):774-80

Tucci A, Liu YT, Preza E, Pitceathly RD, Chalasani A, Plagnol V, Land JM, Trabzuni D, Ryten M, Jaunmuktane Z, Reilly MM, Brandner S, Hargreaves I, Hardy J, Singleton AB, Abramov AY, Houlden H (2014) Novel C12orf65 mutations in patients with axonal neuropathy and optic atrophy.

J Neurol Neurosurg Psychiatry 85(5):486-92

van Meel E, Wegner DJ, Cliften P, Willing MC, White FV, Kornfeld S, Cole FS (2013) Rare recessive loss-of-function methionyl-tRNA synthetase mutations presenting as a multi-organ phenotype. BMC Med Genet 14:106

Vester A, Velez-Ruiz G, McLaughlin HM, Lupski JR, Talbot K, Vance JM, Zuchner S, Roda RH, Fischbeck KH, Biesecker LG, Nicholson G, Beg AA, Antonellis A (2013) A loss-of-function variant in the human histidyl-tRNA synthetase (HARS) gene is neurotoxic in vivo. Hum Mutat 34: 191-9

Weedon MN, Hastings R, Caswell R, Xie W, Paszkiewicz K, Antoniadi T, Williams M, King C, Greenhalgh L, Newbury-Ecob R, Ellard S (2011) Exome sequencing identifies a DYNC1H1 mutation in a large pedigree with dominant axonal Charcot-Marie-Tooth disease. Am J Hum Genet 89: 308-12

Weterman MA, Sorrentino V, Kasher PR, Jakobs ME, van Engelen BG, Fluiter K, de Wissel MB, Sizarov A, Nurnberg G, Nurnberg P, Zelcer N, Schelhaas HJ, Baas F (2012) A frameshift mutation in LRSAM1 is responsible for a dominant hereditary polyneuropathy. Hum Mol Genet 21: 358-70

Zitomer NC, Mitchell T, Voss KA, Bondy GS, Pruett ST, Garnier-Amblard EC, Liebeskind LS, Park H, Wang E, Sullards MC, Merrill AH, Jr., Riley RT (2009) Ceramide synthase inhibition by fumonisin B1 causes accumulation of 1-deoxysphinganine: a novel category of bioactive 1-deoxysphingoid bases and 1-deoxydihydroceramides biosynthesized by mammalian cell lines and animals. J Biol Chem 284: 4786-95

Zuchner S, De Jonghe P, Jordanova A, Claeys KG, Guergueltcheva V, Cherninkova S, Hamilton SR, Van Stavern G, Krajewski KM, Stajich J, Tournev I, Verhoeven K, Langerhorst CT, de Visser M, Baas F, Bird T, Timmerman V, Shy M, Vance JM (2006) Axonal neuropathy with optic atrophy is caused by mutations in mitofusin 2. Ann Neurol 59: 276-81

Chapter 4

Results: Genetic studies in rare known genes of inherited neuropathies and other inherited disorders

Some causative genes for inherited neuropathies have not been studied thoroughly because their mutations are rarely identified. The screening of these genes in specific cohorts is helpful to further understand their phenotypic spectrum and to establish the genetic epidemiological profiles. In this chapter, genetic studies of *NEFL* and the promoter region of *PMP22* in CMT patients are described. Some genes causing other neurological disorders were also investigated due to the overlap with inherited neuropathies. For example, *KIF5A*, the causative gene for SPG10, was screened in both CMT2 patients and HSP cases to investigate the phenotypic spectrum of its mutations. Also, three genes recently identified for SCAs were sequenced in patients with cerebellar ataxia: *PDYN* for SCA23, *AFG3L2* for SCA28 and *KCND3* for SCA22/SCA19.

4.1 Extended phenotypic spectrum of *KIF5A* mutations: from spastic paraplegia to axonal neuropathy

4.1.1 Introduction

Spastic paraplegia type 10 (SPG10) is a rare form of autosomal dominant HSP caused by mutations of the kinesin family member 5A (*KIF5A*) gene (MIM: 602821).(Reid et al. 2002) Axonal neuropathy is frequently associated with SPG10 and has been documented by neurophysiological studies in two-thirds of patients.(Goizet et al. 2009; Musumeci et al. 2010; Schule et al. 2008; Tessa et al. 2008) Interestingly, two mutations in *KIF5A* have been identified in patients with a typical CMT type 2 phenotype but no pyramidal signs. One mutation (p.Glu251Lys, E251K) was carried by the father of a SPG10 patient,(Goizet et al. 2009) and the other (p.Gly235Glu, G235E) was detected in a sporadic case.(Crimella et al. 2012) These findings have raised the hypothesis that *KIF5A* mutations have a broad phenotypic spectrum and SPG10 and CMT2 may be allelic disorders. However, there is still a lack of large-scale studies to address the question. The aim of this study was to establish whether *KIF5A* mutations can be responsible for both HSP associated with neuropathy and for CMT2.

4.1.2 Patients and methods

(1) Patients

The diagnosis of HSP or CMT was based on clinical features, imaging and neurophysiology. Acquired causes of spasticity and neuropathy were excluded. As part of the diagnostic workup patients carrying *KIF5A* mutations had neurological examination and neurophysiological assessment and one patient had a sural nerve biopsy. In patients with an identified *KIF5A* mutation, DNA from affected family members was also tested for segregation where available.

(2) Sanger sequencing

The vast majority of *KIF5A* mutations have been identified mainly in the motor domain,(Blair et al. 2006; Crimella et al. 2012; Fichera et al. 2004; Goizet et al. 2009; Lo Giudice et al. 2006; Musumeci et al. 2010; Reid et al. 2002; Schule et al. 2008; Tessa et al. 2008) therefore, this domain was screened in two series of patients by Sanger sequencing (details of methods are described in Section 2.3). The first series included 186 patients with a clinical diagnosis of HSP with or without neuropathy (HSP series) and the second included 215 patients with axonal neuropathy consistent with CMT2 (CMT2 series). Patients in the HSP series were negative for mutations in *SPAST, REEP1, NIPA1, ATL1* and *BSCL2* and patients in the CMT2 series were usually negative for mutations in *GJB1, MFN2, MPZ, GDAP1, BSCL2, TRPV4, NEFL, HSPB1* and *HSPB8.*

(3) Targeted resequencing

A high-throughput targeted resequencing panel covering all coding exons of *KIF5A* was developed to screen an additional 66 patients with HSP or CMT2 with pyramidal signs. Most of these patients were negative for *ATL1* and *SPAST* mutations. The probe library was designed and enriched by the use of the HaloPlex system (Agilent). Targeted sequencing was performed in the Miseq platform.(Illumina) Details of the methods and variant filtering are described in Section 2.6 and Section 6.2. All mutations identified by the panel were validated by Sanger sequencing.

(3) WES

One patient was analysed by WES. Enrichment of coding exons and flanking intronic regions was performed using the SureSelect Human All Exon 50 Mb kit (Agilent) following the manufacturer's standard protocol. Enriched DNA was subjected to standard sample preparation for the Hiseq2000 instrument (Illumina). BWA and GATK software packages were used to align sequence reads to the NCBI hg19 reference and to call variant positions. All data were then annotated and imported into GEnomes Management Application (GEM.app) for data analysis.(Gonzalez et al. 2013) Variants were filtered as described in Section 2.6.

(4) Pathogenicity evaluation of novel mutations.

For identified novel mutations, in silico prediction of the functional impact of the mutation was performed using Polyphen and SIFT. A search of these mutations was performed in exome sequences from 221 healthy controls, the EVS database, and the Genome Variant Database for Neuromuscular Diseases (NMD database, http://hihg.med.miami.edu/gvd-nmd/).

4.1.3 Results

(1) Genetic results

Five different heterozygous missense *KIF5A* mutations were identified in six unrelated patients. Mutations in two patients were revealed by the panel, three were detected by Sanger sequencing and in one patient, the mutation was identified by WES. Pedigree and the nucleotide changes of these patients are illustrated in figure 4-1, A (p121). R204Q (c.G891A; p.Arg204Gln), R280H (c.G839A; p.Arg280His) and R280C (c.C838T; p.Arg280Cys) have been previously reported in patients with SPG10 (Crimella et al. 2012; Fichera et al. 2004; Goizet et al. 2009) whereas R204W (c.C890T; p.Arg204Trp) and D232N (c.G694A; p.Asp232Asn) were novel mutations. Both novel mutations were not identified in 221 exomes from healthy controls and not reported in either the EVS database or NMD database. Furthermore, they were predicted to be probably damaging and not tolerated by Polyphen and SIFT and each mutation changed a highly conserved amino acid residue (figure 4-1, B). The above evidence supported the pathogenicity of these novel mutations.

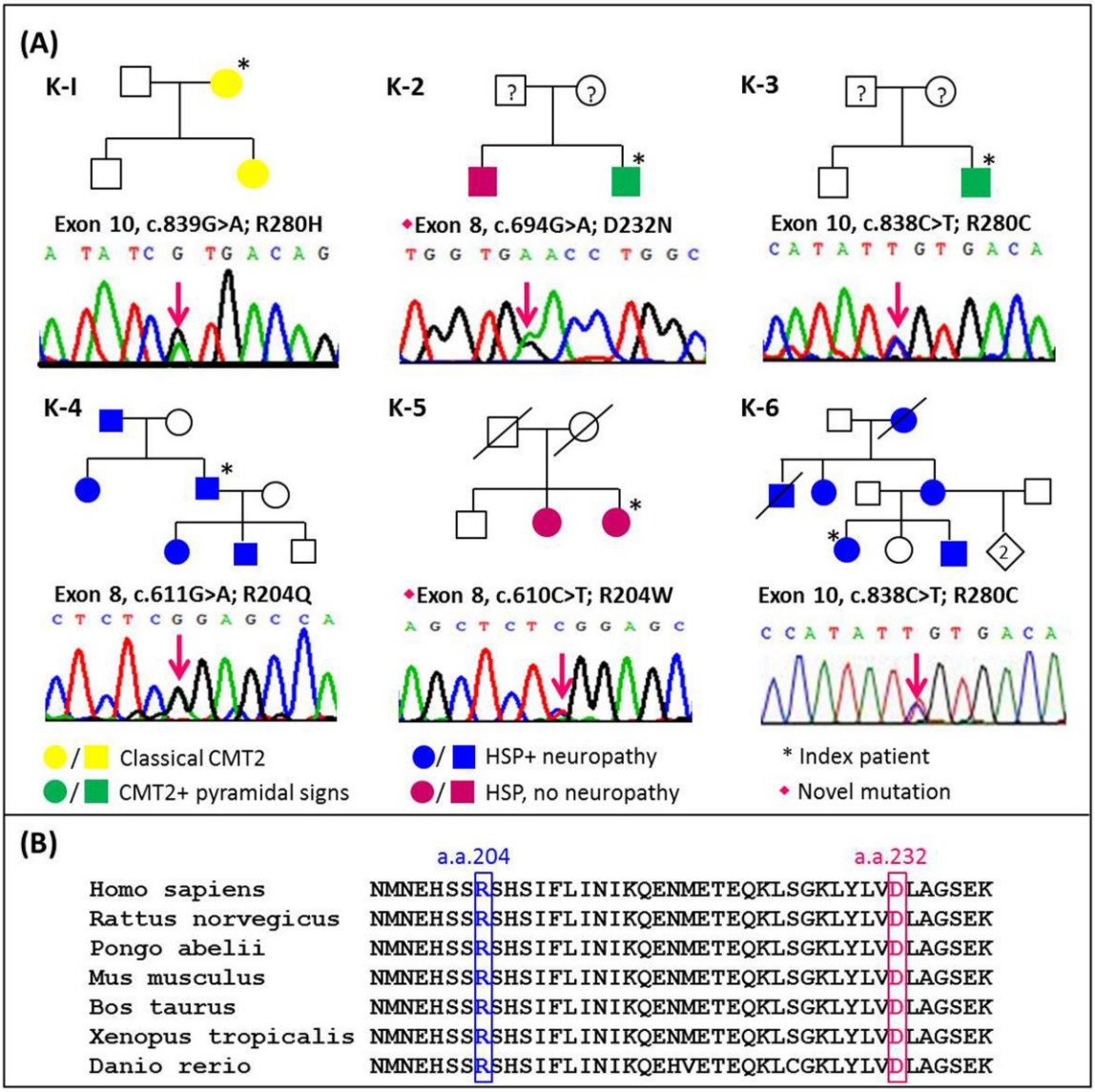

Figure 4-1. *KIF5A* mutations

(A) Chromatographs of the identified mutations and pedigree of the six patients in this study. The phenotypes illustrated in different colors refer to (1) Classical CMT2: classical CMT2 phenotype without pyramidal sign, (2) CMT2 + pyramidal signs: CMT2 is the main manifestation but there are associated pyramidal signs, (3) HSP + neuropathy: complex spastic paraplegia associated with peripheral neuropathy, (4) HSP, no neuropathy: spastic paraplegia without peripheral neuropathy. Parents of K-2 and K-3 were clinically unaffected at least until their sixth decades though they were unavailable for genetic testing. Parents of K-5 died early due to non-neurological diseases.

(B) The amino acid residues where two novel missense mutations (R204W and D232N) occurred were highlighted on kinesin orthologues in various species. The alignment showed their strict conservation during evolution from zebrafish to human beings.

(The figure is cited from Liu et al, 2014)

(2) Clinical and pathological findings

Patients with *KIF5A* mutations presented with a variable phenotype and age of onset. The clinical features of the patients with *KIF5A* mutations are summarized in table 4-1 (p123). Among the three patients who had CMT2 as the predominant phenotype, only K-1 initially presented with a classical CMT2 phenotype whereas the remaining two (K-2, K-3) had some involvement of the pyramidal tracts. The other three patients had spastic paraplegia as the main manifestation and two of them (K-4, K-6) also had peripheral neuropathy. Moreover, some patients had additional features: K-3, K-6 and other affected family members of K-6 had cognitive dysfunction and learning difficulties since their childhood; K-5 and her sister had marked cerebellar ataxia complicating the spasticity.

R280C mutation was identified in two unrelated patients with different phenotypes: K-3 was of British origin and had the clinical diagnosis of CMT2 with mild pyramidal signs whereas K-6 who had lived in Austria for several generations presented with severe spastic paraplegia and mild peripheral neuropathy (figure 4-1, A, K-3, K-6). Variable phenotypes in individuals within the same family were also observed. K-2 who had D232N mutation presented with complex CMT2 associated with spasticity, whereas his brother was affected by pure HSP (figure 4-1, A, K-2).

Table 4-1. Clinical features of the patients with *KIF5A* mutations

Patient	K-1	K-2	K-3	K-4	K-5	K-6
Mutation	R280H	D232N	R280C	R204Q	R204W	R280C
Gender	F	M	M	M	F	F
AO/AE (yr)	42/62	40/50	8/39	<20/38	~30/56	28/32
Predominant phenotype	CMT2	CMT2	CMT2	HSP	HSP	HSP
Additional symptoms	None	Spasticity	Spasticity, Cognitive dysfunction	Peripheral neuropathy	Cerebellar ataxia	Peripheral neuropathy, cognitive dysfunction, Lumbar pain
Presenting symptom	Difficulty in walking	Cramps and pain in LL	Reduced sensation in LL	Stiffness in LL and difficulty in walking	Difficulty in walking	Difficulty in walking
Pyramidal signs	None	Hyperreflexia Hypertonia Spastic gait	Hyperreflexia Hypertonia Extensor plantars	Hyperreflexia except absent ankle jerks Spastic gait	Hyperreflexia with ankle clonus Hypertonia	Hyperreflexia with ankle clonus Spastic gait
Bladder dysfunction	None	Mild urgency	None	Significant urgency	Significant urgency	Significant urgency*
Weakness						
UL	Mild	Mild	Mild	No	No	No
LL	Moderate	Mild	Severe	No	Mild	No
Pinprick						
UL	Moderately abnormal	Mildly abnormal	Normal	Moderately abnormal	Normal	Normal
LL	Moderately abnormal	Mildly abnormal	Normal	Moderately abnormal	Normal	Normal
Vibration						
UL	Normal	Mildly abnormal	Mildly abnormal	Moderately abnormal	Severely abnormal	Normal
LL	Mildly abnormal	Severely abnormal	Mildly abnormal	Moderately abnormal	Severely abnormal	Normal
Aid for walking	Crutch	AFO	Wheelchair	Crutch	Wheelchair	No

AD= autosomal dominant; **AE=** age of examination; **AFO=** ankle foot orthosis; **AO=** age of onset; **CMT2=** Charcot-Marie-Tooth disease type 2; **F=** female; **HSP=** hereditary spastic paraplegia; **M**= male; **UL=** upper limbs; **LL**= lower limbs; **Weakness: mild=** MRC ≥4 in distal muscles, **moderate=** MRC ≤4 in distal muscles, **severe=** proximal weakness (knee flexion and extension, elbow flexion and extension or above); **Pinprick and vibration sense: mildly abnormal**= reduced below wrist/ankle, **Moderately abnormal=** reduced below elbow/knee, **Severely abnormal=** reduced at or above elbow/knee. * Only reported in some family members

Features demonstrating the simultaneous involvement of the peripheral and central nervous systems in our patients are shown in figure 4-2. A sural nerve biopsy from K-3 revealed markedly reduced numbers of large myelinated fibers, compatible with axonal degeneration (figure 4-2, A, B). Meanwhile, spasticity with hyperreflexia was observed on examination. K-2 had wasting of intrinsic foot muscles and pes cavus while the worn-out areas of the shoes indicated a longstanding spastic gait (figure 4-2, E, F).

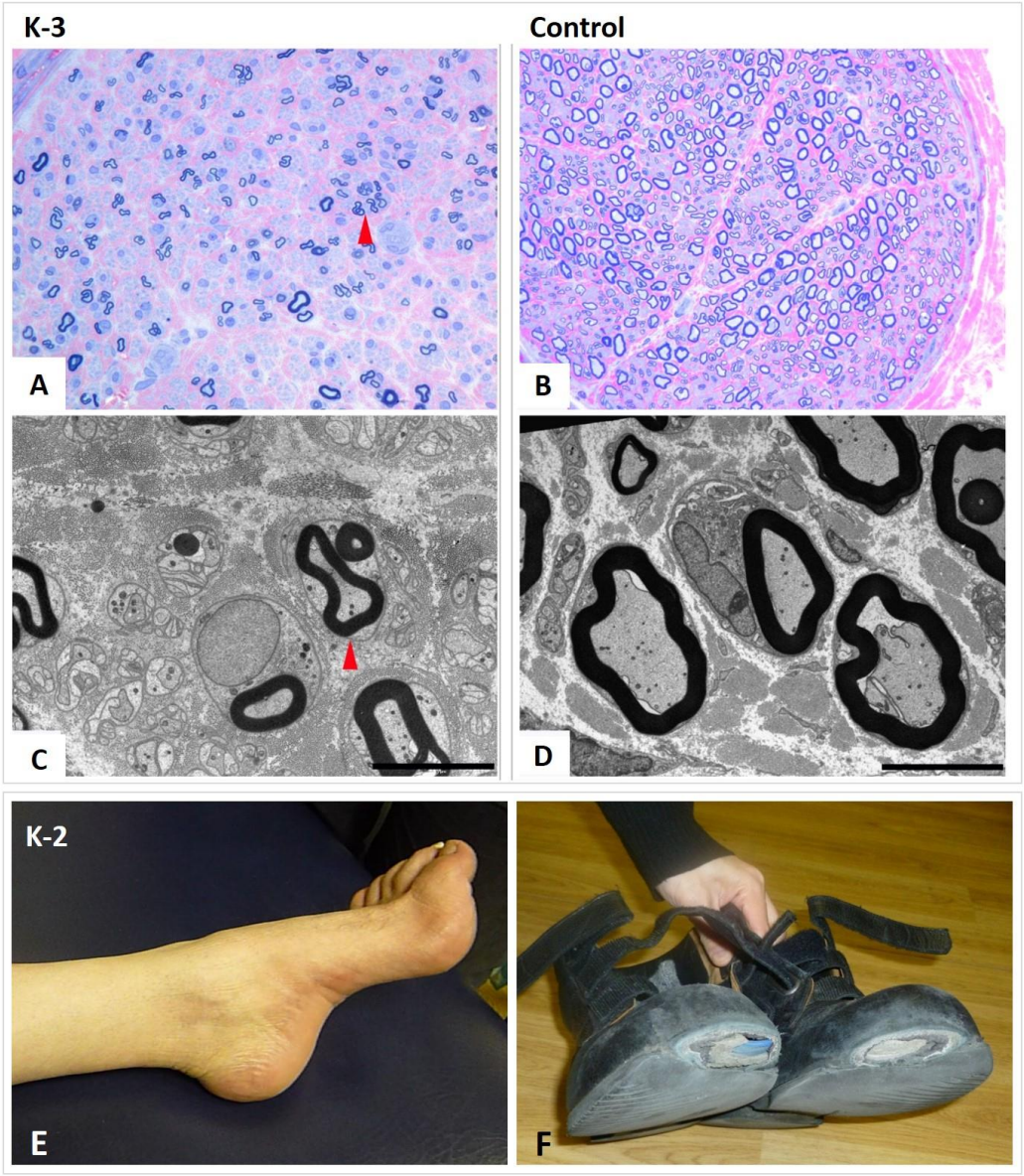

Figure 4-2. Pathological and clinical evidence of peripheral neuropathy in patients with *KIF5A* mutations
Sural nerve biopsy of patient K-3:
A and B. Semi-thin resin section stained with methylene blue azure – basic fuchsin (MBA-BF) showed markedly reduced numbers of large myelinated fibres in patient K-3 (A) as compared with a healthy age-matched control (B). **C and D.** Ultrastructural assessment for patient K-3 revealed numerous regeneration clusters of unmyelinated axons (arrows in A and C) which was not observed in a health age-matched control (D). Scale bar: 45µm (A, B), 5µm (C, D). **Patient K-2:**
E. Pes cavus. **F**. The worn-out areas of the patient's shoes are suggestive of the longstanding spastic gait.

(2) Neurophysiolgical findings

NCS of the five patients who had a clinically recognisable peripheral neuropathy are presented in table 4-2. Neurophysiology showed symmetrically absent or reduced MAPs and SAPs with relatively preserved NCVs in upper and lower limbs, consistent with sensorimotor axonal polyneuropathy.

Table 4-2. Nerve conduction studies of the patients with *KIF5A* mutations

Patient	**K-1**	**K-2**	**K-3**	**K-4**	**K-6**
Mutation	R280H	D232N	R280C	R204Q	R280C
AE (yr)	53	50	32	40	32
Median n.					
Motor DML (ms)	3.5	3.9	6.1	5.5	5.8
CMAP (mV)	6	7.2	4.7	7.8	2.2
MNCV (m/s)	52	44	44	52	36
F-latency (ms)	28	33.2	NR	32.4	NR
SAP (uV)	7	Abs	Abs	2	6.5
SNCV (m/s)	55	Abs	Abs	42	37
Ulnar n.					
Motor DML (ms)	NR	3.2	4.7	3.8	3.4
CMAP (mV)	NR	5.7	6.4	6.5	11.5
MNCV (m/s)	NR	53	50	46	42
SAP (uV)	5	Abs	Abs	4	8.3
SNCV (m/s)	54	Abs	Abs	48	39
Radial n.					
Motor DML (ms)	NR	NR	NR	NR	NR
CMAP (mV)	NR	NR	NR	NR	NR
MNCV (m/s)	NR	NR	NR	NR	NR
SAP (uV)	8	Abs	Abs	9	NR
SNCV (m/s)	54	Abs	Abs	55	NR
Common peroneal n.					
Motor DML (ms)	Abs	Abs	Abs	Abs	7.2
CMAP (mV)	Abs	Abs	Abs	Abs	1.1
MNCV (m/s)	Abs	Abs	Abs	Abs	33
Tibial n.					
Motor DML (ms)	NR	Abs	Abs	Abs	5
CMAP (mV)	NR	Abs	Abs	Abs	4.4
MNCV (m/s)	NR	Abs	Abs	Abs	33
Sural n.					
SAP (uV)	Abs	Abs	Abs	Abs	Abs

AE= age at examination**; Abs**=absent; **CMAP**= compound motor action potential (mV); **DML**=distal motor latency; **MNCV**= motor nerve conduction velocity (m/s); **NR**= not recorded; **n.**= nerve; **SAP**= sensory action potential (uV); **SNCV**= sensory nerve conduction velocity (m/s)

4.1.4 Discussion

This study reports the largest series of HSP and CMT2 patients screened for *KIF5A* mutations. The identification of five different mutations confirms that *KIF5A* is associated with both HSP and CMT2 phenotypes. In this study the first family with a *KIF5A* mutation and associated cerebellar ataxia is reporting broadening the phenotypic spectrum of *KIF5A* mutations.

The identified *KIF5A* mutations and their associated phenotypes are presented in figure 4-3 (p127). HSP and CMT2 represent two different ends of the spectrum of *KIF5A*-related disorders: classical or complex CMT2 is relatively rare while HSP with axonal neuropathy is the commonest phenotype associated with *KIF5A* mutations. However, a specific phenotype-genotype correlation for *KIF5A* mutations could not be defined as some mutations (R280C, R280H and D232N) have been associated with more than one phenotype. The intra-familial phenotypic variability within families with the D232N mutation provides evidence of the allelic relationship of HSP and CMT2.

KIF5A encodes the neuronal kinesis heavy chain (KHC) subunit of kinesin-1, a motor protein which plays a role in axonal transport. Kinesin-1 relies on the highly conserved motor domain of KHC to bind to the microtubules and converts the chemical energy of adenosine-5'-triphosphate (ATP) into mechanical energy required for intracellular trafficking.(Barry et al. 2007; Ebbing et al. 2008; Gunawardena et al.2004; Hirokawa et al. 2009; Xia et al. 1998; Xia et al. 2003) In both CMT2 and SPG10 phenotypes, the majority of the mutations are localized in the motor domain and are clustered around the two switch regions (SWI and SWII in figure 4-3) which carry γ-phosphate-sensing activity and are particularly important in the interaction with microtubules (figure 4-3, p122). Half of the families in this study have mutations at codon R280 and 25% (7/28) of all reported families with a *KIF5A* mutation have an amino acid substitution at this position. Although these families are from different parts of the world, it would be interesting to carry out a haplotype study to investigate a founder effect. The CpG dinucleotide of codon 280 had been proposed as a possible hot spot for *KIF5A* mutations(Goizet et al. 2009) and the findings support the critical role of this codon in the function of *KIF5A*.

A small number of SPG10-associated *KIF5A* mutations (K253N, N256S, R280C and A361V) have been investigated using in-vitro and Drosophila models. The results support a loss of endogenous kinesin-1 function due to a selective dominant-negative mechanism on the kinesin complexes, rather than a toxic gain of function.(Ebbing et al. 2008; Füger et al. 2012) Only mutations localized in the motor domain changed the kinesin gliding properties but not the mutation in the neck (A361V). This suggests that mutations outside of the motor domain may have a different disease mechanism.(Ebbing et al. 2008)

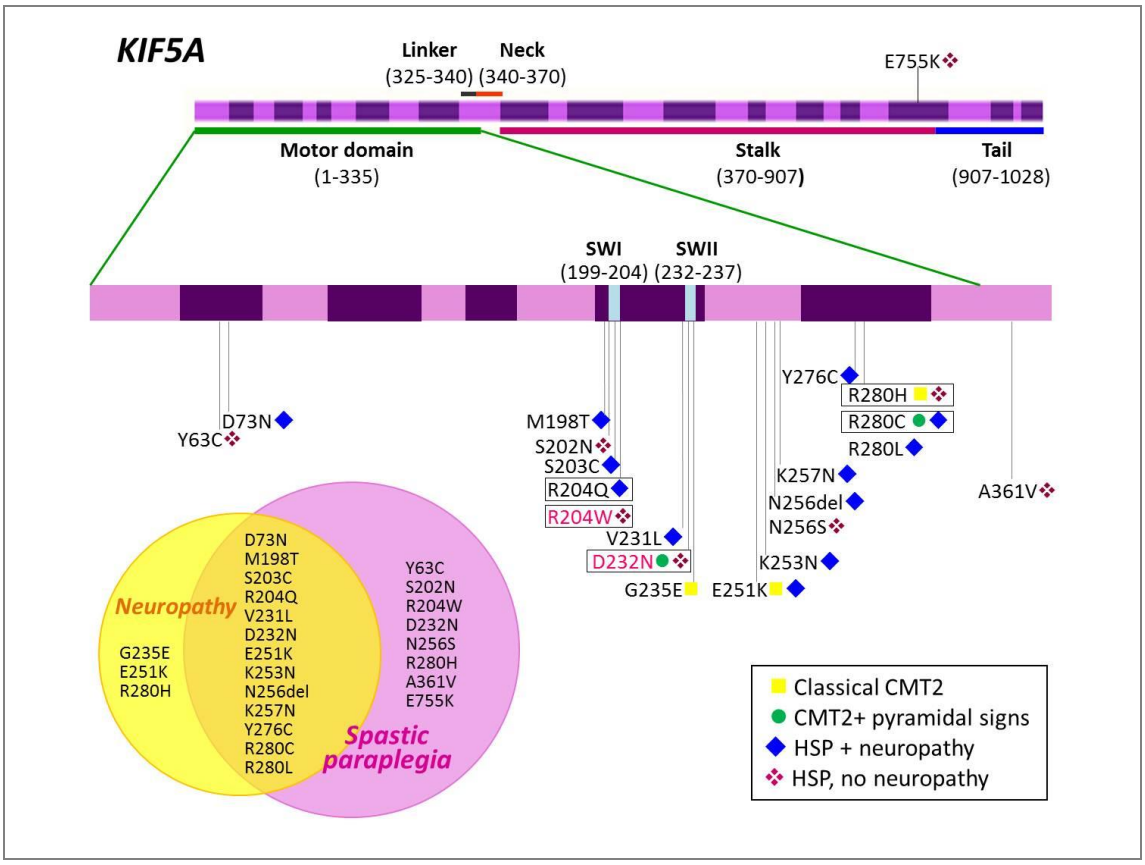

Figure 4-3. Phenotypic spectrum of *KIF5A* mutations

Top. Genomic organization of the human *KIF5A* gene and its mutations. Most of the *KIF5A* mutations are localized in exon 8~10 and many are clustered within or around the switch I regions (SWI) and the switch II region (SWII) which carry γ-phosphate-sensing activity to convert ATP into required energy. *KIF5A* mutations were labelled with the corresponding phenotypes: classical CMT2, CMT2 + pyramidal signs, HSP + neuropathy and HSP, no neuropathy (definitions of the phenotypes have been described in figure 1). The mutations identified in this study were flanked with the two novel mutations in pink.

Bottom left. A Venn diagram representing the overlap and distinct phenotypes of *KIF5A* mutations. The majority of these mutations presented by both spastic paraplegia and neuropathy.

CMT2 and HSP have different target cells: the first primarily affects the peripheral nerves, and the latter principally affects the corticospinal tract. Both the peripheral nerve axons and the long corticospinal tract rely heavily on axonal transport of appropriate cargoes to maintain their normal functions. *KIF5A* is another example of a gene in which mutations can cause axonal neuropathy in association with pyramidal signs and is involved in axonal transport similar to *BSCL2, REEP1, ATL1, SPAST, NIPA1* genes.(Barry et al. 2007; Gunawardena et al. 2004; Timmerman et al. 2012; Xia et al. 2003) Likewise *CCT5, KIF1A*, and *DYNC1H1* are other genes encoding motor proteins which have an important role in axonal transport and their mutations have been identified in patients with complex syndromes involving both the

peripheral and central nervous systems.(Bouhouche et al. 2006; Klebe et al. 2012; Riviere et al. 2011; Weedon et al. 2011; Willemsen et al. 2012) Thus axonal transport represents a potential common pathway in the pathogenesis of both axonal neuropathy and spastic paraplegia. (Timmerman et al. 2012) Mutant motor proteins affecting axonal transport may lead to a neurodegenerative process. However, the mechanism by which mutations of the same gene can either selectively or simultaneously affect the upper motor neurons and the peripheral axons is still not well understood. Other genetic or environmental factors may influence the phenotype. Further studies are needed to understand the function of *KIF5A* and its roles in the peripheral and central nervous systems.

The reported frequency of *KIF5A* mutations may be underestimated as this is not a genetic testing usually included in most of the diagnostic services. The application of targeted resequencing for screening *KIF5A* provides a more comprehensive and cost-effective method. In addition, next-generation targeted sequencing and whole exome sequencing are powerful tools for identifying mutations in patients with atypical complex symptoms. These approaches have effectively facilitated the detection of *KIF5A* mutations and helped broaden the phenotypic spectrum of this gene.

4.2 *NEFL* mutations cause variable CMT phenotypes

4.2.1 Introduction

Neurofilaments are the main cytoskeleton component of vertebrate axons which determine the axonal caliber. Neurofilaments are heteropolymers composed of light, medium, and heavy chains and the neurofilament, light polypeptide (*NEFL*) gene encodes the light chain neurofilament protein (NFL).(Friede et el. 1970; Muma et al. 1993) Mutations in *NEFL* were initially described as a cause of axonal CMT (CMT2E) (De Jonghe et al. 2001; Lupski 2000; Mersiyanova et al. 2000) but subsequently were identified in patients with demyelinating CMT (CMT1F).(Zuchner et al. 2004) In most affected individuals, age of onset is within the first decade of life, the phenotype is usually severe and NCVs are reduced. However, further studies have confirmed that *NEFL* mutations can cause a wide clinical spectrum without an obvious genotype-phenotype correlation.(Miltenberger-Miltenyi et al. 2007; Reilly 2009; Zuchner et al. 2004) *NEFL* mutations are usually transmitted in a dominant fashion; however, de novo dominant mutations and recessive inheritance have been also reported.(Yum et al. 2009) Thus, mutation analysis of *NEFL* should not be restricted to axonal or demyelinating neuropathies, and various inheritance patterns should be taken into consideration. The aim of this study was to screen *NEFL* in a cohort of CMT patients to determine the mutation frequency in a UK population.

4.2.2 Patients and methods

NEFL gene (NM_006158) was sequenced by Sanger sequencing in a cohort of 188 CMT patients in which mutations in *PMP22*, *MPZ*, *GJB1*, *MFN2* or *SH3TC2* genes had been previously excluded. The cohort included patients with variable inheritance and different neurophysiological presentations, including demyelinating, axonal, and intermediate subtypes. The study was part of a large-cohort based genetic study which included 1607 patients with CMT (425 patients attending an inherited neuropathy clinic and 1182 patients whose DNA was sent to the NHNN genetic laboratory for genetic testing) to determine the proportion of different subtypes in a UK population.(Murphy et al. 2012)

4.2.3 Result

(1) Genetic analysis

Two heterozygous mutations were detected in two unrelated patients: p.Leu311Pro (L311P) was a novel mutations while p.Pro8Leu (P8L) had been previously reported.(Jordanova et al. 2003) The mutations and pedigree of patients are described in figure 4-4 (p130).

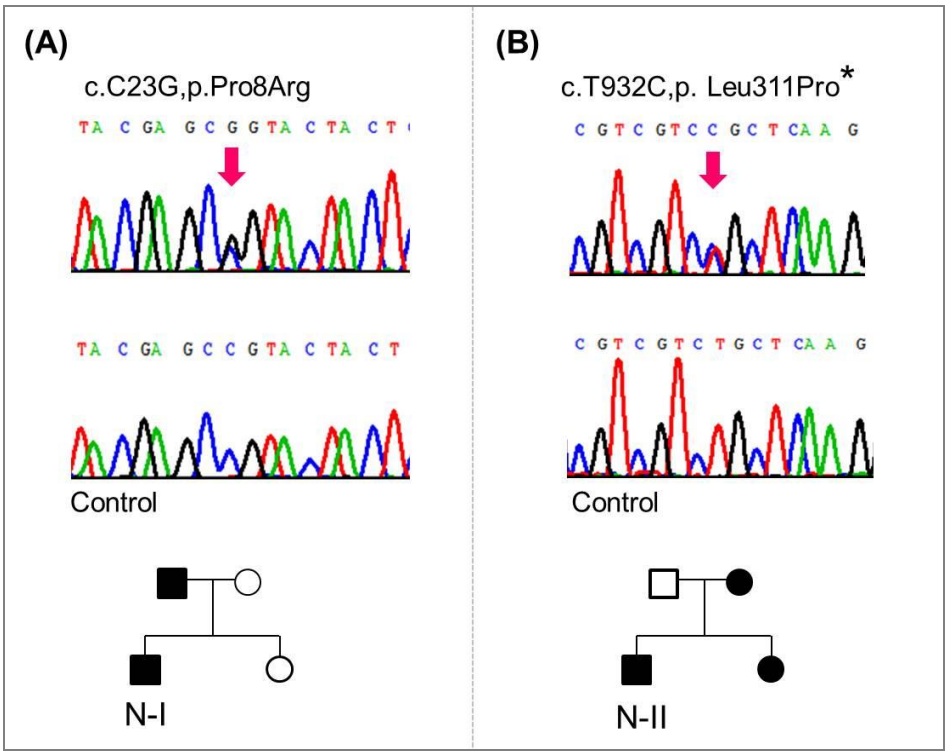

Figure 4-4. Nucleotide sequences and the pedigrees of the patients with *NEFL* mutations

■/●= affected members, □/○= unaffected members. The index patients are labeled with N-I, and N-II.

Each NFL subunit comprises a centralα-helical coil domain flanked by a globular head domain and non-α-helical tail domains. The two mutations were identified in different domains: P8R in the head domain and L311P in the coil domain (figure 4-5, p131). The pathogenicity of the novel mutations was supported by the following evidences: (1) the mutation was absent in 216 control chromosomes; (2) functional prediction using PolyPhen2 and SIFT programs suggested that L311P was probable damaging and intolerable; (3) multispecies alignment of the sequences showed that amino acid codon Leu311 was highly conserved in evolution (figure 4-5).

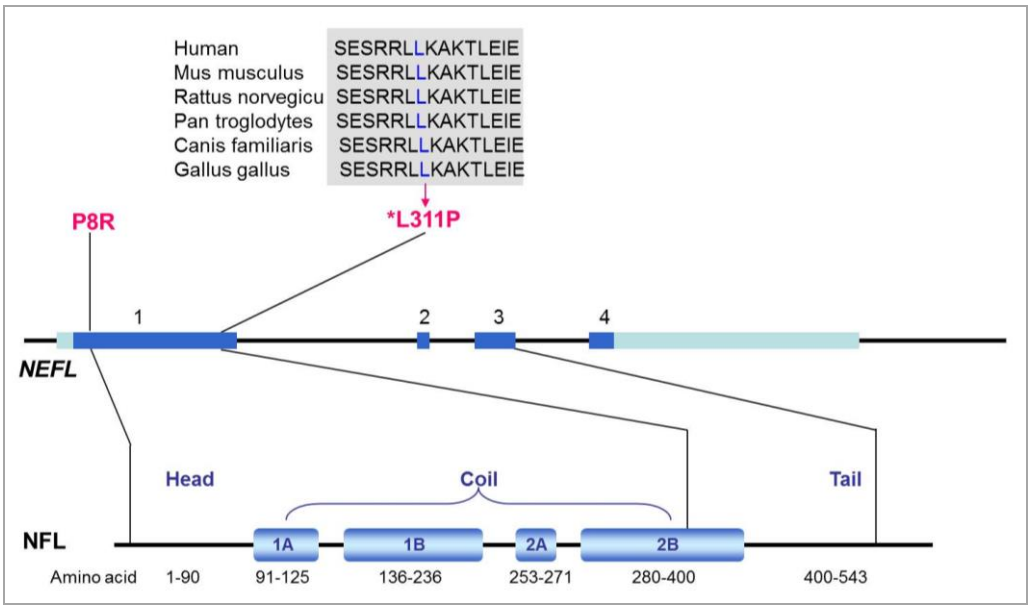

Figure 4-5. *NEFL* mutations and the corresponding protein domains

Genomic organization of the human *NEFL* gene is shown on the top and the functional domains of the coding protein NFL is illustrated on the bottom. The two *NEFL* mutations identified in this study are highlighted. Multispecies alignment of the peptide sequences demonstrated the strict conservation of the amino acid L311 where the novel mutation is localized. Pink star: novel mutation

(2) Clinical features

Clinical features of the patients with *NEFL* mutations are summarised in table 4-3. The two patients presented with distinct phenotypes. N-I who carried P8L mutation had a classical CMT phenotype with onset in the second decade of his life. His father had similar symptoms and signs. NCS revealed a demyelinating neuropathy compatible with CMT1 and the sural nerve biopsy showed features of demyelination and remyelination with onion bulbs. N-II who harboured the L311P mutation had a late-onset sensorimotor neuropathy with walking difficulty as the presenting symptom in the fifth decade. His mother and sister were also affected by peripheral neuropathy. Neurophysiology was compatible with demyelinating neuropathy with secondary axonal loss.

Table 4-3. Clinical features of patients with *NEFL* mutations

Patient	N-I	N-II
DNA No.	38295	49358
Mutation	P8R	L311P*
Gender	M	M
Inheritance	AD	AD
Age of onset	<20y/o	>50y/o
Neurophysiology	CMT1	CMT1

* Novel mutation; M= male; F= female; AD= autosomal dominant; AR= autosomal recessive

4.2.4 Discussion

Two *NEFL* mutations were identified in two unrelated patients, accounting for an approximate 1% hit rate in the selected cohort. In the overall population included in the above mentioned CMT genetic epidemiological study, mutations in *NEFL* were identified in 0.5% of CMT patients who attended the inherited neuropathy clinic at NHNN and in 0.2% of external patients whose DNA samples were sent to our laboratory.(Murphy et al. 2012) These findings suggest that mutations in the *NEFL* gene are a rare cause of CMT in the UK population.

The two patients had variable ages of onset. Our findings suggested that *NEFL* mutation should be considered in CMT patients with variable age of onset when mutations in common genes have been already excluded.

This study identified mutations in two distinct domains of NFL, indicating the significance of their functions. Each domain of NFL has been documented to play an important role in neurofilament formation and transport. In vitro studies have shown that mutations in the head domain caused disruption of neurofilament assembly and transport and affected intracellular localization of mitochondria.(Brownlees et al. 2002; Yates et al. 2009) The coil/rod domain determines neurofilament architecture and *NEFL* mutations in the fragment would cause reduction in self-assembly of NFL .(Lee et al. 2008)

4.3 Mutation analysis of the upstream untranslated region of *PMP22* in CMT1

4.3.1 Introduction

CMT1A, the commonest form of CMT, is caused by a duplication of a 1.4 Mb fragment on chromosome 17 where the *PMP22* gene is localized or by point mutations in the *PMP22* gene. Hereditary neuropathy with liability to pressure palsies (HNPP) is characterised by recurrent nerve palsies at points vulnerable to pressure and is caused by either deletion of the same fragment on chromosome 17 or more rarely by *PMP22* mutations.(Nelis et al. 1998) The identification of the two allelic disorders suggested adose-dependent mechanism of *PMP22*-related diseases.(Braathen 2012; Li et al. 2013) A wide range of age of onset and variable motor or sensory involvement have been observed in patients with *PMP22*-related diseases, both within and among families.(Boerkoel et al. 2002; Li et al. 2013) Additional modifying genetic factors are believed to contribute to the phenotypic heterogeneity.

PMP22 gene encodes peripheral myelin protein 22 (PMP 22) which is mainly expressed in myelinating Schwann cells.(Snipes et al. 1992) *In vivo*, expression of *PMP22* is regulated by two alternate promoters: promoter 1 (P1) containing exon 1A and promoter 2 (P2) containing exon 1B (figure 4-6). High levels of the transcripts expressed by P1 occur in the neural tissue and during myelin formation. Transcripts expressed by P2 are ubiquitously found in non-neural tissues such as lung, intestine, heart, and skeletal muscle.(Manfioletti et al. 1990; Nelis et al. 1998; Suter et al. 1994)

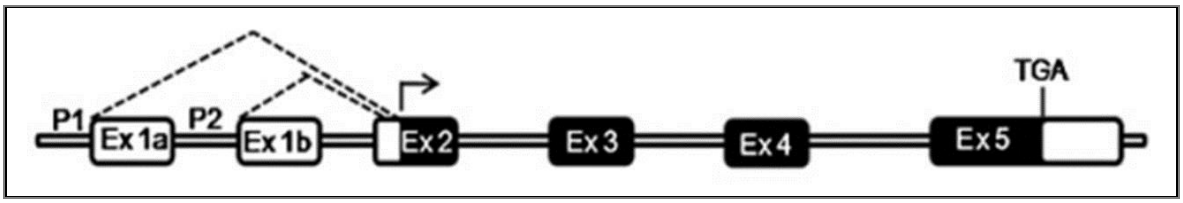

Figure 4-6. Two sets of promoters regulate the transcription of *PMP22*

Exons are identified by numbers above filled boxes. Exon-1a (Ex1a) containing transcripts are predominantly expressed in myelinating schwann cells. Exon-1b (Ex 1b) containing transcripts are expressed in non-neuronal cells. Ex1a and 1b are the transcripts of exon 1 produced by the regulation of promoter 1 (P1) and promoter 2 (P2). (modified from Li 2012)

In addition to the two tissue-specific promoters, there are many other transcriptional regulatory regions in the 5'UTR of *PMP22*. It has been documented that an essential element required for Schwann cell specific expression is contained at 300bp upstream of the start point for transcription.(Suter et al. 1994) Two distinct transcriptional regulatory regions at −1,600 and −2,100 bp of *PMP22* were subsequently identified.(Saberan-Djoneidi et al. 2000) These regions

can regulate *PMP22* expression by interacting with the silencer of the *PMP22* promoter CREB (cAMP response element binding protein) or the enhancer of *PMP22* transcription SREB (sterol regulatory element binding protein).(Desarnaud et al. 2000; transcription SREB (sterol regulatory element binding protein).(Desarnaud et al. 2000; Desarnaud et al. 1998; Li et al. 2013; Saberan-Djoneidi et al. 2000) In another further upstream region (-4000bp of *PMP22*), there are also several microdomains which are potential binding sites for other transcription factors.(Maier et al. 2003; Sinkiewicz-Darol et al. 2010) (figure 4-7).

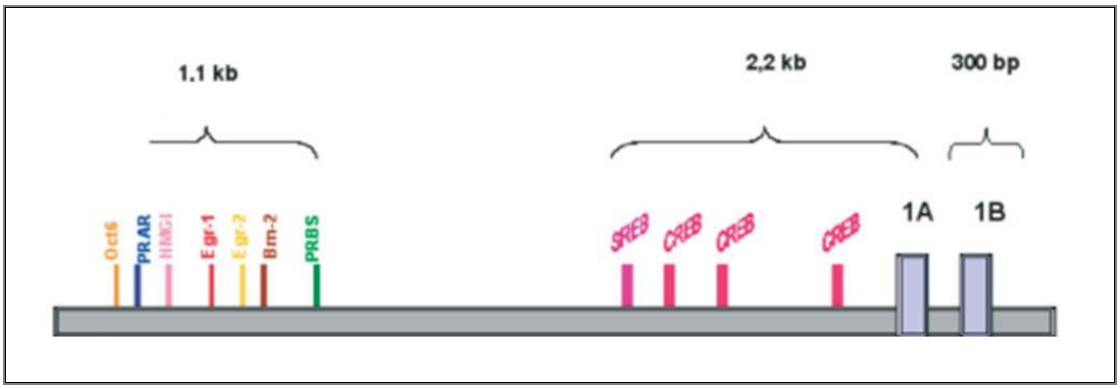

Figure 4-7. The upstream regulatory elements of the human *PMP22* gene.

Potential binding sites for transcription factors Oct6, PRAR, HMGI, Egr-1, Egr-2, Brn-2, PRBS, SREB, CREB in the upstream of human PMP 22 gene and the two promoters were marked.(modified from Sinkiewica-Darol *et al*., 2010)

Previous studies showed that mutations in the nerve specific *PMP22* promoter and 5' untranslated exon were not a common genetic cause of CMT1A. This study was therefore conducted to determine the frequency of mutation/variations in the *PMP22* promoter region in CMT1.

4.3.2 Patients and methods

800bp upstream of the transcription start of *PMP22* including the nerve specific promoter was directly sequenced in 520 patients with clinical diagnosis of CMT1 but negative for *PMP22* duplication or point mutations and mutations in the *MPZ, GBJ1, LITAF* and *GDAP1* genes. Patients included in this cohort belonged to autosomal dominant families or were sporadic.

4.3.3 Result

No nucleotide variation in the *PMP22* promoter region was identified in any of the patients.

4.3.4 Discussion

It has been speculated that variants in the upstream region of PMP22 can alter the expression of the gene and may be either a cause or genetic modifier of CMT. Nelis *et al*. first screened a

500bp long 5' regulatory sequence of *PMP22* in a small group of CMT1A patients using single strand conformation polymorphism (SSCP). Only one –141C>G single nucleotide polymorphism (SNP) variant was found in a single CMT patient..(Nelis et al. 1998) To improve the low mutation detection ratio of SSCP, Sinkiewicz-Darol *et al.* then screened the upstream regulatory regions of *PMP22* by direct sequencing and the investigated region was further extended to -3600 bp encompassing numerous binding sites for transcription factors and regulatory motifs which were recognized after the Nelis study.(Maier et al. 2003; Sinkiewicz-Darol et al. 2010) Nevertheless, the intensive analysis only detected five SNP variants with undetermined significance and indicated that mutations in the promoter are not common in CMT1. Our results supports previous observation that the nerve-specific *PMP22* promoter region and it upstream region are highly conserved in evolution and rarely mutated.

In conclusion this study confirmed that mutations in the upstream untranslated region of *PMP22* are not a common cause of CMT1. The structure of the region containing the nerve specific promoter is highly conserved, supporting the biological significance of the observed arrangement of regulatory regions.

4.4 Mutation analysis of *PDYN, KCND3* and *AFG3L2* in patients with cerebellar ataxias

4.4.1 Introduction

SCAs can be caused by polyglutamine expansions, non-coding expansions and rare conventional mutations in different genes. In the UK, more than 60 % of the SCA families are caused by the common polyglutamine expansions SCAs (SCA1, 2, 3, 6, 7, 12, 17, and DRPLA).(Marelli et al. 2011) The population of patients with conventional mutations is much smaller than those due to polyglutamine expansions. However, the list of SCA genes leading to diseases through conventional mutations is rapidly increasing.(Durr 2010; Sailer et al. 2012) Point mutations in three genes were recently identified causing SCAs: *PDYN* for SCA23, *KCND3* for SCA22/SCA19 and *AFG3L2* for SCA28. Identification of these genes and their biological functions revealed new insights in the pathomechanisms of cerebellar degeneration and potential targets to modulate the disease process.

The locus of SCA23 (MIM_610245) was first mapped to a 6 Mb region on chromosome 20p12.3–p13 in a large autosomal dominant Dutch ataxia family with pure progressive ataxia (Verbeek et al. 2004) and subsequently mutations in the prodynorphin (*PDYN*) gene (MIM_131340) were identified in further families with progressive gait and limb ataxia.(Bakalkin et al. 2010) *PDYN* is the precursor protein for the opioid neuropeptides, α-neoendorphin (α-NE), dynorphins A and B (Dyn A and B). Dynorphins regulate pain processing and modulate the rewarding effects of addictive substances.

The SCA22 locus (MIM_607346) was initially mapped to chromosome 1p21-q23 in a four-generation Chinese family with ADCA.(Chung et al. 2003) Subsequently, the disease loci in a French family and an Ashkenazi Jewish American family were also mapped to this region, overlapping with the locus of SCA19.(Schelhaas et al. 2004; Verbeek et al. 2002) Recently, missense mutations and chromosomal rearrangements in the voltage-gated potassium channel Kv4.3-encoding *(KCND3)* gene were identified in affected families with both SCA22 and SCA19.(Duarri et al. 2012; Lee et al. 2012) Most of the affected individual presented with slowly progressive pure cerebellar ataxia, but a few patients had additional features, such as ophthalmoplegia, sensory neuropathy, hyperreflexia, cogwheel rigidity, or urinary urgency/incontinence in the absence of pyramidal involvement.(Lee et al. 2012) The encoding protein of *KCND3*, Kv4.3, is an alpha subunit of the Shal family of the A-type voltage-gated K^+ channels which is highly expressed in the brain, particularly in the cerebellum.(Tsaur et al. 1997) Kv4.3 is important in membrane repolarization of excitable cells and may play a significant role in the development of the cerebellum.(Hsu et al. 2003; Oberdick et al. 1998; Tsaur et al. 1997) The identification of pathogenic *KCND3* mutations in SCAs emphasizes the important role of

ion channels as key regulators of neuronal excitability in the pathogenesis of cerebellar degeneration.

SCA28 (MIM_610246) is a form of SCA characterized by slowly progressive cerebellar ataxia with hyperreflexia in lower limbs, ophthalmoparesis and ptosis. The onset is usually in in early adulthood.(Cagnoli et al. 2006) but childhood onset has been described in some.(Edener et al. 2010) *AFG3L2*, the causative gene for SCA28, encodes for a subunit of the m-AAA protease (ATPases associated with various cellular activities), a component of the mitochondrial ATP-dependent metalloprotease located on the inner mitochondrial membrane. The m-AAA metalloproteases have been shown to play a role in the control of proteolytic quality and chaperon-like activities in mitochondria by degrading misfolded proteins and promoting the assembly of respiratory chain complexes.(Leonhard et al. 1999) It is also essential for axonal development and maintenance.(Edener et al. 2010) The identification of *AFG3L2* mutations in cerebellar ataxia documented the importance of mitochondrial function in cerebellum and related pathways.

So far, the frequency of mutations in the *PDYN, KCND3* and *AFG3L2* genes in the British population are still unknown and screening of these new identified genes would be useful to determine the frequency of the different genetic subtypes of SCA in UK. The aim of this study was to assess the frequency of mutations in *PDYN, KCND3* and *AFG3L2* in patients with hereditary ataxias. All patients were negative for all common polyglutamine expansion SCAs (SCA1, 2, 3, 6, 7, 17 and DRPLA). The phenotypic-genotypic correlations were also investigated.

4.4.2 Patients and methods

Direct sequencing of the *PDYN* coding exons 3 and 4 (NM_024411) and the flanking introns was performed in a total of 852 patients: 176 cases with autosomal dominant inheritance, 356 sporadic cases and 320 cases with familial cerebellar ataxia (defined as the presence of at least two affected individuals but the inheritance is undetermined). Patients were predominantly from the UK (734 patients), mainly from the south of England. This study also included a group of patients from Greece (83 patients), Egypt (17 patients) and India (18 patients). The predominant phenotype was pure cerebellar ataxia (73%), and the other 27 % had additional features, such as neuropathy, limb spasticity, cognitive decline, myoclonus or seizures. Additional 190 patients with multiple-system atrophy with cerebellar features (MSA-C) were also analysed as this is a phenocopy of SCA23.

Direct sequencing of all coding exons (exon 2 to 8) of the *KCND3* gene (NM_172198) was

performed in 230 unrelated patients with familial cerebellar ataxia defined as above. Since mutations have only been identified in exon 2 and exon 3, these two exons were further sequenced in 180 sporadic patients with a clinical diagnosis of hereditary cerebellar ataxia.

For *AFG3L2* (NM_006796), genetic analyses of all the 17 coding exons and the flanking introns were performed in 174 unrelated patients with familial cerebellar ataxia defined as above.

The diagnosis, the number of patients and the range of sequencing for each gene are listed in table 4-4.

Table 4-4. Genes and studied cohorts of cerebellar ataxias in the chapter

Gene	Studied cohort	No. of patients	Range of sequencing
PDYN (SCA23)	1. ADCAs	176	The two coding exons (exon 3 and exon 4) and the flanking introns
	2. Sporadic ataxia	356	
	3. Familial cerebellar ataxia	320	
AFG3L2 (SCA28)	Familial cerebellar ataxia	174	Coding regions of all 17 exons and the flanking introns
KCDN3 (SCA22/ SCA19)	1. Familial cerebellar ataxia	230	Coding regions of all 6 exons and the flanking introns
	2. Sporadic ataxia	180	Coding regions of exon 2 and 3 and their flanking introns

Familial cerebellar ataxia: defined as the presence of at least two affected members but the inheritance is undetermined.

4.4.4 Results

(1) *PDYN* variants

Three novel heterozygous *PDYN* variants were identified in three unrelated English patients: c.65G>A; p.Cys22Tyr (C22Y), c.74G>A; p.Arg25Gln (R25Q) and c.374G>A; p.Glu159Asp (G159D). C22Y was considered pathogenic because it was not reported in the ESV database or other public genome databases; it was absent in 570 chromosomes from matched British controls; it was predicted to be damaging to protein function by PolyPhen2 and SIFT (table 4-5, p139) and it changed a highly conserved amino acid (figure 4-8, p139). The C22Y mutation was identified in a 55-year-old Caucasian man who developed a slowly progressive cerebellar ataxia at the age of 22 years. There was no history of cerebellar ataxia in his family members. On examination, he had dysarthria, broken pursuit on eye movements and prominent ataxia in the

upper and lower limbs. The reflexes were slightly brisk in the lower limbs. He also had infrequent seizures from the age of 15 years old. His brain MRI showed cerebellar atrophy and left hippocampal sclerosis. His electromyography (EMG), NCS and the muscle biopsy from the quadriceps were normal. The remaining two variants, R25Q and G159D, were present in the ESV database and both were predicted to cause benign amino acid changes and therefore they were rare neutral polymorphisms.

Table 4-5. The *PDYN* mutations and rare variants detected in this study

Case	Nucleotide change	Amino Acid change	Polyphen	SIFT	Sequence
P-1	c.65G>A	C22Y	Damaging	Not tolerated	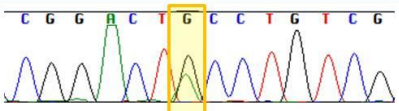
P-2	c.74G>A	R25Q	Benign	Tolerated	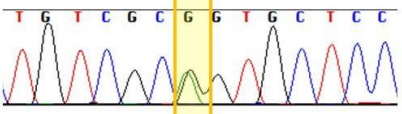
P-3	c.406G>A	G159D	Benign	Tolerated	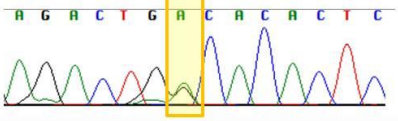

Figure 4-8. Conservation of mutated amino acids in the *PDYN* gene

Three of four previously reported *PDYN* mutations are localized in the dynorphin A (Dyn A) synthesis domain (figure 4-9). The three variants in this study occurred in different regions of the *PDYN*: C22Y and R25Q were located in the opioid peptides α-NE domain in exon 3, while G159D was located in exon 4 and lay within the propeptide region of the gene. The functions of these domains are still unclear.

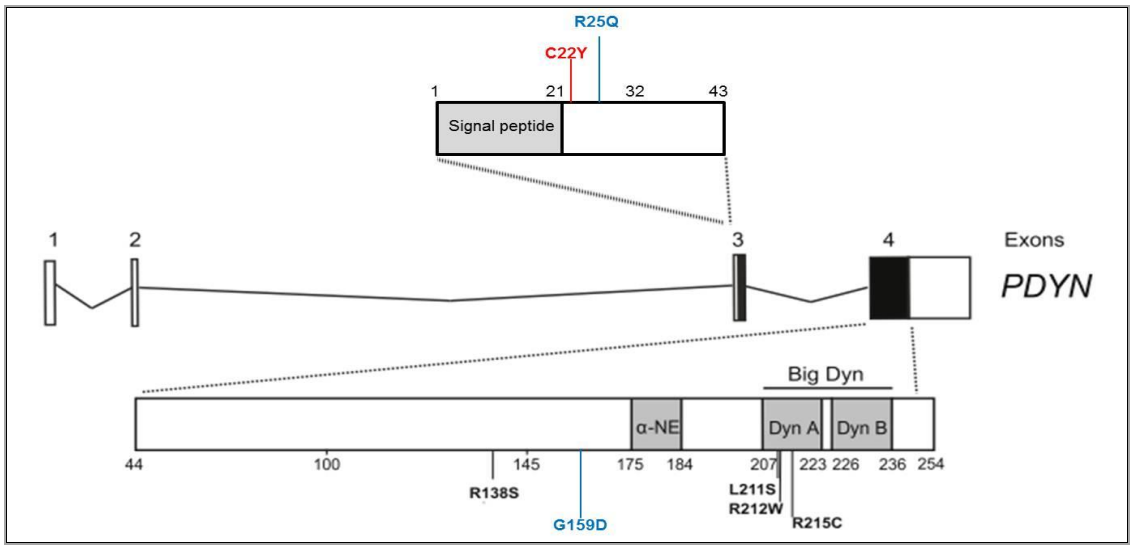

Figure 4-9. Genomic structure and mutations of the *PDYN* gene

The encoding protein, PDYN, contains the domains of the opioid peptides α-neoendorphin (α-NE), prodynorphin (Prodyn), dynorphin A (Dyn A), dynorphin B (Dyn B), and big dynorphin (Big Dyn) encompassing Dyn A and Dyn B. The novel putative pathogenic mutation C22Y (red) and the two rare neutral polymorphisms R25Q and G159D (blue) are all localized in the propeptide region. The locations of previously reported mutations were also shown (black). (modified from Bakalkin et al. 2010)

(2) *KCND3* and *AFG3L2* variants

One heterozygous synonymous mutation and two intronic SNPs were identified in the *KCND3* gene in 410 patients. Nevertheless, no mutation causing an amino acid substitution was identified in the cohort.

As for *AFG3L2*, one missense SNP, c.2314C>T;p.L772F (rs117182113), was identified in one patient. Two synonymous mutations which were not reported in any population were detected from two unrelated patients. An additional eleven non-pathogenic SNPs were identified with variable frequencies. However, no presumed pathological mutation was found in the selected 174 patients.

Details of identified variants in the two genes and their frequencies in patients are listed in table 4-6 (p141).

Table 4-6. *KCND3* and *AFG3L2* variants identified in patients with cerebellar ataxias

Position	dbSNP ID	Mutation type	cDNA Change	Protein Change	MAF in studied cohort (%)	MAF in EVS (%)
KCND3						
1:112329552	unknown	intron	c.1269+14G>T	NA	1.7	0.0077
1:112525085	rs17221819	synonymous	c.264C>T	p.(P88=)	3.9	9.5341
1:112319899	rs72548732	intron	c.1462-4G>T	NA	0.24	1.3225
AFG3L2						
18:12351360	.	synonymous	c.1407C>T	p.(F469=)	0.57	NA
18:12329709	.	synonymous	c.2379G>A	p.(E793=)	0.57	NA
18:12329644	rs117182113	missense	c.2314C>T	p.(L772F)	0.57	0.1461
18:12367018	rs141538541	synonymous	c.498C>T	p.(S166=)	0.57	0.0308
18:12367144	rs111696683	intronic	c.400-28C>T	NA	0.57	NA
18:12371433	rs72875314	intronic	c.214+158T>C	NA	1.15	0.004
18:12337322	rs117096851	intron	c.2175+18G>A	NA	2.87	1.2071
18:12359920	rs8097342	intron	c.752+6C>T	NA	3.16	31.516
18:12348285	rs11553521	synonymous	c.1650A>G	p.(E550=)	3.62	22.074
18:12337288	rs77671335	intron	c.2175+52G>A	NA	4.02	3.6275
18:12358661	rs8091858	intron	c.1026+8G>A	NA	4.6	2.2451
18:12371258	rs9303771	intronic	c.214+333G>T	NA	24.14	0.046
18:12351342	rs11080572	synonymous	c.1389G>A	p.(L463=)	33.33	31.385
18:12329536	rs1129115	3'-utr	c.*28G>C	NA	33.91	27.718

MAF in ESV= the minor-allele frequency data retrieved from ESV database; **NA=** not available; **dbSNP ID=** identifier of Database of single nucleotide polymorphisms (http://www.ncbi.nlm.nih.gov/snp/)

7.2.4 Discussion

This study identified one novel missense mutation (C22Y) in the *PDYN* gene in a patient with early-onset cerebellar ataxia with a negative family history. This mutation was predicted to be damaging and highly conserved suggesting pathogenicity. Two other *PDYN* variants (R25Q and G159D) were found in late-onset ataxia patients. They might be very rare neutral polymorphisms as they were detected in the ESV database; they were not well conserved and they were predicted to be benign and tolerated, despite absence of both changes in 570 controls.

Our results provided evidence that SCA23 caused by *PDYN* mutations is very rare and accounts for a very a small proportion of patients with hereditary cerebellar ataxia. The frequency of *PDYN* mutations in our cohort is approximately 0.1 % (1/734), which is less than the 0.4% (4/1100) in Dutch patients(Bakalkin et al. 2010) and the 0.8% (1/119) in a US cohort.(Fogel et

al. 2012) Given the rarity of its mutations, *PDYN* screening should be considered where the common ataxia genes have been excluded.

Three of the four previously identified *PDYN* mutations (L211S, R212W, R215C) were localized within the DynA domain and have been proved to have toxic gain-of-function mediated through increased expression of Dyn A peptides and increased leakage of ions through the plasma membrane.(Watanabe et al. 2012) R138S was the only *PDYN* mutation which was located in the non-opioid propeptide region reported before our study. This mutation was predicted to create an extra serine phosphorylation site, and thus might affect processing or trafficking of the mutant protein. However, the association of these effects with the motor and coordination dysfunction is still unclear.(Bakalkin et al. 2010) However, the C22Y mutation in this study lies within the propeptide region of PDYN, and was not predicted to increase phosphorylation in this region (predicted by NetPhos 2.0 server, www.cbs.dtu.dk/services/NetPhos/). Further work is needed to explore the influence of the novel mutation on *PDYN* function.

This study also represented the first genetic epidemiological study of *KCND3* and *AFG3L2* mutations in the UK. No pathogenic variants were identified in either of these two genes although many variants were detected. To date, *KCND3* mutations have been identified in patients of diverse ethnic origins.(Lee et al. 2012) Also, SCA28 was estimated to account for 3% of the patients of non-polyglutamine expansion SCAs and for approximately 1.5% of all SCAs in a large-scale study with 366 European-origin patients recruited.(Cagnoli et al. 2010) The absence of *KCND3* or *AFG3L2* mutations in our patients suggests that the prevalence of SCA22/SCA19 and SCA28 vary in different ethnic origins and both may be very rare in the British population.

References

Al-Maawali A, Rolfs A, Klingenhaeger M, Yoon G (2011) Hereditary spastic paraplegia associated with axonal neuropathy: a novel mutation of SPG3A in a large family. J Clin Neuromuscul Dis 12: 143-6

Bakalkin G, Watanabe H, Jezierska J, Depoorter C, Verschuuren-Bemelmans C, Bazov I, Artemenko KA, Yakovleva T, Dooijes D, Van de Warrenburg BP, Zubarev RA, Kremer B, Knapp PE, Hauser KF, Wijmenga C, Nyberg F, Sinke RJ, Verbeek DS (2010) Prodynorphin mutations cause the neurodegenerative disorder spinocerebellar ataxia type 23. Am J Hum Genet 87: 593-603

Barry DM, Millecamps S, Julien JP, Garcia ML (2007) New movements in neurofilament transport, turnover and disease. Exp Cell Res 313: 2110-20

Blair MA, Ma S, Hedera P (2006) Mutation in KIF5A can also cause adult-onset hereditary spastic paraplegia. Neurogenetics 7: 47-50

Boerkoel CF, Takashima H, Garcia CA, Olney RK, Johnson J, Berry K, Russo P, Kennedy S, Teebi AS, Scavina M, Williams LL, Mancias P, Butler IJ, Krajewski K, Shy M, Lupski JR (2002) Charcot-Marie-Tooth disease and related neuropathies: mutation distribution and genotype-phenotype correlation. Ann Neurol 51: 190-201

Bouhouche A, Benomar A, Bouslam N, Chkili T, Yahyaoui M (2006) Mutation in the epsilon subunit of the cytosolic chaperonin-containing t-complex peptide-1 (Cct5) gene causes autosomal recessive mutilating sensory neuropathy with spastic paraplegia. J Med Genet 43: 441-3

Braathen GJ (2012) Genetic epidemiology of Charcot-Marie-Tooth disease. Acta Neurol Scand Suppl: iv-22

Brownlees J, Ackerley S, Grierson AJ, Jacobsen NJ, Shea K, Anderton BH, Leigh PN, Shaw CE, Miller CC (2002) Charcot-Marie-Tooth disease neurofilament mutations disrupt neurofilament assembly and axonal transport. Hum Mol Genet 11: 2837-44

Cagnoli C, Mariotti C, Taroni F, Seri M, Brussino A, Michielotto C, Grisoli M, Di Bella D, Migone N, Gellera C, Di Donato S, Brusco A (2006) SCA28, a novel form of autosomal dominant cerebellar ataxia on chromosome 18p11.22-q11.2. Brain 129: 235-42

Cagnoli C, Stevanin G, Brussino A, Barberis M, Mancini C, Margolis RL, Holmes SE, Nobili M, Forlani S, Padovan S, Pappi P, Zaros C, Leber I, Ribai P, Pugliese L, Assalto C, Brice A, Migone N, Durr A, Brusco A (2010) Missense mutations in the AFG3L2 proteolytic domain account for approximately 1.5% of European autosomal dominant cerebellar ataxias. Hum Mutat 31: 1117-24

Chung MY, Lu YC, Cheng NC, Soong BW (2003) A novel autosomal dominant spinocerebellar ataxia (SCA22) linked to chromosome 1p21-q23. Brain 126: 1293-9

Crimella C, Baschirotto C, Arnoldi A, Tonelli A, Tenderini E, Airoldi G, Martinuzzi A, Trabacca A, Losito L, Scarlato M, Benedetti S, Scarpini E, Spinicci G, Bresolin N, Bassi MT (2012) Mutations in the motor and stalk domains of KIF5A in spastic paraplegia type 10 and in axonal Charcot-Marie-Tooth type 2. Clin Genet 82: 157-64

De Jonghe P, Mersivanova I, Nelis E, Del Favero J, Martin JJ, Van Broeckhoven C, Evgrafov O, Timmerman V (2001) Further evidence that neurofilament light chain gene mutations can cause Charcot-Marie-Tooth disease type 2E. Ann Neurol 49: 245-9

Desarnaud F, Bidichandani S, Patel PI, Baulieu EE, Schumacher M (2000) Glucocorticosteroids stimulate the activity of the promoters of peripheral myelin protein-22 and protein zero genes in Schwann

cells. Brain Res 865: 12-6

Desarnaud F, Do Thi AN, Brown AM, Lemke G, Suter U, Baulieu EE, Schumacher M (1998) Progesterone stimulates the activity of the promoters of peripheral myelin protein-22 and protein zero genes in Schwann cells. J Neurochem 71: 1765-8

Du J, Hu YC, Tang BS, Chen C, Luo YY, Zhan ZX, Zhao GH, Jiang H, Xia K, Shen L (2011) Expansion of the phenotypic spectrum of SPG6 caused by mutation in NIPA1. Clin Neurol Neurosurg 113: 480-2

Duarri A, Jezierska J, Fokkens M, Meijer M, Schelhaas HJ, den Dunnen WF, van Dijk F, Verschuuren-Bemelmans C, Hageman G, van de Vlies P, Kusters B, van de Warrenburg BP, Kremer B, Wijmenga C, Sinke RJ, Swertz MA, Kampinga HH, Boddeke E, Verbeek DS (2012) Mutations in potassium channel kcnd3 cause spinocerebellar ataxia type 19. Ann Neurol 72: 870-80

Durr A (2010) Autosomal dominant cerebellar ataxias: polyglutamine expansions and beyond. Lancet Neurol 9: 885-94

Ebbing B, Mann K, Starosta A, Jaud J, Schols L, Schule R, Woehlke G (2008) Effect of spastic paraplegia mutations in KIF5A kinesin on transport activity. Hum Mol Genet 17: 1245-52

Edener, U., J. Wollner, et al. (2010). Early onset and slow progression of SCA28, a rare dominant ataxia in a large four-generation family with a novel AFG3L2 mutation. Eur J Hum Genet 18(8): 965-8

Fichera M, Lo Giudice M, Falco M, Sturnio M, Amata S, Calabrese O, Bigoni S, Calzolari E, Neri M (2004) Evidence of kinesin heavy chain (KIF5A) involvement in pure hereditary spastic paraplegia. Neurology 63: 1108-10

Fogel BL, Lee JY, Lane J, Wahnich A, Chan S, Huang A, Osborn GE, Klein E, Mamah C, Perlman S, Geschwind DH, Coppola G (2012) Mutations in rare ataxia genes are uncommon causes of sporadic cerebellar ataxia. Mov Disord 27: 442-6

Friede RL, Samorajski T (1970) Axon caliber related to neurofilaments and microtubules in sciatic nerve fibers of rats and mice. Anat Rec 167: 379-88

Fuger P, Sreekumar V, Schule R, et al. (2012) Spastic paraplegia mutation N256S in the neuronal microtubule motor KIF5A disrupts axonal transport in a Drosophila HSP model. PLoS Genet 8:e1003066

Goizet C, Boukhris A, Mundwiller E, Tallaksen C, Forlani S, Toutain A, Carriere N, Paquis V, Depienne C, Durr A, Stevanin G, Brice A (2009) Complicated forms of autosomal dominant hereditary spastic paraplegia are frequent in SPG10. Hum Mutat 30: E376-85

Gonzalez MA, Lebrigio RF, Van Booven D, Ulloa RH, Powell E, Speziani F, Tekin M, Schule R, Zuchner S (2013) GEnomes Management Application (GEM.app): a new software tool for large-scale collaborative genome analysis. Hum Mutat 34: 842-6

Guelly C, Zhu PP, Leonardis L, Papic L, Zidar J, Schabhuttl M, Strohmaier H, Weis J, Strom TM, Baets J, Willems J, De Jonghe P, Reilly MM, Frohlich E, Hatz M, Trajanoski S, Pieber TR, Janecke AR, Blackstone C, Auer-Grumbach M (2011) Targeted high-throughput sequencing identifies mutations in atlastin-1 as a cause of hereditary sensory neuropathy type I. Am J Hum Genet 88: 99-105

Gunawardena S, Goldstein LS (2004) Cargo-carrying motor vehicles on the neuronal highway: transport pathways and neurodegenerative disease. J Neurobiol 58: 258-71

Hewamadduma C, McDermott C, Kirby J, Grierson A, Panayi M, Dalton A, Rajabally Y, Shaw P (2009)

New pedigrees and novel mutation expand the phenotype of REEP1-associated hereditary spastic paraplegia (HSP). Neurogenetics 10: 105-10

Hirokawa N, Noda Y, Tanaka Y, Niwa S (2009) Kinesin superfamily motor proteins and intracellular transport. Nat Rev Mol Cell Biol 10: 682-96

Hsu YH, Huang HY, Tsaur ML (2003) Contrasting expression of Kv4.3, an A-type K+ channel, in migrating Purkinje cells and other post-migratory cerebellar neurons. Eur J Neurosci 18: 601-12

Jordanova A, De Jonghe P, Boerkoel CF, Takashima H, De Vriendt E, Ceuterick C, Martin JJ, Butler IJ, Mancias P, Papasozomenos S, Terespolsky D, Potocki L, Brown CW, Shy M, Rita DA, Tournev I, Kremensky I, Lupski JR, Timmerman V (2003) Mutations in the neurofilament light chain gene (NEFL) cause early onset severe Charcot-Marie-Tooth disease. Brain 126: 590-7

Klebe S, Lossos A, Azzedine H, Mundwiller E, Sheffer R, Gaussen M, Marelli C, Nawara M, Carpentier W, Meyer V, Rastetter A, Martin E, Bouteiller D, Orlando L, Gyapay G, El-Hachimi KH, Zimmerman B, Gamliel M, Misk A, Lerer I, Brice A, Durr A, Stevanin G (2012) KIF1A missense mutations in SPG30, an autosomal recessive spastic paraplegia: distinct phenotypes according to the nature of the mutations. Eur J Hum Genet 20: 645-9

Kumar KR, Sue CM, Burke D, Ng K (2012) Peripheral neuropathy in hereditary spastic paraplegia due to spastin (SPG4) mutation - A neurophysiological study using excitability techniques. Clin Neurophysiol 123(7):1454-9

Lee IB, Kim SK, Chung SH, Kim H, Kwon TK, Min do S, Chang JS (2008) The effect of rod domain A148V mutation of neurofilament light chain on filament formation. BMB Rep 41: 868-74

Lee YC, Durr A, Majczenko K, Huang YH, Liu YC, Lien CC, Tsai PC, Ichikawa Y, Goto J, Monin ML, Li JZ, Chung MY, Mundwiller E, Shakkottai V, Liu TT, Tesson C, Lu YC, Brice A, Tsuji S, Burmeister M, Stevanin G, Soong BW (2012) Mutations in KCND3 cause spinocerebellar ataxia type 22. Ann Neurol 72: 859-69

Leonhard K, Stiegler A, Neupert W, Langer T (1999) Chaperone-like activity of the AAA domain of the yeast Yme1 AAA protease. Nature 398: 348-51

Li J, Parker B, Martyn C, Natarajan C, Guo J (2013) The PMP22 Gene and Its Related Diseases. Mol Neurobiol 47(2):673-98

Liu YT, Laura M, Hersheson J, Horga A, Jaunmuktane Z, Brandner S, Pittman A, Hughes D, Polke JM, Sweeney MG, Proukakis C, Janssen JC, Auer-Grumbach M, Zuchner S, Shields KG, Reilly MM, Houlden H (2014) Extended phenotypic spectrum of KIF5A mutations: From spastic paraplegia to axonal neuropathy. Neurology 83(7): 612-9

Lo Giudice M, Neri M, Falco M, Sturnio M, Calzolari E, Di Benedetto D, Fichera M (2006) A missense mutation in the coiled-coil domain of the KIF5A gene and late-onset hereditary spastic paraplegia. Arch Neurol 63: 284-7

Lupski JR (2000) Axonal Charcot-Marie-Tooth disease and the neurofilament light gene (NF-L). Am J Hum Genet 67: 8-10

Maier M, Castagner F, Berger P, Suter U (2003) Distinct elements of the peripheral myelin protein 22 (PMP22) promoter regulate expression in Schwann cells and sensory neurons. Mol Cell Neurosci 24: 803-17

Manfioletti G, Ruaro ME, Del Sal G, Philipson L, Schneider C (1990) A growth arrest-specific (gas) gene

codes for a membrane protein. Mol Cell Biol 10: 2924-30

Marelli C, Cazeneuve C, Brice A, Stevanin G, Durr A (2011) Autosomal dominant cerebellar ataxias. Rev Neurol (Paris) 167: 385-400

Mersiyanova IV, Perepelov AV, Polyakov AV, Sitnikov VF, Dadali EL, Oparin RB, Petrin AN, Evgrafov OV (2000) A new variant of Charcot-Marie-Tooth disease type 2 is probably the result of a mutation in the neurofilament-light gene. Am J Hum Genet 67: 37-46

Miltenberger-Miltenyi G, Janecke AR, Wanschitz JV, Timmerman V, Windpassinger C, Auer-Grumbach M, Loscher WN (2007) Clinical and electrophysiological features in Charcot-Marie-Tooth disease with mutations in the NEFL gene. Arch Neurol 64: 966-70

Muma NA, Hoffman PN (1993) Neurofilaments are intrinsic determinants of axonal caliber. Micron 24: 677-83

Murphy SM, Laura M, Fawcett K, Pandraud A, Liu YT, Davidson GL, Rossor AM, Polke JM, Castleman V, Manji H, Lunn MP, Bull K, Ramdharry G, Davis M, Blake JC, Houlden H, Reilly MM (2012) Charcot-Marie-Tooth disease: frequency of genetic subtypes and guidelines for genetic testing. J Neurol Neurosurg Psychiatry 83: 706-10

Musumeci O, Bassi MT, Mazzeo A, Grandis M, Crimella C, Martinuzzi A, Toscano A (2010) A novel mutation in KIF5A gene causing hereditary spastic paraplegia with axonal neuropathy. Neurol Sci 32: 665-8

Nelis E, De Jonghe P, De Vriendt E, Patel PI, Martin JJ, Van Broeckhoven C (1998) Mutation analysis of the nerve specific promoter of the peripheral myelin protein 22 gene in CMT1 disease and HNPP. J Med Genet 35: 590-3

Oberdick J, Baader SL, Schilling K (1998) From zebra stripes to postal zones: deciphering patterns of gene expression in the cerebellum. Trends Neurosci 21: 383-90

Reid E, Kloos M, Ashley-Koch A, Hughes L, Bevan S, Svenson IK, Graham FL, Gaskell PC, Dearlove A, Pericak-Vance MA, Rubinsztein DC, Marchuk DA (2002) A kinesin heavy chain (KIF5A) mutation in hereditary spastic paraplegia (SPG10). Am J Hum Genet 71: 1189-94

Reilly MM (2009) NEFL-related Charcot-Marie-tooth disease: an unraveling story. Ann Neurol 66: 714-6

Riviere JB, Ramalingam S, Lavastre V, Shekarabi M, Holbert S, Lafontaine J, Srour M, Merner N, Rochefort D, Hince P, Gaudet R, Mes-Masson AM, Baets J, Houlden H, Brais B, Nicholson GA, Van Esch H, Nafissi S, De Jonghe P, Reilly MM, Timmerman V, Dion PA, Rouleau GA (2011) KIF1A, an axonal transporter of synaptic vesicles, is mutated in hereditary sensory and autonomic neuropathy type 2. Am J Hum Genet 89: 219-30

Saberan-Djoneidi D, Sanguedolce V, Assouline Z, Levy N, Passage E, Fontes M (2000) Molecular dissection of the Schwann cell specific promoter of the PMP22 gene. Gene 248: 223-31

Sailer A, Houlden H (2012) Recent advances in the genetics of cerebellar ataxias. Curr Neurol Neurosci Rep 12: 227-36

Scarano V, Mancini P, Criscuolo C, De Michele G, Rinaldi C, Tucci T, Tessa A, Santorelli FM, Perretti A, Santoro L, Filla A (2005) The R495W mutation in SPG3A causes spastic paraplegia associated with axonal neuropathy. J Neurol 252: 901-3

Schelhaas HJ, Verbeek DS, Van de Warrenburg BP, Sinke RJ (2004) SCA19 and SCA22: evidence for one locus with a worldwide distribution. Brain 127: E6; author reply E7

Schule R, Kremer BP, Kassubek J, Auer-Grumbach M, Kostic V, Klopstock T, Klimpe S, Otto S, Boesch S, van de Warrenburg BP, Schols L (2008) SPG10 is a rare cause of spastic paraplegia in European families. J Neurol Neurosurg Psychiatry 79: 584-7

Schule R, Schols L (2012) Genetics of hereditary spastic paraplegias. Semin Neurol 31: 484-93

Schulte T, Miterski B, Bornke C, Przuntek H, Epplen JT, Schols L (2003) Neurophysiological findings in SPG4 patients differ from other types of spastic paraplegia. Neurology 60: 1529-32

Sinkiewicz-Darol E, Kabzinska D, Moszynska I, Kochanski A (2010) The 5' regulatory sequence of the PMP22 in the patients with Charcot-Marie-Tooth disease. Acta Biochim Pol 57: 373-7

Snipes GJ, Suter U, Welcher AA, Shooter EM (1992) Characterization of a novel peripheral nervous system myelin protein (PMP-22/SR13). J Cell Biol 117: 225-38

Suter U, Snipes GJ, Schoener-Scott R, Welcher AA, Pareek S, Lupski JR, Murphy RA, Shooter EM, Patel PI (1994) Regulation of tissue-specific expression of alternative peripheral myelin protein-22 (PMP22) gene transcripts by two promoters. J Biol Chem 269: 25795-808

Tessa A, Silvestri G, de Leva MF, Modoni A, Denora PS, Masciullo M, Dotti MT, Casali C, Melone MA, Federico A, Filla A, Santorelli FM (2008) A novel KIF5A/SPG10 mutation in spastic paraplegia associated with axonal neuropathy. J Neurol 255: 1090-2

Timmerman V, Clowes VE, Reid E (2012) Overlapping molecular pathological themes link Charcot-Marie-Tooth neuropathies and hereditary spastic paraplegias. Exp Neurol 246: 14-25

Tsaur ML, Chou CC, Shih YH, Wang HL (1997) Cloning, expression and CNS distribution of Kv4.3, an A-type K+ channel alpha subunit. FEBS Lett 400: 215-20

Verbeek DS, Schelhaas JH, Ippel EF, Beemer FA, Pearson PL, Sinke RJ (2002) Identification of a novel SCA locus (SCA19) in a Dutch autosomal dominant cerebellar ataxia family on chromosome region 1p21-q21. Hum Genet 111: 388-93

Verbeek DS, van de Warrenburg BP, Wesseling P, Pearson PL, Kremer HP, Sinke RJ (2004) Mapping of the SCA23 locus involved in autosomal dominant cerebellar ataxia to chromosome region 20p13-12.3. Brain 127: 2551-7

Watanabe H, Mizoguchi H, Verbeek DS, Kuzmin A, Nyberg F, Krishtal O, Sakurada S, Bakalkin G (2012) Non-opioid nociceptive activity of human dynorphin mutants that cause neurodegenerative disorder spinocerebellar ataxia type 23. Peptides 35: 306-10

Weedon MN, Hastings R, Caswell R, Xie W, Paszkiewicz K, Antoniadi T, Williams M, King C, Greenhalgh L, Newbury-Ecob R, Ellard S (2011) Exome sequencing identifies a DYNC1H1 mutation in a large pedigree with dominant axonal Charcot-Marie-Tooth disease. Am J Hum Genet 89: 308-12

Willemsen MH, Vissers LE, Willemsen MA, van Bon BW, Kroes T, de Ligt J, de Vries BB, Schoots J, Lugtenberg D, Hamel BC, van Bokhoven H, Brunner HG, Veltman JA, Kleefstra T (2012) Mutations in DYNC1H1 cause severe intellectual disability with neuronal migration defects. J Med Genet 49: 179-83

Windpassinger C, Auer-Grumbach M, Irobi J, Patel H, Petek E, Horl G, Malli R, Reed JA, Dierick I, Verpoorten N, Warner TT, Proukakis C, Van den Bergh P, Verellen C, Van Maldergem L, Merlini L, De Jonghe P, Timmerman V, Crosby AH, Wagner K (2004) Heterozygous missense mutations in BSCL2 are associated with distal hereditary motor neuropathy and Silver syndrome. Nat Genet 36:

271-6

Xia C, Rahman A, Yang Z, Goldstein LS (1998) Chromosomal localization reveals three kinesin heavy chain genes in mouse. Genomics 52: 209-13

Xia CH, Roberts EA, Her LS, Liu X, Williams DS, Cleveland DW, Goldstein LS (2003) Abnormal neurofilament transport caused by targeted disruption of neuronal kinesin heavy chain KIF5A. J Cell Biol 161: 55-66

Yates DM, Manser C, De Vos KJ, Shaw CE, McLoughlin DM, Miller CC (2009) Neurofilament subunit (NFL) head domain phosphorylation regulates axonal transport of neurofilaments. Eur J Cell Biol 88: 193-202

Yum SW, Zhang J, Mo K, Li J, Scherer SS (2009) A novel recessive Nefl mutation causes a severe, early-onset axonal neuropathy. Ann Neurol 66: 759-70

Zuchner S, Vorgerd M, Sindern E, Schroder JM (2004) The novel neurofilament light (NEFL) mutation Glu397Lys is associated with a clinically and morphologically heterogeneous type of Charcot-Marie-Tooth neuropathy. Neuromuscul Disord 14: 147-57

Chapter 5

Results: Whole exome sequencing in patients with inherited neuropathies and related disorders

An accurate genetic diagnosis has not been achieved in a significant number of patients affected by inherited neurological diseases. For example, the current detection rate of disease-associated mutation in HSN is less than 20%.(Davidson et al. 2012). Similarly, only approximately 60% of patients with cerebellar ataxia receive a definite genetic diagnosis.(Sailer et al. 2012) The difficulty in achieving a genetic diagnosis are likely due to the limitations in genetic technology to test all the possible known genes, but also because many disease-associated genes and mutation types have not been discovered yet. It is possible that many unknown mutations are deep intronic changes, large deletions or insertions or novel repeat expansions. This chapter describes the application of WES in genetic diagnosis of complex syndromes which could not be diagnosed by conventional approach, including HSN complicated by additional features (HSN-plus syndromes), ARCAs and recessive CMT6 (axonal neuropathy with optic atrophy). Mutations in *DNMT1*, *ADCK3* and *SACS* were successfully detected, documenting that WES can identify pathogenic mutations efficiently in genes which are associated with different phenotypes but too large or rare to be routinely screened. WES was also helpful in detecting mutations in novel disease-causing gene, such as the *RNF216* gene in a family with ARCA. A few potential candidate genes for inherited neuropathies were identified through WES including *PDXK* gene in a case of recessive ARCMT2 with optic atrophy and *WFS1* and *NAV2* genes in HSN-plus syndromes.

5.1 Overview

5.1.1 Patients and Methods

WES was performed in patients affected by the following conditions in an attempt to achieve a genetic diagnosis:

(1) A cohort of 17 affected individuals from 12 families who had HSN associated with variable degree of cerebellar ataxia, vestibular failure or sensorineuronal hearing impairment (HSN-plus syndromes). These patients were previously extensively screened and resulted negative for mutations in *SPTLC1, RAB7, WNK1/HSN2, FAM134B, NTRK1 (TRKA)* and *NGFB.*

(2) One patient with axonal neuropathy and optic atrophy (CMT6) belonging to a consanguineous family

(3) A cohort of 18 affected individuals from 16 families with ARCA associated with variable additional symptoms, such as spasticity, neuropathy, dystonia, myoclonus, facial dysmorphism, or hypogonadism. Friedreich's ataxia, AOA1, AOA2, ATM, DYT1, SCA1-3 and acquired aetiologies of cerebellar ataxia were previously excluded in these patients.

5.1.2 Strategy of WES analysis

For each sample, three micrograms of gDNA was used for library preparation and enrichment according to the manufacturer's protocol. Exome-enriched library were subjected to massively parallel sequencing (100 bp paired-end reads) on Hiseq 1000 (Illumina) or Genome Analyzer IIx (illumine). Sequence alignment and variant calling were performed against the reference human genome (UCSC hg19). Details of the methods are described in Section 2.5.

After total variants were generated in an excel file, benign variants were filtered out by the criteria mentioned in Section 2.6.2. Variants in known genes causing similar or related phenotypes were firstly considered. For those patients who did not carry pathogenic variants in known genes but had similar phenotypes, two strategies were applied to look for potential candidate mutation: (1) any mutated gene shared by more than one family was searched; (2) for each family, some variants were selected if there is supportive evidence from their gene expression patterns, types of mutation, *in-silico* prediction of pathogeniticity and functional impacts previously observed in animal or cellular models. For potential variants selected through the two above strategies, they were validated by the following methods: Sanger sequencing, segregation testing if further family members were available and screening of the genes in further cohorts of similar phenotypes. Taking HSN as an example, the pipeline of variants prioritization is summarised in figure 5-1 (p151).

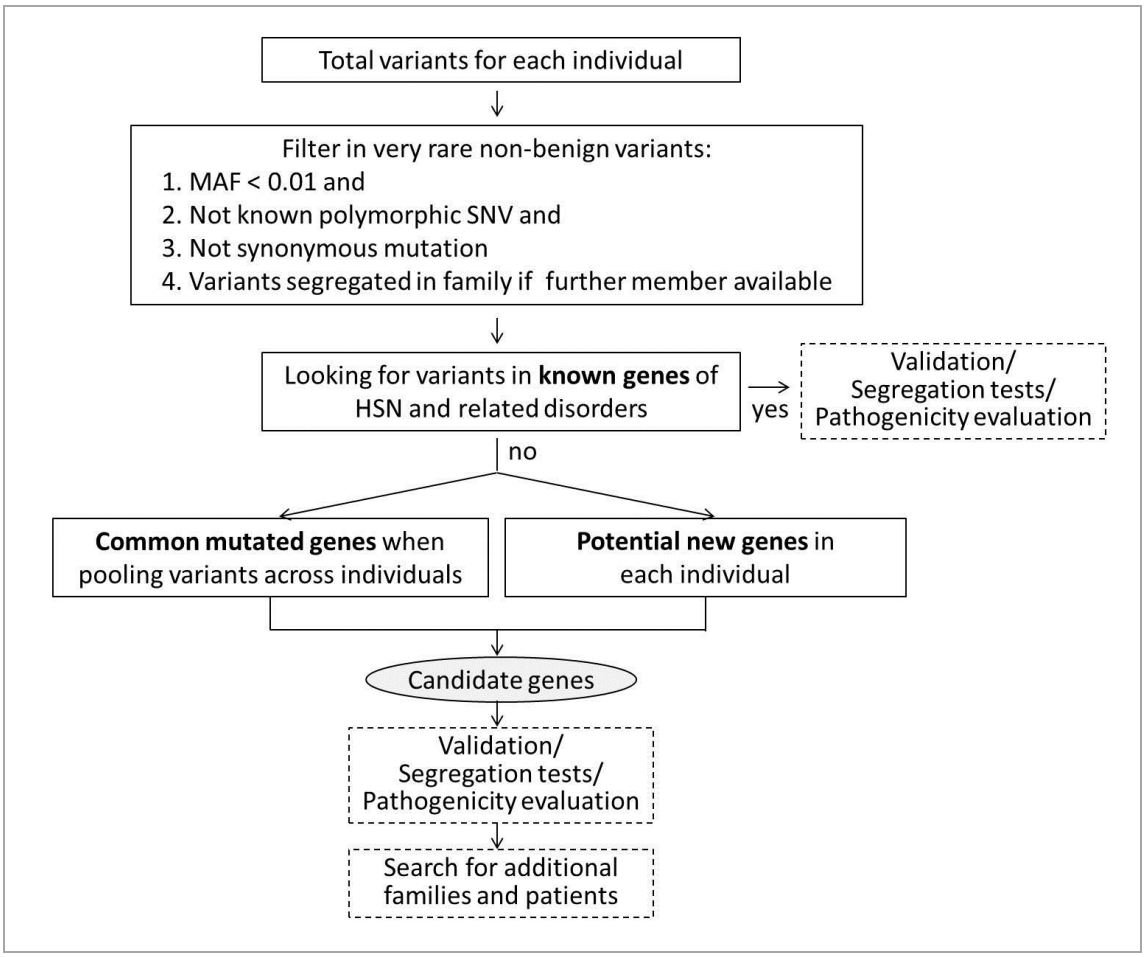

Figure 5-1. Pipeline of exonic variants prioritization

MAF= minor allelic frequency; SNV= single nucleotide variant

5.1.3 Results

Probable pathogenic mutations identified in patients with inherited neuropathies and complex ARCA syndromes are listed in table 5-1 (p152) and table 5-2 (p152) accordingly. The study on the identification of the *ADCK3* mutation in a family with ARCA and myoclonus has been described in Section 3.4.

Table 5-1. Probable pathogenic mutations in inherited neuropathies identified by WES

Phenotype	DNA No.*	Gene	Mutation	
Mutation in known HSN-related genes				
HSN with deafness	58800	*DNMT1*	missense mutation, het	c.1484A>G: p.Y495C
Mutation in potential novel HSN genes				
AD-HSN associated with ataxia and deafness	59547*	*WFS1*	missense mutation, het	c.1067C>A:p.S345Y
Late-onset HSN with ataxia	53596* 49876	*NAV2*	missense mutation, het	1. c.2744C>T:p.S915F 2. c.875A>C:p.Y292S
ARCMT2 with optic atrophy	45077	*PDXK*	missense mutation, hom	c.682G>A:p.A228T

AD= autosomal dominant; AR= autosomal recessive; CMT2: Charcot-Marie-Tooth disease type 2; HSN= hereditary sensory neuropathy; het= heterozygous; hom= homozygous; WES= whole exome sequencing; *only index patient is listed

Table 5-2. Probable pathogenic mutations in complex ARCA syndromes identified by WES

Phenotype	DNA No.*	Gene	Mutation	
Mutation in newly-identified genes				
ARCA with congenital ectodermal dysplasia	54273	*RNF216*	Splice site, hom	c.2453-2A>G
Mutation in known ARCA-related genes				
ARCA with myoclonus and tremor	52627	*ADCK3*	frameshift insertion, hom	c.1844_1845insG: p.S616Lfs
ARCA with spasticity and demyelinating neuropathy	25921	*SACS*	frameshift deletion, hom	c.5557_5561delCTTTT
Mutation in known HSP genes				
ARCA with spasticity and axonal neuropathy	5032	*ZFYVE26* (SPG15)	nonsense mutation, hom	c.4312C>T:p.R1438X
ARCA with spasticity and axonal neuropathy	47681	*PNPLA6* (SPG39)	missense mutation, hom	c.3817G>A:p.V1273M

ARCA= autosomal recessive cerebellar ataxia; HSP= hereditary spastic paraplegia; hom= homozygous; WES= whole exome sequencing

5.2 HSN with deafness caused by a heterozygous missense *DNMT1* mutation

(1) Clinical feature

WES was performed in a 43-year-old patient who developed sensory loss, ulcerations and painless fractures at the age of 30 and progressive hearing loss at the age of 36. He had no family history of neurological diseases. Neurological examination at the age of 43 showed reduced pinprick appreciation, vibration loss and decreased reflexes in the lower limbs. Muscle power was normal. Brain MRI showed mild cerebellar atrophy although there no clinical cerebellar signs were detectable at the age of 42. Neurophysiology was consistent with a sensory axonal neuropathy (table 5-3). Genetic testing for *RAB7, HSN2/WNK1, FAM134B, SPTLC* and *SPTLC1* were negative.

Table 5-3. Neurophysiology of the patient with *DNMT1* Y495C mutation

Sensory conduction	**R**	**L**	**Motor conduction**	**R**	**L**
Median nerve			Median nerve		
SNAP (uV)	NR	Abs	DML (ms)	NR	3.5
CV (m/s)	NR	Abs	CMAP (wrist) (mV)	NR	8.2
Ulnar nerve			CMAP (elbow) (mV)	NR	7.5
SNAP (uV)	NR	Abs	CV (m/s)	NR	53
CV (m/s)	NR	Abs	Minimum F-latency (ms)	NR	28.3
Radial nerve			Ulnar nerve		
SNAP (uV)	NR	4	DML (ms)	NR	2.7
CV (m/s)	NR	56	CMAP (wrist) (mV)	NR	12.6
Sural nerve (calf-ankle)			CMAP (above elbow) (mV)	NR	11.2
SNAP (uV)	Abs	NR	Minimum F-latency (ms)	NR	28.0
CV (m/s)	Abs	NR	Common peroneal nerve		
Superficial Peroneal nerve (calf-ankle)			DML (ms)	3.4	NR
SNAP (uV)	Abs	NR	CMAP (ankle) (mV)	5.3	NR
CV (m/s)	Abs	NR	CMAP (fib. Neck) (mV)	4.2	NR
			CV (fib. Neck-ankle) (m/s)	34	NR
			Minimum F-latency (ms)	54.3	NR
Concentric Needle EMG			Posterior Tibial nerve		
R Tib Ant	No spontaneous activity		DML (ms)	4.9	NR
R FDIO	Normal motor units recruiting		CMAP (ankle) (mV)	5.7	NR
	normally to a full interference pattern		Minimum F-latency (ms)	55.1	NR

Age at examination= 42; Abs= absent; CMAP= compound motor nerve action potential (mV); CV= conduction velocity (m/s); DML= distal motor latency; EMG= electromyography FDIO= first dorsal interosseous; L= left limbs; NR= not recorded; R= right limbs; SNAP= sensory nerve action potential (uV); Tib Ant= tibialis anterior.

(2) Genetic analysis

Both heterozygous and homozygous variants were analysed as the patient is the only known affected member in the family. There were 285 heterozygous variants after filtering out benigh variants. Among them, a heterozygous missense mutation, p.Tyr495Cys (Y495C), in the DNA-methyltransferase 1 gene (*DNMT1*) was considered to be the causative mutation as it has been previously reported in patients with HSN-IE, is a subtype of HSN-I which typically presented by sensory neuropathy and hearing loss as the presenting symptoms between the age of 20 and 35 and dementia subsequently in the fourth decade.(Klein 2012; Klein et al. 2011, also see table 1-2) The mutation was subsequently validated by Sanger sequencing. The process of whole exome analysis is summarised in figure 5-2.

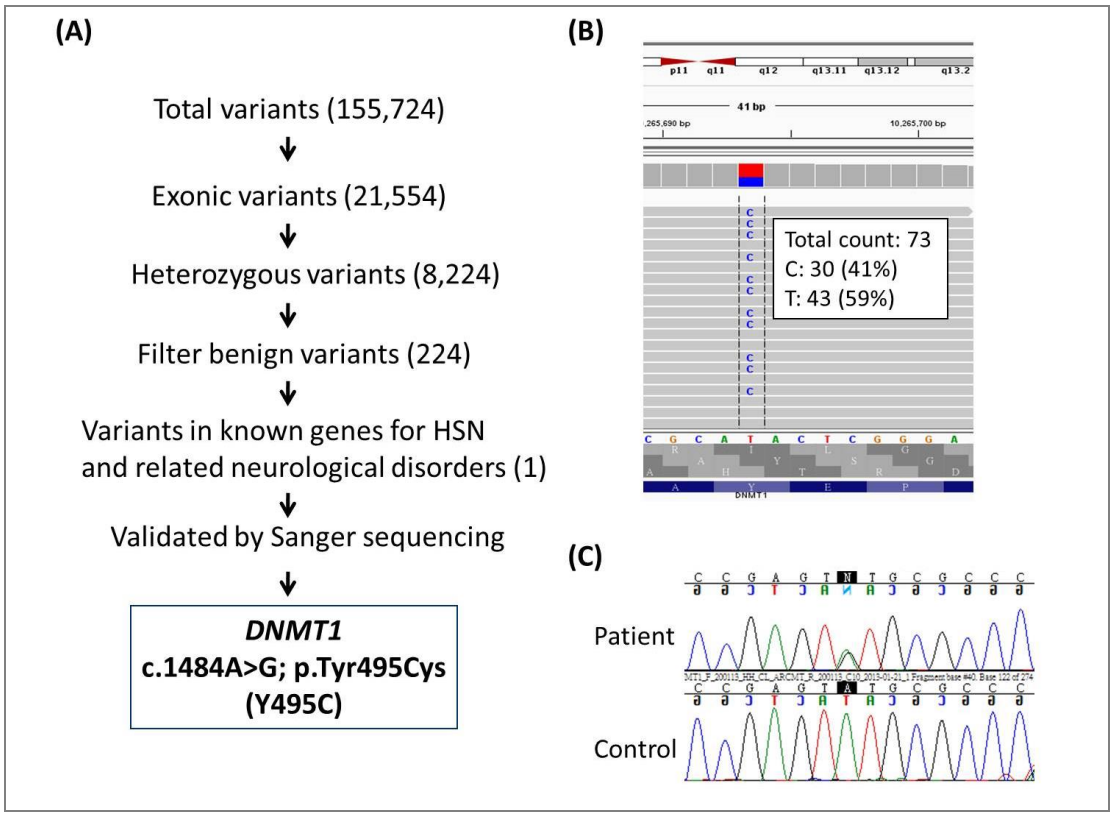

Figure 5-2. Whole exome sequencing of the patient with HSN and deafness

(A) The process of prioritizing exonic variants. *DNMT1* Y495C is revealed as the causative mutation after analysis.

(B) Heterozygosity and the sequencing depth (73X) of the exonic variant shown by IGV.

(C) Chromatogram from the patient. This mutation has been validated by Sanger sequencing.

(3) Discussion

DNMT1 plays a crucial role in maintenance of methylation, gene regulation and chromatin stability. DNA mismatch repair, cell cycle regulation in post-mitotic neurons and neurogenesis are influenced by DNA methylation.(Klein et al. 2011) Mutations in *DNMT1* were first

associated with HSN-IE and subsequently documented in cases of autosomal dominant cerebellar ataxia, deafness and narcolepsy (ADCA-DN), clinically characterised by late-onset (30-40 years) narcolepsy-cataplexy, deafness, cerebellar ataxia and variable dementia.(Winkelmann et al. 2012) Both HSN-IE and ADCA-DN have sensory neuropathy and cerebellar ataxia as parts of the syndrome but present in different ways. Patients with HSN-IE often have sensory neuropathy as the presenting symptoms during early adulthood and the cerebellar involvement usually occurs later and to a lesser degree, whereas patients with ADCA-DN have marked cerebellar dysfunction followed by sensory neuropathy at a later stage of the disease during the sixth decade. So far, all reported HSN patients had dementia or cognitive impairment though the age of onset was variable. (Klein 2012; Klein et al. 2013; Yuan et al. 2013) Clinical features of patients with reported *DNMT1* mutations are summarised in table 5-4 (p157).

This study documents how WES can rapidly detect mutations in a rare gene like *DNMT1* in patients with sensory neuropathy and profound deafness but not developed signs of dementia, atypical to previously reported HSN-IE cases. The mutation in our patient occurred at Tyr495, which is a highly conserved amino acid residue localized within the critical targeting-sequence domain of *DNMT1* (figure 5-3) and has been proposed as a hot spot for HSN-IE associated *DNMT1* mutations.(Klein et al. 2013; Klein et al. 2011; Yuan et al. 2013) Our finding supports the hypothesis.

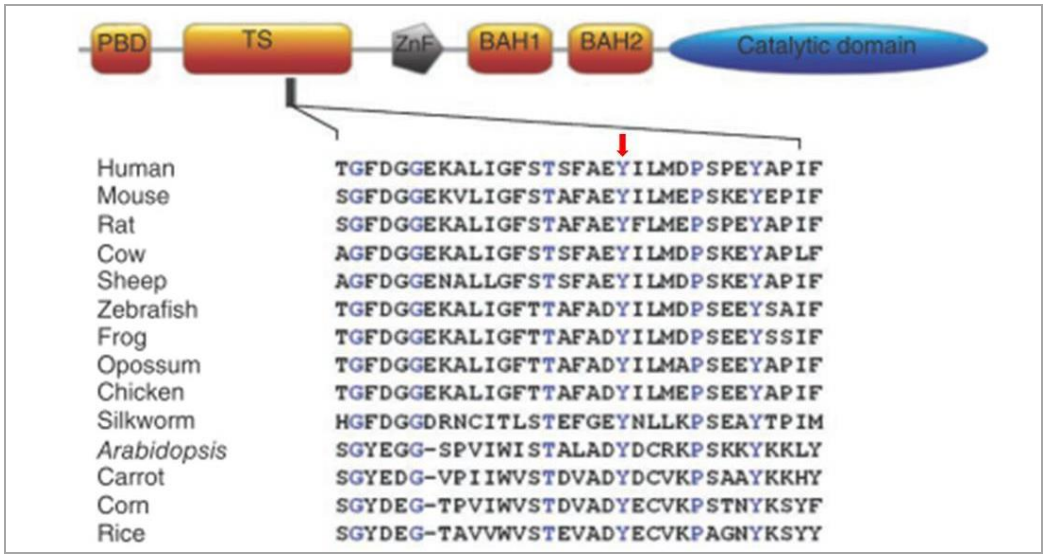

Figure 5-3. Location and conservation of *DNMT1* Thy495.

Top. Functional domains of *DNMT1* in the N-terminal region are illustrated: PBD=PCNA-binding domain; TS= targeting sequence; ZnF= zinc finger; BAH1 & 2= bromo adjacent homology domains 1 and 2. **Bottom.** Alignment of the part of the targeting sequence domain shows Y495 (red arrow head) is strictly conserved across different species. (modified from (Klein et al. 2011)

Our results suggest that *DNMT1* mutations can be associated with HSN and deafness without cognitive involvement although this may develop later since the patient is only 43. A longitudinal follow-up and neuropsychological evaluation are warranted in this patient. The study documented that *DNMT1* mutations can be associated with variable phenotypes. Because of the possibility of cognitive impairment in an advanced course, genetic testing for *DNMT1* mutations in patients with a pure sensory neuropathy will require more ethical consideration and detailed counselling.(Rossor et al. 2013)

Table 5-4. Clinical features of patients with *DNMT1* mutations.

Phenotype	HSN + deafness	HSAN-IE							ADCA-DN			
Mutation	Y495C	Y495C	Y495C	Y495C*	D490E-P491Y	Y495C*	Y495H*	H569R	A570V*	A570V*	G605A*	V606F*
Inheritance	Sporadic	AD	AD	AD	AD	AD	AD	Sporadic	Sporadic	AD	AD	AD
Onset (yr)	20	20s~35	30s	30s	16~28	40s	40s	30	42	35	43	18
First symptom	sensory loss	sensory loss, hearing deficit	sensory loss, hearing deficit	sensory loss, hearing deficit	Hearing deficit	sensory loss, hearing deficit	Hearing deficit	sensory loss	nacrolepsy & cataplexy	cataplexy	cataplexy, hearing loss	excessive daytime sleepiness
SN	Yes	Yes	Yes	Yes	Yes	Yes	Yes	Yes	Yes	Yes	Yes	Yes
	20	20s	30s	30s	20s	47	55	30	47	55	47	49
Hearing deficit	Yes	Yes	Yes	Yes	Yes	Yes	Yes	Yes	Yes	Yes	Yes	Yes
	26	20s	30s	30s	(16~28)	40s	40s	32	43	48	43	32
Dementia/MCI	No	Yes	Yes	Yes	Yes	Yes	Yes	Yes	No	Yes	No	Yes
	-	30s~42	40s	30s	30s	50s (MCI)	50s (MCI)	30s (MCI)	-	54	-	52
Nacrolepsy	No	No	No	No	No	No	No	No	Yes	Yes	Yes	Yes
	/	/	/	/	/	/	/	/	42	35	43	18
CA	No	No	Yes	No	Yes	No	No	No	Yes	Yes	Yes	Yes
	/	/	40s	/	30s	/	/	/	46	48	47	37
Others	MRI: cerebellar atrophy	Autopsies: degeneration of brain including the cerebellum				MRI: cerebral & cerebelllar atrophy	Seizures; MRI & pathology: cerebral & cerebellar atrophy	Bradycardia; MRI: cerebral & cerebelllar atrophy	depression, psychosis, limb lymphedema, optic atrophy	depression, psychosis, optic atrophy, type II DM	depression, optic atrophy,	depression, psychosis, optic atrophy, type II DM
Reference	This study	1	1	1	1	3	3	4	2	2	2	2

CA= cerebellar ataxia; DM= diabetes mellitus; MCI= mild cognitive impairment; MRI= magnetic resonance imaging; SN=sensory neuropathy; * Only index patient for each kindred was listed.

Reference: 1.Klein et al. 2011, 2.Winkelmann et al. 2012, 3.Klein et al. 2013, 4. Yuan et al. 2013.

5.3 ARCA with congenital ectodermal dysplasia caused by a splicing *RNF216* mutation

An autosomal recessive family affected by congenital ectodermal dysplasia and cerebellar ataxia was studied. WES was performed in the index patient and his asymptomatic father. The patient had congenital ectodermal dysplasia and developed cerebellar ataxia in early-adulthood. His parents were consanguineous and of Indian origin (the pedigree is shown in figure 5-4, C, p159). Genetic analysis is summarised in figure 5-4, A. After filtering out benigh variants, 15 homozygous variants were first selected in the index patient as they were shared by the father (FV-2) in heterozygous status. Among these 15 variants, a homozygous splicing variant, c.2453-2A>G, in the ring finger protein 216 gene (*RNF216*) was considered probable pathogenic because that recently homozygous or compound heterozygous mutations in *RNF216* were identified to cause the syndrome of ataxia, hypogonadotropic hypogonadism and dementia in several families.(Margolin et al. 2013; Seminara et al. 2002; Shi et al. 2014) Further evidence supported the pathogenic role of this novel splicing mutation includes: (1) both asymptomatic parent were documented to carry the heterozygous variant (figure 5-4, C), thus confirming the segregation of this mutation; (2) it has so far not reported in any public database; (3) it was absent in 220 control exomes; (4) the mutation was predicted to cause loss of a splice site by five different soft wares (figure 5-5, p160).

The protein encoded by *RNF216* interacts with the receptor-interacting serine/threonine-protein kinase 1 (RIPK1), which is involved in the TNF-induced NF-κB activation pathways and programmed cell death. The variant was predicted to cause loss of a splice site in the zinc finger domain of the encoded protein, which is required for its interaction with RIPK1. The encoded protein may also function as an E3 ubiquitin-protein ligase which accepts ubiquitin from E2 ubiquitin-conjugating enzymes and transfers it to substrates. Knockdown of rnf216 in zebrafish embryos induced defects in the eye, optic tectum, and cerebellum, which were rescued by wild type human *RNF216* mRNA.(Margolin et al. 2013)

RNF216 is a newly-identified gene related to ARCA and its phenotypic spectrum is still not understood completely. The study suggests that different types of *RNF216* mutations may lead to a wide range of phenotypes. Our patient presented differently from other reported patient with *RNF216* mutations: congenital ectodermal dysplasia was first reported and no sign of hypogonadism or cognitive impairment at least until 36 years old. Follow-up is necessary to monitor if signs suggesting dementia will occur in the future.

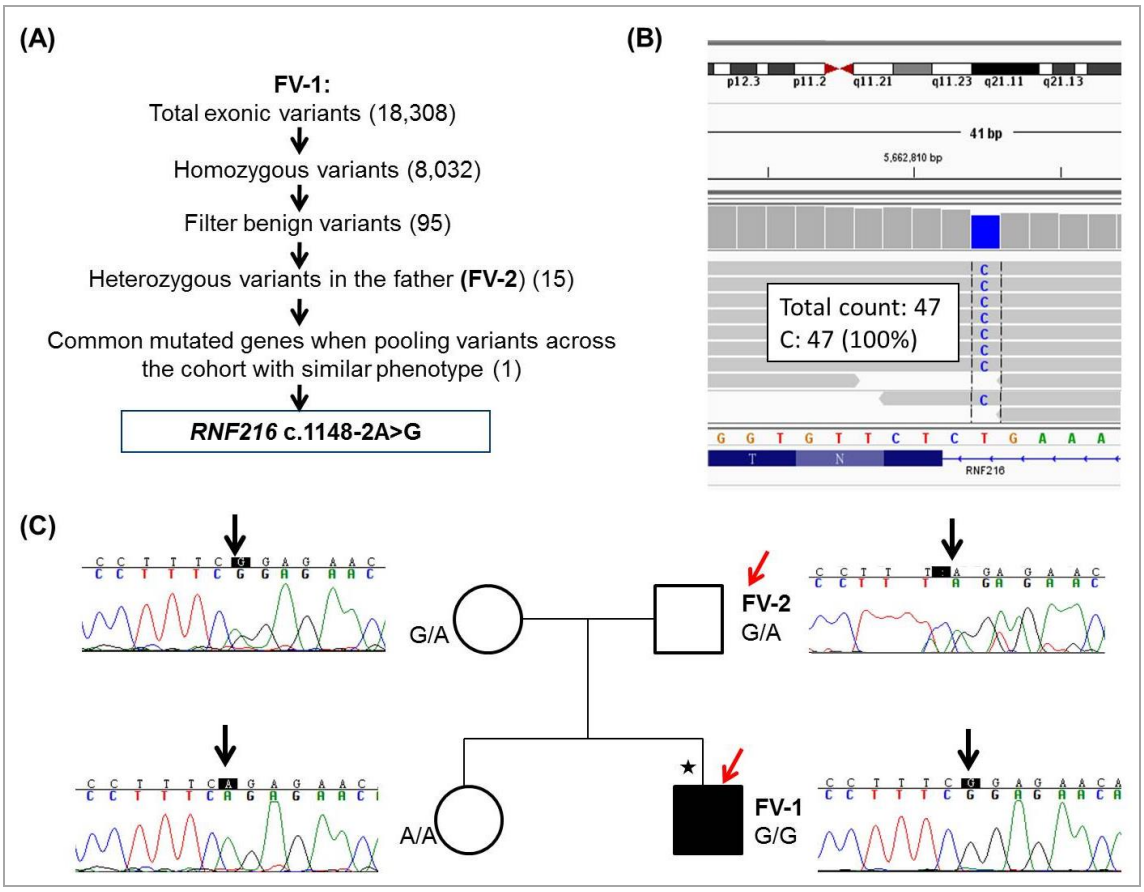

Figure 5-4. Whole exome sequencing of the family with ARCA and congenital ectodermal dysplasia

(A) The process of prioritizing exonic variants. A homozygous splicing mutation in *RNF216* is selected after pooling with the exome of the patient (FV-1), the heterozygous carrier (FV-2) and another family with ARCA.(Margolin et al. 2013; Seminara et al. 2002) Numbers in flank indicate the numbers of exonicvariants pass filtering.

(B) Homozygosity and the sequencing depth (47X) of the mutation shown by IGV.

(**C)Pedigree of the family**.★=Index patient. ■= affected member, □/○= unaffected members.WES was performed in members with a red arrow. Sanger sequencing validated that the mutation is segregated with the phenotype within the family.

Figure 5-5. *RNF216* mutation c.2453-2A>G is predicted to cause loss of a splice site

The five soft wares used to predict the effect of a splicing mutation are listed on the left side. Exonic sequence is shaded grey, intronic sequence is unshaded. Predicted 5' and 3' splice site junctions are highlighted by blue or green arrows. The location of the mutation is highlighted by red bars, linked between the two halves of the screen by a blue line. Green bars (3') illustrate the consensus scores for the 4 splice-site analysis tools used by the software. The maximum score for each program is shown to the left of the bars.(Courtesy of Dr. James Polke from Neurogenetics Unit, National Hospital for Neurology and Neurosurgery, London.)

5.4 Potential candidate genes for inherited neuropathies

5.4.1 A novel heterozygous *WFS1* mutation associated with autosomal dominant sensory neuropathy-ataxia-deafness syndrome

(1) Clinical feature

WES was performed in a family with AD-HSN complicated with cerebellar ataxia and sensorineural hearing loss with the attempt to establish the genetic diagnosis (pedigree shown in figure 5-6, A, p160). The 15-year-old index patient (III-1) had experienced unsteadiness since her childhood. Simultaneously with the onset of gait imbalance, she had numbness and painful sensation in the feet. However, she felt little pain even when she had a fracture of her ankle. Scoliosis was noted at the age of three. Sensorineural hearing loss was diagnosed in her second decade and slowly progressed over the years. One of her older siblings (III-2), had sensory impairment, unsteadiness, scoliosis and hearing loss with the onset in teenage years. Their father (II-1) developed hearing loss and scoliosis in his early 20s. He also had mild ataxic gait and sensory loss in four limbs. The paternal aunt (II-2) was affected by an asymmetric sensory neuropathy with substantial autonomic involvement which was diagnosed as Sjogren's syndrome. The paternal grandmother (I-1) was reported to have scoliosis and gait unsteadiness.

Neurological examination at the age of 14 showed the index patient (III-1) had a wide-based ataxic gait. She had overshooting tremor in her hands. Sensory examination showed reduction of pinprick appreciation distally in the upper limbs up to the elbows and in the lower limbs higher than knees. Vibration and position sense were impaired up to the knees. She was areflexic and plantars were down going. Muscle power was normal. Brain MRI performed at age 14 revealed an atrophic cerebellum. Neurophysiology showed severely reduced or absent SAPs, normal or mildly slowed NCV and normal motor responses in the upper and lower limbs, consistent with a sensory axonal neuropathy. NCS in the father (II-1) was also compatible with a sensory axonal neuropathy but milder than his daughter. Genetic testing for *GJB1, PMP22, FRDA, RAB7, HSN2, NGFB, FAM134B, SPTLC1, POLG,* and *ATL1* were negative.

(2) Genetic analysis

WES was performed in the patient (III-1), her father (II-1) and her aunt (II-2). Genetic analysis is summarised in figure 5-6, B (p162). After filtering out benign variants, 102 heterozygous variants were shared by the patient (III-1) and her father (II-1). Variants were then divided into two groups: those shared by the aunt (II-2) and those not shared by her. A heterozygous missense mutation in *SETX* was first selected because homozygous or compound heterozygous mutations in this gene can cause AOA2. However, the variant was excluded since Sanger sequencing showed that the affected sibling (III-2) does not carry this variant.

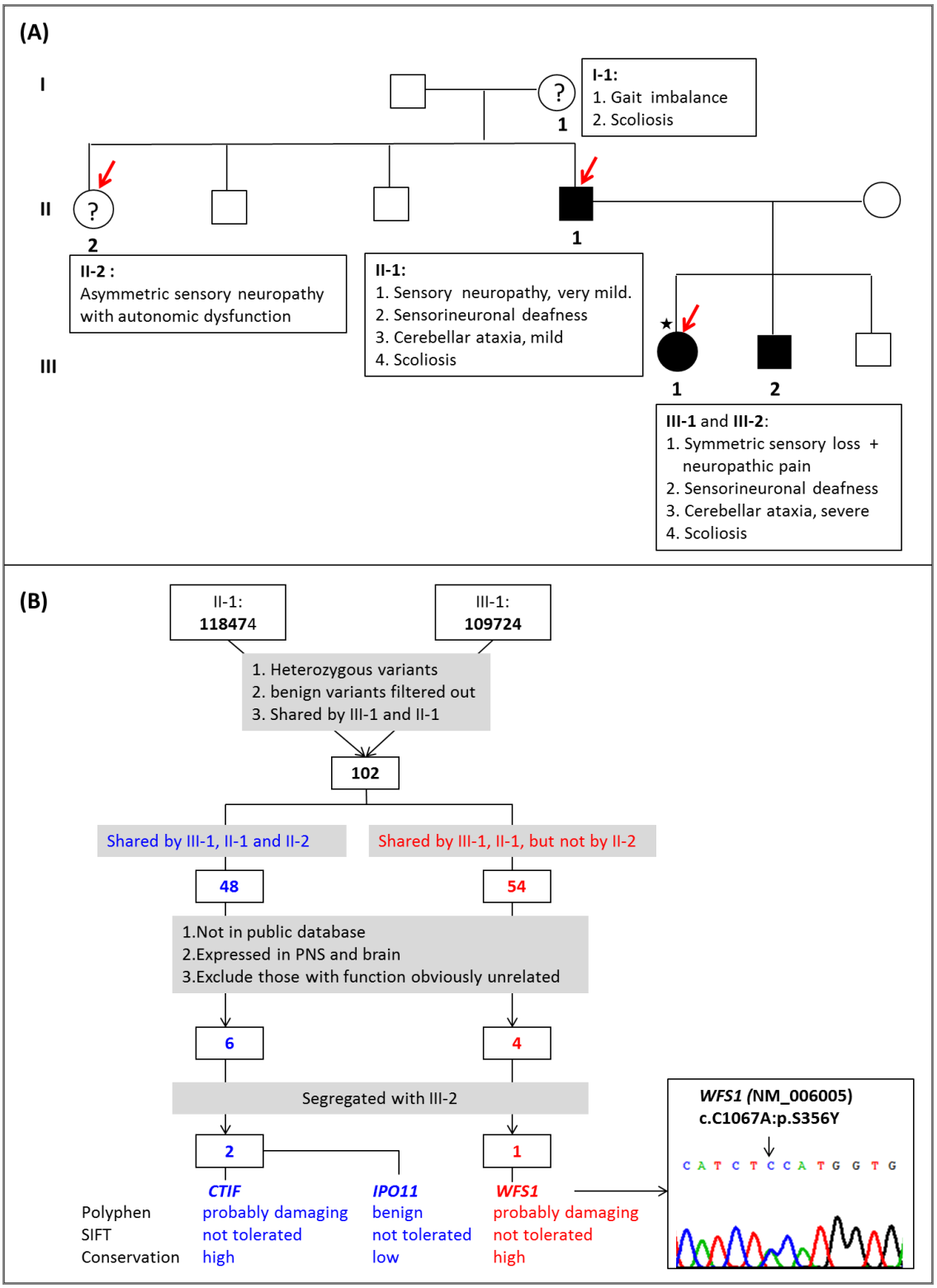

Figure 5-6. Whole exome sequencing of the family with autosomal dominant sensory neuropathy-ataxia-deafness syndrome

(A) Pedigree of the family. The phenotype of each individual is listed in the flank.★=Index patient. ■/●= affected members, □/○= unaffected members,⊘= members who are uncertain affected by the same disease.WES was performed in members with a red arrow.

(B) The process of prioritizing exonic variants. *WFS1* S356Y is determined to be the causative mutation after analysis and validated by Sanger sequencing. Numbers in flank indicate the numbers of exonic variants pass filtering.

Taking into consideration the tissue expression patterns, the evidence from animal or cellular models and interacting protein networks, a total of ten variants, six shared by all three individuals and four shared only by the index case and her father, were selected as potential candidates and then tested in the affected sibling (III-2) by Sanger sequencing. Three variants were also presented in the affected brother. Among them, a novel missense mutation, c.C1067A:p.Ser356Tyr (S345Y), in the Wolfram syndrome 1 gene (*WFS1*) was considered to be a probable pathogenic mutation due to its predicted malignant functional impact and the high conservation of the amino acid Ser356 (figure 5-6, B; figure 5-7, B). *WFS1* mutations have been associated previously with sensorineural hearing loss, ataxia and peripheral neuropathy.

The coding product WFS1 protein, also called wolframin is a type II membrane protein with nine putative transmembrane segments, which is located primarily in the endoplasmic reticulum (ER) and highly expressed in brain, pancreas, heart, and insulinoma beta-cell lines.(Hofmann et al. 2003; Takeda et al. 2001) So far, most of the mutations leading to Wolfram syndrome were detected in the transmembrane domains, particularly in exon 8 (Hansen et al. 2005; Zmyslowska et al. 2011), as well as the S356Y mutation identified in the reported family (figure 5-7, A).

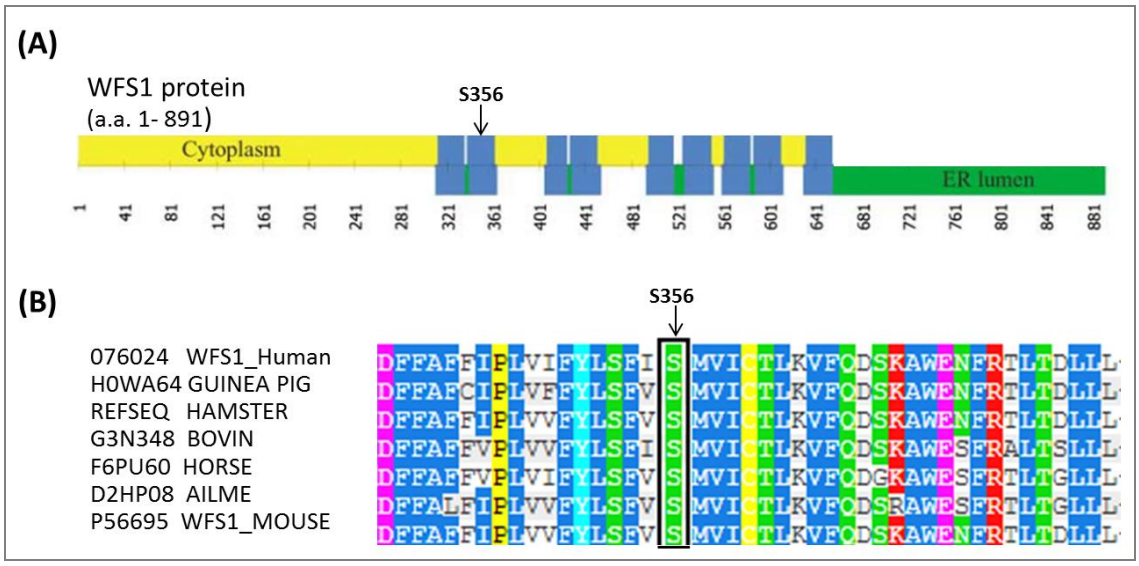

Figure 5-7. Location and conservation of *WFS1* Ser356

(A) Primary and secondary structures of the WFS1 protein. Numbers indicate the amino acid residues. The cytoplasmatic regions are yellow, the endoplasmic regions are green and the transmembrane α-helices are blue. The S356Y mutation is localized in the transmembrane domain.(modified from Hansen et al. 2005)

(B) Alignment of human WFS1 protein with homologs of other species. S356 is a highly conserved among mammals.

(3) Discussion:

Homozygous or compound heterozygous *WFS1* mutations were first recognised to cause the autosomal recessive Wolfram syndrome (WFS), also called Diabetes Insipidus, Diabetes Mellitus, Optic Atrophy, and Deafness (DIDMOAD), a progressive neurodegenerative disorder characterised by childhood to early adolescence onset diabetes mellitus and optic atrophy.(Smith et al. 2004). On the other hand, heretozygous missense mutations in the *WFS1* gene have been appreciated as a frequent cause of autosomal dominant non-syndromic low frequency sensorineural hearing loss (LFSNHL), particularly in Asia.(Bespalova et al. 2001; Fukuoka et al. 2007; Tsai et al. 2007) LFSNHL is a rare dominant condition which affects only 2000 Hz and below is an unusual type of hearing loss that worsens over time without progressing to profound deafness. The identification of *WFS1* as the causative gene subsequently proved that LFSNHL is the allelic disorder of autosomal dominant deafness 6 (DFNA6), another condition characterised by congenital, slowly progressive, low-frequency (<2000 Hz) sensorineural hearing loss and more frequently seen than LFSNHL. Further study reported affected individuals with LFSNHL in the DFNA6 family.(Bespalova et al. 2001; Fukuoka et al. 2007; Tsai et al. 2007) Recently, heterozygous *WFS1* mutations were also identified in many autosomal dominant pedigree with various symptoms, including optic atrophy, hearing loss, psychiatric disorders, ataxia, peripheral neuropathy, dementia and urinary tract abnormalities.(Chakrabarti et al. 2009; Hogewind et a;. 2010; Johansson et al. 2013; McHugh and Friedman 2006) Although the clinical significance of these heterozygous mutations is still undetermined, *WFS1* is suggested to have modifier effects in a broad spectrum of disorders and produce a phenotypic continuum. *WFS1* is ubiquitously expressed and its coding protein interacts diffusely with many molecules, such as ATPase, the adenyl cyclase and ubiquitin ligase.(Fonseca et al. 2012; Gharanei et al. 2013; Guo et al. 2011) This may explain the involvement of multiple neurological and non-neurological systems associated with both homozygous and heterozygous *WFS1* mutations.

As for manifestations of our family, the late-onset sensorineural hearing loss and cerebellar ataxia might be related to a less severe loss-of-function effect brought from a heterozygous mutation when comparing with the typical Wolfram syndrome. To consolidate the pathogenic role of this mutation, screening of a large cohort of similar phenotype and further functional studies are warranted.

5.4.2 *NAV2* mutations associated with late-onset sensory neuropathy and cerebellar ataxia

(1) Genetic analysis

In the cohort of HSN-plus syndromes, two families with late-onset sensory neuropathy and cerebellar ataxia shared a common mutated gene: the neuron navigator 2 gene (*NAV2*) (pedigrees shown in figure 5-8, A). Each family carried a novel heterozygous missense mutation in *NAV2*: c.875A>C;p.Thy292Ser (Y292S) was in FII and c.2744C>T;p.Ser915Phe (S915F) in FIII. Both mutations were not reported in any public database, changed a highly conserved amino acid codon (figure 5-8, C) and were predicted to have damaging effects by Polyphen and SIFT.

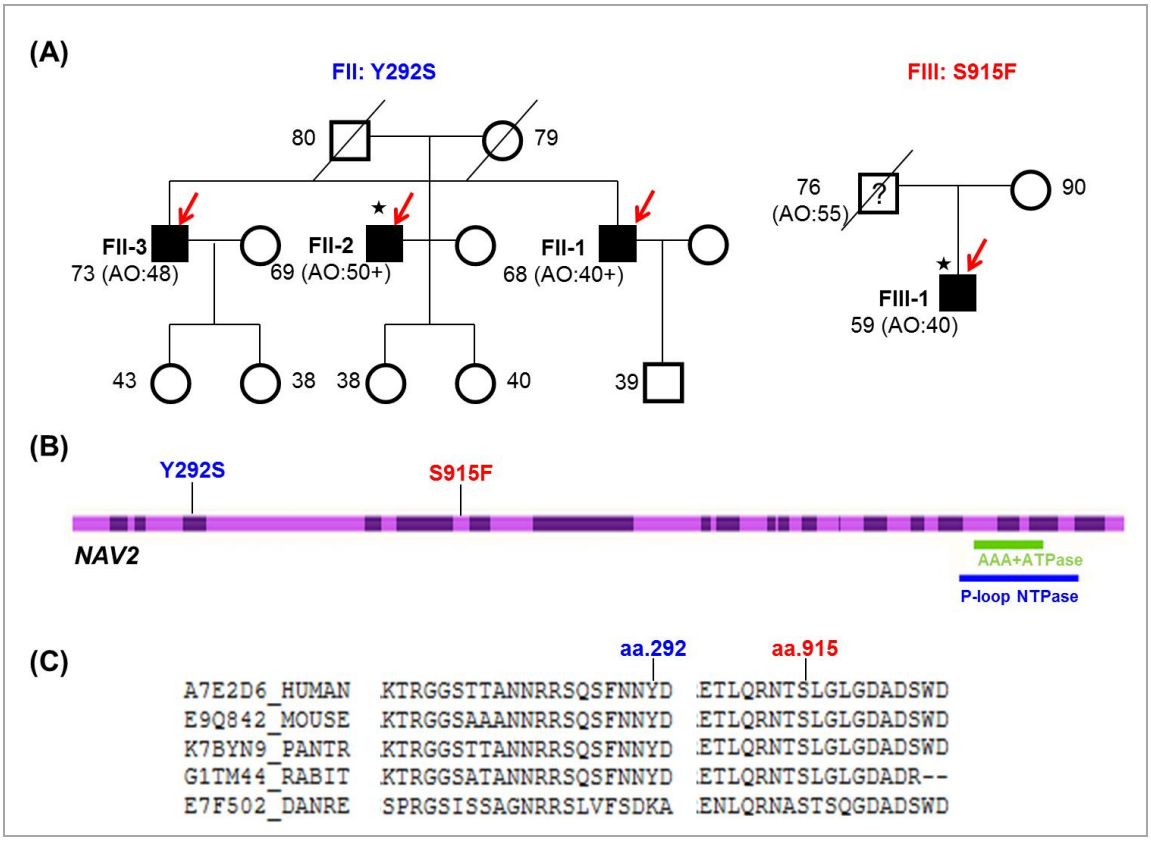

Figure 5-8. *NAV2* mutations in families with late-onset sensory neuropathy and cerebellar ataxia

(A) Pedigree of the two families with *NAV2* mutations. The three affected patients of the family FII carried S915F mutation and patient FIII-1 carried Y292S mutation. ■/●= affected members, □/○= unaffected members, ★=Index patient.WES was performed in members with a red arrow. Numbers in the pedigree refers to the current age or age when deceased. AO= age of onset.

(B) Locations of the two novel *NAV2* mutations. Y292S is in exon 6 whereas S915F is localized in exon 11. The range of the AAA+ATPase (ATPases associated with various cellular activities) domain and the P-loop NTPase domain are also illustrated.

(C) Alignment of the human *NAV2* protein with homologs of multiple species. Both S915F and Y292 are conserved among mammals.

(2) Clinical features

The three affected siblings in family FII developed unsteadiness which was worse in the dark in their fifth decade. They also had numbness in the distal upper and lower limbs. Neurological examination of the three brothers (at the age of 67 for FII-1, 68 for FII-2 and 71 for FII-3) all showed had an ataxic gait, positive Romberg sign and sensory impairment of all modalities in the distal upper and lower limbs. In addition, they all had nystagmus and dysarthria with a variable severity. Their parents were not consanguineous and had no neurological diseases at least until the age of 70. Neurophysiology in the three brothers showed absent SAPs and preserved motor amplitudes in upper and lower limbs, compatible with a sensory axonal neuropathy. Brain MRI of FII-2 performed at the age of 64 was normal. Before WES, they were tested negative for mutations in *SPTLC1*, *MFN2, HSN2, NGFB, RAB7, FRDA, Fragile X, PEO1* hot spots and *POLG*. SCAs type 1, 2, 3, 6, 7 and common mitochondrial mutations were also excluded.

FIII-1 developed unsteadiness and numbness of the distal limbs at the age of 40. Neurological examination at age 57 showed an ataxic gait, dysarthric speech, rotational nystagmus on horizontal and upper gaze and brisk reflexes in lower limbs. His parents were not consanguineous: his father was diagnosed with Parkinson disease at the age of 55, and the mother currently at the age of 90 is quite healthy. NCS of FIII-1 showed absent SAPs in upper and lower limbs with normal motor responses, compatible with a sensory axonal neuropathy.

(3) Discussion

NAV2 encodes a member of the neuron navigator gene family and carries some functionally critical domain like the AAA+ATPase domain. Genes carrying the AAA+ATPase domain have been known to be involved in variable neurological syndromes, like *AFG3L2* mutations in cerebellar ataxia and spasticity (SCA28), *SPAST* and *SPG7* mutations in HSP.

NAV2 was first identified as an all-trans retinoic acid (atRA)-responsive gene in human neuroblastoma cells (retinoic acid-induced in neuroblastoma 1, RAINB1). *NAV2* is essential for neurite outgrowth and axonal elongation. Transgene overexpression of *NAV2* rescued the axonal elongation defect in the Caenorhabditis elegans unc-53 mutant, indicating that Nav2 is an ortholog of unc-53 that is required for cell migration and axonal outgrowth.(Muley et al. 2008)

The coding protein of *NAV2* is located both in the cell body and along the length of the growing neurites of SH-SY5Y cells in a pattern that closely mimics that of neurofilament and microtubule proteins. There is evidence suggesting that the NAV2 protein may also act by facilitating interactions between microtubules and other proteins such as neurofilaments that are

key players in the formation and stability of growing neurites. Transfection of Nav2 deletion constructs in Cos-1 cells revealed a region of the protein (aa 837-1065) that could direct localization with the microtubule cytoskeleton.(Muley et al. 2008) The S915F mutation carried by one of our patients is exactly localised in the region.

Transgenic mice with *Nav2* hypomorphic mutant could develop sensory deficits and impaired hearing, mimicking the manifestations of our patients.(Peeters et al. 2004) Abnormal cerebellar development were also observed in mice lacking the full-length Nav2 transcript.(McNeill et al. 2011) The above evidence supports that *NAV2* is important in the nervous system and maybe a good candidate gene for the HSN-ataxia syndrome. Using a region of *NAV2* that independently associates with the cytoskeleton as bait in a yeast-two-hybrid screen, *NAV2* was recently identified to be able to interact with 14-3-3ε via a 200-amino acid internal domain.(Marzinke et al. 2013) Knockdown of 14-3-3ε leads to a decrease in atRA-mediated neurite outgrowth, similar to the elongation defects observed when *NAV2* is depleted or mutated. Likewise, microtubule defects in C. elegans fed unc-53 RNAi are similar to those fed ftt-2 (a 14-3-3 homolog) RNAi. The discovery provides further insight into the mechanism by which *NAV2* participates in neuronal migration and elongation, and makes sense of *NAV2* mutation in neurodegenerative process.

Considering the late onset of symptoms in our affected individuals and multiple lines of evidence from the *in-vitro* cellular modal and the knock-down animal modal, the two novel missense mutations in *NAV2* are supposed to cause the disease through haplotype insufficiency or loss of function. In order to confirm its pathogenicity, it is necessary to do further studies, including validation by Sanger sequencing in affected individuals, familial segregation analysis, and screening in larger cohorts of patients with similar phenotype and cellular or animal studies.

5.4.3 A homozygous *PDXK* mutation associated with recessive CMT2 and optic atrophy

(1) Clinical feature

WES was performed in a patient (II-6 in figure 5-9, B, p169) from a Greek Cypriot-origin family who was affected by childhood-onset motor and sensory neuropathy followed by optic atrophy during adulthood. The proband (II-6) developed distal wasting and weakness of the lower limbs at the age of 7 and upper limbs weakness at the age of 12. The symptoms were progressive and at the age of 57 he had difficulty in climbing stairs and weakness of grip. Sensation of all modalities in all limbs was reduced. He developed progressive vision impairment at the age of 47. Neurological examination at the age of 7 showed distal weakness and wasting of the intrinsic muscles of the hands and the distal lower limbs. He had pes cavus, areflexia and flexor plantar responses. There was glove and stocking sensory loss to all modalities. Romberg's sign was positive. Visual fields were constricted with a central scotoma. Fundoscopy showed bilateral optic disc atrophy. NCS at the age of 57 showed absent SAPs in the upper and lower limbs, absent motor responses or severely reduced MAPs with preserved MNCV, compatible with sensorimotor axonal neuropathy in CMT2. Optic nerve and chiasm CT was normal. His sister (II-7) developed wasting and weakness of the lower limbs when aged 9 years and weakness of the upper limbs when aged 12. At the age of 54, she could not run or walk more than 200 yards, and had significant weakness of grip. Impaired vision was noted at the age of 50. Examination at age 54 revealed reduced glove and stocking sensory loss of all modalities, positive Romberg's sign, pes cavus, wasting of the intrinsic muscles of the hand and pronounced weakness of dorsiflexion and plantar flexion of the feet. She was areflexic with flexor plantar responses. Her gait was high stepping and there was bilateral optic disc pallor. NCS at the same age also showed features suggesting sensorimotor axonal neuropathy: unrecordable SAP in all sampling nerves, absent CMAP in lower limbs and reduced CMAP in upper limbs with preserved NCV. The third sibling (II-4) was considered affected on the basis of history provided by relatives. She developed distal wasting and weakness when aged 10 years and had progressive impairment of vision from the age of 50 years. Other siblings did not have any neurological or ophthalmological complaints at least until 59 years old (II-5) and 69 years old (case II-1). The two children of II-6 were unaffected when examined at aged 30 and 36.Their parents who were consanguineous and unaffected at the age of 99 and 85 years. Mitochondrial DNA analysis did not show pathogenic Leber's hereditary optic neuropathy mutation. WES was performed in the proband to identify the disease-causing mutation.

(2) Genetic analysis

WES was performed in the index case (II-6). The process of prioritizing exonic variants is summarised in figure 5-9, A (p169). After filtering benigh variants, 18 homozygous variants

were identified. Five variants were kept after filtered out non-framshift indels, false positive variants and genes with irrelevant functions like *HLA*. Sanger sequencing to validate the five variants were subsequently performed for the patient (II-6) and his affected sister (II-7). A homozygous missense mutation, c.G682A;p.Ala228Thr (A228T) in the pyridoxal kinase gene (*PDXK)* was shared by the two affected individuals (figure 5-9, C). *PDXK* encodes the enzyme catalysing the ATP-dependent phosphorylation reaction of pyridoxine (vitamin B6).(Cao et al. 2006; Musayev et al. 2007) A228T was absent in the ESV database, 221 exome sequences from healthy controls at UCL and 65 in-house exomes from patients with ataxia at ION. Its pathogenicity is further supported by the damaging effects predicted by Polyphen and SIFT.

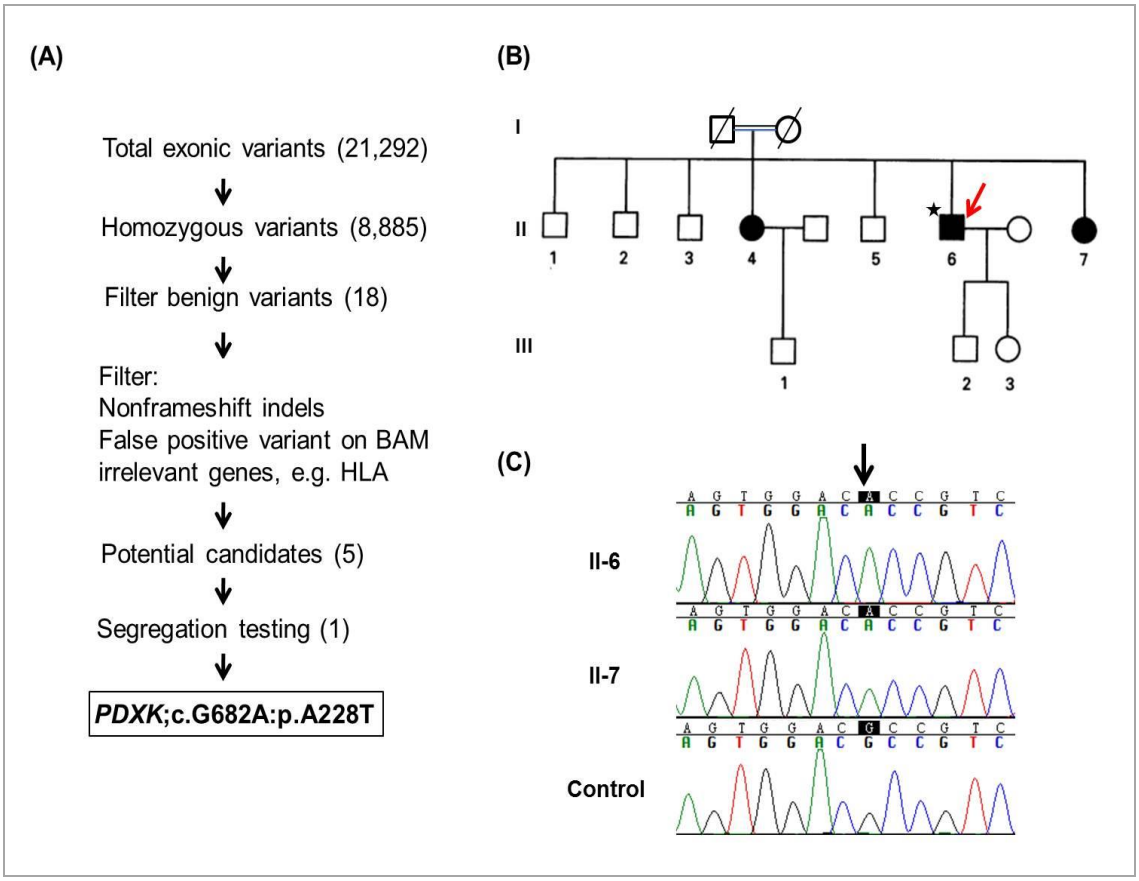

Figure 5-9. Whole exome sequencing of the family with recessive axonal neuropathy and optic atrophy

(A) The process of prioritizing exonic variants. *PDXK* A228T is probably a pathogenic mutation after analysis.

(B) Pedigree of the family. ■/●= affected members, □/○= unaffected members, ⍁/⌀= diseased members ★=Index patient.WES was performed in members with a red arrow. (modified from (Chalmers et al. 1997)

(C) Chromatography from the patient and the affected sibling. The homozygous mutation segregates within the family.

The Ala228 is a highly conserved amino acid localized in the overlapping region of pyridoxal phosphate biosynthesis domain and the phosphomethylpyrimidine kinase domain (figure 5-10). Both of the two domains harbor critical functions. The pyridoxal phosphate biosynthesis domain is the key region participating in the biosynthesis of pyridoxal-5-phosphate (PLP), the active form of vitamin B6 (pyridoxine or pyridoxal). The phosphomethylpyrimidine kinase domain, also known as HMP-phosphate kinase, catalyses the phosphorylation of HMP-P to HMP-PP in the thiamine pyrophosphate (TPP) synthesis pathway.

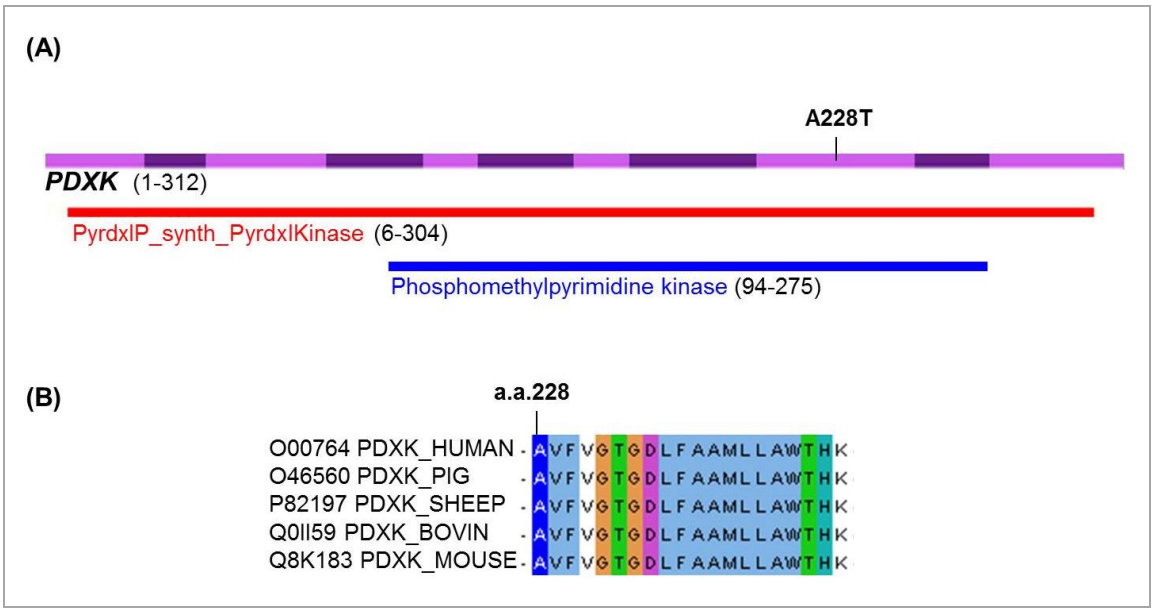

Figure 5-10. Localisation and conservation of *PDXK* A228T mutation

(A) Localisations of the novel *PDXK* A228T mutations. PyrdxlP_synth_PyrdxlKinase: the domain responsible for synthesis of pyridoxal-5-phosphate (PLP), Phosphomethylpyrimidine kinase: the domain participating the Thiamine pyrophosphate synthesis pathway. Numbers indicate amino acids.

(B) Alignment of the human *PDXK* protein with homologs of multiple species. A228 is highly conserved among mammals.

(3) Discussion

Recent advancement of genetics has documented some forms of hereditary neurological diseases are treatable as they are vitamin-responsive disorders, like ataxia with vitamin E deficiency, CoQ10 deficiency caused by *ADCK3* mutations (Section 3.4) and riboflavin-responsive Brown-Vialetto-Van Laere syndrome caused by *C20orf54* mutations.(Green et al. 2010) Being one of vitamins, the important role of pyridoxin in the nervous system is well recognized as it can involve both CNS and PNS. Deficiency of pyridoxine would lead to diffident neurological disorders, encephalopathy to peripheral neuropathy.

PDXK has dual important physiological functions: (1) it catalyses the step required for the synthesis of PLP, which is the active form of pyridoxine and is an important cofactor for over 100 enzymes involved in amino acid, sugar and neurotransmitter metabolisms; (2) it is involved in the biosynthesis of TPP, another essential cofactor for many enzymes. Recently, PLP-dependent pathways have been suggested to play a role in the pathogenesis of Huntington's disease and epilepsy.(Dolina et al. 2012; Sorolla et al. 2010)

This study suggests that *PDXK* may be a candidate gene for inherited axonal neuropathy with optic atrophy. However, there are still some questions needed to answer in order to confirm the hypothesis. Genetically, it is necessary to perform segregating test in other family members and to extensively screen more patients with similar phenotype. If more evidence comes out from genetic study, *in vitro* and *in vivo* models should be developed since there is no available animal model and little is known about the molecular mechanisms of *PDXK* mutations at present.

References

Bespalova IN, Van Camp G, Bom SJ, Brown DJ, Cryns K, DeWan AT, Erson AE, Flothmann K, Kunst HP, Kurnool P et al (2001) Mutations in the Wolfram syndrome 1 gene (WFS1) are a common cause of low frequency sensorineural hearing loss. Hum Mol Genet 10(22):2501-08

Cao P, Gong Y, Tang L, Leung YC, Jiang T (2006) Crystal structure of human pyridoxal kinase. J Struct Biol 154: 327-32

Chakrabarti B, Dudbridge F, Kent L, Wheelwright S, Hill-Cawthorne G, Allison C, Banerjee-Basu S, Baron-Cohen S (2009) Genes related to sex steroids, neural growth, and social-emotional behavior are associated with autistic traits, empathy, and Asperger syndrome. Autism Res 2: 157-77

Chalmers RM, Riordan-Eva P, Wood NW (1997) Autosomal recessive inheritance of hereditary motor and sensory neuropathy with optic atrophy. J Neurol Neurosurg Psychiatry 62: 385-7

Davidson GL, Murphy SM, Polke JM, Laura M, Salih MA, Muntoni F, Blake J, Brandner S, Davies N, Horvath R, Price S, Donaghy M, Roberts M, Foulds N, Ramdharry G, Soler D, Lunn MP, Manji H, Davis MB, Houlden H, Reilly MM (2012) Frequency of mutations in the genes associated with hereditary sensory and autonomic neuropathy in a UK cohort. J Neurol 259(8):1673-85

Dolina S, Margalit D, Malitsky S, Pressman E, Rabinkov A (2012) Epilepsy as a pyridoxine-dependent condition: quantified urinary biomarkers for status evaluation and monitoring antiepileptic treatment. Med Hypotheses 79: 157-64

Fonseca SG, Urano F, Weir GC, Gromada J, Burcin M (2012) Wolfram syndrome 1 and adenylyl cyclase 8 interact at the plasma membrane to regulate insulin production and secretion. Nat Cell Biol 14: 1105-12

Fukuoka H, Kanda Y, Ohta S, Usami S (2007) Mutations in the WFS1 gene are a frequent cause of autosomal dominant nonsyndromic low-frequency hearing loss in Japanese. J Hum Genet 52(6):510-5

Gharanei S, Zatyka M, Astuti D, Fenton J, Sik A, Nagy Z, Barrett TG (2013) Vacuolar-type H+-ATPase V1A subunit is a molecular partner of Wolfram syndrome 1 (WFS1) protein, which regulates its expression and stability. Hum Mol Genet 22: 203-17

Green P, Wiseman M, Crow YJ, Houlden H, Riphagen S, Lin JP, Raymond FL, Childs AM, Sheridan E, Edwards S et al (2010) Brown-Vialetto-Van Laere syndrome, a ponto-bulbar palsy with deafness, is caused by mutations in c20orf54. Am J Hum Genet 86(3):485-9

Guo X, Shen S, Song S, He S, Cui Y, Xing G, Wang J, Yin Y, Fan L, He F, Zhang L (2011) The E3 ligase Smurf1 regulates Wolfram syndrome protein stability at the endoplasmic reticulum. J Biol Chem 286: 18037-47

Hansen L, Eiberg H, Barrett T, Bek T, Kjaersgaard P, Tranebjaerg L, Rosenberg T (2005) Mutation analysis of the WFS1 gene in seven Danish Wolfram syndrome families; four new mutations identified. Eur J Hum Genet 13: 1275-84

Hofmann S, Philbrook C, Gerbitz KD, Bauer MF (2003) Wolfram syndrome: structural and functional analyses of mutant and wild-type wolframin, the WFS1 gene product. Hum Mol Genet 12: 2003-12

Hogewind BF, Pennings RJ, Hol FA, Kunst HP, Hoefsloot EH, Cruysberg JR, Cremers CW (2010) Autosomal dominant optic neuropathy and sensorineual hearing loss associated with a novel mutation of WFS1. Mol Vis 16: 26-35

Johansson S, Irgens H, Chudasama KK, Molnes J, Aerts J, Roque FS, Jonassen I, Levy S, Lima K, Knappskog PM, Bell GI, Molven A, Njolstad PR (2013) Exome sequencing and genetic testing for MODY. PLoS One 7: e38050

Klein CJ (2012) DNMT1-Related Dementia, Deafness, and Sensory Neuropathy. In: Pagon RA, Adam MP, Bird TD, Dolan CR, Fong CT, Stephens K, editors. SourceGeneReviews™ [Internet]. Seattle (WA): University of Washington, Seattle; 1993-2013. 2012 Feb 16 [updated 2012 May 17]. In: Pagon RA, Bird TD, Dolan CR, Stephens K, Adam MP, editors. GeneReviews™ [Internet]. Seattle (WA): University of Washington, Seattle; 1993-.2012 Feb 16 [updated 2012 May 17].

Klein CJ, Bird T, Ertekin-Taner N, Lincoln S, Hjorth R, Wu Y, Kwok J, Mer G, Dyck PJ, Nicholson GA (2013) DNMT1 mutation hot spot causes varied phenotypes of HSAN1 with dementia and hearing loss. Neurology 80(9):824-8

Klein CJ, Botuyan MV, Wu Y, Ward CJ, Nicholson GA, Hammans S, Hojo K, Yamanishi H, Karpf AR, Wallace DC, Simon M, Lander C, Boardman LA, Cunningham JM, Smith GE, Litchy WJ, Boes B, Atkinson EJ, Middha S, PJ BD, Parisi JE, Mer G, Smith DI, Dyck PJ (2011) Mutations in DNMT1 cause hereditary sensory neuropathy with dementia and hearing loss. Nat Genet 43: 595-600

Margolin DH, Kousi M, Chan YM, Lim ET, Schmahmann JD, Hadjivassiliou M, Hall JE, Adam I, Dwyer A, Plummer L, Aldrin SV, O'Rourke J, Kirby A, Lage K, Milunsky A, Milunsky JM, Chan J, Hedley-Whyte ET, Daly MJ, Katsanis N, Seminara SB (2013) Ataxia, dementia, and hypogonadotropism caused by disordered ubiquitination. N Engl J Med 368: 1992-2003

Marzinke MA, Mavencamp T, Duratinsky J, Clagett-Dame M (2013) 14-3-3epsilon and NAV2 interact to regulate neurite outgrowth and axon elongation. Arch Biochem Biophys 540(1-2):94-100

McHugh RK, Friedman RA (2006) Genetics of hearing loss: Allelism and modifier genes produce a phenotypic continuum. Anat Rec A Discov Mol Cell Evol Biol 288: 370-81

McNeill EM, Klockner-Bormann M, Roesler EC, Talton LE, Moechars D, Clagett-Dame M (2011) Nav2 hypomorphic mutant mice are ataxic and exhibit abnormalities in cerebellar development. Dev Biol 353: 331-43

Muley PD, McNeill EM, Marzinke MA, Knobel KM, Barr MM, Clagett-Dame M (2008) The atRA-responsive gene neuron navigator 2 functions in neurite outgrowth and axonal elongation. Dev Neurobiol 68: 1441-53

Musayev FN, di Salvo ML, Ko TP, Gandhi AK, Goswami A, Schirch V, Safo MK (2007) Crystal Structure of human pyridoxal kinase: structural basis of M(+) and M(2+) activation. Protein Sci 16: 2184-94

Peeters PJ, Baker A, Goris I, Daneels G, Verhasselt P, Luyten WH, Geysen JJ, Kass SU, Moechars DW (2004) Sensory deficits in mice hypomorphic for a mammalian homologue of unc-53. Brain Res Dev Brain Res 150: 89-101

Rossor AM, Polke JM, Houlden H, Reilly MM (2013) Clinical implications of genetic advances in Charcot-Marie-Tooth disease. Nat Rev Neurol 9(10):562-71

Sailer A, Houlden H (2012) Recent advances in the genetics of cerebellar ataxias. Curr Neurol Neurosci Rep 12: 227-36

Seminara SB, Acierno JS, Jr., Abdulwahid NA, Crowley WF, Jr., Margolin DH (2002) Hypogonadotropic

hypogonadism and cerebellar ataxia: detailed phenotypic characterization of a large, extended kindred. J Clin Endocrinol Metab 87: 1607-12

Shi CH, Schisler JC, Rubel CE, Tan S, Song B, McDonough H, Xu L, Portbury AL, Mao CY, True C, Wang RH, Wang QZ, Sun SL, Seminara SB, Patterson C, Xu YM (2014) Ataxia and hypogonadism caused by the loss of ubiquitin ligase activity of the U box protein CHIP. Hum Mol Genet 23(4):1013-24

Smith CJ, Crock PA, King BR, Meldrum CJ, Scott RJ (2004) Phenotype-genotype correlations in a series of wolfram syndrome families. Diabetes Care 27: 2003-9

Sorolla MA, Rodriguez-Colman MJ, Tamarit J, Ortega Z, Lucas JJ, Ferrer I, Ros J, Cabiscol E (2010) Protein oxidation in Huntington disease affects energy production and vitamin B6 metabolism. Free Radic Biol Med 49: 612-21

Takeda K, Inoue H, Tanizawa Y, Matsuzaki Y, Oba J, Watanabe Y, Shinoda K, Oka Y (2001) WFS1 (Wolfram syndrome 1) gene product: predominant subcellular localization to endoplasmic reticulum in cultured cells and neuronal expression in rat brain. Hum Mol Genet 10: 477-84

Tsai HT, Wang YP, Chung SF, Lin HC, Ho GM, Shu MT (2007) A novel mutation in the WFS1 gene identified in a Taiwanese family with low-frequency hearing impairment. BMC Med Genet 8: 26

Winkelmann J, Lin L, Schormair B, Kornum BR, Faraco J, Plazzi G, Melberg A, Cornelio F, Urban AE, Pizza F, Poli F, Grubert F, Wieland T, Graf E, Hallmayer J, Strom TM, Mignot E (2012) Mutations in DNMT1 cause autosomal dominant cerebellar ataxia, deafness and narcolepsy. Hum Mol Genet 21: 2205-10

Yuan J, Higuchi Y, Nagado T, Nozuma S, Nakamura T, Matsuura E, Hashiguchi A, Sakiyama Y, Yoshimura A, Takashima H (2013) Novel mutation in the replication focus targeting sequence domain of DNMT1 causes hereditary sensory and autonomic neuropathy IE. J Peripher Nerv Syst 18: 89-93

Zmyslowska A, Borowiec M, Antosik K, Szalecki M, Stefanski A, Iwaniszewska B, Jedrzejczyk M, Pietrzak I, Mlynarski W (2011) Wolfram syndrome in the Polish population: novel mutations and genotype-phenotype correlation. Clin Endocrinol (Oxf) 75: 636-41

Chapter 6

Results: Targeted resequencing in inherited neuropathies and related disorders

Targeted resequencing is an NGS technology which allows massively parallel sequencing of DNA molecules with a library containing only the exons which are specifically designed and relevant to diseases of interest. Using a customised design of specific exons to a gene, and developing a library, targeted resequencing can support a wider range of genomic applications in a faster and more cost effective way. In this chapter, the applications of targeted resequencing in two groups of patients are reported. The first resequencing panel for ARCMT1 was a pilot project with the attempt to evaluate if targeted sequencing could be used as a diagnostic tool. The second panel was aimed to screen mutations in patients with HSP or axonal neuropathy with spasticity thus covering numerous genes for both HSP and neuropathy. The two panels were designed and executed through different platforms. The experience gained from the reliability and efficiency of their performance would help optimize the use of targeted resequencing in the future.

6.1 Targeted resequencing as a diagnostic tool in inherited neuropathies: a pilot study on ARCMT1

6.1.1 Introduction

ARCMT1 patients generally have an earlier onset and a more severe phenotype than patients with typical ADCMT1. Weakness often progresses to involve proximal muscles and may result in early loss of ambulation. At least 16 causative genes have been identified for ARCMT1.(Reilly et al. 2011; Rossor et al. 2013) However, the underlying genetic aetiology is still unknown in a significant number of patients. The overlaps in phenotypes between different genotypes increases the number of genes to test and cause difficulty in diagnosis. Therefore, targeted resequencing may be considered as a diagnostic tool for ARCMT1.

This study was aimed to apply a resequencing panel for ARCMT1 to evaluate the efficiency and reliability of targeted resequencing in mutation detection and its application in the diagnostic process for inherited neuropathies. At the time of panel development, mutations in *SH3TC2, GDAP1* and *FGD4* genes have been identified in the British population. Large-scale genetic studies confirmed that *SH3TC2* is the commonest mutated gene, accounting for 21.7% of the molecular diagnoses of ARCMT1 in a referral population.(Murphy et al. 2012) Mutations in *GDAP1* were identified in either ARCMT1 or ARCMT2. *FGD4* is another gene which mutations have been identified in British patients with ARCMT1.(Houlden et al. 2009). Samples from these genetic-diagnosed patients could provide positive controls for the panel. Therefore, the ARCMT1 panel was designed to target coding regions of these three genes.

6.1.2 Methods

(1) Patients and clinical evaluation

The study cohort comprised 91 patients with a clinical diagnosis of ARCMT1. As part of the diagnostic workup all patients had neurological examination and neurophysiological assessment. The patients were previously tested and resulted negative for chromosome 17 duplication and *PMP22* point mutations. In eight of these patients a single heterozygous non-polymorphic variant in *SH3TC2* was previously by Sanger sequencing.

(2) Design of the custom targeted resequencing panel

The targeted sequencing panel was designed to amplify coding exons of three genes: *SH3TC2, GDAP1* and *FGD4* (table 6-1, p177). Custom oligonucleotide probes of 67 amplicons were first designed to capture 38 targeted exons via the web-based DesignStudio (https://icom.illumina.com) (Details of the method were described in Section 2.5)

Table 6-1. Targeted resequencing panel for ARCMT1

Number of targeted exons: 38 Number of attempted amplicons: 67 Cumulative target (bp): 7,994					
Gene	Targeted region	Coding exon	Amplicons	Ref seq	CCDS
GDAP1	chr8:75,262,647-75,276,652	6	22	NM_018972.2	CCDS34911.1
FGD4	chr12:32,729,242-32,793,518	15	12	NM_139241.2	CCDS8727.1
SH3TC2	chr5:148,384,223-148,442633	17	33	NM_024577.3	CCDS 4293.1
Total		**38**	**67**		

Chr: chromosome; Target regions were defined by CCDS of the target genes. Each target region was then divided into amplicons of around 250bps in length. Ref seq: reference sequence according to UCSC iGenomes (hg19) (Homo sapiens) (http://genome.ucsc.edu).

(3) Experimental procedure and data analysis

Two hundred and 50 ng gDNA was used for library preparation according to the TruSeq sample preparation protocol (Illumina). There were totally 96 samples recruited on the panel: one negative control provided by the commercial Kit, four positive controls with known mutations in the three genes and samples from 91 ARCMT1 patients. DNA libraries were then hybridized to exome-capture probes with the TruSeq Kit (Illumina). Automated cluster generation and sequencing were performed on the Miseq system (Illumina). All non-polymorphic rare variations reported by the panel were validated by Sanger sequencing. (Details of experimental procedures were described in Section 2.5.1~2.5.3)

6.1.3 Results

(1) Sequencing yields and optimal target base coverage

A total of 1.5 Gb sequences were generated with 92.1% passing quality filter Q30, which infers a base call accuracy higher than 99.9%. Table 6-2 (p178) lists the coverage of each targeted exon. 74% (28/38) of the targeted exons had the coverage more than 80%. There were four failed exons which had the coverage lower than 50%: exon 2, exon 4, exon 8 and exon 14 in *SH3TC2*.

Table 6-2. Coverage of targeted exons on the ARCMT1 panel

Chr	Start	Stop	Exon	Coverage
5	148442534	148442585	SH3TC2_ex1	75.7%
5	148431705	148431803	SH3TC2_ex2	0.0%
5	148427425	148427552	SH3TC2_ex3	93.5%
5	148424096	148424201	SH3TC2_ex4	34.2%
5	148422257	148422400	SH3TC2_ex5	98.9%
5	148420979	148421180	SH3TC2_ex6	98.4%
5	148420167	148420240	SH3TC2_ex7	82.8%
5	148417858	148418053	SH3TC2_ex8	26.4%
5	148411117	148411250	SH3TC2_ex9	64.6%
5	148408240	148408281	SH3TC2_ex10	100.0%
5	148406423	148408117	SH3TC2_ex11	100.0%
5	148406135	148406315	SH3TC2_ex12	97.4%
5	148392147	148392297	SH3TC2_ex13	96.2%
5	148389833	148389955	SH3TC2_ex14	15.0%
5	148388414	148388564	SH3TC2_ex15	87.5%
5	148386444	148386640	SH3TC2_ex16	75.3%
5	148384274	148384465	SH3TC2_ex17	65.6%
8	75262697	75262813	GDAP1_ex1	100.0%
8	75263509	75263701	GDAP1_ex2	99.2%
8	75272372	75272545	GDAP1_ex3	100.0%
8	75274119	75274213	GDAP1_ex4	98.7%
8	75275174	75275288	GDAP1_ex5	91.4%
8	75276220	75276602	GDAP1_ex6	96.0%
12	32729292	32729383	FGD4_ex3	76.8%
12	32734894	32735401	FGD4_ex4	61.1%
12	32751431	32751520	FGD4_ex5	51.4%
12	32754212	32754357	FGD4_ex6	93.2%
12	32755095	32755251	FGD4_ex7	99.8%
12	32760891	32761029	FGD4_ex8	100.0%
12	32763710	32763768	FDG4_ex9	94.8%
12	32764071	32764217	FGD4_ex10	98.6%
12	32772632	32772804	FGD4_ex11	100.0%
12	32777356	32777386	FGD4_ex12	100.0%
12	32777910	32778002	FGD4_ex13	100.0%
12	32778588	32778713	FGD4_ex14	98.1%
12	32786483	32786623	FGD4_ex15	100.0%
12	32791589	32791729	FGD4_ex16	100.0%
12	32793210	32793467	FGD4_ex17	91.1%
Panel coverage				83.2%

Coverage is generated from the BEDtools and defined as the total number of none-overlapping bases covered by amplicons divided by the total numbers of bases in CCDS of the targeted exon. For each exon, the mean coverage of all samples is listed in the table. Panel coverage is defined as the mean coverage of all exons. Chr: chromosome, ex: exon.

(2) Sensitivity and specificity

The sensitivity of the panel is defined as proportion of true positives detected by the panel in the positive controls with known mutations. There are totally six mutations in the three genes from four positive control samples. Every mutation was reported by the panel with a satisfactory sequencing depth and a robust variant frequency (table 6-3). Therefore, the panel successfully detected all known mutations in the positive controls and gave 100% sensitivity.

Table 6-3. Mutations of the positive controls successfully detected by the ARCMT1 panel

DNA No.	Gene	Mutation		POS	Base depth	REF (depth)	ALT (depth)	Quality filter
44730	*SH3TC2*	R641C	Het	5:148407374	1877	G (978)	A (897)	PASS
44730	*SH3TC2*	R954X	Het	5:148406435	4630	G (2238)	A (2382)	PASS
14605	*SH3TC2*	S433L	Het	5:148407997	4308	G (2112)	A (2190)	PASS
46116	*GDAP1*	P153L	Het	8:75272519	817	C (403)	T (414)	PASS
46116	*GDAP1*	Q163X	Het	8:75274121	307	C (168)	T (138)	PASS
44338	*FGD4*	R275X	Hom	12:32754344	6	C (0)	T (6)	Q30

POS: the position of the mutation, REF: reference allele, ALT: alternated allele, Het: heterozygous, Hom: homozygous.

Quality scores measure the probability that a base is called incorrectly. Each base in a read is assigned a quality score by a phred-like algorithm (Ewing et al. 1998a; Ewing et al. 1998b), similar to that originally developed for Sanger sequencing experiments. The quality score of a given base, Q, is defined by the equation Q = -10log10(e) where e is the estimated probability of the base call being wrong. Thus, a higher quality score indicates a smaller probability of error. Q30 represents an error rate of 1 in 1000, with a corresponding call accuracy of 99.9%.

Specificity and negative predictive value of the ARCMT1 panel are listed in table 6-4 (p180). The specificity is defined as proportion of true positives in the patient cohort detected by the resequencing panel, which could be confirmed by Sanger sequencing. After filtering out synonymous, silent and non-coding variants, a total of 114 variants were tested by Sanger sequencing. All 62 variants passing quality filter Q30 were validated, giving the 100% specificity. Among the 52 variants which failed to pass Q30, 49 of them were reconfirmed as false, thus a negative predictive value of 94%.

Table 6-4. Specificity and negative predictive value of the ARCMT1 panel

Number of variants		Sanger sequencing		Compatible rate
passing Q30	62	TRUE	62	100% *
		FALSE	0	0%
not passing	52	TRUE	3	6%
		FALSE	49	94% #

* Specificity= the proportion of true positives in the patient cohort detected by the resequencing microarray, which could be confirmed by Sanger sequencing.

Negative predictive value = the proportion of subjects with a negative test result who are correctly diagnosed.

(3) Variants detected by the panel

Among the 91 patients, 48 (52.7%) were identified to have at least one non-synonymous rare variants (MAF<0.01) in the coding regions of the three genes. Seven unrelated patients (7.6%) were identified to carry reported or novel mutations which were probably pathogenic: four had homozygous mutations and three had two heterozygous mutations (table 6-5). Some patients have rare variants in more than one gene.

Table 6-5. Rare variants detected by the ARCMT1 panel

Pathogenic grade		No. of patients	*SH3TC2*	*GDAP1*	*FGD4*
Positive		48	42	3	3
Reported or probable pathogenic mutation	**Hom**	**4**	**2**	**1**	**1**
	Double Het	**3**	**1**	**1**	**1**
Hom or double Het, with at least one none-pathogenic SNP		12	12	0	0
Single Het		29	27	1	1
Negative		43	/	/	/

Rare variants are defined as: non-synomic variants in the coding regions with MAF<0.01.

No.: number of patients, Hom: homozygous variant, Het: heterozygous variant, Double Het: two heterozygous variants in one sample, allele unknown, SNP: single nucleotide polymorphism

Details of mutations in the seven patients are listed in table 6-6 (p181). All mutations were confirmed by Sanger sequencing (figure 6-1, p182). Two patients carried *FGD4* mutations. One with early-onset demyelinating neuropathy carried a homozygous *FGD4* R442H mutation and co-segregation with the phenotype was confirmed within the family (figure 6-1, A). The other patients had two heterozygous *FGD4* mutations: G620V is a novel mutation, and R577Q has

been reported as a very rare variant with unknown clinical significance (figure 6-1, B). Both mutations are predicted to generate damaging effects by Polyphen and SIFT. In two patients *GDAP1* mutations were identified. One patient carried homozygous *GDAP1* M116R mutation, an already reported pathogenic mutation (figure 6-1, C). The second case had two heterozygous *GDAP1* mutations: a known pathogenic mutation L238F and a novel G327D mutation (figure 6-1, D). In S*H3TC2*, the hot-spot mutation R954X was identified in three patients. Two had homozygous mutations (figure 6-1, E). The third one was previously known to carry a single heterozygous R954X mutation and a further novel heterozygous mutation Y290X was identified through the panel (figure 6-1, F). For patients harbouring two heterozygous mutations, parental samples will be tested to confirm whether the two mutations are compound heterozygous mutations.

Table 6-6. Reported or probable pathogenic mutations detected by the ARCMT1 panel

Gene	Mutation	Pathogenicity prediction
FGD4	[p.R442H ; p.R442H]	Reported pathogenic mutation
	[p.R577Q (;) p.G620V]	R577Q: Vary rare variant without SNP ID, MAF=0.016%, highly conserved GERD:5.29, PolyPhen: probably damaging
		G620V: Novel mutation, presumed pathogenic; MAF=N/A, PolyPhen: probably damaging
GDAP1	[p.M116R ; p.M116R]	Reported pathogenic mutation
	[p.G327D (;) p.L239F]	L239F: Reported pathogenic mutation (rs104894080)
		G327D: : Novel mutation, presumed pathogenic, MAF=N/A, GERD:4.99, PolyPhen: probably damaging
SH3TC2	[p.R954X ; p.R954X] (n=2)	Reported pathogenic mutation (rs80338933)
	[p.Y290X ; p.R954X]	Y290X: Novel mutation, presumed pathogenic, MAF=N/A
		R954X: Reported pathogenic mutation (rs80338933)

SNP: single-nucleotide polymorphism, MAF: minor allele frequency, N/A: not available

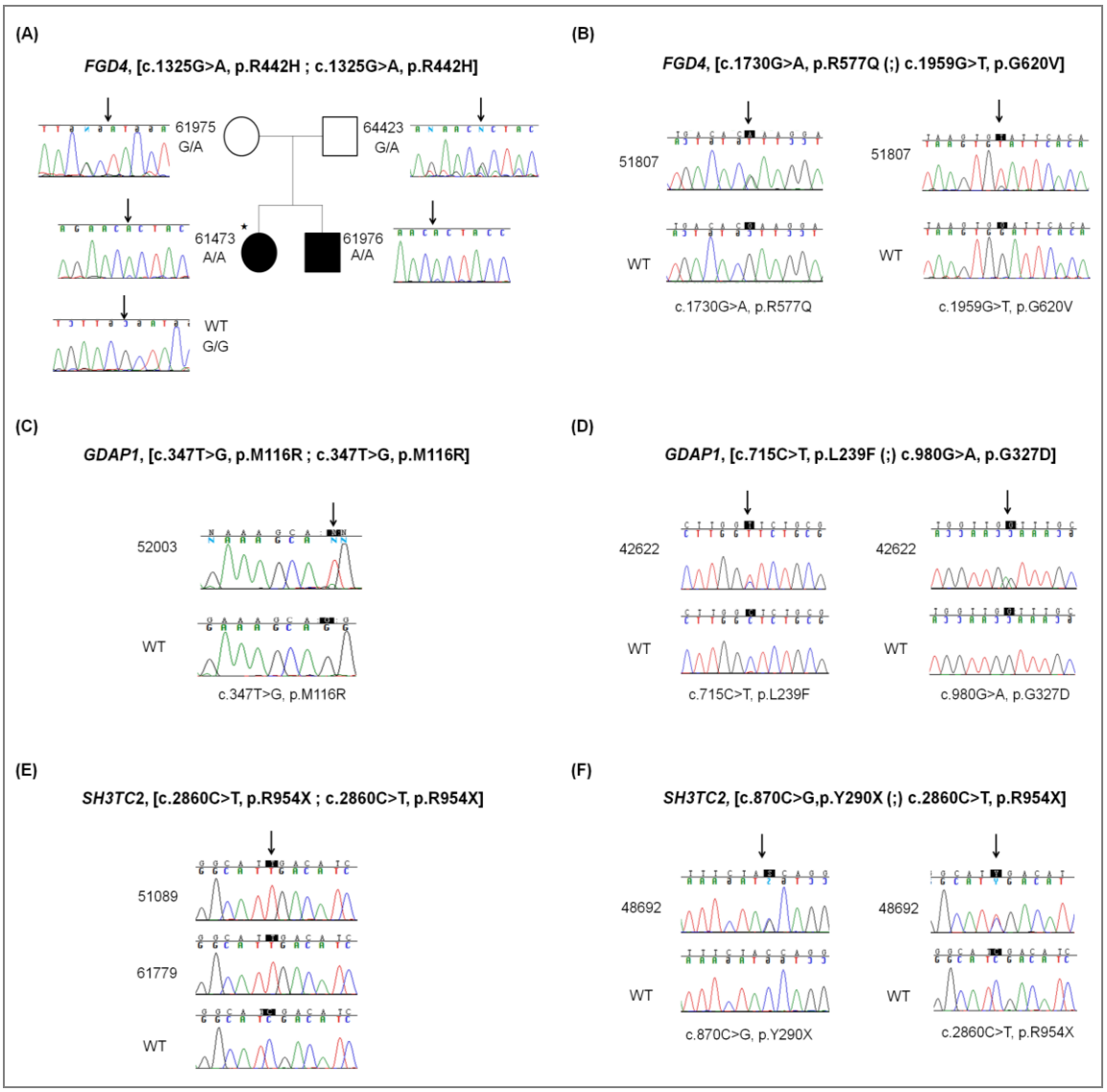

Figure 6-1. Mutations detected by the ARCMT1 panel validated by Sanger sequencing

A total of 1002 rare non-pathogenic SNPs annotated in dbSNP (build 138) corresponding to 38 distinct sequence variations were found in the 95 analysed patients: SNP (n) in *FGD4*=16, in *GDAP1*=6, and in *SH3TC2*=16. The frequencies of these SNPs in the cohort on the ARCMT1 panel are much higher than their MAF in 1000 Genomes Project (table 6-7).

Table 6-7. Rare single-nucleotide polymorphisms (SNPs) detected by the ARCMT1 panel

Chr	Position	SNP ID	Number	Frequency in panel	MAF
chr12	32735236	rs904582	58	0.6105	0.000459
chr12	32754367	rs41276676	6	0.0632	0.000458
chr12	32755058	rs4931641	26	0.2737	0.000459
chr12	32755259	rs12823621	15	0.1579	0.000459
chr12	32763668	rs1004969	17	0.1789	0.000459
chr12	32763975	rs76666307	1	0.0105	0.000467
chr12	32764184	rs10844253	56	0.5895	0.000459
chr12	32777362	rs11052110	37	0.3895	0.000459
chr12	32777889	rs17539792	18	0.1895	0.000459
chr12	32778742	rs17539848	19	0.2000	0.000459
chr12	32778830	rs79100182	4	0.0421	0.000458
chr12	32778913	rs1909510	68	0.7158	0.000459
chr12	32786460	rs76834265	2	0.0211	0.00046
chr12	32786700	rs59572242	26	0.2737	0.000459
chr12	32791796	rs4575368	17	0.1789	0.000459
chr12	32793164	rs74073032	15	0.1579	0.000459
chr8	75262536	rs4541908	17	0.1789	0.000458
chr8	75262798	rs7828201	6	0.0632	0
chr8	75262841	rs4321999	6	0.0632	0.000458
chr8	75272287	rs3780014	64	0.6737	0.000459
chr8	75274141	rs11554166	51	0.5368	0.000459
chr8	75275312	rs4463412	93	0.9789	0
chr5	148384455	rs146920285	1	0.0105	0.000457
chr5	148386525	rs6871030	58	0.6105	0.000459
chr5	148386569	rs142451273	1	0.0105	N/A
chr5	148388420	rs55853803	4	0.0421	0.000459
chr5	148392362	rs11954893	36	0.3789	0.000459
chr5	148406032	rs10075404	30	0.3158	0.000459
chr5	148406386	rs17722209	33	0.3474	0.000459
chr5	148407481	rs186864272	1	0.0105	0.00045
chr5	148407708	rs1432794	95	1.0000	0.000458
chr5	148407892	rs6874630	2	0.0211	0.000456
chr5	148407893	rs6875902	37	0.3895	0.000459
chr5	148407945	rs17722227	4	0.0421	0.000459
chr5	148408101	rs1432793	69	0.7263	0.000459
chr5	148420221	rs144963732	1	0.0105	N/A
chr5	148421065	rs80227512	3	0.0316	0.000456
chr5	148422274	rs17722293	5	0.0526	0.000459

Chr: chromosome, Number: number of patients who had the SNP on the panel, MAF: minor allele frequency, N/A: not available

6.1.4 Discussion

This study documented that targeted resequencing could detect single base substitutions with a reliable accuracy. The ARCMT1 panel which was developed and performed by Truseq system provided an excellent sensitivity, specificity and negative predictive value. Also, by simultaneously screening several genes per patient, the panel significantly improved the cost-efficiency of CMT testing and reduced diagnostic turn-around times.

Our results confirmed that mutation in *SH3TC2* is the commonest genetic aetiology in patients with ARCMT1. This study also illustrated how a resequencing panel can be a comprehensive tool for Sanger sequencing. For example, in one patient who was already known to carry a heterozygous R954X mutation in *SH3TC2*, a second heterozygous mutation R290X was detected through the panel. The frequency of *GDAP1* mutations may be underestimated because many patients with *GDAP1* mutations have been diagnosed through conventional diagnostic process and were not included on the panel. Alternatively, the frequency of *FGD4* mutations using targeted resequencing may be higher than previously reported since mutation analysis of *FGD4* was not routinely screened in most diagnostic laboratories. The application of target resequencing will probably broaden the phenotypic spectrum of *FGD4* mutations and may reshape our understanding of genotypes and phenotypes related to CMT in the near future.

In our CMT cohort, the frequency of rare SNPs detected through the panel was much higher than their MAF in 1000 Genomes Project. In other studies employing resequencing panels, higher occurrence rates of SNPs were also observed.(Dufke et al. 2012) Their clinical significance is still unclear.

The results of the pilot panel suggested that a small disease-specific panel covering a particular phenotype, e.g. ARCMT1, is a more feasible strategy in the design of panels in comparison with a more complete panel that includes several genes (currently, more than 60 genes) causing most CMT phenotypes. A small phenotype-specific panel may be more advantageous than a complete CMT panel as it may be more cost-effective and, more importantly, the number of non-pathogenic variants likely to be detected may be lower. This is particularly important when interpreting the results and thus helps reduce substantially the time and the cost of validating results. Furthermore, the frequency with which phenotype-specific panels will have to be upgraded will be less than that for a panel including all CMT genes as new genes are keeping increasing. Based on the experience learned from the ARCMT1 pilot panel, currently four phenotype-specific panels are being developed in the diagnostic genetic service at the NHNN: a CMT1-intermediate CMT panel, a CMT2-intermediate CMT panel, a distal HMN panel and a HSN panel. The panels have been designed to cover a broad spectrum

of CMT phenotypes but at the same time they benefit from known phenotype-genotype correlation. They are part of the integrative approach of genetic diagnosis of CMT patients which combines NGS and conventional Sanger sequencing (figure 6-2).

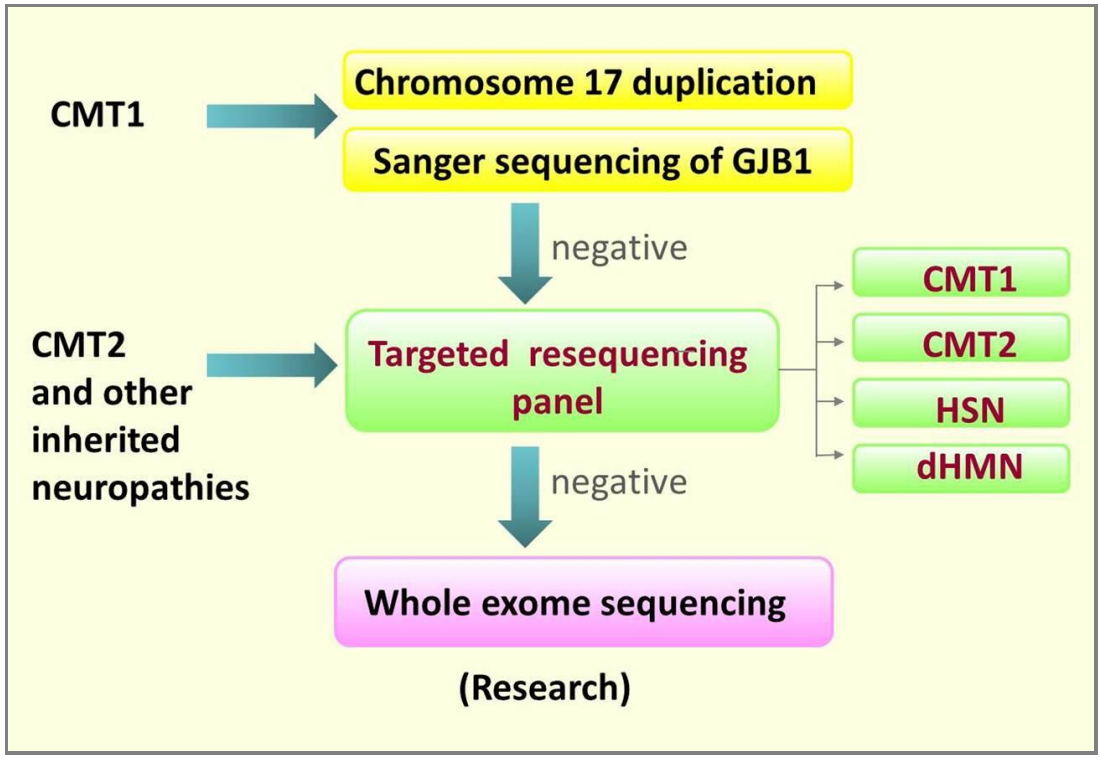

Figure 6-2. Integrative approach of genetic diagnosis of CMT which combines targeted resequencing and Sanger sequencing

Genetic diagnosis starts with the categorization of patients with CMT1, CMT2 and other phenotypes. CMT1Patients will be firstly tested for chromosome17 duplication or *GJB1* gene mutation as these are the most common causes of CMT. After exclusion of these mutations patients will be sequenced by the CMT1 panel which includes known genes for the demyelinating and intermediate types of CMT. In patients with CMT2, HSN and dHMN the specific panel will be performed. Some genes are included in more than one panel as they can cause several phenotypes. Whole exome sequencing will be performed in selected patients in which causative gene mutations are still unknown after targeted resequencing.

6.2 Mutation analysis of genes for HSP and axonal neuropathy by targeted resequencing

6.2.1 Introduction

More than 52 loci and 31 genes have been identified to cause dominant, recessive, and X-linked forms of HSP.(Fink 2013) The genetic diagnosis of HSP is becoming challenging due to the complicated phenotype-genotype correlations. At least two forms of HSP may manifest as both AR and AD disorders: SPG7 was originally described as a recessive disorder due to homozygous or compound heterozygous S*PG7*/paraplegin gene mutations but subsequently reports of HSP syndromes due to heterozygous *SPG7* mutation have been published.(Arnoldi et al. 2008; Brugman et al. 2008; McDermott et al. 2001) Homozygous or compound heterozygosous *CYP7B1* mutations were known to cause recessive SPG5, but a heterozygous missense change was recently reported in a dominant HSP family.(Schule et al. 2009) This is further complicated by the increasing genetic and clinical overlaps with inherited neuropathies. As mentioned previously in Section 1.2.1, many forms of HSP are frequently associated with peripheral neuropathy, e.g. *ATL1* (SPG3A), *SPAST* (SPG4), *BSCL2* (SPG17) and KIF5A (SPG10).(Al-Maawali et al. 2011; Du et al. 2011; Goizet et al. 2009; Guelly et al. 2011; Ivanova et al. 2007; Kumar et al. 2012; Musumeci et al. 2010; Scarano et al. 2005; Schule et al. 2003; Windpassinger et al. 2004) Because of the clinical and genetic heterogeneity of HSP, it may be more time and cost effective using targeted resequencing rather than Sanger sequencing, particularly when dealing with a large scale of patients. Target resequencing is also an ideal tool to screen genes for other diseases which may cause phenotypes overlapping with HSP.

This study reported the design and application of a resequencing panel targeting the coding regions of 31 genes related to HSP and axonal neuropathy. The purpose was to establish the epidemiological profile of a group of patients with HSP or axonal neuropathy with spasticity. The efficiency and reliability of high-throughput genotyping technology in screening multiple genes were also investigated.

6.2.2 Patient and methods

(1) Patients

The study cohort comprised 66 unrelated patients with HSP or axonal neuropathy associated with spasticity. Twenty four patients had AD inheritance, 5 belonged to consanguineous family with a definite AR inheritance and 37 were sporadic cases. Most patients (58/66) had been already screened and resulted negative for mutation in *SPAST* and *ATL1* genes. Sixteen patients had neurophysiological-documented sensorimotor axonal neuropathy.

(2) Design of the custom targeted resequencing panel

The targeted sequencing panel was designed to amplify the coding regions of 31 genes: 11 for AD-HSP, 16 for AR-HSP, 3 for X-liked HSP and *MFN2* (gene for CMT2A) (table 6-8, p188). *MFN2* was included on the panel as patients carrying its mutations can present by axonal neuropathy in association with spasticity, overlapping with the complex HSP phenotype. Custom oligonucleotide probes were designed through the web-based Agilent Halo Design Wizard (http://www.halogenomics.com/haloplex/custom-reagent-kits).

(3) Experimental procedure and data analysis

250ng of Genomic DNA was used for library preparation and then hybridized to exome-capture probes with the HaloPlex system (Agilent). 72 samples were included on the panel: five positive controls with known mutations in *ATL1, SPAST, REEP1, NIPA1* and *BSCL2*, 66 samples from the patient cohort mentioned above and one negative control provided by the commercial kit. The total number of samples was sequenced by two runs on the Miseq platform in order to investigate the optimized sequencing capacity of the panel. Twelve samples were pooled and submitted in Flow cell A for the first run, and the rest 60 samples were pooled and submitted in Flow cell B for the second run. Samples with different indexes were pooled with equimolar amounts of each sample. The final HaloPlex enrichment pool was ready for 150 + 150 bp paired-end sequencing using chemistry on the Illumina MiSeq. Before aligning reads to the reference genome, reads were trimmed from HaloPlex adaptor sequences with NextGene software (Softgenetics). Sequence alignment and variant calling were then performed against the reference human genome (UCSC hg19). An overview of the workflow is shown in figure 6-3. (Details of experimental procedures were described in Section 2.5)

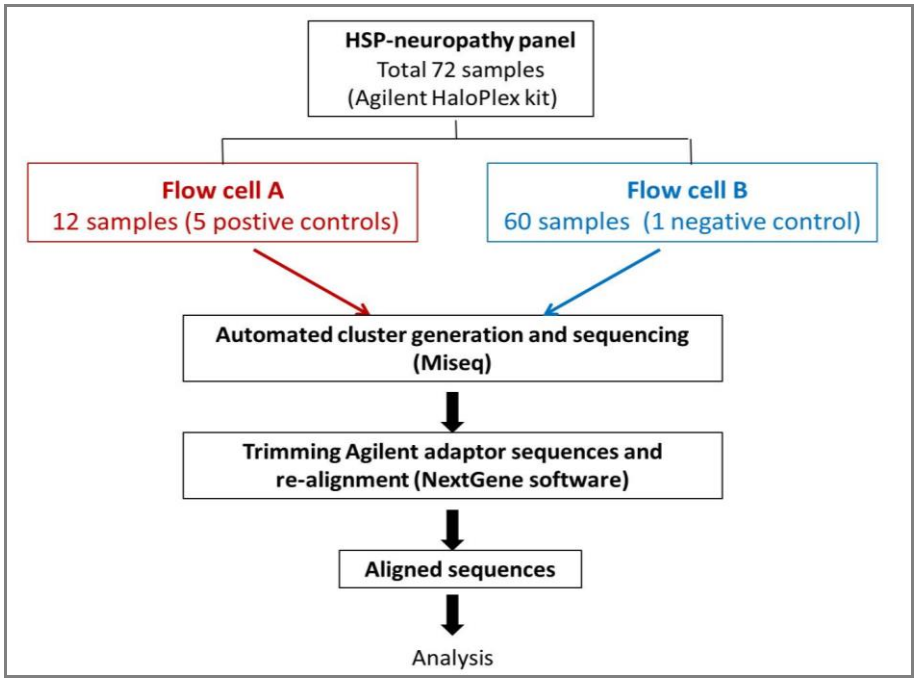

Figure 6-3. Workflow of the HaloPlex panel for HSP and axonal neuropathy

Table 6-8. Targeted resequencing panel for HSP and axonal neuropathy

Number of Targeted exons: 463 Cumulative Target (bp): 94,164 Predicted coverage: 99.8%				
AD (12 genes)				
Disease	Gene	Location	Ref seq	CCDS
SPG3	*ATL1*	chr7:4,815,262-4,834,026	NM_014855	CCDS47528.1
SPG4	*SPAST*	chr2:32,288,680-32,382,706	NM_014946	CCDS1779.1, CCDS1778.1
SPG6	*NIPA1*	chr15:23,048,850-23,086,324	NM_001095784	CCDS45190.1, CCDS10011.1
SPG8	*KIAA0196*	chr2:198,351,308-198,364,998	NM_199440	CCDS33357.1
SPG10	*KIF5A*	chr12:57,943,847-57,978,554	NM_004984	CCDS8945.1
SPG12	*RTN2*	chr19:45,988,546-46,000,313	NM_005619	CCDS12665.1, CCDS12666.1
SPG13	*HSPD1*	chr17:42,875,816-42,907,607	NM_005497	CCDS1569.1
SPG17	*BSCL2*	chr14:51,026,743-51,099,784	NM_015915	CCDS32077.1, CCDS9700.1
SPG31	*REEP1*	chr2:86,441,120-86,565,206	NM_001164730	CCDS1989.1
SPG33	*ZFYVE27*	chr10:99,496,878-99,520,664	NM_001174122	CCDS31262.1, CCDS31263.1, CCDS31264.1
SPG42	*SLC33A1*	chr3:155544301-155572248	NM_004733	CCDS3173.1
CMT2	*MFN2*	chr1:12,040,238-12,073,572	NM_014874	CCDS30587.1
AR (16 genes)				
Disease	Gene	Location	Ref seq	CCDS
SPG5	*CYP7B1*	chr5:10,250,282-10,266,501	NM_012073	CCDS3877.1
SPG7	*SPG7*	chr16:89,574,805-89,624,174	NM_003119	CCDS10977.1, CCDS10978.1
SPG11	*SPG11*	chr15:44,854,894-44,955,876	NM_025137	CCDS10112.1
SPG15	*ZFYVE26*	chr14:68,213,237-68,283,306	NM_015346	CCDS9788.1
SPG18	*ERLIN2*	chr8:65,508,529-65,711,348	NM_004820	CCDS6180.1
SPG20	*SPG20*	chr13:36,875,775-36,944,317	NM_001142294	CCDS9356.1
SPG21	*SPG21*	chr15:65,255,362-65,282,284	NM_016630	CCDS45279.1, CCDS10198.1
SPG35	*FA2H*	chr8:37,594,097-37,615,319	NM_007175	CCDS6095.1, CCDS34879.1
SPG39	*PNPLA6*	chr19:7,599,038-7,626,653	NM_006702	CCDS32891.1
SPG44	*GJC2*	chr16:74,746,856-74,808,729	NM_024306	CCDS10911.1
SPG47	*AP4B1*	chr1:114,437,371-114,447,741	NM_006594	CCDS865.1
SPG48	*KIAA0415*	chr8:126,036,503-126,104,061	NM_014846	CCDS6355.1
SPG50	*AP4M1*	chr7:99,699,130-99,704,803	NM_004722	CCDS5685.1
SPG51	*AP4E1*	chr15:51,200,869-51,298,097	NM_007347	CCDS32240.1
SPG52	*AP4S1*	chr14:31,494,676-31,555,008	NM_007077	CCDS9642.1, CCDS45093.1
Spasticity + SN	*CCT5*	chr11:62,457,734-62,475,179	NM_001122955	CCDS8031.1, CCDS44627.1
X-linked (3 genes)				
Disease	Gene	Location	Ref seq	CCDS
SPG1	*L1CAM*	chrX:153,126,969-153,141,500	NM_000425	CCDS14733.1, CCDS14734.1, CCDS48192.1
SPG2	*PLP1*	chrX:103,031,439-103,047,547	NM_001128834	CCDS14514.1, CCDS14513.1
SPG22	*SLC16A2*	chrX:73,641,328-73,753,764	NM_006517	CCDS14426.1

AD: autosomal dominant; AR: autosomal recessive; chr: chromosome; Ref seq: reference sequence according to UCSC iGenomes (hg19) (Homo sapiens) (http://genome.ucsc.edu); Target regions were defined by CCDS of the target genes; SN: sensory neuropathy

(4) Validation of reported variants by Sanger sequencing:

Synonymus, silent and non-coding variants were filtered out first from all variants reported by the panel. The following strategy was then adopted to validate the rest variants by Sanger sequencing: (1) Variants which were compatible with the patient's inheritance were tested. For example, single heterozygous variant in known AD-HSP genes were validated in patients with dominant inheritance whereas homozygous or double heterozygous variants in AR-HSP genes were selected in patients from a recessive family. (2) For sporadic cases with undetermined inheritance, both heterozygous variants in AD genes and homozygous/double heterozygous variants in AR- genes were tested. (3) Variants in *MFN2*, *SPG7* and *CYP7B1* were considered in both AD and AR inheritance as mutations in these genes have been reported in heterozygous and homozygous status. (4) Variants on chromosome X were tested only when they presented in male patients when there was no male to male transmission.

6.2.3 Results

(1) Sequencing yields and optimal target base coverage

A total of 3 Gb sequences were generated by two runs, 1.5 Gb sequences per run. Table 6-9 lists the distribution of target base coverage of each targeted exon on the panel. The mean coverage of all 465 targeted exons in Flow cell A with 12 pooled samples was higher than 80%, better than 72% in Flow cell B which pooled 60 samples together. In Flow cell A, more than half (55.3%) of the exons had the coverage higher than 80%, but the proportion dropped to 42.8% in Flow cell B.

Table 6-9. Coverage of the targeted exons on the panel for HSP and axonal neuropathy

	Flow cell A (*n*=12)		**Flow cell B (*n*=60)**	
Coverage	**No. of exons**	**%**	**No. of exons**	**%**
X ≧80%	256	55.1	198	42.6
50% ≦ X <80%	89	19.1	182	39.1
10% ≦ X <50%	62	13.3	75	16.1
X <10%	58	12.5	10	2
Panel coverage	**81%**		**72%**	

Coverage per exon is generated from the BEDtools and defined as the total number of none-overlapping bases covered by amplicons divided by the total numbers of bases in CCDS of the targeted exon. X represents the mean coverage of all samples per exon. Panel coverage is defined as the mean coverage of all exons.

Nineteen out of the 31 genes (61%) had the coverage above 70%. Genes were then listed from high to low in the order of the average coverage in table 6-10 (p190). Failed exons with the coverage less than 50% were listed in the table. In some genes, only one or two failed exons

lowered the average coverage of the gene significantly.

Table 6-10. Coverage of the genes on the panel for HSP and axonal neuropathy

Gene	Coverage	coding exons	Failed exon (coverage<50%)
FA2H	100.0%	7	
SLC33A1	97.6%	6	
GJC1	94.5%	1	
AP4B1	85.9%	10	AP4B1_ex5
NIPA1	85.5%	5	
ZFYVE27	80.9%	13	ZFYVE27_ex1
AP5Z1	80.8%	17	AP5Z1_ex1, AP5Z1_ex11
ATL1	80.7%	14	
KIF5A	80.5%	28	KIF5A_ex5
MFN2	79.9%	17	MFN2_ex8
CCT5	79.5%	11	
RTN2	78.8%	11	RTN2_ex1
SPG7	77.6%	17	SPG7_ex17
KIAA0196	76.9%	28	KIAA0196_ex25, KIAA0196_ex24
ZFYVE26	75.2%	41	ZFYVE26_ex33, ZFYVE26_ex29, ZFYVE26_ex16
PLP1	72.1%	7	PLP1_ex7, PLP1_ex8
ERLIN2	71.8%	12	ERLIN2_ex6
SPG20	70.7%	8	SPG20_ex9,SPG20_ex6, SPG20_ex3
BSCL2	70.3%	11	BSCL2_ex10
SPAST	68.6%	17	SPAST_ex5, SPAST_ex6
AP4E1	66.2%	21	AP4E1_ex8
PNPLA6	66.2%	33	PNPLA6_ex35, PNPLA6_ex3, PNPLA6_ex18
SPG11	65.4%	40	SPG11_ex25, SPG11_ex37, SPG11_ex17
AP4S1	65.0%	6	AP4S1_ex6
AP4M1	64.4%	15	AP4M1_ex1, AP4M1_ex15
REEP1	62.0%	7	REEP1_ex1, REEP1_ex5
L1CAM	60.3%	29	L1CAM_ex26, L1CAM_ex3
HSPD1	59.0%	11	HSPD1_ex3, HSPD1_ex12, HSPD1_ex8
CYP7B1	57.2%	6	CYP7B1_ex6, CYP7B1_ex1
SPG21	63.3%	8	SPG21_ex7, SPG21_ex6
SLC16A2	52.7%	6	SLC16A2_ex5, SLC16A2_ex4

Coverage listed in the table is the mean of coverage of all exons for each gene. The better coverage among two runs is chosen to show the optimal performance of the probes. ex: exon

(2) Sensitivity and specificity

There were in total five mutations in five genes from five positive controls on the panel. Each of the five mutations was detected as a robust variant which has a satisfactory sequence depth and variant frequency (table 6-11). Therefore, the panel successfully detected all known mutations in the positive controls and gave 100% sensitivity.

Table 6-11. Mutations of the positive controls successfully detected by the panel for HSP and neuropathy

DNA No.	Gene	Mutation		POS	Base depth	REF (depth)	ALT (depth)	Quality filter
49028	*BSCL2*	N88S	Het	chr11:62469971	5	T (2)	C (3)	PASS
52069	*NIPA1*	G304V	Het	chr15:23048908	85	C (35)	A (50)	PASS
60379	*ATL1*	V253I	Het	chr14:51081124	18	G (7)	A (11)	PASS
60483	*REEP1*	Y35X	Het	chr2:86509294	24	T (5)	A (19)	PASS
65223	*SPAST*	R562X	Het	Chr2:32370073	18	C (12)	T (6)	PASS

POS: the position of the mutation, REF: reference allele, ALT: alternated allele, Het: heterozygous

Among all the variants reported by the panel, 446 rare variants (MAF<0.01) were kept after filtering synonymus, silent and non-coding variants. Applying the strategy mentioned before, a total of 260 variants in 31 genes were tested by Sanger sequencing. Only 17 variants passed the validation, suggesting a low specificity of the panel although not all variants reported by the panel were tested. A significant number of false positive variants were caused by the remnants of restrict enzyme cutting sites, as illustrated in figure 6-4 (p192).

Figure 6-4. Example of a false positive report caused by a restriction enzyme cutting site on the HaloPlex panel

The panel reports the variant on the top sample (pointed by the red arrow). However, the variant was not detected by Sanger sequencing and thus a false positive report. Alignment of the sample with the other two samples revealed that the variant is localised in a restriction enzyme cutting site.

(3) Probable pathogenic mutations detected by the panel

Nine unrelated patients were identified to carry reported or novel mutations which are probably pathogenic (table 6-12, p193). All mutations were confirmed by Sanger sequencing (figure 6-5, p194).

Two heterozygous *MFN2* mutations were identified in two unrelated patients. S231P is a novel mutation detected in a sporadic case who had an early-onset sensorimotor axonal neuropathy with hyperreflexia (figure 6-5, A). R519C was a very rare variant only reported on ESV with an extremely low frequency (MAF<0.007%) (figure 6-5, B). The pathogenic role of this variant was supported by the predicted damaging effect and high conservation of the substituted codon. The patient with R519C mutation had peripheral neuropathy and additional CNS involvement like spastic paraperesis and learning difficulty.

There are other heterozygous mutations in AD-HSP genes. One *ATL1* mutation (R239C) was identified in a sporadic patient with pure HSP (figure 6-5, C*)*. This is a previously reported pathogenic mutation related to HSP. A novel I226T mutation in *KIAA0196* was detected in a patient with spastic paraplegia and sensory axonal neuropathy which was DOPA responsive (figure 6-5, D). She was from a dominant family as her daughter was also affected by spasticity

and sensory impairment. Two previously reported pathogenic mutations in *SPAST* were identified in two patients. The patient with the missense mutation S44L had a pure HSP phenotype and AD inheritance (figure 6-5, E). The other heterozygous was 1pb deletion at the splicing cite (c.1494-2delT) which was carried by a patient with HSP, visual impairment, learning difficulties and nystagms (figure 6-5, F).

Mutations in AR-HSP gene were also identified. One patient was identified to carry two heterozygous mutations in FA2H: p.R154C is a presumed pathogenic novel mutation and p.T207M is a very rare variant with predicted damaging effects (figure 6-5, G). Parents of the individual will be tested in the future to confirm if the two mutations are compound heterozygous mutations. Two heterozygous missense mutations in *KIF5A* were detected and have been described in Section 4-1.

Table 6-12. Reported or probable pathogenic mutations detected by the panel for HSP and axonal neuropathy

DNA No.	Gene	Mutation	Significance	Inheritance	Phenotype
66679	*MFN2*	S231P (Het)	Novel mutation, presumed pathogenic	sporadic	Sensorimotor axonal neuropathy with hyperreflexia
30156	*MFN2*	R519C (Het)	Vary rare variant without SNP ID; MAF <0.007% on ESV, PolyPhen: damaging	sporadic	cHSP with neuropathy and learning difficulty, childhood-onset
66681	*ATL1*	R239C (Het)	Reported pathogenic mutation (rs119476046)	sporadic	pHSP, early onset
62182	*KIAA0196*	I226T (Het)	Novel mutation, presumed pathogenic	AD	cHSP: L-Dopa responsive spasticity with sensory axonal neuropathy, early onset
45020	*SPAST*	S44L (Het)	Reported pathogenic mutation (rs121908515)	AD	pHSP, two children are affected
23578	*SPAST*	c.1494-2delT (Het)	Reported pathogenic mutation (CD023280)	sporadic	cHSP with visual impairment, learning difficulties, nystagmus
51210	*FA2H*	[p.R154C (;) p.T207M]	p.R154C: novel mutation, presumed pathogenic; p.T207M: vary rare variant without SNP ID	sporadic	Spastic ataxia (cHSP with ataxia)
60113	*KIF5A*	R204W (Het)	Novel mutation, presumed pathogenic	AD	Spastic ataxia (cHSP with ataxia), dystonia, adult-onset, one affected sister
48092	*KIF5A*	R204Q (Het)	Reported pathogenic mutation	AD	cHSP with sensorimotor axonal neuropathy, two children affected

AD: autosomal dominant, AR: autosomal recessive, cHSP: complex HSP, Het: heterozygous variant, pHSP: pure HSP, SNP: single nucleotide polymorphism, MAF: minor allele frequency.

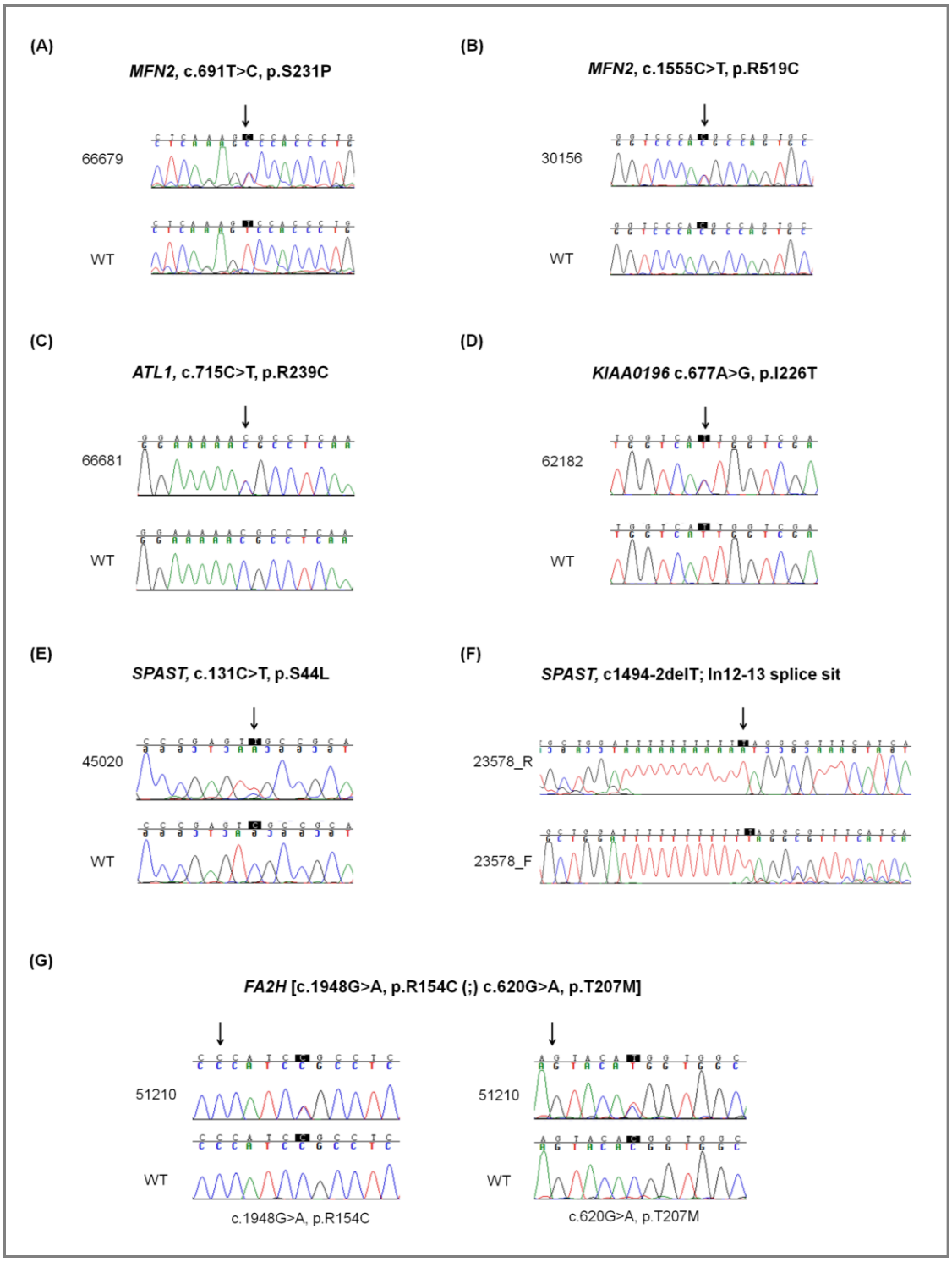

Figure 6-5. Reported or probable pathogenic mutations detected by the panel for HSP and axonal neuropathy were validated by Sanger sequencing

6.2.4 Discussion

The panel has helped identify reported or probable pathogenic mutations in 9 patients from the 66 index patients. The overall diagnosis rate was 13.6% and the hit rate was 13.1% (8/61) in *SPAST*-negative cases. Previous studies conducted by Sanger sequencing revealed that *SPAST* is the commonest causative HSP gene, accounting for approximately 50% of AD-HSP

cases(Hazan et al. 1999), and *ATL1* is the second most common causative gene explaining another 10% of AD-HSP cases.(Hazan et al. 1999) Mutations in most of the AR-HSP genes are much rarer and little information about the prevalence are available.(Dufke et al. 2012) Recently, it has been reported that a genetic diagnosis could be established only in 11% of *SPAST*-negative AD-HSP cases by resequencing technology.(Dufke et al. 2012) The higher detection rates in our study provided evidence that targeted resequencing is a competent tool to simultaneously screen a large number of genes for diseases of high genetic heterogeneity, like HSP.

The panel was aimed to screen mutations in patients with various inheritance modes, not limited in AD cases. This was because that a significant number of our patients were sporadic thus genes related to different inheritance patterns should all be considered. Our results showed five patients were sporadic cases among the nine patients diagnosed though the panel. This study suggested that a panel including numerous genes could substantially raise the genetic diagnosis rate of HSP patients since it encompassed most subtypes.

Eight missense mutations and one deletion were identified in patients with HSP or axonal neuropathy by the resequencing panel, documenting that targeted resequencing could successfully detect both single base substitutions and small indels.

Genetic findings in this study have greatly contributed to broaden the phenotypic spectrums of many HSP genes. For example, the patient harbouring a novel *KIAA0196* I226T mutation presented with a L-Dopa responsive spastic paraplegia and sensory neuropathy. This is a new phenotype since previous reported patients with *KIAA0196* mutations were clinically characterised by pure HSP.(Rocco et al. 2000; Valdmanis et al. 2007) Furthermore, the panel detected the first *KIF5A* mutation associated with cerebellar ataxia (*KIF5A* R204W in table 6-12, details of *KIF5A* mutations were described in Section 4.1). The accumulation of genetic data generated by targeted resequencing will increase rapidly our understanding of phenotypic-genotypic correlations of many rare genes and will improve the process of genetic diagnosis in the future.

This was also the first resequencing panel designed for the genetic diagnosis of complex syndromes spanning over more than one group of neurological disorders. For the two patients with *MFN2* mutations, both had axonal neuropathy complicated with pyramidal tract involvement, clinically overlapped with cHSP. The findings highlighted *MFN2* is a must gene to screen in patient affected by spastic paraperesis when there is simultaneous involvement of peripheral nerves. The experience from the HSP-axonal neuropathy panel indicates that more

CMT2 genes which may cause both LMN and UMN signs can be recruited together when studying HSP patients. Conversely, it is reasonable to put some HSP genes which have a high association with peripheral neuropathy on the panel for CMT2 genes. This study documented that targeted resequencing is flexible and powerful in studying patients whose symptoms involve more than one neurological system.

A major challenge in the application of targeting resequencing is how to interpret the data when variants in multiple genes were detected simultaneously. Several ways could help to determine the clinical significance of a variant, including Sanger sequencing, segregation tests in family members, screening in controls or larger cohorts, in silico prediction, conservation of the affected base and amino acid in evolution. However, sometimes it was still very difficult in distinguishing which mutation was likely to be pathogenic.

Another critical issue is to achieve sufficient read depths and satisfactory sequencing coverage for use in clinical practice. If the sequence yields fail to cover the target regions well, the costs and time to do Sanger sequencing for the missing regions would be considerably high. This study performed sequencing in two conditions by the use of the same library probes, and the run which pooled less samples yielded sequences with a better coverage. Our results pointed out the importance to get the balance between number of targeted regions and amount of testing samples. This would be helpful for the future design of resequencing panels.

Although there are some issues in sequence generation and data processing, targeted resequencing still shows its excellent efficiency of screening mutations in a lot of known genes. Considering the high cost and huge size of data generated by WES or even whole genome sequencing (WGS), it is an efficient way to utilise a custom-designed panel to screen most of the related known genes in selective groups of patients first. WES or WGS can be reserved for those whose pathogenic mutations are still unknown after targeted resequencing.

References

Al-Maawali A, Rolfs A, Klingenhaeger M, Yoon G (2011) Hereditary spastic paraplegia associated with axonal neuropathy: a novel mutation of SPG3A in a large family. J Clin Neuromuscul Dis 12: 143-6

Arnoldi A, Tonelli A, Crippa F, Villani G, Pacelli C, Sironi M, Pozzoli U, D'Angelo MG, Meola G, Martinuzzi A, Crimella C, Redaelli F, Panzeri C, Renieri A, Comi GP, Turconi AC, Bresolin N, Bassi MT (2008) A clinical, genetic, and biochemical characterization of SPG7 mutations in a large cohort of patients with hereditary spastic paraplegia. Hum Mutat 29: 522-31

Brugman F, Scheffer H, Wokke JH, Nillesen WM, de Visser M, Aronica E, Veldink JH, van den Berg LH (2008) Paraplegin mutations in sporadic adult-onset upper motor neuron syndromes. Neurology 71: 1500-5

Du J, Hu YC, Tang BS, Chen C, Luo YY, Zhan ZX, Zhao GH, Jiang H, Xia K, Shen L (2011) Expansion of the phenotypic spectrum of SPG6 caused by mutation in NIPA1. Clin Neurol Neurosurg 113: 480-2

Dufke C, Schlipf N, Schule R, Bonin M, Auer-Grumbach M, Stevanin G, Depienne C, Kassubek J, Klebe S, Klimpe S, Klopstock T, Otto S, Poths S, Seibel A, Stolze H, Gal A, Schols L, Bauer P (2012) A high-throughput resequencing microarray for autosomal dominant spastic paraplegia genes. Neurogenetics 13: 215-27

Ewing B, Green P (1998a) Base-calling of automated sequencer traces using phred. II. Error probabilities. Genome Res 8: 186-94

Ewing B, Hillier L, Wendl MC, Green P (1998b) Base-calling of automated sequencer traces using phred. I. Accuracy assessment. Genome Res 8: 175-85

Fink JK (2013) Hereditary spastic paraplegia: clinico-pathologic features and emerging molecular mechanisms. Acta Neuropathol 126: 307-28

Goizet, C, Boukhris A, Mundwiller E, Tallaksen C, Forlani S, Toutain A, Carriere N, Paquis V, Depienne C, Durr A, Stevanin G, Brice A (2009) Complicated forms of autosomal dominant hereditary spastic paraplegia are frequent in SPG10. Hum Mutat 30(2): E376-85

Guelly C, Zhu PP, Leonardis L, Papic L, ZidarJ, Schabhuttl M, Strohmaier H, Weis J, Strom TM, Baets J, Willems J, De Jonghe P, Reilly MM, Frohlich E, Hatz M, Trajanoski S, Pieber TR, Janecke AR, Blackstone C, Auer-Grumbach M (2011) Targeted high-throughput sequencing identifies mutations in atlastin-1 as a cause of hereditary sensory neuropathy type I. Am J Hum Genet 88(1): 99-105

Hazan J, Fonknechten N, Mavel D, Paternotte C, Samson D, Artiguenave F, Davoine CS, Cruaud C, Durr A, Wincker P, Brottier P, Cattolico L, Barbe V, Burgunder JM, Prud'homme JF, Brice A, Fontaine B, Heilig B, Weissenbach J (1999) Spastin, a new AAA protein, is altered in the most frequent form of autosomal dominant spastic paraplegia. Nat Genet 23: 296-303

Houlden H, Hammans S, Katifi H, Reilly MM (2009) A novel Frabin (FGD4) nonsense mutation p.R275X associated with phenotypic variability in CMT4H. Neurology 72: 617-20

Ivanova N, Claeys KG, Deconinck T, Litvinenko I, Jordanova A, Auer-Grumbach M, Haberlova J, Lofgren A, Smeyers G, Nelis E, Mercelis R, Plecko B, Priller J, Zamecnik J, Ceulemans B, Erichsen AK, Bjorck E, Nicholson G, Sereda MW, Seeman P, Kremensky I, Mitev V, De Jonghe P (2007) Hereditary spastic paraplegia 3A associated with axonal neuropathy. Arch Neurol 64: 706-13

Kumar KR, Sue CM, Burke D, Ng K (2012) Peripheral neuropathy in hereditary spastic paraplegia due to

spastin (SPG4) mutation - A neurophysiological study using excitability techniques. Clin Neurophysiol 123(7):1454-9

McDermott CJ, Dayaratne RK, Tomkins J, Lusher ME, Lindsey JC, Johnson MA, Casari G, Turnbull DM, Bushby K, Shaw PJ (2001) Paraplegin gene analysis in hereditary spastic paraparesis (HSP) pedigrees in northeast England. Neurology 56: 467-71

Murphy SM, Laura M, Fawcett K, Pandraud A, Liu YT, Davidson GL, Rossor AM, Polke JM, Castleman V, Manji H, Lunn MP, Bull K, Ramdharry G, Davis M, Blake JC, Houlden H, Reilly MM (2012) Charcot-Marie-Tooth disease: frequency of genetic subtypes and guidelines for genetic testing. J Neurol Neurosurg Psychiatry 83: 706-10

Reilly MM, Murphy SM, Laura M (2011) Charcot-Marie-Tooth disease. J Peripher Nerv Syst 16: 1-14

Rocco P, Vainzof M, Froehner SC, Peters MF, Marie SK, Passos-Bueno MR, Zatz M (2000) Brazilian family with pure autosomal dominant spastic paraplegia maps to 8q: analysis of muscle beta 1 syntrophin. Am J Med Genet 92: 122-7

Rossor AM, Polke JM, Houlden H, Reilly MM (2013) Clinical implications of genetic advances in Charcot-Marie-Tooth disease. Nat Rev Neurol 9(10):562-71

Scarano V, Mancini P, Criscuolo C, De Michele G, Rinaldi C, Tucci T, Tessa A, Santorelli FM, Perretti A, Santoro L, Filla A (2005) The R495W mutation in SPG3A causes spastic paraplegia associated with axonal neuropathy. J Neurol 252: 901-3

Schule R, Brandt E, Karle KN, Tsaousidou M, Klebe S, Klimpe S, Auer-Grumbach M, Crosby AH, Hubner CA, Schols L, Deufel T, Beetz C (2009) Analysis of CYP7B1 in non-consanguineous cases of hereditary spastic paraplegia. Neurogenetics 10: 97-104

Schulte T, Miterski B, Bornke C, Przuntek H, Epplen JT, Schols L (2003) Neurophysiological findings in SPG4 patients differ from other types of spastic paraplegia. Neurology 60: 1529-32

Valdmanis PN, Meijer IA, Reynolds A, Lei A, MacLeod P, Schlesinger D, Zatz M, Reid E, Dion PA, Drapeau P, Rouleau GA (2007) Mutations in the KIAA0196 gene at the SPG8 locus cause hereditary spastic paraplegia. Am J Hum Genet 80: 152-61

Windpassinger C, Auer-Grumbach M, Irobi J, Patel H, Petek E, Horl G, Malli R, Reed JA, Dierick I, Verpoorten N, Warner TT, Proukakis C, Van den Bergh P, Verellen C, Van Maldergem L, Merlini L, De Jonghe P, Timmerman V, Crosby AH, Wagner K (2004) Heterozygous missense mutations in BSCL2 are associated with distal hereditary motor neuropathy and Silver syndrome. Nat Genet 36: 271-6

Chapter 7

General discussion

This chapter provides an overview of the genetic studies in this thesis. Mutations in several genes for inherited neuropathies and related disorders have been identified by these studies. These genetic findings contribute to both clinical diagnosis and the understanding of molecular genetics. Most of these mutations were identified from patients with new and unexpected phenotypes, broadening the phenotypic spectrum of these mutated genes. Screening studies in large cohorts also defined more accurately the frequency of specific gene mutations. Understanding the molecular genetics of these genes can provide a comprehensive perspective on the pathogenesis of inherited neuropathies. Many mutations were detected through NGS. The challenges faced when applying NGS in genetic diagnosis and how to address these challenges in the future will also be discussed.

7.1 Contribution of this thesis to clinical diagnosis

Genetic findings in this thesis are summarised in table 7-1 (p202). Knowledge gained from these findings is very helpful for decision making of how to approach genetic testing in clinical practice. The contributions of this thesis to clinical diagnosis are described below:

(1) Screening studies in large cohorts

The aim of these studies was to define more accurately the frequency of specific gene mutations and their phenotypic spectrum. From this thesis, the mutation frequencies of *NEFL* mutations in CMT, *SPTLC2* mutations in HSN-I and *PDYN* mutations in ADCA in the British population was documented. The two *NEFL* mutations were associated with early-onset CMT1 and late-onset cases individually, suggesting that mutation analysis of *NEFL* should be considered in CMT patients with variable age of onset when mutations in common genes have been already excluded. It could also be inferred that mutations in the *PMP22 promoter*, *KCND3*, or *AFG3L2* are very rare from the negative screening.

(2) Identification of novel genes for inherited neuropathies:

Two novel genes for CMT2 identified by WES were described in this thesis: *MARS and C12orf65. A* novel missense mutation in the *MARS* gene was detected in a family with late-onset CMT2. Identification of this mutation highlights the importance to take incomplete penetrance into consideration when determining the inheritance of a patient with a late-onset course. The *C12orf65* mutation is the first mutation documented in patients with a recessive form of axonal neuropathy with optic atrophy (CMT6). Although only rare mutations were reported, multiple symptoms in PNS, CNS and extra-neurological systems are the features of these patients with *C12orf65* mutations.

(3) Mutations in known rare gene identified through NGS

Many mutations in known rare genes were identified through NGS in this thesis. Most of these genes are not tested in most of the diagnostic labs routinely because it is not cost effective to screen those genes which are very rarely mutated or very large in size. The introduction of NGS has made sequencing in these "difficult genes" much easier. In parallel with the identification of more mutations, the understanding of mutation frequencies and the phenotypic spectrum of these genes is expanding. This is best illustrated by mutation analysis of *KIF5A* by the combination of NGS and Sanger sequencing. Through this study, *KIF5A* has been confirmed to be one of the causative genes for CMT2. The phenotypic spectrum of *KIF5A* mutations has also been broadened showing that cerebellar ataxia can be an associated feature. Another example is the *DNMT1* mutation identified by WES in this thesis. Although the pathogenic mutation has

been reported before, this is the first time that a *DNMT1* mutation has been shown to cause a sensory neuropathy only with no cognitive impairment. The learning point of this genetic finding is to include *DNMT1* mutations in the possible aetiologies of patients with HSN and sensorineuronal loss, even when cognitive function is not impaired. This thesis also identified new phenotypes for *RNF216, KIAA0196, SPAST* and *ADCK3* (see table 7-1).

Most of the patients carrying the mutations described above presented with a complex syndrome involving more than one part of the nervous system. Mutations in *C12orf65, KIF5A* and many other HSP genes have affected both the PNS and CNS. WES also detected pathogenic mutations in two HSP genes (*PNPLA6* and *ZFYVE26)* in ARCA families. These results suggest a significant overlap between cerebellar ataxia and HSP. The clinical and genetic overlap between inherited neuropathies and HSP and/or cerebellar ataxia has been further reinforced by these genetic findings (illustrated by figure 7-1). Therefore, various associated features should be looked for carefully and taken into consideration when evaluating a patient with inherited neuropathy of undetermined caused. Screening of genes causing other overlapping diseases may be considered for these patients. It is not uncommon for these mutations to be identified in sporadic cases. Absence of family history cannot be an exclusion criterion of inherited neuropathy.

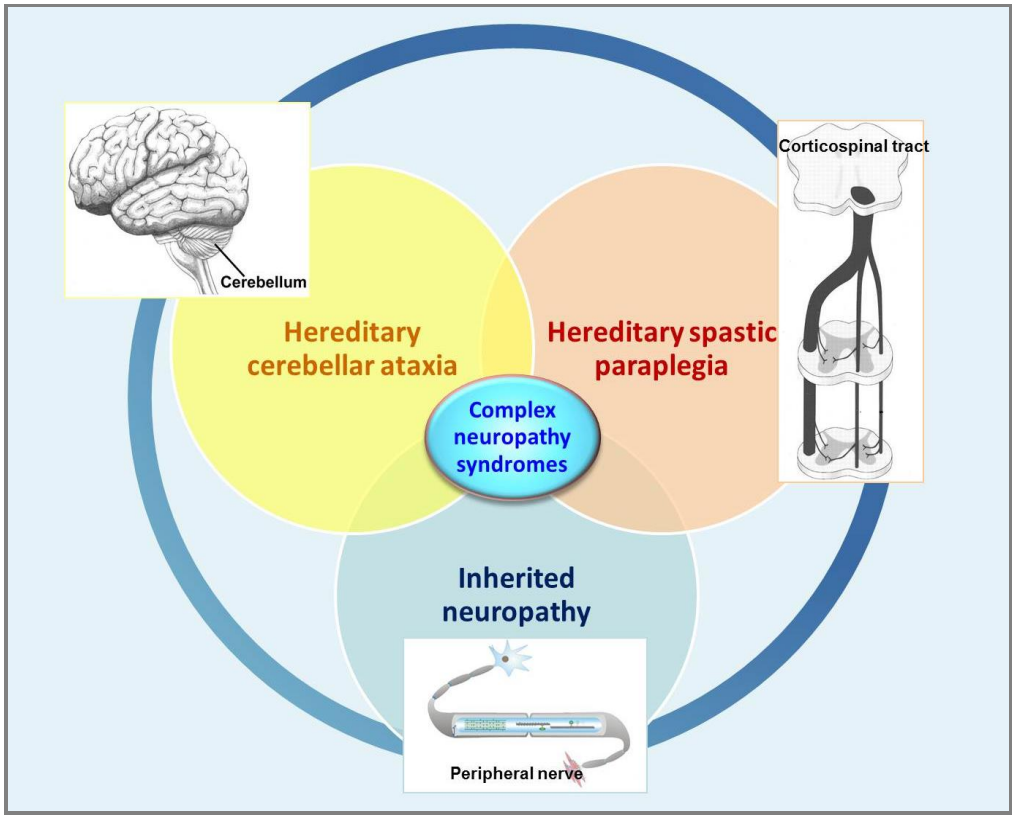

Figure 7-1. Complex neuropathy syndromes representing the overlap between inherited neuropathy, hereditary spastic spastic paraglegia, and cerebellar ataxia

Table 7-1. Genetic findings of studies in this thesis

	Gene	Mutation	Phenotype
Screening studies in large cohorts by Sanger sequencing	*NEFL*	P8R, L311P*	ADCMT1, early and late onset
	SPTLC2	A182P*	AD-HSN (HSN type I)
	PMP22 promoter	None	
	PDYN	C22Y*	ADCA
	KCND3	None	
	AFG3L2	None	
Novel genes for inherited neuropathies	*C12orf65*	V116X*	ARCMT2 with optic atrophy and pyramidal signs
	MARS	R618C*	ADCMT2, late-onset and incomplete penetrance
Mutations in known rare gene identified through NGS	**Genes for inherited neuropathies**		
	SH3TC2	[p.R954X ; p.R954X] (n=2),	ARCMT1
	GDPA1	[p.M116R ; p.M116R], [p.G327D (;) p.L239F]*	ARCMT1
	FGD4	[p.R442H ; p.R442H], [p.R577Q (;)	ARCMT1
	MFN2	S231P*, R519C	CMT2 with spasticity, cHSP with neuropathy and learning difficulty
	DNMT1	Y495C	HSN with deafness
	Genes for HSP		
	KIF5A++	R204Q, R204W*, D232N*, R280H,	CMT2#, CMT2 with spasiticity#, pHSP, cHSP with axonal
	ATL1	R239C	pHSP
	KIAA0196	I226T*	L-Dopa responsive spasticity with sensory axonal neuropathy#
	SPAST	S44L, c.1494-2delT	pHSP, cHSP with visual impairment, learning difficulty#
	FA2H	[p.R154C (;) p.T207M]	cHSP with cerebellar ataxia#
	ZNFVE26	R1438X	ARCA with spasticity and axonal neuropathy
	PNPLA6	V1273M	ARCA with spasticity and axonal neuropathy
	Genes for hereditary cerebellar ataxia		
	RNF216	c.2453-2A>G*	ARCA with congenital ectodermal dysplasia
	ADCK3	S616Lfs	ARCA with tremor, myoclonus and dystonia#
	SACS	c.5557_5561delCTTTT	ARCA with spasticity and demyelinating neuropathy

* novel mutation, # novel phenotype for the gene, ++mutations were identified by both large-cohort screening and NGS

(4) Identification for mutations with treatable hereditary disorders

WES detected a novel *ADCK3* mutation causing CoQ10 deficiency in one patient and CoQ10 supplement helped her improve the clinical symptoms substantially. Introduction of NGS can lead to identification of more mutations in some treatable hereditary diseases, and therefore benefit more patients. Moreover, the identification of a novel *SPTLC2* mutation in HSN-1 has highlighted the role of deoxy-sphingolipids as a potential screening biomarker for sensory neuropathy which is under investigation currently. The toxic effects of deoxy-sphingolipids generated by mutated SPT also represent a potential target for treatment in the future and this is currently undergoing further investigations by our group.

7.2 Contribution of this thesis to molecular genetics

Mutations identified in this thesis will help understand the roles of these mutated genes in the pathogenesis of inherited neuropathy and even provide insights into the underlying mechanisms of other neurological disorders. Their proposed pathomechanisms are summarised in figure 7-2.

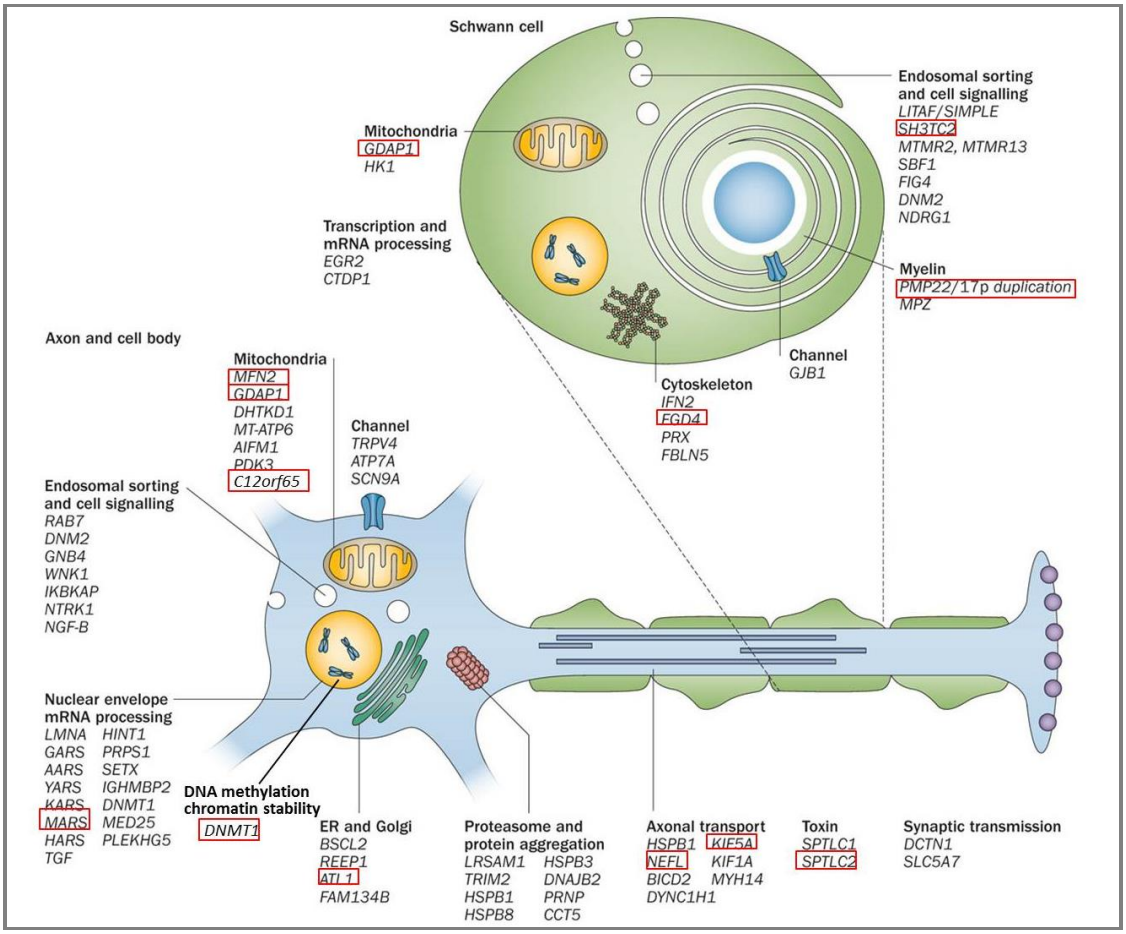

Figure 7-2. Genes causing inherited neuropathies and their biological functions

Genes flanked in red are those studied in this thesis.(modified from Rossor et al. 2013

Biological functions of these genes can be categorized into the following pathways:

(1) Intracellular trafficking and mutant protein processing

Many mutant genes that cause inherited neuropathies are involved in intracellular trafficking and related pathways. These diverse processes occur in subcellular organelles such as ER, Golgi apparatus, endosomes, lysosome and phagosomes. Below are some examples. *SH3TC2* expression is restricted to Schwann cells. The gene product, SH3TC2, localizes to the perinuclear recycling compartment and has been shown to participate in endosomal recycling.(Stendel et al. 2010). Atlastin-1, the dynamin-like GTPase responsible for spastic paraplegia SPG3A, remodels lipid membranes and may form tubules and vesicles in the

ER.(Muriel et al. 2009) As mentioned earlier, *SPTLC2* encodes for a subunit of an enzyme involved in the pathways of sphingolipid metabolism and mutant protein is believed to cause accumulation of atypical sphingolipids that may have a neurotoxic effect.(Rotthier et al. 2012)

Many other genes cause inherited neuropathies through abnormal protein processing and trafficking. For example, the aminoacyl-tRNA synthetase (ARS) gene family is composed of ubiquitously expressed housekeeping genes which are important for protein synthesis. Previously, four genes in this family, *GARS, YARS, AARS* and *KARS* have been identified as causes of CMT or related inherited neuropathies. The identification of a *MARS* mutation in a CMT2 family in this thesis further supports the hypothesis that genes in the ARS family are closely associated with axonal degeneration. This strongly indicates that these genes may harbour nerve-specific functions which are currently not completely understood yet. One hypothesis is the high metabolic demand of motor neurons and axons make them more vulnerable to dysfunction of t-RNA synthetases.(Antonellis et al. 2006; Jordanova et al. 2006)

(2) Axonal transport and cytoskeleton organization

Many mutant genes identified in peripheral neuropathies encode motor proteins or proteins directly interacting with cytoskeletons, e.g *KIF5A, NEFL* and *FGD4*. The *FGD4* gene encodes a protein which contains an actin filament-binding domain and is involved in the regulation of the actin cytoskeleton and cell shape.(Delague et al. 2007; Stendel et al. 2007) *NEFL* encodes NFL, the major intermediate filament in neurons and axons and is required for axon calibre and nerve conduction. It is involved in cytoskeleton maintenance and indirectly in axonal transport. The encoded proteins of *KIF5A*, KIF5s, are microtubule-directed, ATP-dependent motors that move cargo in anterograde axonal transport. In humans, KIF5s are necessary for axonal transport of neurofilament subunits and mitochondria.(Ebbing et al. 2008; Hirokawa et al. 2009) KIF5 proteins also regulate transport of cargoes in dendrites and have roles in a number of membrane traffic pathways in the cell body, including in ER-to-Golgi, Golgi-to-ER, Golgi to plasma membrane, and recycling endosomes and lysosomes.

The net effect of various mutant protein processing events frequently converges on deficiencies in axonal transport. Therefore, many genes participating in mutant protein processing can affect axonal transport, like *ATL1*. Also, some cellular studies showed that mutations in *YARS* and *GARS* impaired axonal transport and affected synaptic plasticity, suggesting these ARS genes are involved in axonal transportation in addition to protein processing.(Rossor et al. 2012;)

(3) Mitochondrial dysfunction

Mitochondria dysfunction can be caused by defects of either mitochondrial DNA or the nuclear genome encoding subunits of the mitochondrial respiratory chain. *C12orf65* is a newly identified gene for recessive axonal neuropathy and optic atrophy and plays a role in mitochondrial complex assembly and respiration. Interestingly, mutations in *MFN2* can cause a dominant form of axonal CMT and optic atrophy also due to mitochondrial dysfunction. *MFN2* encodes an outer mitochondrial membrane protein. Loss of *MFN2* affects mitochondria movements and transport along the axon, suggesting that this may be the cause of the length-dependent axonal degeneration observed in CMT2A.(Misko et al. 2010) Some other gene mutations have been demonstrated to cause mitochondrial dysfunction in CMT including *GDAP1* and *NEFL*. *GDAP1* encodes another mitochondrial outer membrane protein. Recessive *GDAP1* mutants reduce mitochondrial fission activity, whereas dominant ones interfere with the fusion process.(Niemann et al. 2009) Mitochondrial dysfunction is thought to contribute to the pathogenesis of *NEFL* mutations as rounding of mitochondria occurred before disruption of the neurofilament network in a model of CMT2E.(Tradewell et al. 2009) *C12orf65* is a newly identified neuropathy-related gene which is implicated in mitochondrial function. Furthermore, *KIF5A* is indirectly associated with the normal function of mitochondria because the KIF5 motors participate in mitochondrial transport.(Hirokawa et al. 2009) These genetic findings provide evidence that mitochondrial dysfunction is a common mechanism underlying axonal neuropathy.

(4) Myelin formation

PMP22 encodes peripheral myelin protein 22, which is mainly expressed in Schwann cells.(Snipes et al. 1992) The severity of CMT1A seems to be associated with the number of extra PMP22 copies, providing evidence that PMP22 duplications cause the demyelinating neuropathy though a gene dosage effect.(Lupski et al. 1992) Multiple studies in transgenic PMP22 mice also support the hypothesis that a dosage effect is the major determinant of the type and extent of the neuropathy.(Patzko et al.2011; Schenone et al. 2011)

(5) Epigenetic modification and regulation

DNMT1 plays a crucial role in maintenance of methylation, gene regulation and chromatin stability. DNA methylation in important in DNA mismatch repair, cell cycle regulation in post-mitotic neurons and neurogenesis.(Klein et al. 2011; Winkelmann et al. 2012) Clinically, *DNMT1* mutations have been associated with sensory neuropathy, deafness, ataxia, dementia and psychiatric symptoms, in parallel with the multiple functions of the gene.

Molecular genetic studies have been critical in understanding pathophysiological links between

inherited neuropathies and other neurological disorders. Inherited neuropathies, cerebellar ataxias, and HSPs are highly genetically heterogeneous disorders caused by mutations in many genes. Although the genes responsible for these neurological disorders are different, many of them play similar roles in the nervous system or participate in the same cellular pathways (table 7-2, p208).

Inherited neuropathies caused by mutations in genes associated with mitochondrial function have been mentioned earlier. Many other diseases have mitochondrial dysfunction as the main pathological process, like *ADCK3* mutations in cerebellar ataxia and *SPG7* mutations in HSP. The strong association between mitochondrial function and various components of the motor system may be due to the heavy energy consumption demands of the long axons, the corticospinal tract, motor neurons and Purkinje cells.(Blackstone et al. 2010)

Axonal transport represents a potential common pathway in the pathogenesis of both axonal neuropathies and spastic paraplegia.(Timmerman et al. 2012) *KIF5A* mutations provide further evidence for this with a wide phenotypic spectrum ranging from CMT2 to HSP. Like axonal neuropathies, many forms of HSP have mutants genes which are involved in axonal transport, like *BSCL2, REEP1, ATL1, SPAST* and *NIPA1* .(Barry et al. 2007; Gunawardena et al. 2004; Timmerman et al. 2012; Xia et al. 2003)

Genes associated with vesicle trafficking and protein processing are another group which commonly have a dual pathological effect on both the PNS and CNS. Mutations in these genes can cause CMT/dHMN with pyramidal features (*FIG4, GARS, TRPV4*) or cHSP with axonal neuropathy (*KIAA0196, ZFYVE26*).(Blackstone et al. 2010; Timmerman et al. 2012)

Table 7-2. Genes responsible for inherited neuropathies, cerebellar ataxias and hereditary spastic paraplegia and their functions

Functional groups	Mutant genes of different neurological disorders				
	CMT	**HSN**	**dHMN**	**CA**	**HSP**
Intracellular processing of proteins					
Protein misfolding and vesicle trafficking	***PMP22***, *MPZ, BSCL2, HSPB8, RAB7, LITAF, MTMR2,MTMR 1FIG4,****SH3TC2, FGD4***	*RAB7, HSN2(WNK1), FAM134B, ATL1*	*BSCL2, HSPB8, DCTN1,ATP7A*		***ATL1,SPAST, NIPA1,KIAA0196 SPG11,RTN2, ZFYVE26, BSCL2,SPG20, SPG21,REEP1, KIAA0415***
Protein synthesis	*GARS,YARS, AARS,KARS,* ***MARS*** *HSPB1,HSPB8*		*GARS,HSPB1, HSPB8,IGHMBP2*		
Channel function	*TRPV4*	*SCN9A*	*TRPV4*	*CACNA1A,* ***KCND3***	
Phospholipid homeostasis		*SPTLC1,* ***SPTLC2***		*TDP1*	***PNPLA6***
Axonal transport and cytoskeleton organization	***NEFL****,GARS,* ***FGD4, KIF5A,*** *KIF1B,LMNA*	*KIF1A,IKBKAP, CCT5, NTRK, NGFB,DNMT, ATL1*	*DCTN1,GARS*	*SPTBN2*	***ATL1, KIF5A***
Mitochondrial function	***MFN2, NEFL, GDAP1, PMP22, C12orf65***			*ATXN2, CACNA1A, ATXN7, ATN1, PPP2R2B,* ***AFG3L2,*** *PDSS1, PDSS2, COQ2,* ***ADCK3,*** *POLG*	***SPG7, HSPD1, C12orf65***
Toxic accumulation of aggregates and intranuclear inclusions	***PMP22***			*ATXN1, ATXN2, ATXN3, ATXN7, TBP, ATN1, ATXN8, ATXN10*	
RNA regulation and epigenetic modification	*EGR2, MED25*	***DNMT1***		*ATXN1, ATXN2, ATXN3, ATXN7, ATXN8, TBP, ATN1, BEAN-TK2*	
Myelination	***PMP22,*** *MPZ, GJB1,* ***NEFL, GDAP1,*** *EGR2, PRX, SOX10*				***PLP1, FA2H, GJC2***

CA: cerebellar ataxia. Genes studied in this thesis are expressed in bold.

Functional classification for genes are based on Durr et al. 2010, Anheim 2011, Matilla-Duenas et al.2010, Timmerman et al. 2012, Blacktson et al. 2011, Tucci et al. 2013 and Liu et al. 2014.

7.3 Challenges and future perspectives for next-generation sequencing

Over the past three years, NGS has been demonstrated to be a powerful tool in identifying disease-associated variants in several inherited human diseases. The introduction of high-throughput sequencing technologies has radically changed the approach of clinical geneticists towards human diseases and the nature of biomedical research.(Goh et al.2012; Torkamani et al. 2011) However, the current wide-spread availability of these techniques and the potential to generate large amounts of sequence data means that scientists are now faced with the challenges associated with the design of large-scale projects and analysis of the vast data generated. This poses significant challenges at various stages of the projects including planning, sample preparation, run processing and downstream analyses.(Kircher et al. 2011)

(1) Challenges of project design

Although a few studies have reported small indels which were detected by WES or targeted resequencing, the identification of long-fragment gene rearrangements still represents one of the major limitations. For targeted resequencing, it is possible to customize the library to target specific functional elements not in the coding region, such as introns, promoters, enhancers, silencers, microRNA binding sites, conserved regions, etc. However, it may reduce the panel's clinical utility when these non-coding regions are included. Moreover, the need of continually updating a panel due to newly discovered genes can markedly increase cost for targeting resequencing when applied in genetic diagnosis.

(2) Challenges of data production

Different commercial platforms provide users with the ability to construct application-specific sequencing libraries using a variety of protocols and different sequencing primers. The most important requirement for a DNA library to be sequenced on the Illumina platform is the presence of specific outer adapter sequences, complementary to the oligonucleotides on the flow cell used for cluster generation. Library adapters can be added by a variety of approaches, e.g. single strand ligation, double strand blunt-end ligation, double strand overhang ligation, and restriction enzyme overhangs in, or by extension from overhanging primers (e.g. multiplex PCR or molecular inversion probes). Each of these approaches has a different susceptibility to the creation of library adapter dimers, chimeric sequences and other library artifacts. The above conditions lead to generation of artifact sequences, which may have a negative impact on the image analysis and base-calling by overrepresentation of certain sequence populations and thus the generation of a false positive report.(Kircher et al. 2011) In this thesis, false-positive reports were found to increase substantially when the adapters were added by restriction enzyme overhangs (details described in Section 6.2). Sequencing of large numbers of such artifacts is

not cost effective and lowers the potential number of informative sequences that can be generated per run.

Other problems in data production come from samples. Results in this thesis showed that small amounts of input materials caused by a failure of library enrichment generated a higher fraction of library artifacts. This may be due to the relative abundance of adapter oligonucleotides compared to insert molecules. Sample contamination during library preparation from other DNA sources is another important issue. Library preparations starting from low amounts of sample DNA and protocols using single strand ligation procedures are more prone to contamination.(Kircher et al. 2011)

(3) Challenges of data analysis

Interpretation of the clinical significance of rare variants can be challenging. This is a critical issue when multiple variants in related genes are identified simultaneously from the same individual by NGS. To determine the pathogenicity of a variant one needs to consider all the following evidence: novelty of a variant, the knowledge that other variants in the same gene have been shown to cause the disease, the damage a particular variant may cause, the association of a variant with the gene expression in tissues of relevance to the disease. A documented segregation within the family is strongly supportive, whereas a functionally relevant protein interacting network of the mutated gene provides soft evidence. Unfortunately, it is common that either not all requirements can be fulfilled perfectly or there are more than one variant which can satisfy the criteria.

It is also challenging to analysis data when dealing with cases with limited clinical information (especially inheritance pattern) as currently WES has been applied frequently in patients who are sporadic or from small families where the inheritance pattern cannot always be determined. In WES studies for the cohort of ARCA in this thesis, a clear recessive inheritance greatly reduced the number of potential variants as only homozygous or compound heterozygous variants were taken into consideration, thus facilitating the process of gene identification. On the contrary, for sporadic HSN patients with uncertain inheritance, the lack of other affected members made it hard to reduce the number of candidate variants and progress further in the analysis.

(4) Future perspectives

With WES becoming increasingly available and cost effective, a larger number of variants will be identified. It is estimated that the total number of disease-associated variants will increase by approximately 37% in the next four years.(Cassa et al. 2012) To overcome the challenges of

interpreting NGS data, it is important to collect more human genome sequences and through collaboration with multiple collaborating groups, the accumulated data will help clarify the clinical significance of some rare variants. Development of user-friendly international databases and bioinformatic platforms are also vital to facilitate data sharing and statistical analysis. For instance, GEnomes Management Application (GEM.app) is a software tool developed to annotate, manage, visualize, and analyze large genomic datasets (https://genomics.med.miami.edu/). GEM.app currently contains more than 1,600 whole exomes from 50 different phenotypes studied by 40 principal investigators from 15 different countries.(Gonzalez et al. 2013) In the context of disease risk predictions, longitudinal and clinical studies exploring the role of multiple variants must be pursued.(Torkamani et al. 2011)

Meanwhile, the establishment of genome database, the accumulation of information about biological processes, molecular functions and the cellular components of a gene via diverse gene ontology (GO) databases will be helpful in the identification of novel disease-causing genes. The proteomic information is particularly useful when analyzing genetic defects in genes which involve specific tissues or systems, e.g. inherited peripheral neuropathies, cerebellar ataxia or HSP. Taking CMT as the example, genes which are highly expressed or have evidence of unique alternative splicing in peripheral nerves or are associated with known pathways causing neuropathy are excellent disease causing candidates.

NGS is rapidly revolutionizing genetic testing in hereditary neurological disorders. An integrated approach for genetic diagnosis will be established by the combination of NGS and conventional Sanger sequencing. With the reduction of costs, it will be possible in the near future to employ NGS at an earlier stage in the diagnostic pathway. Customized genetic screening panels will be more wildly used in clinical practice, and even WES will be adopted in the diagnostic process as routine for patients who have not a genetically confirmed inherited disorder in the next few years.(Rossor et al. 2013)

Reference

Anheim M (2011) Autosomal recessive cerebellar ataxias. Rev Neurol (Paris) 167: 372-84

Antonellis A, Lee-Lin SQ, Wasterlain A, Leo P, Quezado M, Goldfarb LG, Myung K, Burgess S, Fischbeck KH, Green ED (2006) Functional analyses of glycyl-tRNA synthetase mutations suggest a key role for tRNA-charging enzymes in peripheral axons. J Neurosci 26: 10397-406

Barry DM, Millecamps S, Julien JP, Garcia ML (2007) New movements in neurofilament transport, turnover and disease. Exp Cell Res 313: 2110-20

Blackstone C, O'Kane CJ, Reid E (2010) Hereditary spastic paraplegias: membrane traffic and the motor pathway. Nat Rev Neurosci 12: 31-42

Cassa CA, Savage SK, Taylor PL, Green RC, McGuire AL, Mandl KD (2012) Disclosing pathogenic genetic variants to research participants: quantifying an emerging ethical responsibility. Genome Res 22: 421-8

Delague V, Jacquier A, Hamadouche T, Poitelon Y, Baudot C, Boccaccio I, Chouery E, Chaouch M, Kassouri N, Jabbour R, Grid D, Megarbane A, Haase G, Levy N (2007) Mutations in FGD4 encoding the Rho GDP/GTP exchange factor FRABIN cause autosomal recessive Charcot-Marie-Tooth type 4H. Am J Hum Genet 81: 1-16

Durr, A. (2010). Autosomal dominant cerebellar ataxias: polyglutamine expansions and beyond. Lancet Neurol 9(9): 885-94

Ebbing B, Mann K, Starosta A, Jaud J, Schols L, Schule R, Woehlke G (2008) Effect of spastic paraplegia mutations in KIF5A kinesin on transport activity. Hum Mol Genet 17: 1245-52

Goh G, Choi M (2012) Application of whole exome sequencing to identify disease-causing variants in inherited human diseases. Genomics Inform 10: 214-9

Gonzalez MA, Lebrigio RF, Van Booven D, Ulloa RH, Powell E, Speziani F, Tekin M, Schule R, Zuchner S (2013) GEnomes Management Application (GEM.app): a new software tool for large-scale collaborative genome analysis. Hum Mutat 34: 842-6

Gunawardena S, Goldstein LS (2004) Cargo-carrying motor vehicles on the neuronal highway: transport pathways and neurodegenerative disease. J Neurobiol 58: 258-71

Hirokawa N, Noda Y, Tanaka Y, Niwa S (2009) Kinesin superfamily motor proteins and intracellular transport. Nat Rev Mol Cell Biol 10: 682-96

Jordanova A, Irobi J, Thomas FP, Van Dijck P, Meerschaert K, Dewil M, Dierick I, Jacobs A, De Vriendt E, Guergueltcheva V, Rao CV, Tournev I, Gondim FA, D'Hooghe M, Van Gerwen V, Callaerts P, Van Den Bosch L, Timmermans JP, Robberecht W, Gettemans J, Thevelein JM, De Jonghe P, Kremensky I, Timmerman V (2006) Disrupted function and axonal distribution of mutant tyrosyl-tRNA synthetase in dominant intermediate Charcot-Marie-Tooth neuropathy. Nat Genet 38: 197-202

Kircher M, Heyn P, Kelso J (2011) Addressing challenges in the production and analysis of illumina sequencing data. BMC Genomics 12: 382

Klein CJ, Botuyan MV, Wu Y, Ward CJ, Nicholson GA, Hammans S, Hojo K, Yamanishi H, Karpf AR, Wallace DC, Simon M, Lander C, Boardman LA, Cunningham JM, Smith GE, Litchy WJ, Boes B, Atkinson EJ, Middha S, PJ BD, Parisi JE, Mer G, Smith DI, Dyck PJ (2011) Mutations in DNMT1 cause hereditary sensory neuropathy with dementia and hearing loss. Nat Genet 43: 595-600

Liu YT, Laura M, Hersheson J, Horga A, Jaunmuktane Z, Brandner S, Pittman A, Hughes D, Polke JM,

Sweeney MG, Proukakis C, Janssen JC, Auer-Grumbach M, Zuchner S, Shields KG, Reilly MM, Houlden H (2014) Extended phenotypic spectrum of KIF5A mutations: From spastic paraplegia to axonal neuropathy. Neurology 83(7): 612-9

Lupski JR, Wise CA, Kuwano A, Pentao L, Parke JT, Glaze DG, Ledbetter DH, Greenberg F, Patel PI (1992) Gene dosage is a mechanism for Charcot-Marie-Tooth disease type 1A. Nat Genet 1: 29-33

Matilla-Duenas A, Sanchez I, Corral-Juan M, Davalos A, Alvarez R, Latorre P (2010) Cellular and molecular pathways triggering neurodegeneration in the spinocerebellar ataxias. Cerebellum 9(2): 148-66

Misko A, Jiang S, Wegorzewska I, Milbrandt J, Baloh RH (2010) Mitofusin 2 is necessary for transport of axonal mitochondria and interacts with the Miro/Milton complex. J Neurosci 30: 4232-40

Muriel MP, Dauphin A, Namekawa M, Gervais A, Brice A, Ruberg M (2009) Atlastin-1, the dynamin-like GTPase responsible for spastic paraplegia SPG3A, remodels lipid membranes and may form tubules and vesicles in the endoplasmic reticulum. J Neurochem 110(5): 1607-16.

Niemann A, Wagner KM, Ruegg M, Suter U (2009) GDAP1 mutations differ in their effects on mitochondrial dynamics and apoptosis depending on the mode of inheritance. Neurobiol Dis 36: 509-20

Patzko, A.and M. E. Shy (2011) Update on Charcot-Marie-Tooth disease. Curr Neurol Neurosci Rep 11(1): 78-88.

Rossor AM, Kalmar B, Greensmith L, Reilly MM (2012) The distal hereditary motor neuropathies. J Neurol Neurosurg Psychiatry 83: 6-14

Rossor AM, Polke JM, Houlden H, Reilly MM (2013) Clinical implications of genetic advances in Charcot-Marie-Tooth disease. Nat Rev Neurol 9(10):562-71

Rotthier A, Baets J, Timmerman V, Janssens K (2012) Mechanisms of disease in hereditary sensory and autonomic neuropathies. Nat Rev Neurol 8: 73-85

Schenone, A. L Nobbio, et al. (2011). Inherited neuropathies. Curr Treat Options Neurol 13(2): 160-79.

Snipes U, Suter A, Welcher A, Shooter EM (1992) Characterization of a novel peripheral nervous system myelin protein (PMP-22/SR13). J Cell Biol 117(1): 225-38

Stendel C, Roos A, Deconinck T, Pereira J, Castagner F, Niemann A, Kirschner J, Korinthenberg R, Ketelsen UP, Battaloglu E, Parman Y, Nicholson G, Ouvrier R, Seeger J, De Jonghe P, Weis J, Kruttgen A, Rudnik-Schoneborn S, Bergmann C, Suter U, Zerres K, Timmerman V, Relvas JB, Senderek J (2007) Peripheral nerve demyelination caused by a mutant Rho GTPase guanine nucleotide exchange factor, frabin/FGD4. Am J Hum Genet 81: 158-64

Stendel C, Roos A, Kleine H, Arnaud E, Ozçelik M, Sidiropoulos PN, Zenker J, Schüpfer F, Lehmann U, Sobota RM, Litchfield DW, Lüscher B, Chrast R, Suter U, Senderek J (2010) SH3TC2, a protein mutant in Charcot-Marie-Tooth neuropathy, links peripheral nerve myelination to endosomal recycling. Brain 133(Pt 8): 2462-74.

Timmerman V, Clowes VE, Reid E (2012) Overlapping molecular pathological themes link Charcot-Marie-Tooth neuropathies and hereditary spastic paraplegias. Exp Neurol 246: 14-25

Torkamani A, Scott-Van Zeeland AA, Topol EJ, Schork NJ (2011) Annotating individual human genomes. Genomics 98: 233-41

Tradewell ML, Durham HD, Mushynski WE, Gentil BJ (2009) Mitochondrial and axonal abnormalities

precede disruption of the neurofilament network in a model of charcot-marie-tooth disease type 2E and are prevented by heat shock proteins in a mutant-specific fashion. J Neuropathol Exp Neurol 68: 642-52

Tucci A, Liu YT, Preza E, Pitceathly RD, Chalasani A, Plagnol V, Land JM, Trabzuni D, Ryten M, Jaunmuktane Z, Reilly MM, Brandner S, Hargreaves I, Hardy J, Singleton AB, Abramov AY, Houlden H (2014) Novel C12orf65 mutations in patients with axonal neuropathy and optic atrophy. J Neurol Neurosurg Psychiatry 85(5):486-92

Winkelmann J, Lin L, Schormair B, Kornum BR, Faraco J, Plazzi G, Melberg A, Cornelio F, Urban AE, Pizza F, Poli F, Grubert F, Wieland T, Graf E, Hallmayer J, Strom TM, Mignot E (2012) Mutations in DNMT1 cause autosomal dominant cerebellar ataxia, deafness and narcolepsy. Hum Mol Genet 21(10):2205-10

Xia CH, Roberts EA, Her LS, Liu X, Williams DS, Cleveland DW, Goldstein LS (2003) Abnormal neurofilament transport caused by targeted disruption of neuronal kinesin heavy chain KIF5A. J Cell Biol 161: 55-66